

**Western Australian School of Mines: Minerals, Energy and Chemical
Engineering**

Self-Propelled Micro/Nanomotors (MNM)s and Their Applications

Heng Ye

**This thesis is presented for the Degree of
Doctor of Philosophy
of
Curtin University**

October 2018

Declaration

To the best of my knowledge and belief this thesis contains no material previously published by any other person except where due acknowledgment has been made. This thesis contains no material which has been accepted for the award of any other degree or diploma in any university.

Signature: Heng Ye (Heng Ye)
Date: 04/10/2018

Acknowledgements

Firstly, I would like to express my utmost gratefulness to my principal advisor professor Shaobin Wang for his kind and supportive instruction, guidance, tolerance, assistance, and encouragement. Without his selfless help and arrangement, I cannot complete my academic research and publications.

My sincere gratitude also gives to my co-supervisor professor Hongqi Sun for his understanding of the difficulties of conducting research in a totally new research topic in our group and the kind suggestion when I encounter problems. His selfless input contributes to my publications and the thesis.

I would also like to thank professor Shaomin Liu as the chairperson of the thesis committee for his kind encouragement and suggestions during the project.

I am also grateful to my undergraduate and graduate period mentor professor Changsheng Liu from Northeastern University and professor Haifeng Zhang from the Institute of Metal Research of the Chinese Academy of Sciences, you teach me a lot in every aspect of my life both academically and personally.

I also want to give my gratitude to the technicians at Curtin University, Yu, Jimmy, Andrew, Guanliang, Ann, Jason, Araya, Melina, Dipok, Hao Gao, Elaine Miller, Kelly Merigot, and Anja for helping me prepare the chemicals and training me on the use of equipments. Special thanks also give to the supporting team and friends at the University of Western

Australia (UWA) and Edith Cowan University (ECU), professor Martin Saunders, professor Alexandra Suvorova, professor Xiaozhi Hu, professor Wen Lei, professor Andrew Johnson, professor Peta Clode, professor Paul Rigby, Dr Thomas Becker, Dr Aaron, Dr Yujing Liu, Dr Hua Li, Shunxing, Jincheng, Alysia, Irma, Andrea, and Lyn for their constant help, understanding, and encouragement to facilitate my research.

I also appreciate the support, help, and assistance from all my friends and colleagues at Curtin University, professor Degang Li, professor Linfeng Zhai, professor Peiqiang Li, professor Jianchao Ma, professor Jian Liu, Dr Lihong, Dr Lei Shi, Dr Yu Yin, Dr Lei Li, Dr Zhengyu, Dr Xiaoguang, Dr Wei, Spark, Hao Tian, Meiwen, Stacey, Muhammad, Min Ao, Rui Diao, Chi Zhang, Ping Liang, Yuxian, Wenran, Jinxiu, Chen Wang, Jian Kang, Xiaochen, Huayang, Wenjie, Qi Yang, Stacey, Yee Wen Chua, Sui Boon Liaw, Jun Ke, Jie Liu, Fuping, Lily Zhou, Qiaoran, Leon Liu, Yazhi, Fern, Xiaojie, Shiyong, Shuai He, Qi Zhang, Panpan, Ning Han, Ruofei, Panda Yao, Jingqiang, Hong Wu, Shanshan, and Jiaquan.

Last but not the least, I would like to express my deepest love and gratitude to my family and relatives. I truly thank you all for your tremendous support and unreserved love in my entire study period as a student. I love you all dearly.

Abstract

Micro/nanomotors (MNMs) would enable humankind to perform diverse tasks and operations that would be unimaginable in the past. The development of motion-based micro/nano scale devices, platforms, and MNMs are realizing the dream of manipulating the tiny entities, which means that a whole range of possible opportunities is open for the nanoscience, chemistry, biomedicine, and analysis. Previously, the majority of the catalytic MNMs use the precious noble metal platinum (Pt) as the catalyst to decompose hydrogen peroxide (H_2O_2) for propulsion. However, the Pt catalyst suffers from high-cost, scarcity, and possibility of deactivation in various media, researchers have been searching for new catalytic materials and propelling mechanisms. In this thesis, we tried to use the low-cost manganese dioxide (MnO_2) based materials as the catalytic part to construct MNMs. The MnO_2 based MNMs have already demonstrated many applications, but the performance of MnO_2 cannot compete with Pt for MNMs purposes, due to the intrinsic low catalytic performance for H_2O_2 decomposition. we explore the possibility of MnO_2 as an alternative for Pt for the fabrication of high-performance and low-cost MNMs. Different fabrication and modification methods have been utilized to construct four types of MnO_2 based MNMs. Especially interestingly, the most high-performance iron oxide doped MnO_2 based MNMs could lower the minimal fuel concentration to nearly one order of magnitude than the commonly used Pt-based MNMs. We believe that these MnO_2 based MNMs will show great potential applications for biomedical and environmental sciences.

Publications by the Author

Published and accepted papers:

1. **H. Ye**, H.Q. Sun, S.B. Wang. Electrochemical synthesis of graphene/MnO₂ in an architecture of bilayer microtubes as micromotors. Chem. Eng. J. 2017; 324; 251-258.
2. **H. Ye**, G.F. Ma, J. Kang, H.Q. Sun, S.B. Wang. Pt-Free microengines at extremely low peroxide levels. Chem. Commun. 2018; 54; 4653-4656. **(Front outside cover)**
3. **H. Ye**, J. Kang, G.F. Ma, H.Q. Sun, S.B. Wang. High-speed graphene@Ag-MnO₂ micromotors at low peroxide levels. J. Colloid Interface Sci. 2018; 528; 271-280.
4. G.F. Ma, **H. Ye**, H.L. Zhang, C.L. He, L.N. Sun, H.F. Zhang, Z.Q. Hu, The relation between wetting and interfacial chemistry in the Zr-Based BMGs/W system. J. Alloy Compd. 2017; 690; 903-908.
5. G.F. Ma, **H. Ye**, H.L. Zhang, C.L. He, H.F. Zhang, Wettability of molten Sn on AlCoCrCu_xFeNi high-entropy alloy. Mater. Chem. Phys. 2017; 199; 1-6.

Manuscripts submitted or in preparation:

1. **H. Ye**, H.Q. Sun, S.B. Wang. Surfactant independent propulsion of MnO₂ based micromotors. **(To be submitted)**
2. **H. Ye**, H.Q. Sun, S.B. Wang. How surfactant affects the motion of silver-containing MnO₂ based micromotors. **(In preparation)**

Content

Declaration	i
Acknowledgement	ii
Abstract	iv
Publications by the Author	v
Content	vi
Chapter 1. Introduction	1
1.1 Background of micro/nanomotors (MNMs) for environmental applications	1
1.2 Research objectives	4
1.3 Thesis organization.....	5
References	7
Chapter 2. Literature Review	11
2.1 Introduction	11
2.2 The underlying physics for MNMs propulsion	17
2.2.1 The Reynolds number	19
2.2.2 The effect of thermal fluctuation induced Brownian motion ..	19

2.3 The propelling and motion mechanisms of MNMs	20
2.3.1 Self-electrophoresis propelled MNMs.....	21
2.3.2 Self-diffusiophoresis propelled MNMs	23
2.3.3 Bubble propulsion of MNMs	24
2.3.4 Propulsion of MNMs by surface tension	25
2.3.5 Motion control of micro/nanomotors by external stimuli	25
2.4 The fabrication of MNMs	26
2.4.1 Materials selection for MNMs	26
2.4.2 Fabrication techniques for MNMs	28
2.5 MNMs responding to the environments	30
2.5.1 The pH-responsive applications of MNMs.....	31
2.5.2 How surfactants affect the motion behaviors of MNMs	32
2.5.3 How other environmental conditions influence the motion of MNMs	33
2.6 MNMs based environmental applications	33
2.6.1 Self-propelled MNMs for catalytic degradation of pollutants. 36	
2.6.2 MNMs for adsorption removal of aquatic contaminants.....	37

2.6.3 MNMs for separation of oil and water	39
2.6.4 MNMs for the killing of bacterial	41
2.6.5 MNMs based sensing, detection, monitoring, and analysis	43
2.6.5.1 Optical microscope based analytical applications of the MNMs	44
2.6.5.2 Electrochemical based analytical applications of MNMs .	46
2.7 Conclusions and perspectives	48
References	49
Chapter 3. Electrochemical Synthesis of MnO₂ Based Micromotors in an Architecture of Bilayer Microtubes by an Anodic Oxidation Deposition Method	64
Abstract	64
3.1 Introduction	65
3.2 Experimental section	67
3.2.1 Materials and reagents	67
3.2.2 Fabrication of graphene/MnO ₂ bilayer microtubes.....	67
3.2.3 Equipment and characterization	68
3.2.4 Motion behavior observations	70

3.3 Results and discussion	70
3.4. Conclusions	84
References	85
Chapter 4. High-Speed Graphene/Ag-MnO₂ Micromotors at Low Peroxide Levels by Cathodically Electrochemical Deposition	91
Abstract	91
4.1. Introduction	92
4.2. Experimental section	94
4.2.1 Materials and reagents	94
4.2.2 Fabrication of MnO ₂ based micromotors	95
4.2.3 Characterization of the micromotors	96
4.2.4 Motion behavior observation	97
4.3 Results and discussion	98
4.4 Conclusions	116
References	117
Chapter 5. High-Performance Pt-Free Microengines at Extremely Low Peroxide Levels.....	124
Abstract	124

5.1 Introduction	125
5.2 Experimental section	126
5.2.1 Materials and reagents	126
5.2.2 Fabrication of MnO ₂ based micromotors	127
5.2.3 Characterization of the micromotors	128
5.2.4 Motion behavior observation	129
5.3 Results and discussion	129
5.4 Conclusions	141
References	141
Chapter 6. Robust MnO₂ Based Microengines for Surfactant Independent Propulsion	146
Abstract	146
6.1 Introduction	147
6.2 Experimental section	149
6.2.1 Materials and reagents	149
6.2.2 Fabrication of MnO ₂ based micromotors	150
6.2.3 Motion behaviors observation	151

6.3 Results and discussions.....	152
6.4 Conclusions	161
References	163
Chapter 7. How Surfactants Affect the Mobility of Silver-Containing Microengines.....	169
Abstract.....	169
7.1 Introduction	170
7.2 Experimental section	173
7.2.1 Materials and reagents	173
7.2.2 Fabrication of graphene/Ag-MnO ₂ micromotors.....	174
7.2.3 Motion behavior observation	175
7.3 Results and discussion	176
7.4 Conclusions	184
References	185
Chapter 8. Conclusions and Perspectives.....	191
8.1 Conclusions	191
8.1.1 Graphene/MnO ₂ micromotors by anodic electrosynthesis	191

8.1.2 MnO ₂ based micromotors by cathodic electrofabrication	192
8.1.3 High-performance graphene/FeO _x -MnO ₂ micromotors	192
8.1.4 The role of surfactants in MnO ₂ based micromotors system.	193
8.2 Perspectives and suggestions for future work	193
8.2.1 Environmental applications of the developed micromotors ..	193
8.2.2 Development of new types of metal oxide based MNMs	194
8.2.3 MNMs based analytical applications.....	194
Appendix	196

Chapter 1. Introduction

1.1 Background of micro/nanomotors (MNMs) for environmental applications

In 1959, Richard Feynman in his famous speech “There’s plenty of room at the bottom” forecasted the use of micro/nano-scale tools and devices to perform tasks at nanoscale.¹ Several years later, in a science fiction based movie the *fantastic voyage*, a crew of miniaturized scientists and doctors in a mini-submarine solved the medical problem in a human brain. The development of nanosciences and nanotechnology are realizing the dream of manipulating small-scale entities, such as delivery of drugs for cancer treatment and sorting of cells, as various small-scale motion platforms are developed in the last half-century.² In 2016, the Nobel Prize in chemistry was awarded to Jean-Pierre Sauvage, Sir J. Fraser Stoddart and Bernard L. Feringa "for the design and synthesis of molecular machines".³ These molecular scaled tools and devices would open a new gate for the materials scientists, chemists and biologists to manipulate and assemble similar dimensional scale atoms and molecules. Thus, it is possible to construct the molecular factories, which would fundamentally change the nanoscience and nanofabrication.

Slightly larger than the molecular machines, synthetic micro/nanomotors (MNMs) are also motion reactors, whose fabrication is one of the most dynamic research areas in nanoscience since the first demonstration by Whitesides et al.⁴ in 2002. Whitesides et al. designed a sub-centimeter sized floating semi-cylindrical plate with a small porous platinum (Pt) plate as the engine, and ever since a great deal of man-made MNMs have been developed based on different fabrication techniques, construction materials, propelling mechanisms, and geometry shape.⁵ Due to the good

catalytic activity for hydrogen peroxide (H_2O_2) decomposition, Pt has always been the most widely used materials for the MNMs fabrication. Different geometry materials, such as bilayer microtubes,^{6, 7} Janus particles,⁸ bi-segment nanorods⁹, and nano bottles,¹⁰ have been tested based on the Pt as a catalyst. It seems that other catalysts are far less inefficient than Pt for the activation of motion at a micro/nano scale. Physical vapor deposition (PVD) and electrochemical deposition method have been widely used to fabricate MNMs with diverse applications.^{6, 11-13} Apart from the deposition methods, Pt nanoparticles were also incorporated as the catalyst for MNMs by chemical reaction methods.^{14, 15}

Although the Pt/ H_2O_2 based MNMs are the most widely used propulsion systems, the Pt catalyst suffers from several severe drawbacks, such as high cost, scarcity, and deactivation, impeding its further applications.^{16, 17} Hence, the research communities for MNMs are searching for alternative catalysts and propelling mechanisms to replace Pt as the next generation MNMs.¹⁸ Manganese oxide based catalysts are good catalytic materials for H_2O_2 decomposition and various catalytic MNMs are developed using MnO_2 as the catalyst. However, until now, pure MnO_2 based catalytic propellers are not able to surpass the speed of Pt-based catalytic MNMs, due to the intrinsic lower catalytic activity for H_2O_2 decomposition. The use of MnO_2 as the catalytic part for the MNMs provides the following advantages. Firstly, the MnO_2 based materials are far less expensive than the noble metal-based catalysts, which means that it is possible to reduce the cost of MNMs for various applications. Secondly, these MnO_2 based catalysts are more robust than the Pt-based catalyst, which means that the MnO_2 based catalytic MNMs could be used in various biological as well as natural waterbody media. Thirdly, various fabrication and modification techniques could be utilized to construct the

MnO₂ based MNMs, as already been demonstrated by the energy-related researchers for MnO₂ as the electrode materials for batteries and supercapacitors.¹⁹ Fourthly, the MnO₂ based materials are good catalysts for various environmental based applications.^{20, 21}

Due to human activities over the last decades, environmental deterioration is developing at an alarming rate.²² The problems relating to reservation and utilization of clean water resources affect millions of people as large amount of different types of contaminants, such as heavy metals, persistent organic pollutants, are discharged into the natural water body without proper post-treatment.²³ These environmental pollutants originated from the improper human activities are widely existed in the industrial, agricultural, and municipal wastewaters.²⁴ Various decontamination methods are developed to protect our precious clean and freshwater resources, such as membrane filtration,²⁵ coagulation,²⁶ adsorptions,²⁷ and catalytic degradation²¹. Very recently, the development of MNMs has been tested as micro/nano cleaners to address diverse environmental issues, such as adsorption of heavy metals,²⁸ catalytic degradation of organics,¹¹ separation of oil and water,²⁹ and anti-bacterial applications.³⁰ What is more, the development of MNMs would provide an excellent motion based analytic tool and platform for the analysis, monitoring, detection, and sensing of the environmental contaminants.³¹
³² Hence, the combination of the development of MNMs with the handling of environmental issues will provide many possibilities for the environmental sustainability; this will benefit the human society. The advantages of micro/nano cleaners are the motion enhanced fast treatment and the higher efficiency compared with the static method.³³ The agitation brought by the motion of the MNMs enable the efficient mixing of the decontaminants and the pollutants without external stirring. The motion

of micro cleaner would then enable better contact and reach for adsorption removal and catalytic degradation of pollutants.³⁴

1.2 Research objectives

The main objective of this research is to develop MNMs based on the feasibilities of addressing environmental issues using cheap and reliable materials and simple methods. Considering the basic research facilities available, we focus on the fabrications of MNMs using electrochemical deposition methods. We choose the graphene oxide for potential applications as adsorbents. We choose MnO₂ based materials as the engine part and potentially use as the catalyst for the catalytic degradation of organic pollutants.

More specific research objectives are listed below:

- a. Demonstrating the use of MnO₂ to replace Pt for the construction of a graphene/MnO₂ bilayer tubular micromotor.
- b. Improving the motion performance of MnO₂ catalyzed micromotors by changing the synthetic methods.
- c. Improving the performance of MnO₂ based micromotors by introducing a metal dopant, silver is chosen to improve the motion performance and potentially with improved catalytic degradation and anti-bacterial properties.
- d. Improving the motion performance by doping the MnO₂ with iron oxide.
- e. Evaluating the motion performance of these micromotors in different surfactant solutions.

- f. Evaluating the catalytic degradation of organic dyes and adsorption of metals using the graphene/MnO₂ based materials.

1.3 Thesis organization

Chapter 1: Introduction.

This chapter introduced the current development of MNMs with an emphasis on the environmental-based applications. Some fundamental questions were also introduced in this chapter and will be answered in the following chapters. The research objectives and thesis organization are also presented.

Chapter 2: Literature review.

This chapter summarized the development of MNMs as environmental cleaners. The underlying physics, propelling mechanisms, construction materials, fabrication techniques and environmental based applications of MNMs are summarized. For the environmental applications of MNMs, we divided it into five parts including catalytic degradation of pollutants, MNMs as adsorbents for contaminants, separation of oil and water using MNMs, anti-bacterial applications of MNMs, and MNMs based detection, sensing, and analysis.

Chapter 3: Electrochemical fabrication of graphene/MnO₂ bilayer tubular micromotors. (Chem. Eng. J. 2017, 324, 251-258)

This chapter described the use of MnO₂ to replace Pt as catalytic MNMs and the motion behaviors are characterized. The MnO₂ was fabricated by anodic oxidation method.

Chapter 4: High-speed graphene/Ag-MnO₂ micromotors at low peroxide levels by cathodic electrochemical deposition. (J. Colloid and Interface Sci. 2018, 528, 271-280)

In this chapter, fabrication of the graphene/MnO₂ bilayer tubular micromotors by the cathodic electrochemical method will be introduced. The fabrication of un-doped pure MnO₂ based micromotors with improved motion performance than previously developed MnO₂ based micromotors by anodic deposition. Synthesis of the graphene/Ag-MnO₂ bilayer tubular micromotors by cathodic electrochemical co-deposition are discussed. Introducing the silver dopant to further enhance the motion performance of the MnO₂ based micromotors by cathodic deposition.

Chapter 5: Fabrication of the graphene/FeO_x-MnO₂ bilayer tubular micromotors using the cathodic electrochemical co-deposition and the related environmental applications. (Chem. Commun. 2018, 54, 4653-4656)

The introduction of iron oxide to the MnO₂ matrix by cathodic electrochemical co-deposition resulting in the high-performance MnO₂ based micromotors with extremely low fuel for propulsion.

Chapter 6: The surfactant independent propulsion of the cathodically fabricated MnO₂ based tubular microengines.

Evaluation of these MnO₂ based micromotors' motion behaviors in different surfactant conditions and solving the problems of how surfactants affect the motion behaviors for the further applications of the MnO₂ based micromotors.

Chapter 7: How the surfactants affect the mobility of silver containing micromotors.

Evaluation of these silver-containing micromotors' motion behaviors in different surfactant conditions and solving the problems of how surfactants affect the motion behaviors for the further applications of the silver-containing micromotors.

Chapter 8: Conclusions and perspectives.

Highlights the meaningful findings in this study and proposes suggestions for further research in the field.

References

1. Feynman RP. There's plenty of room at the bottom. *Engineering and science*. 1960; 23(5):22-36.
2. Ozin GA, Manners I, Fournier-Bidoz S, Arsenault A. Dream nanomachines. *Adv. Mater.* 2005; 17(24):3011-3018.
3. Cheng C, Stoddart JF. Wholly synthetic molecular machines. *Chemphyschem*. 2016; 17(12):1780-1793.
4. Ismagilov RF, Schwartz A, Bowden N, Whitesides GM. Autonomous movement and self-assembly. *Angew. Chem. Int. Ed.* 2002; 41(4):674-676.
5. Wang H, Pumera M. Fabrication of micro/nanoscale motors. *Chem. Rev.* 2015; 115(16):8704-8735.
6. Gao W, Sattayasamitsathit S, Orozco J, Wang J. Highly efficient catalytic microengines: Template electrosynthesis of polyaniline/platinum microtubes. *J. Am. Chem. Soc.* 2011; 133(31):11862-11864.

7. Martin A, Jurado-Sanchez B, Escarpa A, Wang J. Template electrosynthesis of high-performance graphene microengines. *Small*. 2015; 11(29):3568-3574.
8. Gibbs JG, Zhao YP. Autonomously motile catalytic nanomotors by bubble propulsion. *Appl. Phys. Lett.* 2009; 94(16):163104.
9. Paxton WF, Baker PT, Kline TR, et al. Catalytically induced electrokinetics for motors and micropumps. *J. Am. Chem. Soc.* 2006; 128(46):14881-14888.
10. Tu Y, Peng F, Sui X, et al. Self-propelled supramolecular nanomotors with temperature-responsive speed regulation. *Nat. Chem.* 2017; 9(5):480-486.
11. Soler L, Magdanz V, Fomin VM, Sanchez S, Schmidt OG. Self-propelled micromotors for cleaning polluted water. *ACS Nano*. 2013; 7(11):9611-9620.
12. Lee C-S, Gong J, Oh D-S, Jeon J-R, Chang Y-S. Zerovalent-iron/platinum Janus micromotors with spatially separated functionalities for efficient water decontamination. *ACS Appl. Nano Mater.* 2018; 1(2):768-776.
13. Lin Z, Wu Z, Lin X, He Q. Catalytic polymer multilayer shell motors for separation of organics. *Chem-Eur. J.* 2016; 22(5):1587-1591.
14. Wang S, Jiang Z, Ouyang S, Dai Z, Wang T. Internally/externally bubble-propelled photocatalytic tubular nanomotors for efficient water cleaning. *ACS Appl. Mater. Inter.* 2017; 9(28):23974-23982.
15. Wilson DA, Nolte RJ, van Hest JC. Autonomous movement of platinum-loaded stomatocytes. *Nat. Chem.* 2012; 4(4):268-274.
16. Wang H, Zhao GJ, Pumera M. Blood proteins strongly reduce the mobility of artificial self-propelled micromotors. *Chem-Eur. J.* 2013; 19(49):16756-16759.

17. Wang H, Zhao G, Pumera M. Blood metabolite strongly suppresses motion of electrochemically deposited catalytic self-propelled microjet engines. *Electrochem. Commun.* 2014; 38:128-130.
18. Wang H, Zhao GJ, Pumera M. Beyond platinum: Bubble-propelled micromotors based on Ag and MnO₂ catalysts. *J. Am. Chem. Soc.* 2014; 136(7):2719-2722.
19. Wei WF, Cui XW, Chen WX, Ivey DG. Manganese oxide-based materials as electrochemical supercapacitor electrodes. *Chem. Soc. Rev.* 2011; 40(3):1697-1721.
20. Wani OM, Safdar M, Kinnunen N, Janis J. Dual effect of manganese oxide micromotors: Catalytic degradation and adsorptive bubble separation of organic pollutants. *Chem-Eur. J.* 2016; 22(4):1244-1247.
21. Wang YX, Sun HQ, Ang HM, Tade MO, Wang SB. 3D-hierarchically structured MnO₂ for catalytic oxidation of phenol solutions by activation of peroxymonosulfate: Structure dependence and mechanism. *Appl. Catal. B.* 2015; 164(0):159-167.
22. Pimentel D, Rodrigues G, Wang T, et al. Renewable energy - economic and environmental-issues. *Bioscience.* 1994; 44(8):536-547.
23. Postel SL. Entering an era of water scarcity: The challenges ahead. *Ecol. Appl.* 2000; 10(4):941-948.
24. Vorosmarty CJ, Green P, Salisbury J, Lammers RB. Global water resources: Vulnerability from climate change and population growth. *Science.* 2000; 289(5477):284-288.
25. Pendergast MM, Hoek EMV. A review of water treatment membrane nanotechnologies. *Energ. Environ. Sci.* 2011; 4(6):1946-1971.
26. Sanchez NP, Skeriotis AT, Miller CM. Assessment of dissolved organic matter fluorescence PARAFAC components before and after

coagulation-filtration in a full scale water treatment plant. *Water Res.* 2013; 47(4):1679-1690.

27. Liu S, Peng W, Sun H, Wang S. Physical and chemical activation of reduced graphene oxide for enhanced adsorption and catalytic oxidation. *Nanoscale.* 2014; 6(2):766-771.

28. Vilela D, Parmar J, Zeng Y, Zhao Y, Sanchez S. Graphene-based microbots for toxic heavy metal removal and recovery from water. *Nano Lett.* 2016; 16(4):2860-2866.

29. Pan D, Mou FZ, Li XF, et al. Multifunctional magnetic oleic acid-coated MnFe_2O_4 /polystyrene Janus particles for water treatment. *J. Mater. Chem. A.* 2016; 4(30):11768-11774.

30. Mou FZ, Pan D, Chen CR, et al. Magnetically modulated pot-like MnFe_2O_4 micromotors: Nanoparticle assembly fabrication and their capability for direct oil removal. *Adv. Funct. Mater.* 2015; 25(39):6173-6181.

31. Jurado-Sanchez B, Escarpa A. Milli, micro and nanomotors: Novel analytical tools for real-world applications. *Trends Analyt. Chem.* 2016; 84:48-59.

32. Duan W, Wang W, Das S, et al. Synthetic nano- and micromachines in analytical chemistry: Sensing, migration, capture, delivery, and separation. *Annu. Rev. Anal. Chem.* 2015; 8(1):311-333.

33. Moo JG, Pumera M. Chemical energy powered nano/micro/macromotors and the environment. *Chem-Eur. J.* 2015; 21(1):58-72.

34. Gao W, Wang J. The environmental impact of micro/nanomachines: A review. *ACS Nano.* 2014; 8(4):3170-3180.

Every reasonable effort has been made to acknowledge the owners of copyright material. I would be pleased to hear from any copyright owner who has been omitted or incorrectly acknowledged.

Chapter 2. Literature Review

2.1 Introduction

The abilities to make and use tools and machines are the most fundamental and important attribute that separates the mankind from the rest of the living things on the Earth. Motors and machines are so much a part of everyday life that it is hard to imagine a world without them. The invention of peculiar motors, such as the steam engines and the internal combustion engines, played a major role in the generation of modern civilization, enabling the productivities and industrial capacities of human society to increase and expand greatly. It is fair to say that modern civilization eras are based on the motors we use. The development of the steam engines to the electric generators marked the human society's transfer from the steam age to the era of electricity. It is envisioned that the high-performance thrust adjustable aerospace engines, developed by the space exploration company in California, would open a new era for the human society as a multi-planetary species. The age of human as a multi-planetary species is coming, due to the development of a thrust adjustable "Merlin" engine by Elon Musk's team,¹ which allows the construction of the reusable rockets and boosters for low-cost space travel. While the macro motors and engines have already played a key role in the civilization progress of human history, the micro/nanomotors (MNMs) have just attracted enormous research interests for the micro/nanoscience and technology communities and are showing great potential and profound and long-lasting influences on multidisciplinary basic science at present.^{2, 3}

Man had long been dreaming of shrinking the machines down to micro/nano scale and perform tasks that would be unimaginable in the macro world.^{4, 5} In 1959, Richard Feynman in his historical speech "There

is plenty of room at the bottom” forecasted the use of micro/nano scale tools and devices to perform tasks and address issues at nanoscale.⁶ In recent decades, the development of nanoscience and nanotechnology entered a new era of motion based micro/nano scale tools and devices.⁷ In 2016, the Nobel prize of chemistry was awarded to Jean-Pierre Sauvage, Sir J. Fraser Stoddart and Bernard L. Feringa" for the design and synthesis of molecular machines".⁸ Slightly larger than the molecular machines are the artificial micro/nanomachines, which could show motion behaviors or perform works at the micro/nano scale.⁹

The development of artificial micro/nanomotors was inspired by their natural counterparts, the protein motors in the live cells or organisms.¹⁰ These man-made small-scale tools and machines would fundamentally change the nanoscience and nanofabrication, suggesting that a gate full of opportunities and challenges is open for the chemistry, materials science, biology, medical science, robotics, and the related interdisciplinary basic science.¹¹⁻¹⁵ The application of these small-scale tools and devices would generate a plethora of applied science and technology knowledge for the environmental monitoring and remediation, chemical analysis and sensing, nanoscale assembling and manipulating, biomedical imaging and drug delivery, bionic systems and nanosurgery.¹⁶⁻²⁷ Hence, since the beginning of the new millennium, there are great interests in the design, fabrication, and application of the MNMs.^{4,9}

In the micro/nanoscale, many macro-scale rules do not apply due to the dimensional scale effect.⁷ A macro object can maintain its motion with the inertia, such as the move of the Earth. As the dimension of an object decreases, it is becoming harder to maintain motion.²⁰ This means that to maintain motion at the micro/nanoscale, it is essential to apply a constant

force on the microparticles to overcome the viscous force for continuous motion. Based on the above-mentioned reasons, the design of MNMs should overcome the low inertial force and high viscous force. Thus, various propulsion strategies have been applied to design the MNMs. The motion of MNMs could be provoked by external stimuli as well as internally generated chemical gradients and fields. These external stimuli include light, acoustic, electric, and magnetic fields.² The self-generated fields propelled MNMs usually have an asymmetry structure, for example, the asymmetry in particle composition, geometry shape, or surface chemistry. Generally, the design of self-propelled MNMs has to break the symmetry of the micro/nano-particles.²⁸ In this design, one part of the micro/nanomotor serves as the engine and another part of the particle works as a functional material. Then, it is possible to fabricate the self-propelled MNMs with various demonstrated functionalities.

As the traditional chemical reaction method, such as hydrothermal reactions, cannot break the symmetry of the resulted particles, the new method should be applied to design the asymmetrical structures.²⁹ The most widely used methods to break the symmetry are the physical vapor deposition (PVD) and the electrochemical deposition methods.³⁰ More specifically, PVD methods include the e-beam evaporation, magnetron sputtering, and atom layer deposition methods. These physical vapor deposition methods have already been applied to break the symmetry of the micro/nano particles, while they require the high vacuum pumping systems.^{17, 31} The electrochemical deposition method can avoid the use of high vacuum systems, while, it usually requires the use of the templates, such as the polycarbonate membranes and the anodic aluminum oxide (AAO) membranes to direct the growth of MNMs.³² These methods could fabricate MNMs, but they usually suffer from sophisticated synthetic

procedures and low yields. Besides the synthetic materials, the use of high-cost materials, such as gold and platinum, is another drawback for the further applications. Hence, the search for low-cost materials with good motion performance is highly desirable.^{33, 34} MnO_2 could be a good alternative for the precious Pt as the catalytic part due to its polycrystallinity and feasible fabrication and modification methods.³⁵

The propulsion of MNMs is highly dependent on the surrounding environment they swim; hence, it is essential to study how different environmental conditions affect the motion behaviors of these micro/nano scale swimmers.³⁶⁻³⁸ It has been demonstrated that the Pt catalyst suffers from deactivation in various biological media and natural water body.^{39, 40} The deactivation agents are widely existing in the environment, and will eventually affect the motion behaviors and functionalities of these micro/nano scale motors. Besides the deactivation of the catalyst, the aquatic environment these MNMs swim has a lot of other variable conditions, such as pH value, the dissolved salts, and temperature also have significant effects on the motion behaviors. For catalytic bubble propelled MNMs, the choice of surfactants also affects the motion of these micro/nano swimmers, as the surfactants are quite indispensable for the motion behaviors.^{37, 41} How different surfactants condition affect the motion behaviors of the MNMs needs to be addressed before the applications of the MNMs. The knowledge generated here could facilitate the further MNMs based analysis, sensing, and detection applications. The direct observation of changing motion behaviors would provide a new venue for the analytical chemists and will have many applications in the developments of sensors, detectors for food science and biochemistry related realms.⁴²

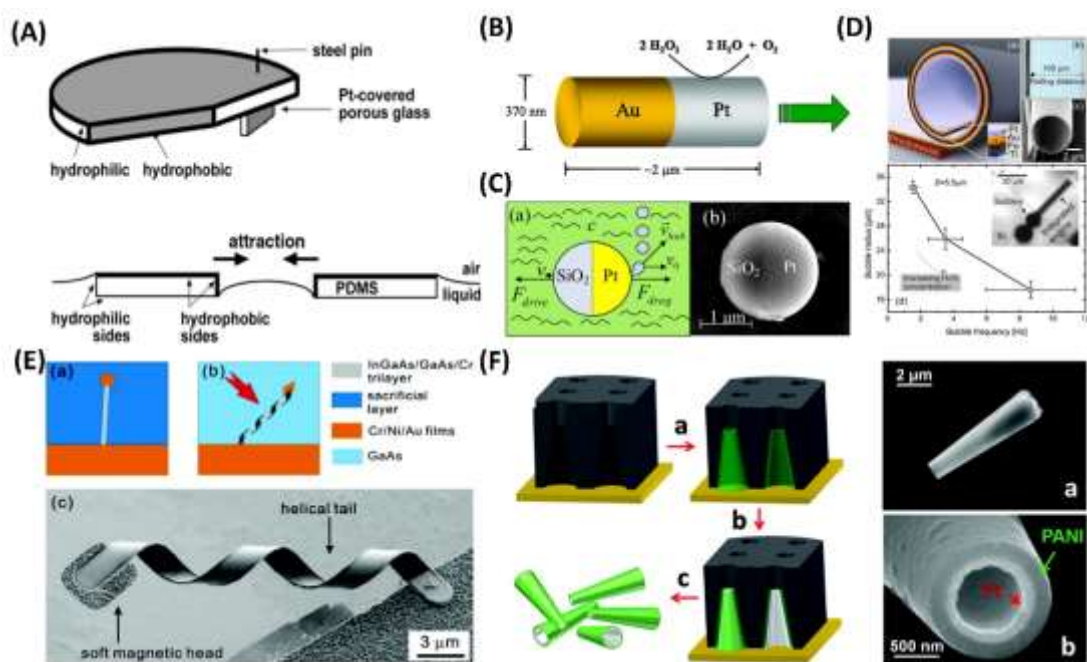


Figure 2.1. (A) Schematic illustration of a self-propelled sub-centimeter sized cylindrical plate. Reproduced with permission.⁹ Copyright 2002, Wiley-VCH. (B) Schematic of a bi-segment nanorods nanomotor. Reproduced with permission.⁴³ Copyrights 2004, American Chemical Society. (C) Schematic illustration of the Janus particle micromotors. Reprinted with the permission of AIP Publishing.⁴⁴ (D) Schematic of a rolled-up microtube consisting of Pt/Au/Fe/Ti multilayers on a photoresist sacrificial layer: top) optical and SEM images of the rolled-up microtube; bottom) bubble radius as a function of the bubble frequency with increasing H_2O_2 concentration (from 3% to 15%). The inset shows an optical image of a rolled-up microtube integrated on the Si wafer. Reproduced with permission.⁴⁵ Copyright 2009, Wiley-VCH. (E) Illustration of an artificial bacterial flagella micromotors. Reproduced with permission.⁴⁶ Copyright 2009, American Chemical Society. (F) Schematic of the template-assisted fabrication of the PANI/Pt bilayer microtubes and SEM images of the released microtubes. Reproduced with permission.³² Copyright 2011, American Chemical Society.

Figure 2.1 shows the typical examples of synthetic artificial motors systems. These pioneering works demonstrated the prototype of the micro/nano machines and pave the way for the further application of MNMs. MNMs have demonstrated tremendous proof-of-concept applications in the biomedical and environmental science fields. The

motion of MNMs would have a great impact on the wide technological applications relating to biomedicine, nanofabrication, catalyst, environment, and bioassay. Currently, the most widely studied application areas for MNMs are the biomedical and the environmental fields. In this thesis, we mainly focus on the use of MNMs for environmental based applications. So, we will summarize the results of the environmental-based applications using MNMs. Generally, the environmental-based applications could be divided into five categories, adsorption, catalytic degradation, oil-water separation, the killing of the pathogenic bacteria, and the motion based analysis, monitoring, sensing, and detections. Using the MNMs as an innovative tool to handle environmental issues offers the following advantages: The motion-based catalytic degradation and adsorption are much faster and more efficient than the static methods. This is especially favorable for field applications, where the external agitation is not possible or unwanted. The functional MNMs based water treatment processes offer a direct and explicit optical observation for the potential environmental applications in detection, analysis, sensing and monitoring of pollutants. These tiny environmental cleaners are also potent analyzing tools for the handling of environmental issues.

Although researchers have already demonstrated a lot of environmental based applications and many proof-of-concept biomedical applications, the development of MNMs is still at its infancy. The limit for the applications of MNMs is only the human imaginations as various progress related to speed and motion could be regulated by MNMs. While showing such fascinating advantages as the micro/nano scale tools, there are still a lot of challenges facing the MNMs research community. The use of high-cost materials, the sophisticated synthetic equipment and procedures, and the low output of the MNMs are the most challenging hurdles for their

widespread applications. The use of untreated raw materials also demonstrates motion behaviors and has already been used in many environmental applications, but the motion performance is quite low due to the lower degree of asymmetry. For specific applications, special MNMs could be developed. While there are still very limited in vivo applications demonstrated, the use of MNMs in biological tissues is still quite impossible, as the most of these self-propelled MNMs require the highly toxic fuels and the surfactants. Therefore, it is very favorable to design MNMs based on the biocompatible fuels and biological enzyme-catalyzed reactions. These MNMs would be more favorable for the biological based applications, while the chemically powered catalytic MNMs are more favorable for the environmental-based applications.

2.2 The underlying physics for MNMs propulsion

We live in the macroscopic world, so the motion behaviors of the micro/nano objects are quite different from the experience we get in the real macroscopic world. It is very essential to study the underlying physical rules of how these MNMs swim in the fluid. At small scale, the inertial force no longer plays a crucial part in motion, as the inertial declines much faster with the decrease in body length. When the dimension of MNMs decreases to smaller than 1 μm , another factor takes into effect, i.e. Brownian motion. The collision with fluid molecules becomes increasingly significant as the sizes of particles decreases, which makes the active directional movement quite difficult. Based on the fundamental physical rules for motion at small scale, various motion mechanisms were proposed to guide the design and fabrication of MNMs. The self-propelled MNMs could be activated by bubble propulsion and the self-generated fields or chemical gradients.

Table 2.1. Typical examples of synthetic self-propelled MNMs

Developer	Shape & Size	Catalyst or reactive material	Fuel	Propelling mechanisms	Comment
Whitesides et al. ⁹	half cylindrical plate Less than 1 cm.	Pt	H ₂ O ₂	Bubble Propulsion	Generally recognized as the first synthetic motors
Mallouk et al. ^{43,47}	Pt-Au nanorod	Pt	H ₂ O ₂	Self-electrophoresis	Demonstration of nanomotors
Gibbs et al. ⁴⁴	SiO ₂ -Pt Janus particle nanomotors	Pt	H ₂ O ₂	Bubble Propulsion	Janus nanomotors
Mei et al. ⁴⁵	Rolled-up microtubes 100 μm	Pt	H ₂ O ₂	Bubble Propulsion	First tubular micromotors
Wang et al. ³²	PANI/Pt bilayer microtubes	Pt	H ₂ O ₂	Bubble Propulsion	Electrochemically synthesized microtubes
Pumera et al. ⁴⁸	mm scale polymer capsule	solvent	H ₂ O	Surface tension	Fuel loaded motors
Pumera et al. ⁴⁹	Iridium (Ir) doped graphene micromotors	Ir	H ₂ O ₂	Bubble Propulsion	Irregular shape bubble propulsion
Wang et al. ⁵⁰	Ir-SiO ₂ Janus particle micromotors	Ir	N ₂ H ₄	Self-diffusiophoresis or osmotic effect	Extremely low N ₂ H ₄ fuel levels
Wilson et al. ⁵¹	Pt-loaded stomatocytes nanomotors	Pt	H ₂ O ₂	Bubble Propulsion	Bowl-shaped polymer by chemical reaction synthesis
Gao et al. ⁵²	Ti/Al-Ga	Al	H ₂ O	Bubble propulsion	Water powered
Pumera et al. ⁵³	Micromotors by raw materials	Ag or MnO ₂	H ₂ O ₂	Bubble Propulsion	Demonstration of raw materials for MNMs
Ye et al. ³³	Graphene/FeO _x -MnO ₂ microtubes	Iron oxide modified MnO ₂	H ₂ O ₂	Bubble Propulsion	Outperform the best Pt-based microengines by MnO ₂ based materials

2.2.1 The Reynolds number

At the macroscale, objects can maintain their motions with inertial, such as the movement of the celestial body. However, as the particle size decreases, inertial, which scales with volume, becomes negligible compared to viscous forces that scale with L , where L is the characteristic length of the object. The Reynolds number (Re) is a dimensionless number that represents the ratio of these two forces:

$$Re = \frac{\text{Inertial}}{\text{Viscous force}} = \frac{\rho v^2}{\mu v/L} = \frac{\rho v L}{\mu} \quad \text{Eq. (2.1)}$$

where ρ is the density, v is the particle velocity and μ is the dynamic viscosity of the medium.⁷ A person in the swimming pool has a Reynolds number of roughly 10^4 , whereas the bacterial in the swimming pool has a Reynolds number of 10^{-4} . Most of the MNMs will have a Reynolds number close to the value of the bacteria. At low Reynolds number, the inertial force does not contribute a lot to the motion, which means that the motion could only be maintained by a constant force.⁵⁴

2.2.2 The effect of thermal fluctuation induced Brownian motion

The moving of nanoscale particles is strongly influenced by the thermal fluctuation, leading to the well-known Brownian motion. As their sizes decrease, the collisions of fluid molecules with the MNMs become increasingly significant. Brownian motion induced by these small molecules strongly affect the directionality of these MNMs. Resulting in the random motion patterns for the MNMs. Thus, long distance, translational migration is quite difficult because the average distance with this random motion is proportional to the square root of time. The same regime applies as the passive diffusion process.⁵⁴ A stationary asymmetry

induced by chemically anisotropic motors generates a constant driving force, while a transient force only generates random fluctuation. The fabrication of directional moving MNMs is desired for many applications, such as the active cargo transportation and drug delivery, where the MNMs could show fast directional motion and the distances are proportional to the time. Hence, it is preferable for the design of MNMs to break the symmetry to overcome the random Brownian fluctuation for enhanced directional active motion.

2.3 The propelling and motion mechanisms of MNMs

While external fields and the chemical or thermal gradients could be applied to manipulate and regulate the motion behaviors of MNMs, the propulsion of self-propelled MNMs is mainly dependent on the self-generated fields, chemical or thermal gradient, and the expelled microbubbles. The external electric, magnetic, or acoustic field could be applied to generate an asymmetrical charge distribution, torque, or imbalance of forces upon the MNMs' conducting surface, magnetic metal part, or the long axis, which is an effective method to regulate the speed and the directionality of MNMs. The fuel-free external field driven MNMs usually require the complex, high-cost, external energy source facilities, such as the light source for light propulsion, and the magnetic coils for the generating of magnetic fields for speed and direction control. The fuel driven, self-propelled MNMs offer the advantage of ease of applications and lots of choices and reactions available for propulsion. These reactions include the bio-enzyme based catalytic reactions, the reactions of water or acid with reactive metals, and the catalytic decomposition of H_2O_2 , but not limited to these reactions.

2.3.1 Self-electrophoresis propelled MNMs

Electrophoresis is the motion of a dispersed particle in a fluid under the influence of an applied spatially uniform electric field. At low Reynold numbers, the resistance for a moving particle is only the fluid viscous force. Hence, in the case of low Reynold number and moderate electric field E , the drifting velocity of a charged particle v is simply proportional to the applied field, which leaves the electrophoretic mobility μ_e defined as:

$$\mu_e = \frac{v}{E} \quad \text{Eq. (2.2)}$$

The above equation is the basic physics rule guiding the design and application of the electric field driven MNMs. The more well-known theory about electrophoresis is developed by Smoluchowski in 1903:

$$\mu_e = \frac{\varepsilon_r \varepsilon_0 \zeta}{\eta} \quad \text{Eq. (2.3)}$$

where the ε_r is the dielectric constant of the dispersion media, ε_0 is the permittivity of free space, η is the dynamic viscosity of the dispersion fluid and ζ is the zeta potential of the particle surface, which relate to the surface charge.⁷ Based on the above theory, it is possible to design a micro/nano system exploiting the asymmetry electrochemical reactions to generate an asymmetrically distributed electric field around the particles and to drive the motion of the particles. This is the theory for self-electrophoresis, where charged particles move in a self-generated electric field due to the asymmetry electrochemical reactions around the particles. The first self-electrophoresis nanomotors were developed by Thomas E. Mallouk's group at Pennsylvania State University, where gold-platinum bi-segment nanorods were observed to demonstrate directional motion behaviors towards the Pt end with a speed of around 10 $\mu\text{m/s}$.⁴⁷ These bi-segment

nanorods were fabricated by the template-assisted multi-step electrochemical deposition method using the anodized alumina (AAO) membrane as the template. Upon the first demonstration, various multi-segment nanorods nanomotors with different composition and electrochemical reactions were developed such as the Au/Ni,⁵⁵ Cu/Pt,⁵⁶ Pt/Ag-Au alloy nanomotors,⁵⁷ and Au/Pt-CNT⁵⁸ nanorods. The slightly larger speed of the nanomotors could be obtained by designing a larger mixed potential difference between the two electrodes.^{57, 59} These self-electrophoreses show various applications, such as pumping,⁶⁰ rotation,⁵⁵ sense,⁶¹ and cargo transportation,⁶² but they suffer from the following drawbacks. These self-propelled nano swimmers usually rely on toxic fuels, such as H₂O₂ and hydrazine for propulsion. Br₂ and I₂ were also demonstrated as the fuels for nanomotors, but they are also not biocompatible. Another drawback for these nanomotors is the limitation from the high ionic strength, which means that its motion in biological media is nearly impossible. Moreover, these nano swimmers have an extremely low power output, indicating that their further applications as nanocarriers are quite impossible.

Figure 2.2 demonstrated the four types of propelling mechanisms of the self-propelled MNMs. Bubble propulsion, self-diffusiophoresis, self-electrophoresis, and propulsion by surface tension are the most commonly used methods to design the self-propelled MNMs. MNMs could also be propelled by external stimuli such as electric, magnetic, and acoustical field and light. These methods are more capable as a method for the motion control of MNMs.

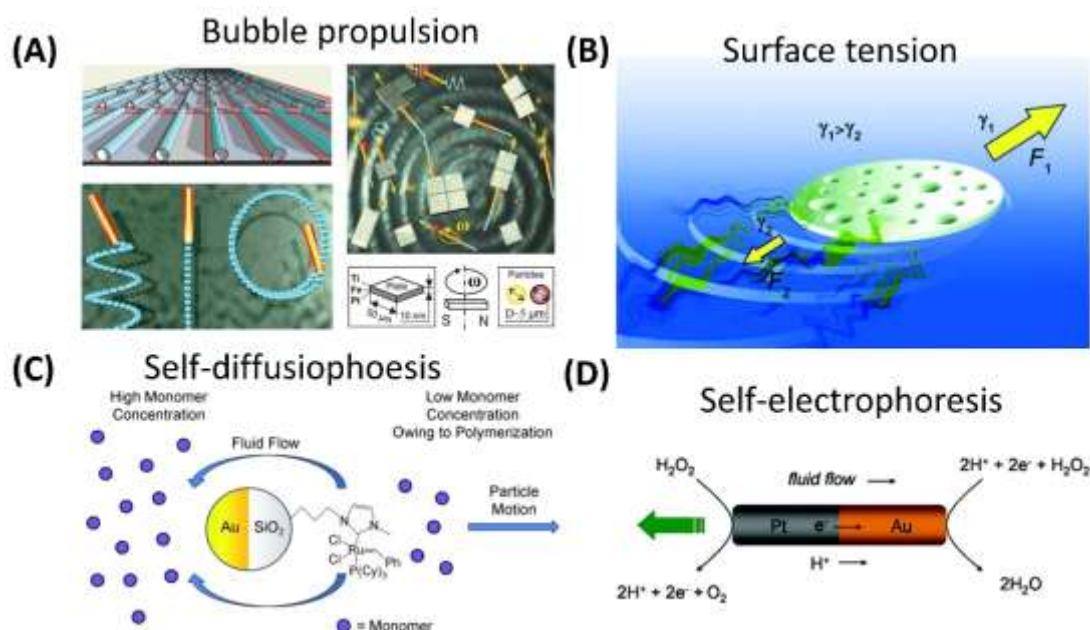


Figure 2.2. (A) Schematic illustration of a bubble propelled tubular micromotors. Reproduced with permission.⁶³ Copyright 2010, Wiley-VCH. (B) Schematic of a micromotor propelled by surface tension. Reproduced with permission.⁴⁸ Copyrights 2011, Wiley-VCH. (C) Schematic illustration of the Janus particle micromotors. Reproduced with permission.⁶⁴ Copyrights 2011, Wiley-VCH. (D) Schematic of a Pt-Au bi-segment nanorod nanomotors powered by self-electrophoresis. Reproduced with permission.⁴⁷ Copyright 2006, American Chemical Society.

2.3.2 Self-diffusiophoresis propelled MNMs

Diffusiophoresis is a physical chemistry phenomenon in which the motion of particles is driven by a concentration gradient of solutes.⁶⁵ According to the charging properties of the solute molecules, the diffusiophoresis can be classified into two categories, the electrolyte and nonelectrolyte diffusiophoresis.⁷ The self-diffusiophoresis can be termed and classified as the non-ionic self-diffusiophoresis and the ionic self-diffusiophoresis. Self-diffusiophoresis means that the propulsion mechanism is due to the solute concentration gradient generated by the motor's surface chemical reactions. Usually, the asymmetrically distributed catalytic or reactive materials on the motors will trigger the formation of the asymmetrically

distributed solutes, and thus the formation of the small molecule chemical gradient for the propulsion. It is generally acknowledged that the asymmetry in particle shape and geometry will also result in the formation of the unbalanced local chemical gradient, which will apply a constant force on the particles. The self-diffusiophoresis propulsion can lead to the motion of a particle moving at 1-10 $\mu\text{m/s}$. Under certain external stimuli, the self-diffusiophoresis shows reversible collective behaviors, which may provoke other novel applications such as the mimic of biological systems.⁶⁶ Usually, the ionic self-diffusiophoresis can lead to slightly higher speed than the non-ionic self-diffusiophoresis, while the non-ionic self-diffusiophoresis is more tolerant to the higher ionic strength.

2.3.3 Bubble propulsion of MNMs

By far, bubble propulsion is the most powerful and effective motion strategy for the self-propelled catalytic MNMs.^{45, 67} Both Janus particles and the tubular microengines demonstrate fast and efficient propulsion with the catalytic generated bubbles. Both catalytic and the reactive chemical reactions have been employed to design the bubble propelled MNMs. The most commonly used propulsion catalytic reactions are the decomposition of H_2O_2 with the Pt as the catalyst.⁴⁵ The propulsion of MNMs using the reactive metals with water and acid to generate the hydrogen bubbles is also a very promising strategy, while it usually demonstrates a very short lifetime.^{52, 68} The gaseous products undergo nucleation, bubble formation, and growth, and subsequently detachment expelling the fluid away from the MNMs will generate the transient force needed to overcome the viscous for propulsion. The continuous generation and flow of microbubbles will apply a constant force for the self-propulsion. The bubble propulsion strategy has been the most widely used propulsion mechanism for the MNMs with various demonstrated

applications, such as water purification, killing of bacterial and drug delivery.⁶⁹

2.3.4 Propulsion of MNMs by surface tension

The generation of an unbalanced surface tension at the different sides of MNMs will result in a constant net force for the self-propulsion of MNMs. This is the mechanism of the surface tension propulsion. The Sen's group first demonstrated the propulsion of surface tension gradient by the depolymerization of a polymer.⁷⁰ This motion strategy demonstrates very robust motion behaviors in various media and the high ionic strength solutions. Pumera's group demonstrated the use of self-exfoliation of the naphthalene distributed MoS₂ particles as motors.⁷¹ The propulsion is based on the generation of the imbalanced surface tension with the self-exfoliation process. Wang et al designed a self-propelled motor by the simultaneous release of sodium dodecyl sulfate (SDS) surfactant for propulsion.⁷² The propulsion is based on the surfactant-induced imbalance of the surface tension distribution.

2.3.5 Motion control of micro/nanomotors by external stimuli

The use of external stimuli to control the motion of MNMs has been demonstrated with various fascinating motion maneuvers. The external stimuli such as light, electric, acoustic, magnetic field have been widely applied to control the speed and directionality of motion. As this thesis focuses on the fabrication of self-propelled MNMs, the in-depth review of the motion control by external stimuli is not provided. Briefly speaking, ferromagnetic materials such as iron, cobalt, and nickel could be incorporated into the MNMs as the magnetic layer, thus allows for the magnetic control. These microengines will align according to the direction of the magnetic field. Both UV light and visible light have been applied to

activate the motion of MNMs.⁷³ Upon the light irradiation, the asymmetry photo induced electrochemical reactions occur at the different sides of the micro/nanomotors, which will result in the asymmetry distribution of the photo-induced reaction products, thus the diffusiophoresis will occur and a propelling force is generated for motion. Near-infrared light (NIR) could also be a promising strategy for biomedical relation MNMs applications due to the generation of a thermal gradient upon irradiation. MNMs could also be propelled by the acoustic field, especially the ultrasound, which is a high-frequency sound wave above the threshold value of normal human hearing. Nanorods with concave or convex ends could be used to concentrate or dissipate the acoustic wave energy, therefore the formed asymmetric structure of the nanorods led to uneven distribution of acoustic pressure, which serves as the propelling force of the nanorods.^{74,}

75

2.4 The fabrication of MNMs

Due to the high viscous resistance compared with the inertial force at the micro/nano scale movement and the thermal fluctuation induced by Brownian motion for the impedance of the directionality of these micro/nano scale swimmers, it is necessary to break the symmetry for the construction of the self-propelled MNMs. The breaking of symmetry is the need for the generation of the net propelling force for continuous motion.⁷⁶ From materials selection to the fabrication techniques, we can use various methods to generate the asymmetrical chemical reactions at different sides of the MNMs for the directional motion.⁷⁷

2.4.1 Materials selection for MNMs

Different types of materials have been used to fabricate the self-propelled MNMs based on different geometry design and propelling mechanisms.

There is always new kind of materials as promising MNMs with good functionalities. Generally, commonly used materials for the engine parts of the self-propelled MNMs could be divided into the following categories: the pure metals, the metal oxides, and the enzymes.

By now, the most widely used catalyst for self-propelled catalytic MNMs is Pt, because of the high catalytic activities for the H_2O_2 decomposition.⁷⁸ Pt-based MNMs could be fabricated with different geometries, such as Janus particles, and tubular microengines, have been demonstrated with various applications. Other metals could be also used for the MNMs purposes, such as the iridium (Ir) and gold have been as the engine parts. Ir could be used as the catalyst for the decomposition of hydrazine (N_2H_4) for the design of the bubble propelled or the diffusiophoresis based MNMs.⁵⁰ Gold is also a widely used material for the self-electrophoresis propelled and the thermophoresis propelled MNMs. These precious rare metals based MNMs suffer from the high-cost, scarcity, and possibility of deactivation in various media impeded their further applications. Silver is also a good catalyst for H_2O_2 decomposition and various silver-based MNMs have been designed and tested for the anti-bacterial based applications.⁷⁹ Silver-containing compounds, such as the silver chloride, have been demonstrated with self-diffusiophoresis motion under light irradiation. Nano zero valence iron particles have been demonstrated to show motion behaviors in acid conditions with good environmental based applications.⁸⁰ Zinc and magnesium have been used to design water powered MNMs. Aluminum has been used to design the MNMs in alkaline environmental conditions.^{81, 82}

Metal oxides, such as the manganese dioxide, are also good catalytic materials for H_2O_2 decomposition, emerging as the low-cost alternative

for the precious metal based MNMs. While various applications have been demonstrated, the MnO_2 based MNMs cannot compete with the precious metal Pt-based MNMs, due to the intrinsic low catalytic activities. Various other metal oxide materials, such as the titanium dioxide have been used to design the light steered MNMs. A mixed metal oxide such as the MnFe_2O_4 has been employed to design the magnetic steered MNMs with good environmental applications.

The enzyme catalyzed MNMs have been designed and tested with moderate motion performances.⁸³ Various bio-catalytic reactions could be utilized to design the enzyme-based MNMs.⁸⁴ Enzyme-based MNMs are very favorable for the biomedical reactions because of the mild environmental conditions and the avoidance of the highly toxic fuels. While enzyme based MNMs are very favorable for the biomedical related applications, they are not as suitable as the manganese oxide-based MNMs for the environmental-based applications, as the enzymes will suffer from the deactivation in harsh environmental conditions, such as high salt and high temperatures.

2.4.2 Fabrication techniques for MNMs

The fabrication techniques are chosen to serve the purpose of generating the net propulsion force needed. Generally, due to the need of breaking the symmetry in the structural design, multi-step fabrication processes are needed. Traditional chemical reactions, such as hydrothermal reactions, cannot break the symmetry of the resulted particles, hence, novel fabrication strategies should be adopted for the efficient propulsion. For self-propelled MNMs, the incorporation of the catalytic or reactive materials should be asymmetrically distributed. In this regard, physical vapor deposition, and electrochemical deposition methods are widely used

in the fabrications of MNMs with different geometry, such as the Janus particles, multi-segment micro/nano rods, and multi-layer tubular microengines.

PVD method vaporizes the condensed materials and then deposition as a form of thin films. The most widely used thin film deposition methods are sputtering and evaporations. Sputtering relies on the bombardment of a target source material with an ionized inert gas such as argon (Ar). The kinetic energy is transferred from the ionized gas atoms to the target materials which then undergo vaporization and deposition as a thin layer of film. Evaporation is also a widely used deposition, which can use the energy of electricity or an electron beam to vaporize target materials. Various catalytic materials, such as Pt and Ir could be deposited as a thin layer of catalyst to generate the propulsion force needed. Non-reactive materials such as titanium (Ti) could also be deposited to block the reaction on one side of the Janus particles for the breaking of the symmetry.⁵² The deposition of a layer of magnetic materials such as iron could provide the MNMs with magnetic properties for magnetic guidance and recovery, which is very crucial for the design of the intelligent micro/nano scale robotic systems.

Electrochemical deposition method is also widely used to deposit various MNMs, such as the tubular microengines and the bi-segment nanorods. Pt could also be electrochemically deposited as the engine part for MNMs using the commercially available Pt plating solutions. Template-assisted electrochemical deposition method could be adopted to control the outside dimension of the MNMs. The commonly used template could be the track etched polycarbonate (PC) membrane and the AAO membrane. The PC membranes with pore diameters of several micrometers are very suitable

for the fabrication of multi-layer tubular microengines. By now, the most highly efficient and powerful micro/nano scale motion strategy is based on this design. The use of porous AAO membrane with a diameter ranging from 20 to 400 nm is very suitable for the fabrication of rod shape nanomotors.

MNMs could also be fabricated by the traditional chemical reaction methods. Such as the layer by layer assembly of functional materials, chemical synthesis of the manganese oxide microparticles and the encapsulation of micro/nano particles. The assembly of micro/nano particles is very useful for nanofabrication, thus it is very likely to be used for MNMs fabrication.

2.5 MNMs responding to the environments

MNMs could also be used as the motion-based analysis platform for the sensing, detection, and monitoring of environmental situations. Self-propelled MNMs rely on the environmental factors to propel, and the locally available fuels are indispensable for the self-propelling motion behaviors. Higher speed could be obtained by the bubble propulsion strategy with the assistance of a tiny amount of surfactants. Environmental conditions, such as light, temperature, pH values, and other solutes will affect the motion behaviors of MNMs.⁸⁵ Hence, the direct observation of the motion behaviors of MNMs could provide a route to sense the environmental solutes. The study on the MNMs responding to the environment could generate a plethora of applied knowledge for the water quality testing, food analysis, chemical sensing, and electrochemical analysis. It is very important to study how these micro/nano scale swimmers respond to the environments, as the environmental conditions are very complicated. There are heavy metals, and various persistent

organic pollutants, such as dyes, phenolic compounds, pesticides, pathogenic organisms in the industrial and agricultural wastewater, due to the improper human activities. Thus, it is essential to study how these environmental conditions influence the motion behaviors of MNMs. Biological media also contains very complicated biological entities, such as electrolytes, blood cells, and various proteins and carbohydrates. Further biomedical applications of MNMs demand the understanding of how these biological objects affect the micro/nano scale propulsion.

2.5.1 The pH-responsive applications of MNMs

In industrial wastewater and biological media, the pH values are varying to a very large range. Studying how these environmental conditions influence the motion behaviors of MNMs will pave the way for the future applications in biomedicine and environmental cleaning. Some of the MNMs show motion behaviors in the strong acid environment, while others could be activated in the strong basic environment. So, it is very essential to investigate the motion behaviors of MNMs in acid or base conditions. Base on the reactive metals, such as Mg, Zn, and iron with water or acid for generating of hydrogen bubbles for propulsion, a lot of MNMs have been designed and tested. These MNMs based on the reactive reactions other than catalytic reactions usually have a very short lifetime. Chattopadhyay et al.⁸⁶ demonstrated a pH taxis behavior of an intelligent microbot. The smart micro swimmer could move at a speed of 20 body length per second towards a targeted location based on the pH taxis mechanism. Pumera's group studied the influence of pH on the motion behaviors of catalytic Janus particles and tubular microjets.³⁶ They found that higher pH values above neutral condition lead to faster decomposition of H₂O₂, resulting in a greater activity and higher velocity. Structural changes would inevitably occur as the acidity environment and would then

result in the corrosion of the metal-based MNMs. Hence, the motion behaviors would change and reflect the environmental acidity. Dong et al.⁸⁷ designed a cartridge-case-like micromotor using Pt nanoparticles as the inside catalyst and the gelatin materials as the shell. Due to the pH-dependent “open” and “close” feature of the pH-responsive gelatin material. The micromotor can be utilized as a motion based pH sensor over the whole pH range. Li and Wang et al. designed an acid-driven micromotor for pH-responsive payload release in a mouse’s stomach.⁸⁸

2.5.2 How surfactants affect the motion behaviors of MNMs

Surfactants are quite indispensable for bubble propelled MNMs system. Surfactants would lower the surface tension of the fluid and facilitate the bubble propulsion process.⁴¹ The formation of bubbles is quite dependent on the surfactant conditions. Without a surfactant, it is very difficult to form stable microbubbles. So, there are always a minimal surfactant range requirement for the catalytic bubble propelled MNMs. Under very high surfactant levels, the bubble propelled MNMs system would decrease the speed due to the high viscous force. What’s more, under certain surfactant conditions, Pt-based MNMs would lose the mobility.³⁷ Pumera’s group studied the effect of different types of surfactants on the motion behaviors of a Pt-based tubular micromotor.³⁷ They found that Pt-based micromotors are more active and faster in anodic surfactant SDS than non-ionic surfactant tween 20. What’s more, these microjets lost the mobility totally in a cationic surfactant cetrimonium bromide. Surfactants can also be used as the fuel for propulsion based on the imbalanced distribution of surface tension at different sides of the motors.⁸⁹

2.5.3 How other environmental conditions influence the motion of MNMs

The self-propelled MNMs rely on the catalytic or reactive chemical reactions for propulsion. If the catalysts are deactivated by certain chemicals, the MNMs would lose their mobility. Under some special conditions, the environmental solutes would promote the underlying reaction mechanisms for propulsion, and the MNMs show drastically a speed increase. The environmental conditions matter for the self-propelled MNMs. Pumera's group found that the Pt-based tubular micromotors were poisoned by the sulfur-containing molecules⁹⁰ and some blood proteins.³⁹ They also demonstrated that blood electrolytes strongly influence the mobility of microjets. Usually, these electrolytes will have an adverse effect on the propulsion of the Pt-based microengines, especially at slightly higher concentrations.⁹¹ Wang et al. studied the effect of the real-life environments on the motion of the polymer/Pt tubular microengines.³⁸ It was found that the polymer/Pt tubular micromotors are very robust in various real waters, such as sea water, river water, lake water, tap water, apple juice, and human serum, etc. Although the speed decreased as the volume of the real-life environment increased to 90%, in such a high content of real-life fluid condition, the propulsion is still very prominent. This finding is very important for the real practical application of the Pt-based MNMs for biomedicine and environmental remediation, as a lot of other studies showed that the speed dramatically decreases in certain environmental conditions.

2.6 MNMs based environmental applications

Self-propelled MNMs show diverse environmental applications, such as catalytic degradation of organic pollutant, adsorption of metals, the killing

of bacteria, oil-water separation. By converting the locally available chemical energy into mechanical movement, self-propelled MNMs would provide the environmental experts with more degrees of freedom in pollutant disposal onsite and offsite. The mechanical agitation brought by the self-propelled synthetic motor systems enables efficient mixing of the solution. The ejection and rising of microbubbles can serve as an additional mixing agent. As most of the catalytic degradation and adsorption removal processes are diffusion limited, the additional mechanical agitation would accelerate the catalytic and adsorption reaction for a better degradation and removal progress. MNMs are an excellent platform for chemical processes. But, the development of MNMs cannot be limited to these areas, as other types of applications could also be demonstrated. For example, the micromotors developed at Wang's group have been applied for the biomimetic carbon dioxide sequestration.⁹² The developed mobile CO₂ scrubbing platform leads to the dramatic increase in the CO₂ sequestration efficiency while greatly decreasing the reaction time because of the self-mixing and convection brought by the self-motile behaviors. The same group also demonstrated the use of self-propelled nanomotors to seek and repair cracks autonomously.⁹³ Besides these novel applications, MNMs can be integrated with the lab-on-chip devices for various purposes.⁹⁴

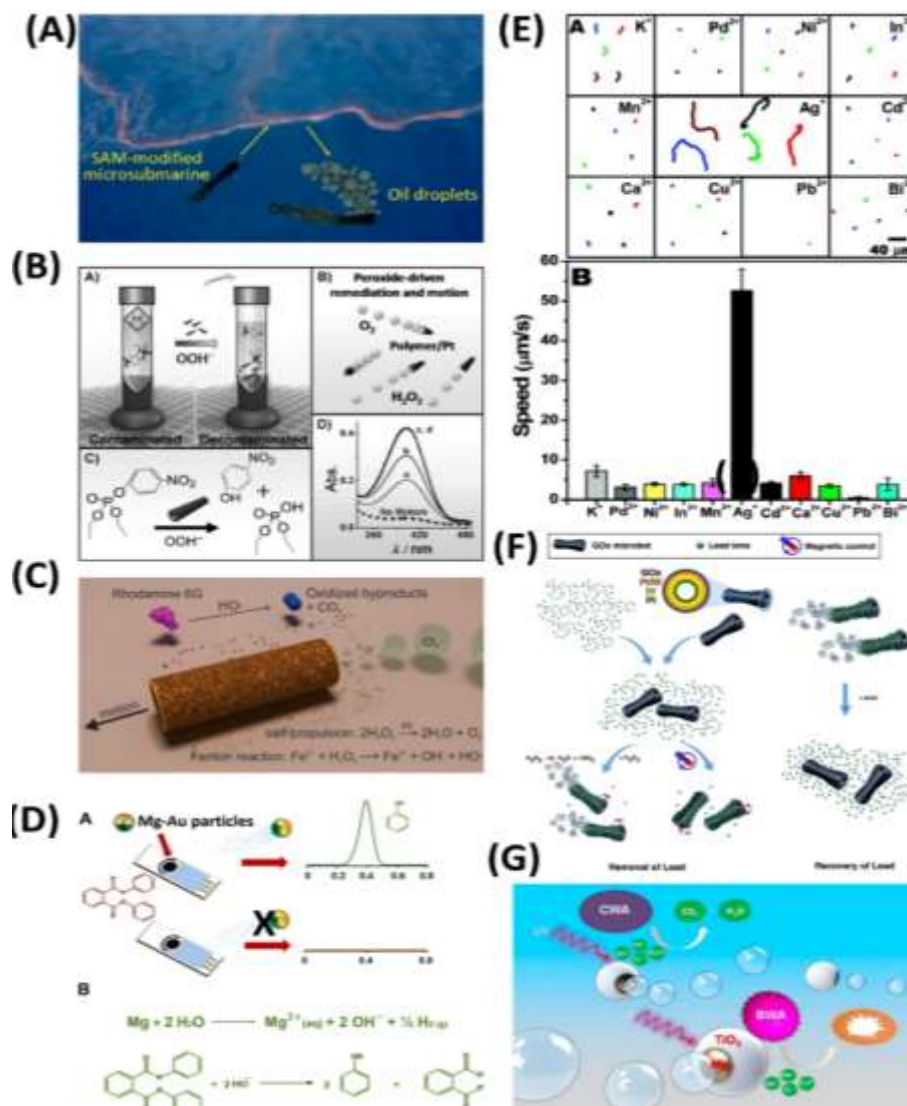


Figure 2.3. (A) Micromotors for transportation of oil drops. Adapted with permission.⁹⁵ Copyright 2012, American Chemical Society. (B) Micromotors based detoxification of chemical threats. Adapted with permission.⁹⁶ Copyright 2013, Wiley-VCH. (C) Catalytic degradation of organic pollutants by micromotors. Adapted under the terms of the ACS AuthorChoice License.⁹⁷ Copyright 2013, American Chemical Society. (D) Micromotors for degradation and detection of organics. Reproduced with permission.⁹⁸ Copyright 2016, American Chemical Society. (E) Nanomotor for selective detection of silver ions. Reproduced with permission.⁶¹ Copyright 2009, American Chemical Society. (F) Graphene-based micromotors for lead decontamination and collection. Adapted under the term of the Creative Commons Attribution (CC-BY) License.⁹⁹ Copyright 2016, the authors, published by American Chemical Society. (G) Photo-degradation of chemical and biological warfare agent. Reproduced with permission.¹⁰⁰ Copyright 2014, American Chemical Society.

2.6.1 Self-propelled MNMs for catalytic degradation of pollutants

MNMs self-propelled by the locally available fuel are a very promising strategy for catalytic degradation of organic pollutant. Here, the most widely used H_2O_2 fuel for propulsion could also serve as the oxidizing agent for generating reactive hydroxyl species to degrade the pollutants. Wang et al. demonstrated the use of polymer/Pt tubular micromotor for fast and efficient degradation of organophosphate (OP) nerve agent at low peroxide levels without external stirring.⁹⁶ Based on the Fenton reaction using the iron as the catalyst and the Pt metal for catalytic generating of oxygen bubbles for propulsion, reusable rolled-up Fe/Pt microtubes were developed by Schmidt's group for catalytic degradation organic contaminants.^{97, 101} The same group also demonstrated the use of a self-propelled Ti/Fe/Cr/Pd rolled-up microjet for the catalytic conversion of a 4-nitrophenol pollutant under the presence of sodium borohydride (NaBH_4) as a reductant. The improved intermixing of the micromotors made the degradation rate 10 times higher to its nonmotile counterpart.¹⁰² The use of water-powered photocatalytic degradation is very promising for a wide range of environmental and defense applications. Wang et al.¹⁰⁰ designed the water driven propulsion of $\text{TiO}_2/\text{Au}/\text{Mg}$ micromotors for the photocatalytic degradation of the chemical and biological warfare agents. Mushtaq et al. designed the highly efficient reusable coaxial $\text{TiO}_2\text{-PtPd}$ tubular nanomachines for photocatalytic decontamination of organic dyes with a diverse propulsion strategy.¹⁰³ Inorganic microparticles such as the MnO_2 have been applied for the MNM propulsion as well as the catalyst for catalytic degradation of aquatic contaminants.^{104, 105} Iron containing oxides such as the MnFe_2O_4 and the zero valence iron-based materials have been incorporated as the MNMs for the catalytic degradation of organic pollutants, with an added advantage of the magnetic recovery.^{80.}

^{106, 107} Parmar et al. designed the cobalt ferrite based micromotors for catalytic oxidation degradation of the tetracycline antibiotic.¹⁰⁸ Wang et al. designed the multifunctional silver-exchanged zeolite micromotors for catalytic detoxification of chemical and biological environmental threats.¹⁰⁹ Mushtaq et al.¹¹⁰ designed a magnetically driven hybrid for wide spectrum photocatalytic degradation of dyes. The as-prepared structure contains a ferromagnetic CoNi segment and a bismuth-based photocatalytic segment and is of good catalytic performance and reusability. Zhang et al. designed the light-driven Au-WO₃@C Janus particle micromotors for rapid photodegradation of dye pollutants.¹¹¹ Li et al.¹¹² designed a bubble propelled Janus particles micromotor, using Fe₃O₄ nanoparticles loaded onto mesoporous SiO₂ as the matrix and the silver nanoparticles as the catalyst for propulsion. The micromotors demonstrated a good motion performance and water remediation capability. Tang et al.¹¹³ designed a 3D Prussian blue-reduced graphene oxide hydrogel as the self-propelling motors for the catalytic degradation of aquatic dyes.

2.6.2 MNMs for adsorption removal of aquatic contaminants

The wastewater usually contains cationic and anionic ions, organics and oil, which have a poisonous and toxic effect on the ecosystem. Adsorption is a widely-used, effective, low-cost, and simple method for the decontamination of aquatic pollutants.¹¹⁴ Traditional adsorption purification relies on the diffusion process and physiochemical property of the adsorbent, which is usually a time-consuming process.^{115, 116} Recently, the development of nanoscience and nanotechnology-enabled researchers to design the motion-based micro/nano cleaners for accelerated adsorption decontamination of wastewater.¹¹⁷ The newly developed motion based purification techniques utilize the self-propelling

behaviors of the adsorbents and would break the limitation of the natural diffusion process for an accelerated adsorption decontamination.¹⁸ Solution mixing is critical for improving the efficiency and speed of many physical-chemical processes, including the adsorption. By self-mixing, the MNMs can remove the pollutants more efficiently with less operation time.²⁴ Due to the above-mentioned advantages of MNMs for adsorption water purification, different types of pollutants, such as heavy metals,⁹⁹ nerve agent,¹⁰⁹ biochemistry toxin,¹¹⁸ and dyes have been decontaminated with good adsorption performances.^{119, 120}

Heavy metals, such as lead, mercury, cadmium, are a potential hazard to the wildlife and human. Vilela et al. designed the graphene oxide based microbots as the active self-propelled micromotors for the capture, transfer, and removal of a heavy metal of lead, and the subsequent recovery for reuse. The effective adsorption of lead on the graphene surface of the graphene oxide that covered micromotors is based on the strong interactions produced between the oxygen functional groups on graphene oxide and the Pb^{2+} ions.⁹⁹ Uygun et al.¹¹⁹ designed the water-powered ligand-modified micromotors that offer efficient “on-the-fly” chelation of metal ions contaminants. The micromotors are prepared by functionalizing the Janus Mg/Au microsphere with a self-assembled monolayer of meso-2,3-dimercaptosuccinic acid (DMSA). The resulted micromotors demonstrated autonomous motion in complex environmental and biological matrices. Such self-propelling micromotors offer significantly shorter operation time and more efficient water remediation process, compared to the commonly used static remediation agents. Pumera et al. designed a tubular micromotor with DNA immobilized on the gold outer surface for dynamic adsorption of mercury ions from the waterbody.¹²¹

MNMs could also be used as the motion-based platform for the adsorption of organic pollutants. Singh et al designed the zirconia/GO hybrid tubular micromotors for selective capture of nerve agents.¹²² The coupling of surface nanomaterials with fast moving ability holds considerable promise for defense and sustainability prospects. The same group also demonstrated the fabrication of activated carbon-based Janus particle micromotors for efficient and rapid adsorption of various kinds of contaminants, such as heavy metals, nitroaromatic explosives, organophosphorus nerve agent the and the azo-dyes compounds.¹²³ Li et al. designed the self-propelled multilayered micromotors for adsorption removal of the methyl-paraoxon and rhodamine 6G.¹²⁰ He et al. designed the catalytic polymer multilayer shell motors for separation of organic dyes by layer-by-layer assembly of polyelectrolyte using the template. This micromotor could adsorb nearly 90% of the dye molecules and subsequently release them at neutral pH in a microfluidic device. The adsorption and separation behaviors of the micromotors hold considerable promise for water analysis. Wu et al. designed the cell membrane coated nanomotors driven by the acoustic field for effective and accelerated neutralization of the membrane-damaging toxins.¹¹⁸

2.6.3 MNMs for separation of oil and water

Oil is a major source of ocean and groundwater pollutants. Oils are hard to decompose by the natural process and will block the sunshine from the sun, thus would have a very detrimental effect on the microorganisms and the wildlife. The removal of spilled oils and organic solvents from contaminated water is of great importance and scientific interest in minimizing its environmental hazards.¹²⁴ The development of the MNMs could provide an efficient and accelerated cleanup strategy for the oils and solvents contaminates in the aquatic environment.

Guix and co-workers demonstrated the use of a super-hydrophobic alkanethiol coated self-propelled micro submarines for the efficient removal of oil for the first time.⁹⁵ The oil collection micromotors are based on modifying microtubular engines with a superhydrophobic layer which enable the engines to adsorb oil by means of the strong adhesion to a long chain of self-assembled monolayers of alkanethiols created on the rough outer surface of the gold layers of the devices. The resulted alkanethiol coated Au/Ni/PEDOT/Pt multilayer microtubes display a continuous interaction with large oil droplets and are capable of loading and transporting multiple small oil droplets. This result demonstrates that the multilayer tubular microengines can be useful for a facile, rapid, and efficient collection of oil in water sample and other hydrophobic targets, such as the anti-cancer drugs. Gao and his co-workers demonstrated the use of water-powered Mg-based micromotors for capture and transport of oil in water.⁶⁹ By similar surface modification as Guix's method, the biocompatible fuel and composition of the water-powered Mg-based micromotor showed a great potential for diverse applications in biomedicine and environmental remediation. However, the above-mentioned micromotors developed at Joseph Wang's group suffer from the disadvantages of complex structures, sophisticated fabrication process, and the high cost of materials, which greatly hinder their widespread applications. Mou et al. designed the pot like micromotors using the "growing-bubble"-templated self-assembly of hydrophobic nanoparticles (NPs) by a volatile droplet method. In this approach, the hydrophobic MnFe_2O_4 @oleic acid NP in an oil droplet of chloroform and hexane was assembled into a dense NP shell layer due to the hydrophobic interactions between the NP surfaces. With the encapsulated oil continuously vaporizing into high-pressured gas bubbles, the dense MnFe_2O_4 NP shell layer then bursts, forming an asymmetric pot-like micromotor by creating

a single hole in it. For this structure of pot like micromotor, the catalytically generated O_2 molecules nucleate and grow into bubbles preferentially on the inner concave surface other than the outer convex surface, resulting in the continuous propelling force by the ejection of the oxygen bubbles from the opening. This work demonstrates a simple-structured, low-cost magnetically modulated micromotor with pot-like hollow microparticles structure as well as facile, versatile, and large-scale assembly fabrication. The magnetically steerable pot-like micromotor can autonomously move in water with H_2O_2 as fuel and can be directly used for oil removal without any further surface modification.

2.6.4 MNMs for the killing of bacterial

The contamination of drinking water with bacterial represents a major public health problem in view of the continuous rise of antimicrobial resistance. Biological warfare agent and other life-threatening outbreak of infectious diseases caused by different pathogenic bacteria require efficient protocols for the rapid and effective killing of bacteria. What is more, the increasing threat of multi-drug resistant bacteria strains against conventional antibiotic therapies represents a significant worldwide health risk and intensify the need for novel antibacterial treatment. The development of MNMs could provide a good tool for mankind to handle the problem of the bacterial outbreak and water disinfection. Many different types of materials have been incorporated in the fabrication of MNMs and used as the bactericide for water treatment.

Kiristi and co-workers in Joseph Wang's group designed an ultrasound propelled porous gold nanowire nanomotor for rapid bacterial killing using the lysozyme as the active agent, which could cleave the glycosidic bonds of peptidoglycans present in the bacterial cell wall.¹²⁵ Coupling the

antibacterial activity of the enzyme with the rapid movement of the high specific surface area porous gold nanorod nanomotor, contribute to the greatly enhanced bacterial-killing capability.¹²⁵ The same group demonstrated that silver-exchanged zeolite micromotors could be used for the detoxification of chemical warfare agents and killing of bacteria.¹⁰⁹ The use of silver-based materials for water disinfection has attracted great interest for scientific communities due to the strong antibacterial activity against a broad spectrum of bacteria, viruses, and fungi. The antibacterial properties of silver species depend largely upon the contact of bacteria with silver species. The self-propulsion of the micromotors would greatly enhance the contact kill effect. Hence, the micromotor based contact killing of pathogenic bacteria is very promising water treatment technology with higher efficiency and better outcome. Dong et al.¹²⁶ from Soochow University developed a dual fuel driven bactericidal micromotor, which showed motion behavior and bacterial killing effect in water or hydrogen peroxide containing solutions. The motion-based strategy can kill bacteria about nine times faster than that of the static one, thus demonstrating a great potential for the environmental hygiene applications.¹²⁶ Nelson et al.⁷⁹ from ETH Zurich designed the magnetically driven silver-coated nano coils for efficient bacterial contact killing, the low cytotoxicity along with the capability of precise magnetic locomotion makes the proposed nano coils an ideal candidate to combat multidrug-resistant bacteria in the field of environmental and biomedical applications. Vilela et al.¹²⁷ designed the Ag NP coated Mg-based Janus particle micromotor with an intermediate iron layer for magnetic recovery. This micromotor can capture the bacteria and kill them. After recovery from the water, leaving the water without biological contaminations, demonstrating great potentials for public health applications. Simmchen and co-workers demonstrated the fabrication of photoactive AgCl micro

stars for the decontamination of polluted water with dyes and the bacteria.¹²⁸ The micromotors can inhibit the bacterial growth. Delezuk et al.¹²⁹ designed a chitosan-based water powered micromotor for bacterial killing applications. The use of natural non-toxic biopolymer chitosan-based antimicrobial agents presented with a low toxicity and biocompatibility are very attractive for designing bactericide MNMs.

2.6.5 MNMs based sensing, detection, monitoring, and analysis

MNMs provide an excellent motion based analytical tool for various environmental, defense, security, chemical process, and food safety fields.^{18, 19, 42, 130, 131} There are two major analytical methods employed in the MNMs based detection, sensing, analysis, and testing applications. One is the direct optical observation strategy which monitors the motion behavior variation and the fluorescence-based “on-off” detection using the functionalized MNMs to interfere with the analytes’ response.^{21, 61} Since the MNMs will react with the analytes and the motion behaviors of MNMs will change to a marked degree due to the related enhanced chemical reaction offered by the increased fluid convection, various analytes could be detected based on the explicit, simple, direct and highly reproducible motion behavior changing recognition. The new sensing platforms offer great possibilities for the design of the field-portable analytical system. Another category of MNMs related analytical application is based on the electrochemical signal variation offered by the changes in chemical process and analytes response due to the MNMs’ reaction with the analytes.¹³² The MNMs based sensing, detection, monitoring, and analysis applications are very appealing due to the following advantages compared with static or traditional methods.¹³¹ Both the optical observation and the electrochemical detection demand extremely low quantity of the reagents and samples, thus significantly lower the generation of chemical waste.¹³³

More importantly, at micro/nano scale levels, greater control of molecular interaction is achieved, thus a higher sensibility could be obtained compared with other traditional methods.^{5, 134-136}

2.6.5.1 Optical microscope based analytical applications of the MNMs

Kogan and co-workers reported the first example of using catalytic nanomotors for motion-based chemical sensing, and particularly for specific detection of trace silver ions.⁶¹ Orozco and his co-workers designed the artificial enzyme catalyzed micro fish for water-quality testing purposes.¹³³ The micromotors based strategy for water quality testing is done by direct observation of the changes in the propulsion behavior of artificial bio-catalytically driven microswimmers in the presence of an aquatic pollutant. The micromotor based toxicity testing concept mimics the live-fish water testing and relies on the toxin-induced inhibition of the enzyme catalase, responsible for the bio-catalytic bubble propulsion behavior. The enzyme-powered biocompatible polymeric (PEDOT)/Au-catalase tubular microengines offer highly sensitive direct optical visualization of changes in the swimming behavior in the presence of a broad range of common contaminants and hence can do a direct real-time assessment of the water quality. The use of enzyme-powered micro fish addresses major standardization and reproducibility problems as well as the ethical concerns associated with the live fish toxicity assays and hence offers an attractive alternative to the common use of aquatic organisms for water quality testing. Pumera's group designed a biomimetic artificial inorganic micromotor for selective detection of Pb^{2+} in water based on the highly efficient Pt catalyst for enzyme-free self-propulsion.¹³⁷ The self-propelled Pt-based micro fish showed a specific response to Pb^{2+} compared to other heavy metals, such as Cd^{2+} , and can be used for selective determination of Pb^{2+} in water.

Besides the detection of metal ions in the aquatic environment, MNMs based analytic tools are showing great potentials for detection of toxin and nerve agent, biochemistry related analysis, and food safety control. Singh et al. demonstrated the use of enzyme-powered nanomotors responsive to the presence of nerve agents in the surrounding atmosphere for remote detection and monitoring.¹³⁴ This finding demonstrated the first example of MNMs to detect the atmospheric chemical warfare agents. The same group also demonstrated the use of Janus Si/Pt micromotors coated with fluoresceinamine for real-time “on-the-fly” field detection of sarin and soman simulants.¹³⁵ The dye-coated micromotors demonstrated an extremely fast fluorescent “on-off” detection of these chemical warfare agents. The same group also demonstrated the use of aptamer-modified graphene-based catalytic micromotors for “Off-On” fluorescent detection of the extremely poisonous natural toxin ricin.¹³⁶ Escarpa and his co-workers demonstrated the use of graphene/Pt micromotors for simultaneous, fast, and reliable assessment of two highly concerning mycotoxins.¹³⁸ The detection is based on the selective recognition from aptamers to the target mycotoxins and further “on-the-move” fluorescence quenching of the free aptamer in the outer layer of unmodified electrochemical reduced graphene oxide micromotors. Later, the same group demonstrated the use of magnetocatalytic phenylboronic acid (PABA) modified graphene quantum dots (GQDs) decorated Janus micromotors for ultrafast detection of deadly bacteria endotoxins lipopolysaccharides (LPSs).¹³⁹ The Janus micromotors were synthesized by the bottom-up method to generate the iron oxide and Pt NP on one side of the micromotors for catalytic propulsion and magnetic steering. Fluorescence quenching was observed upon the interaction of GQDs with the LPS endotoxin. Here, the PABA tags serve as highly specific recognition receptors of the LPS core polysaccharide region.¹³⁹ Current

enzyme-based assays are highly susceptible to the pH and temperature changes and require tedious sample-preparation procedures. The highly adaptive operation with highly specific detection holds considerable promise for diverse clinical, diagnostic, and food safety applications. Pacheco and co-workers at Escarpa's group studied the use of Janus micromotors as mobile sensors for the detection of toxins released by enterobacteria as indicators of food contamination.¹⁴⁰ The micromotor based assays can detect ultra-low levels of endotoxin and be applied in food samples. Such reliable and ultrafast approach holds considerable promise for food contamination screening related safety and defense applications.

2.6.5.2 Electrochemical based analytical applications of MNMs

Self-propelled MNMs are very attractive and promising for next-generation electroanalytical detection applications.^{21, 22, 141} Amperometric, impedance or photo-electrochemical based sensors are particularly attractive for detecting chemical and biological targets in terms of electrochemical environmental changes at electrode interfaces.²¹ Such signal variations can be easily converted into a digital readout, holding a great promise for the development of next-generation low-cost, portable, sensitive and easy to operate miniaturized analytical devices. Bubble-propelled autonomous MNMs have been shown to induce efficient fluid transport-mixing, enhancing the yield of classical chemical processes.^{42, 142} Such unique behaviors can be very beneficial for the electrochemical-based analytical applications. In 2015, Cinti et al. demonstrated the first example of using micromotors assisted electrochemical measurements at printable sensor strips.¹⁴¹ They observed the dramatically enhanced amperometric signal of organophosphorus (OP) nerve agent in the presence of the bubble generating magnesium Janus particle micromotors.

The generated microbubbles greatly enhanced the mass transportation and localized convection, thus leading to a higher sensitivity. The use of Mg-based Janus particle micromotor would generate the hydroxyl ions, which would react with the paraoxon and produce the electrochemically active and detectable p-nitrophenol by-product. The simple design and operation with an extremely low sample volume would greatly enhance the disposable test strip based analytical methods for a variety of target analytes with extremely high sensitivity and reproducibility. Such MNMs assisted printable electrode based electrochemical analytical method can be readily extended to different electrochemical sensing platforms with different analytes while eliminating the need for additional stimuli, instrument or external stirring to homogenize ultra-small samples at faster speeds. Rojas et al. demonstrated the Janus micromotors-based strategy for simultaneous degradation and detection POPs, for the first time in food and biological samples.⁹⁸ The Mg/Au Janus micromotors are used as novel analytical platforms for the degradation of non-electroactive DPP into phenol, which is directly measured by difference pulse voltammetry on disposable screen-printed electrodes. The increased fluid convection improves dramatically the analytical signal, increasing the sensitivity while lowering the detection potential. The first demonstrated determination in food and biological samples by the MNMs assisted technology holds considerable promises for its application in food and biological control in analytical applications with a high significance. Escarpa and co-workers demonstrated the fabrication of CdS and ZnS nanocrystals decorated polymer/Pt bilayer tubular micromotors for photocatalytic degradation of bisphenol A. They demonstrated the use of screen-printed electrodes for electrochemical analysis of the photocatalytic degradation processes. Pumera's group demonstrated the use of electrochemical analysis methods to evaluate the numbers of the

micromotors and the velocities of these self-propelled objects.¹⁴³ The perturbances of the diffusion layer at the electrode interface from the locomotion of the micromotors in solution resulted in spikes that were recorded by the electrochemical signals.

2.7 Conclusions and perspectives

Due to the advances in materials science and chemistry fields, self-propelled MNMs are developed as an innovative tool for diverse applications. Currently, there are two major application areas for MNMs, the biomedical science, and the environmental-based applications. A plethora of proof-of-concept applications has been achieved, such as drilling of biological tissue, transportation of cargos, delivery of genes, minimally invasive surgery, catalytic degradation of organic pollutant, the killing of bacteria, oil and water separation, and adsorption removal of heavy metals. The progress suggests that these MNMs based small-scale tools are very capable of addressing challenging issues facing mankind. Although there is numerous progress that has been made regarding the synthesis and application of self-propelled MNMs, the development of this area are still at its early stage. There are still many obstacles for the real and practical usage as nanocarriers for nanomedicines or environmental catalysts.

The MNMs always relying on the expensive materials such as Pt or sophisticated synthesis equipment and multi-step procedures. These drawbacks of MNMs need to be addressed before its large-scale applications. Up to now, there is no research on the fabrication of MNMs at industrial scale. The use of cheap and reliable materials with large-scale production ability will greatly facilitate the practical application of MNMs as micro cleaners. Novel fabrication methods could be developed to

fabricate the asymmetry structure for solving the problem of large-scale industrial fabrication with cheap and reliable basic materials.

The use of ferromagnetic materials is very attractive for the fabrication of magnetically recoverable MNMs. The coupling of photocatalytic materials with MNMs are very promising for the design of light controlled nanomotors for diverse environmental and biomedical applications. The MNMs could also show communication and collective behaviors, which means that these micro/nano scale tools could work together cooperatively to perform tasks in the future. Since this area of research will have wide follow-on applications for the analytical, environmental, biomedical and related cross-disciplinary basic science, we anticipate that a myriad of new MNMs will be developed with various functionalities that would greatly reshape the nanoscience and nanotechnology today.

References

1. Vance A. Elon musk: How the billionaire CEO of SpaceX and Tesla is shaping our future. Random House; 2015.
2. Xu T, Gao W, Xu LP, Zhang X, Wang S. Fuel-free synthetic micro-/nanomachines. *Adv. Mater.* 2017; 29(9):1603250.
3. Xu L, Mou F, Gong H, Luo M, Guan J. Light-driven micro/nanomotors: From fundamentals to applications. *Chem. Soc. Rev.* 2017; 46(22):6905-6926.
4. Ozin GA, Manners I, Fournier-Bidoz S, Arsenault A. Dream nanomachines. *Adv. Mater.* 2005; 17(24):3011-3018.
5. Sanchez S, Pumera M. Nanorobots: The ultimate wireless self-propelled sensing and actuating devices. *Chem-Asian J.* 2009; 4(9):1402-1410.

6. Feynman RP. There's plenty of room at the bottom. *Engineering and science*. 1960; 23(5):22-36.
7. Wang W, Duan WT, Ahmed S, Mallouk TE, Sen A. Small power: Autonomous nano- and micromotors propelled by self-generated gradients. *Nano Today*. 2013; 8(5):531-554.
8. Cheng C, Stoddart JF. Wholly synthetic molecular machines. *Chemphyschem*. 2016; 17(12):1780-1793.
9. Ismagilov RF, Schwartz A, Bowden N, Whitesides GM. Autonomous movement and self-assembly. *Angew. Chem. Int. Ed*. 2002; 41(4):674-676.
10. Mirkovic T, Zacharia NS, Scholes GD, Ozin GA. Nanolocomotion - catalytic nanomotors and nanorotors. *Small*. 2010; 6(2):159-167.
11. Patra D, Sengupta S, Duan W, et al. Intelligent, self-powered, drug delivery systems. *Nanoscale*. 2013; 5(4):1273-1283.
12. Abdelmohsen LKEA, Peng F, Tu YF, Wilson DA. Micro- and nano-motors for biomedical applications. *J. Mater. Chem. B*. 2014; 2(17):2395-2408.
13. Armstrong MJ, Hess H. The ecology of technology and nanomotors. *ACS Nano*. 2014; 8(5):4070-4073.
14. JianFeng, Cho S. Mini and micro propulsion for medical swimmers. *Micromachines*. 2014; 5(1):97-113.
15. Moo JG, Pumera M. Chemical energy powered nano/micro/macromotors and the environment. *Chem-Eur. J*. 2015; 21(1):58-72.
16. J Suematsu N, Nakata S. Self propelled object response to environment. *Curr. Phys. Chem*. 2015; 5(1):21-28.
17. Sanchez S, Soler L, Katuri J. Chemically powered micro- and nanomotors. *Angew. Chem. Int. Ed*. 2015; 54(5):1414-1444.

18. Singh VV, Wang J. Nano/micromotors for security/defense applications. A review. *Nanoscale*. 2015; 7(46):19377-19389.
19. Kherzi B, Pumera M. Self-propelled autonomous nanomotors meet microfluidics. *Nanoscale*. 2016; 8(40):17415-17421.
20. Li JX, Rozen I, Wang J. Rocket science at the nanoscale. *ACS Nano*. 2016; 10(6):5619-5634.
21. Jurado-Sanchez B, Escarpa A. Janus micromotors for electrochemical sensing and biosensing applications: A review. *Electroanalysis*. 2017; 29(1):14-23.
22. Li JX, de Avila BEF, Gao W, Zhang LF, Wang J. Micro/nanorobots for biomedicine: Delivery, surgery, sensing, and detoxification. *Sci. Robot*. 2017; 2(4):eaam6431.
23. Xu BR, Zhang BR, Wang L, Huang GS, Mei YF. Tubular micro/nanomachines: From the basics to recent advances. *Adv. Funct. Mater*. 2018; 28(25).
24. Safdar M, Khan SU, Janis J. Progress toward catalytic micro- and nanomotors for biomedical and environmental applications. *Adv. Mater*. 2018:1703660.
25. Ning HP, Zhang Y, Zhu H, et al. Geometry design, principles and assembly of micromotors. *Micromachines*. 2018; 9(2):75.
26. Karshalev E, Esteban-Fernandez de Avila B, Wang J. Micromotors for "chemistry-on-the-fly". *J. Am. Chem. Soc*. 2018; 140(11):3810-3820.
27. Guix M, Weiz SM, Schmidt OG, Medina-Sanchez M. Self-propelled micro/nanoparticle motors. *Part. Part. Syst. Char*. 2018; 35(2):1700382.
28. Dey KK, Sen A. Chemically propelled molecules and machines. *J. Am. Chem. Soc*. 2017; 139(23):7666-7676.
29. Yi D, Zhang Q, Liu Y, et al. Synthesis of chemically asymmetric silica nanobottles and their application for cargo loading and as

nanoreactors and nanomotors. *Angew. Chem. Int. Ed.* 2016; 55(47):14733-14737.

30. Wang H, Pumera M. Fabrication of micro/nanoscale motors. *Chem. Rev.* 2015; 115(16):8704-8735.

31. Dong R, Hu Y, Wu Y, et al. Visible-light-driven BiOI-based Janus micromotor in pure water. *J. Am. Chem. Soc.* 2017; 139(5):1722-1725.

32. Gao W, Sattayasamitsathit S, Orozco J, Wang J. Highly efficient catalytic microengines: Template electrosynthesis of polyaniline/platinum microtubes. *J. Am. Chem. Soc.* 2011; 133(31):11862-11864.

33. Ye H, Ma G, Kang J, Sun H, Wang S. Pt-Free microengines at extremely low peroxide levels. *Chem. Commun.* 2018; 54:4653-4656.

34. Ye H, Sun H, Wang S. Electrochemical synthesis of graphene/MnO₂ in an architecture of bilayer microtubes as micromotors. *Chem. Eng. J.* 2017; 324:251-258.

35. Wei W, Cui X, Chen W, Ivey DG. Manganese oxide-based materials as electrochemical supercapacitor electrodes. *Chem. Soc. Rev.* 2011; 40(3):1697-1721.

36. Moo JG, Wang H, Pumera M. Influence of pH on the motion of catalytic Janus particles and tubular bubble-propelled micromotors. *Chem-Eur. J.* 2016; 22(1):355-360.

37. Wang H, Zhao GJ, Pumera M. Crucial role of surfactants in bubble-propelled microengines. *J. Phys. Chem. C.* 2014; 118(10):5268-5274.

38. Gao W, Sattayasamitsathit S, Orozco J, Wang J. Efficient bubble propulsion of polymer-based microengines in real-life environments. *Nanoscale.* 2013; 5(19):8909-8914.

39. Wang H, Zhao GJ, Pumera M. Blood proteins strongly reduce the mobility of artificial self-propelled micromotors. *Chem-Eur. J.* 2013; 19(49):16756-16759.

40. Wang H, Zhao G, Pumera M. Blood metabolite strongly suppresses motion of electrochemically deposited catalytic self-propelled microjet engines. *Electrochem. Commun.* 2014; 38:128-130.
41. Simmchen J, Magdanz V, Sanchez S, et al. Effect of surfactants on the performance of tubular and spherical micromotors - a comparative study. *RSC Adv.* 2014; 4(39):20334-20340.
42. Jurado-Sanchez B, Escarpa A. Milli, micro and nanomotors: Novel analytical tools for real-world applications. *Trends Analyt. Chem.* 2016; 84:48-59.
43. Paxton WF, Kistler KC, Olmeda CC, et al. Catalytic nanomotors: Autonomous movement of striped nanorods. *J. Am. Chem. Soc.* 2004; 126(41):13424-13431.
44. Gibbs JG, Zhao YP. Autonomously motile catalytic nanomotors by bubble propulsion. *Appl. Phys. Lett.* 2009; 94(16):163104.
45. Solovev AA, Mei Y, Bermudez Urena E, Huang G, Schmidt OG. Catalytic microtubular jet engines self-propelled by accumulated gas bubbles. *Small.* 2009; 5(14):1688-1692.
46. Zhang L, Abbott JJ, Dong L, et al. Characterizing the swimming properties of artificial bacterial flagella. *Nano Lett.* 2009; 9(10):3663-3667.
47. Paxton WF, Baker PT, Kline TR, et al. Catalytically induced electrokinetics for motors and micropumps. *J. Am. Chem. Soc.* 2006; 128(46):14881-14888.
48. Zhao G, Seah TH, Pumera M. External-energy-independent polymer capsule motors and their cooperative behaviors. *Chem-Eur. J.* 2011; 17(43):12020-12026.
49. Wang H, Sofer Z, Eng AY, Pumera M. Iridium-catalyst-based autonomous bubble-propelled graphene micromotors with ultralow catalyst loading. *Chem-Eur. J.* 2014; 20(46):14946-14950.

50. Gao W, Pei A, Dong RF, Wang J. Catalytic iridium-based Janus micromotors powered by ultralow levels of chemical fuels. *J. Am. Chem. Soc.* 2014; 136(6):2276-2279.
51. Wilson DA, Nolte RJ, van Hest JC. Autonomous movement of platinum-loaded stomatocytes. *Nat. Chem.* 2012; 4(4):268-274.
52. Gao W, Pei A, Wang J. Water-driven micromotors. *ACS Nano.* 2012; 6(9):8432-8438.
53. Wang H, Zhao GJ, Pumera M. Beyond platinum: Bubble-propelled micromotors based on Ag and MnO₂ catalysts. *J. Am. Chem. Soc.* 2014; 136(7):2719-2722.
54. Yamamoto D, Shioi A. Self-propelled nano/micromotors with a chemical reaction: Underlying physics and strategies of motion control. *Kona Powder Part J.* 2015; (32):2-22.
55. Fournier-Bidoz S, Arsenault AC, Manners I, Ozin GA. Synthetic self-propelled nanorotors. *Chem. Commun.* 2005; (4):441-443.
56. Liu R, Sen A. Autonomous nanomotor based on copper-platinum segmented nanobattery. *J. Am. Chem. Soc.* 2011; 133(50):20064-20067.
57. Demirok UK, Laocharoensuk R, Manesh KM, Wang J. Ultrafast catalytic alloy nanomotors. *Angew. Chem. Int. Ed.* 2008; 47(48):9349-9351.
58. Laocharoensuk R, Burdick J, Wang J. Carbon-nanotube-induced acceleration of catalytic nanomotors. *ACS Nano.* 2008; 2(5):1069-1075.
59. Wang Y, Hernandez RM, Bartlett DJ, Jr., et al. Bipolar electrochemical mechanism for the propulsion of catalytic nanomotors in hydrogen peroxide solutions. *Langmuir.* 2006; 22(25):10451-10456.
60. Jun IK, Hess H. A biomimetic, self-pumping membrane. *Adv. Mater.* 2010; 22(43):4823-4825.

61. Kagan D, Calvo-Marzal P, Balasubramanian S, et al. Chemical sensing based on catalytic nanomotors: Motion-based detection of trace silver. *J. Am. Chem. Soc.* 2009; 131(34):12082-12083.
62. Gao W, Kagan D, Pak OS, et al. Cargo-towing fuel-free magnetic nanoswimmers for targeted drug delivery. *Small.* 2012; 8(3):460-467.
63. Alexander AS, Samuel S, Martin P, Yong Feng M, Oliver GS. Magnetic control of tubular catalytic microbots for the transport, assembly, and delivery of micro-objects. *Adv. Funct. Mater.* 2010.
64. Pavlick RA, Sengupta S, McFadden T, Zhang H, Sen A. A polymerization-powered motor. *Angew. Chem. Int. Ed.* 2011; 123(40):9546-9549.
65. Golestanian R, Liverpool TB, Ajdari A. Propulsion of a molecular machine by asymmetric distribution of reaction products. *Phys. Rev. Lett.* 2005; 94(22):220801.
66. Duan W, Liu R, Sen A. Transition between collective behaviors of micromotors in response to different stimuli. *J. Am. Chem. Soc.* 2013; 135(4):1280-1283.
67. Manjare M, Yang B, Zhao YP. Bubble driven quasioscillatory translational motion of catalytic micromotors. *Phys. Rev. Lett.* 2012; 109(12):128305.
68. Gao W, D'Agostino M, Garcia-Gradilla V, Orozco J, Wang J. Multi-fuel driven Janus micromotors. *Small.* 2013; 9(3):467-471.
69. Gao W, Feng X, Pei A, et al. Seawater-driven magnesium based Janus micromotors for environmental remediation. *Nanoscale.* 2013; 5(11):4696-4700.
70. Zhang H, Duan W, Liu L, Sen A. Depolymerization-powered autonomous motors using biocompatible fuel. *J. Am. Chem. Soc.* 2013; 135(42):15734-15737.

71. Wang H, Sofer Z, Moo JG, Pumera M. Simultaneous self-exfoliation and autonomous motion of MoS₂ particles in water. *Chem. Commun.* 2015; 51(48):9899-9902.
72. Orozco J, Vilela D, Valdes-Ramirez G, et al. Efficient biocatalytic degradation of pollutants by enzyme-releasing self-propelled motors. *Chem-Eur. J.* 2014; 20(10):2866-2871.
73. Chen C, Mou F, Xu L, et al. Light-steered isotropic semiconductor micromotors. *Adv. Mater.* **2017**; 29(3):1603374.
74. Xu T, Soto F, Gao W, et al. Ultrasound-modulated bubble propulsion of chemically powered microengines. *J. Am. Chem. Soc.* 2014; 136(24):8552-8555.
75. Wang W, Duan W, Zhang Z, et al. A tale of two forces: Simultaneous chemical and acoustic propulsion of bimetallic micromotors. *Chem. Commun.* 2015; 51(6):1020-1023.
76. Gao W. *Synthetic micro/nanomachines and their applications: Towards 'fantastic voyage'*. San Diego: University of California, San Diego; 2014.
77. Mei Y, Solovev AA, Sanchez S, Schmidt OG. Rolled-up nanotech on polymers: From basic perception to self-propelled catalytic microengines. *Chem. Soc. Rev.* 2011; 40(5):2109-2119.
78. Claussen JC, Daniele MA, Geder J, et al. Platinum-paper micromotors: An urchin-like nanohybrid catalyst for green monopropellant bubble-thrusters. *ACS Appl. Mater. Inter.* 2014; 6(20):17837-17847.
79. Hoop M, Shen Y, Chen XZ, et al. Magnetically driven silver-coated nanocoils for efficient bacterial contact killing. *Adv. Funct. Mater.* 2016; 26(7):1063-1069.

80. Teo WZ, Zboril R, Medrik I, Pumera M. Fe⁰ nanomotors in ton quantities (10²⁰ units) for environmental remediation. *Chem-Eur. J.* 2016; 22(14):4789-4793.
81. Wu ZG, Li JX, de Avila BEF, et al. Water-powered cell-mimicking Janus micromotor. *Adv. Funct. Mater.* 2015; 25(48):7497-7501.
82. Chen C, Karshalev E, Guan J, Wang J. Magnesium-based micromotors: Water-powered propulsion, multifunctionality, and biomedical and environmental applications. *Small.* 2018:1704252.
83. Ma X, Hortelao AC, Patino T, Sanchez S. Enzyme catalysis to power micro/nanomachines. *ACS Nano.* 2016; 10(10):9111-9122.
84. Ma X, Hortelao AC, Miguel-Lopez A, Sanchez S. Bubble-free propulsion of ultrasmall tubular nanojets powered by biocatalytic reactions. *J. Am. Chem. Soc.* 2016; 138(42):13782-13785.
85. Karshalev E, Kumar R, Jeerapan I, et al. Multistimuli-responsive camouflage swimmers. *Chem. Mater.* 2018; 30(5):1593-1601.
86. Dey KK, Bhandari S, Bandyopadhyay D, Basu S, Chattopadhyay A. The pH taxis of an intelligent catalytic microbot. *Small.* 2013; 9(11):1916-1920.
87. Su Y, Ge Y, Liu L, et al. Motion-based pH sensing based on the cartridge-case-like micromotor. *ACS Appl. Mater. Inter.* 2016; 8(6):4250-4257.
88. Li J, Angsantikul P, Liu W, et al. Micromotors spontaneously neutralize gastric acid for pH-responsive payload release. *Angew. Chem. Int. Ed.* 2017; 56(8):2156-2161.
89. Seah TH, Zhao GJ, Pumera M. Surfactant capsules propel interfacial oil droplets: An environmental cleanup strategy. *Chempluschem.* 2013; 78(5):395-397.

90. Zhao GJ, Sanchez S, Schmidt OG, Pumera M. Poisoning of bubble propelled catalytic micromotors: The chemical environment matters. *Nanoscale*. 2013; 5(7):2909-2914.
91. Wang H, Zhao G, Pumera M. Blood electrolytes exhibit a strong influence on the mobility of artificial catalytic microengines. *Phys. Chem. Chem. Phys.* 2013; 15(40):17277-17280.
92. Uygun M, Singh VV, Kaufmann K, et al. Micromotor-based biomimetic carbon dioxide sequestration: Towards mobile microscrubbers. *Angew. Chem. Int. Ed.* 2015; 54(44):12900-12904.
93. Li J, Shklyayev OE, Li T, et al. Self-propelled nanomotors autonomously seek and repair cracks. *Nano Lett.* 2015; 15(10):7077-7085.
94. Maria-Hormigos R, Jurado-Sanchez B, Escarpa A. Labs-on-a-chip meet self-propelled micromotors. *Lab Chip*. 2016; 16(13):2397-2407.
95. Guix M, Orozco J, Garcia M, et al. Superhydrophobic alkanethiol-coated microsubmarines for effective removal of oil. *ACS Nano*. 2012; 6(5):4445-4451.
96. Orozco J, Cheng G, Vilela D, et al. Micromotor-based high-yielding fast oxidative detoxification of chemical threats. *Angew. Chem. Int. Ed.* 2013; 52(50):13276-13279.
97. Soler L, Magdanz V, Fomin VM, Sanchez S, Schmidt OG. Self-propelled micromotors for cleaning polluted water. *ACS Nano*. 2013; 7(11):9611-9620.
98. Rojas D, Jurado-Sanchez B, Escarpa A. "Shoot and sense" Janus micromotors-based strategy for the simultaneous degradation and detection of persistent organic pollutants in food and biological samples. *Anal. Chem.* 2016; 88(7):4153-4160.
99. Vilela D, Parmar J, Zeng Y, Zhao Y, Sanchez S. Graphene-based microbots for toxic heavy metal removal and recovery from water. *Nano Lett.* 2016; 16(4):2860-2866.

100. Li J, Singh VV, Sattayasamitsathit S, et al. Water-driven micromotors for rapid photocatalytic degradation of biological and chemical warfare agents. *ACS Nano*. 2014; 8(11):11118-11125.
101. Parmar J, Vilela D, Pellicer E, et al. Reusable and long-lasting active microcleaners for heterogeneous water remediation. *Adv. Funct. Mater.* 2016; 26(23):4152-4161.
102. Srivastava SK, Guix M, Schmidt OG. Wastewater mediated activation of micromotors for efficient water cleaning. *Nano Lett.* 2015.
103. Mushtaq F, Asani A, Hoop M, et al. Highly efficient coaxial TiO₂-PtPd tubular nanomachines for photocatalytic water purification with multiple locomotion strategies. *Adv. Funct. Mater.* 2016; 26(38):6995-7002.
104. Wani OM, Safdar M, Kinnunen N, Janis J. Dual effect of manganese oxide micromotors: Catalytic degradation and adsorptive bubble separation of organic pollutants. *Chem-Eur. J.* 2016; 22(4):1244-1247.
105. He X, Bahk YK, Wang J. Organic dye removal by MnO₂ and Ag micromotors under various ambient conditions: The comparison between two abatement mechanisms. *Chemosphere*. 2017; 184:601-608.
106. Lee C-S, Gong J, Oh D-S, Jeon J-R, Chang Y-S. Zerovalent-iron/platinum Janus micromotors with spatially separated functionalities for efficient water decontamination. *ACS Appl. Nano Mater.* 2018; 1(2):768-776.
107. Pan D, Mou FZ, Li XF, et al. Multifunctional magnetic oleic acid-coated MnFe₂O₄/polystyrene Janus particles for water treatment. *J. Mater. Chem. A*. 2016; 4(30):11768-11774.
108. Parmar J, Villa K, Vilela D, Sanchez S. Platinum-free cobalt ferrite based micromotors for antibiotic removal. *Appl. Mater. Today*. 2017; 9:605-611.

109. Singh VV, Jurado-Sanchez B, Sattayasamitsathit S, et al. Multifunctional silver-exchanged zeolite micromotors for catalytic detoxification of chemical and biological threats. *Adv. Funct. Mater.* 2015; 25(14):2147-2155.
110. Mushtaq F, Guerrero M, Sakar MS, et al. Magnetically driven Bi₂O₃/BiOCl-based hybrid microrobots for photocatalytic water remediation. *J. Mater. Chem. A.* 2015; 3(47):23670-23676.
111. Zhang Q, Dong R, Wu Y, et al. Light-driven Au-WO₃@C Janus micromotors for rapid photodegradation of dye pollutants. *ACS Appl. Mater. Inter.* 2017; 9(5):4674-4683.
112. Li ZL, Wang W, Li M, et al. Facile fabrication of bubble-propelled micromotors carrying nanocatalysts for water remediation. *Ind. Eng. Chem. Res.* 2018; 57(13):4562-4570.
113. Hao J, Yang W, Zhang Z, Tang J. Surfactant-assisted fabrication of 3D prussian blue-reduced graphene oxide hydrogel as a self-propelling motor for water treatment. *Nanoscale.* 2015; 7(23):10498-10503.
114. Wang SB, Peng YL. Natural zeolites as effective adsorbents in water and wastewater treatment. *Chem. Eng. J.* 2010; 156(1):11-24.
115. Bradder P, Ling SK, Wang SB, Liu SM. Dye adsorption on layered graphite oxide. *J. Chem. Eng. Data.* 2011; 56(1):138-141.
116. Shukla P, Wang SB, Sun HQ, Ang HM, Tade M. Adsorption and heterogeneous advanced oxidation of phenolic contaminants using Fe loaded mesoporous SBA-15 and H₂O₂. *Chem. Eng. J.* 2010; 164(1):255-260.
117. Eskandarloo H, Kierulf A, Abbaspourrad A. Nano- and micromotors for cleaning polluted waters: Focused review on pollutant removal mechanisms. *Nanoscale.* 2017; 9(37):13850-13863.

118. Wu ZG, Li TL, Gao W, et al. Cell-membrane-coated synthetic nanomotors for effective biodetoxification. *Adv. Funct. Mater.* 2015; 25(25):3881-3887.
119. Uygun DA, Jurado-Sanchez B, Uygun M, Wang J. Self-propelled chelation platforms for efficient removal of toxic metals. *Environ Sci-Nano.* 2016; 3(3):559-566.
120. Li TL, Li LQ, Song WP, et al. Self-propelled multilayered microrockets for pollutants purification. *ECS J. Solid State Sci. Technol.* 2015; 4(10):S3016-S3019.
121. Wang H, Khezri B, Pumera M. Catalytic DNA-functionalized self-propelled micromachines for environmental remediation. *Chem.* 2016; 1(3):473-481.
122. Singh VV, Martin A, Kaufmann K, de Oliveira SDS, Wang J. Zirconia/graphene oxide hybrid micromotors for selective capture of nerve agents. *Chem. Mater.* 2015; 27(23):8162-8169.
123. Jurado-Sanchez B, Sattayasamitsathit S, Gao W, et al. Self-propelled activated carbon Janus micromotors for efficient water purification. *Small.* 2015; 11(4):499-506.
124. Radetic M, Ilic V, Radojevic D, et al. Efficiency of recycled wool-based nonwoven material for the removal of oils from water. *Chemosphere.* 2008; 70(3):525-530.
125. Kiristi M, Singh VV, Esteban-Fernandez de Avila B, et al. Lysozyme-based antibacterial nanomotors. *ACS Nano.* 2015; 9(9):9252-9259.
126. Ge Y, Liu M, Liu LM, et al. Dual-fuel-driven bactericidal micromotor. *Nano-Micro Lett.* 2016; 8(2):157-164.
127. Vilela D, Stanton MM, Parmar J, Sanchez S. Microbots decorated with silver nanoparticles kill bacteria in aqueous media. *ACS Appl. Mater. Inter.* 2017.

128. Simmchen J, Baeza A, Miguel-Lopez A, et al. Dynamics of novel photoactive AgCl microstars and their environmental applications. *ChemNanoMat*. 2017; 3(1):65-71.
129. Delezuk JA, Ramirez-Herrera DE, Esteban-Fernandez de Avila B, Wang J. Chitosan-based water-propelled micromotors with strong antibacterial activity. *Nanoscale*. 2017; 9(6):2195-2200.
130. Guix M, Mayorga-Martinez CC, Merkoci A. Nano/micromotors in (bio)chemical science applications. *Chem. Rev.* 2014; 114(12):6285-6322.
131. Duan W, Wang W, Das S, et al. Synthetic nano- and micromachines in analytical chemistry: Sensing, migration, capture, delivery, and separation. *Annu. Rev. Anal. Chem.* 2015; 8(1):311-333.
132. Jurado-Sánchez B, Wang J, Escarpa A. Ultrafast nanocrystals decorated micromotors for on-site dynamic chemical processes. *ACS Appl. Mater. Inter.* 2016; 8(30):19618-19625.
133. Orozco J, Garcia-Gradilla V, D'Agostino M, et al. Artificial enzyme-powered microfish for water-quality testing. *ACS Nano*. 2013; 7(1):818-824.
134. Singh VV, Kaufmann K, Esteban-Fernandez de Avila B, Uygun M, Wang J. Nanomotors responsive to nerve-agent vapor plumes. *Chem. Commun.* 2016; 52(16):3360-3363.
135. Singh VV, Kaufmann K, Orozco J, et al. Micromotor-based on-off fluorescence detection of sarin and soman simulants. *Chem. Commun.* 2015; 51(56):11190-11193.
136. Esteban-Fernández de Ávila B, Lopez-Ramirez MA, Báez DF, et al. Aptamer-modified graphene-based catalytic micromotors: Off-on fluorescent detection of ricin. *ACS Sensors*. 2016; 1(3):217-221.
137. Moo JG, Wang H, Zhao G, Pumera M. Biomimetic artificial inorganic enzyme-free self-propelled microfish robot for selective detection of Pb²⁺ in water. *Chem-Eur. J.* 2014; 20(15):4292-4296.

138. Molinero-Fernandez A, Moreno-Guzman M, Lopez MA, Escarpa A. Biosensing strategy for simultaneous and accurate quantitative analysis of mycotoxins in food samples using unmodified graphene micromotors. *Anal. Chem.* 2017; 89(20):10850-10857.
139. Jurado-Sanchez B, Pacheco M, Rojo J, Escarpa A. Magnetocatalytic graphene quantum dots Janus micromotors for bacterial endotoxin detection. *Angew. Chem. Int. Ed.* 2017:n/a-n/a.
140. Pacheco M, Jurado-Sanchez B, Escarpa A. Sensitive monitoring of enterobacterial contamination of food using self-propelled Janus microsensors. *Anal. Chem.* 2018; 90(4):2912-2917.
141. Cinti S, Valdes-Ramirez G, Gao W, et al. Microengine-assisted electrochemical measurements at printable sensor strips. *Chem. Commun.* 2015; 51(41):8668-8671.
142. Wang J. Self-propelled affinity biosensors: Moving the receptor around the sample. *Biosens. Bioelectron.* 2015.
143. Moo JGS, Pumera M. Self-propelled micromotors monitored by particle-electrode impact voltammetry. *ACS Sensors.* 2016; 1(7):949-957.

Every reasonable effort has been made to acknowledge the owners of copyright material. I would be pleased to hear from any copyright owner who has been omitted or incorrectly acknowledged.

Chapter 3. Electrochemical Synthesis of MnO₂ Based Micromotors in an Architecture of Bilayer Microtubes by an Anodic Oxidation Deposition Method

Abstract

Micro/nanomotors (MNMs) that could perform diverse tasks are the most dynamic research areas in nanoscience and nanotechnology. Up to now, the majority of micromotors contain the precious metal platinum (Pt) as the catalyst for propulsion. High cost and scarcity of Pt seriously impede its practical application. The exploration of manganese oxide based MNMs provides a route to circumvent the drawback of Pt. In this chapter, graphene/MnO₂ microtubes as a highly efficient micromotor were fabricated by a template-assisted electrochemical process. The resulting micromotors show a good motion behavior in a wide range of hydrogen peroxide (H₂O₂) concentrations. Owing to its robust motion, easy functionalization, a large quantity of surface functional groups for modification, along with simple synthesis, these fine micromotors hold a great promise for biomedicine and environmental applications.

3.1 Introduction

Self-propelled micro/nanomotors (MNMs) are at the frontier of the micro- and nanotechnology.¹⁻⁷ MNMs show great potentials in diverse applications, such as the selective capture of nerve agents,⁸ oil and water separation,⁹ cargo delivery and release,^{10, 11} efficient water cleaning,¹² rapid dye degradation,¹³ pH meters¹⁴, and lab-on-chip devices.¹⁵ The synthesis of chemically powered, bubble-propelled MNMs is of the great interest and challenge in this field.^{1, 16-18} The bubble formation and motion behaviors of micromotors have been modeled and it is generally accepted that the continuous generation and detachment of microbubbles from the catalytic surface result in the propelling force.¹⁹⁻²¹

Platinum (Pt) has always been the most widely used catalyst in designing MNMs because of its high efficiency in catalytic decomposition of hydrogen peroxide (H_2O_2).^{3, 22} Although the Pt-based MNMs show the best motion behavior, they also suffer from several drawbacks. Firstly, platinum is an expensive noble metal, which is the major obstacle in its large-scale application in environmental clean-up. Secondly, the platinum-based micromotors can be deactivated by certain proteins and sulfate-containing molecules that exist widely in biological media as well as natural water matrices.²³ Thus, the search for alternative catalytic materials is highly in demand. Iron, iridium, and silver have been tested for their performances in MNMs constructions. Although iron could be used as the reaction part with acids to generate hydrogen bubbles for propulsion, it shows no catalytic activity for catalytic H_2O_2 decomposition.²⁴ Iridium is also a noble metal which has the same limitations as platinum.¹⁵ Silver is a good alternative for designing micromotors.²⁵ The enzyme could be another good candidate, but it suffers

from the strict requirement to operating temperature and will deactivate in a short period of time.²⁶

The use of manganese dioxide (MnO_2) for MNMs fabrication becomes highly desirable due to its low cost, wide fuel concentration range, easiness of fabrication, tunable crystal structure, and surface morphology, controllable size and geometry, high efficiency and long lifespan. However, very few reports on MNMs studies were based on the robust MnO_2 as the catalyst.²⁷ MnO_2 can be fabricated by a hydrothermal or electrochemical method. Both the methods offer great opportunities for tuning MnO_2 shape, size, surface geometry, and chemistry.^{28, 29} Efforts were mainly made to the electrochemical fabrication because asymmetry is difficult to be achieved in hydrothermal synthesis. Wang and his co-workers³⁰ demonstrated the use of commercial MnO_2 particles as micromotors, which required a very high concentration of fuel, showing a motion performance of about $120 \mu\text{m s}^{-1}$ in 21% H_2O_2 . Feng et al.³¹ designed a “sandwich”-like $\text{MnO}_2/\text{Graphene}/\text{Au}$ micromotor, which could be propelled in a very low concentration of H_2O_2 , down to 0.15% at a speed of $15.8 \mu\text{m s}^{-1}$ (2.18 body-lengths s^{-1}). Salfar et al.³² designed a conducting polymer PEDOT/ MnO_2 bilayer microtube micromotors. The MnO_2 -based micromotor showed good motion behaviors from 5% to 15% of H_2O_2 concentration range. Very recently, they also studied the crystalline forms and geometry on the motion of the MnO_2 based micromotors. The individual hollow spherical MnO_2 microparticles reached a maximum speed of $\sim 1600 \mu\text{m s}^{-1}$ and the average speed is about $1000 \mu\text{m s}^{-1}$ in 10% H_2O_2 .³³ Wang et al. tested the PEDOT/ MnO_2 tubular micromotors for drug delivery.³⁴ Singh et al.³⁵ designed a self-propelling paperbots that could be magnetically guided, but it requires at least 9%

H₂O₂ solution to become motile. The maximum speed of these paperbots is about 1600 μm s⁻¹ (about 2 body lengths s⁻¹) and the lifetime is 6 min.

Herein, we demonstrated the synthesis of electrochemically reduced graphene oxide (erGO)/MnO₂ bilayer microtubes as micromotors, which can be propelled efficiently in varying H₂O₂ concentrations at above 3%. The rough, porous inner surface of the MnO₂ microtubes with the nanoscale sheet-like microstructure is responsible for its good activity in catalytic decomposition of H₂O₂ for fast and efficient propelling. This platinum-free MnO₂ based micromotors with superior motion behaviors hold a great promise for biomedical as well as environmental applications.

3.2 Experimental section

3.2.1 Materials and reagents

Manganese (II) acetate tetrahydrate, sodium sulfate, ethanol, dichloromethane, sodium dodecyl sulfate (SDS), H₂O₂ (30%), and sulfate acid (98%) were purchased from Sigma-Aldrich. Aluminum oxide paste (catalog no. F1200, code: 361544) were purchased from Kemet, NSW, Australia. Porous polycarbonate (PC) membranes (Catalogue no. 7060-2513) with an average pore diameter of 5 μm were purchased from Whatman Inc., NY, USA. Ultrapure water (Milli-Q) was used in all experiments. Nano-sized graphene oxide (GO) was purchased from graphene supermarket, New York, USA.

3.2.2 Fabrication of graphene/MnO₂ bilayer microtubes

The graphene/MnO₂ bilayer microtubes were fabricated using a common template-directed electrochemical deposition protocol. A cyclopore polycarbonate membrane containing 5 μm maximum diameter conical-shaped micropores was employed as the template. An 80 nm of gold film

was first deposited on one side of the porous membranes to serve as the working electrode using the Emitech K950X gold evaporator and the evaporation deposition was performed at room temperature under high vacuum of below 1×10^{-3} mBar at a direct current of 5 to 6 A. The deposition rate was about 1 nm s^{-1} . A Pt wire and Ag/AgCl with 3 M KCl were used as counter and reference electrodes, respectively. The membrane was then assembled in a self-designed plating cell with an aluminum foil serving as a contact for the working electrode. The detailed information about the plating cell is described below. A solution containing 0.1 mg mL^{-1} GO in 0.5 M of Na_2SO_4 and 0.1 M H_2SO_4 was prepared as the electrolyte for the electrochemical growth of the graphene outer layer. The GO in the solution was reduced using a cyclic voltammetry from 0.3 to -1.5 V for five cycles. After three washing with 10 mL of ultrapure water, MnO_2 inner layer was deposited using a Potentiostat (PS) method at a voltage of + 0.75 V for approximately 0.3 C of charge transfer. The plating solution contains 0.1 M manganese acetate tetrahydrate as the MnO_2 source and 0.1 M sodium sulfate as the electrolyte to increase the conductivity. Following the deposition, the gold layer was removed by hand polishing gently with alumina slurry, which contains 3 μm diameter alumina particles. Then the templates were dissolved in dichloromethane for 15 min to release the micromotors. Finally, the micromotors were collected by centrifuge at 7000 rpm for 3 min while being repeatedly washing with dichloromethane, ethanol, and ultrapure water, three times each. All the micromotors were stored in ultrapure water at room temperature for further use.

3.2.3 Equipment and characterization

An Emitech K950X gold evaporator was used to deposit a layer of gold onto the PC template membranes. Electrochemical deposition was carried

out using an electrochemical workstation (Zennium Zahner, Germany) connected to a computer and controlled by the Thalse software. The deposition procedure was conducted at room temperature (25 °C) using a three-electrode arrangement. A platinum wire electrode was utilized as a counter electrode and Ag/AgCl with 3 M KCl was used as a reference electrode. A customized plating cell was used in all plating process. The ultrasonication process was carried out using an ultrasonication cleaner (Model FXP12D, Unisonics), and centrifuge was carried out using an Eppendorf centrifuge (Model 5430). Scanning electronic microscopy (SEM/EDX) analysis was conducted using a Zeiss Neon 40 EsV FIBSEM with a field emission electron gun and the Oxford EDS detector operated by the Aztec software and the Zeiss 1555 VP-FESEM with a field emission electron gun and the Oxford EDS detector operated by the Aztec software. SEM images were taken at an accelerating voltage of 2, 3 and 5 kV. EDX analysis was taken using the coupled Oxford detector and operated by the Aztec software at an acceleration voltage of 15 kV. Optical microscopy videos and images were obtained using the Olympus IX81 inverted microscope with a Nikon digital sight DS-2Mv camera connected to a computer and operated by the Nikon NIS Elements software and a Nikon Eclipse ME600 microscope with a Toupcam UCMOS14000KPA camera operated by a ToupView 3.7 software. A digital hand-held "Pocket" H₂O₂ refractometer (Model: Atago, PAL-39S) was used to calibrate the concentrations of the H₂O₂ solutions used. The videos were edited by the Virtual Dub 1.10.4 software and free Fiji software was used to track the speed of the micromotors and to extract images.³⁶⁻³⁸ XPS was carried out on a thermos ESCALAB 250 XPS microscope with monochromatic Al-K α X-rays at a photo energy of 1486.7 eV. The measurement was carried out using a Kratos AXIS Ultra DLD system under UHV conditions with a base pressure of less than 1 \times 10⁻

⁹ mBar. Spectra were acquired with the pass energy of 20 eV and fitted using CasaXPS software. All the spectra are calibrated to yield a primary C 1s component at 284.6 eV with the Shirley background, and the component fitting applied Voigt functions with a 30% Lorentzian component.

3.2.4 Motion behavior observations

A transparent plastic glass bottom microwell dish (Part No. P35G-1.5-10-C, Mat Tek Corporation, MA, USA) with the holed bottom covered by thin glass slides was used as the container to prepare different fuel concentrations for all motion behavior observation. The 10 mm diameter bottom hole of a 35mm diameter plastic petri dish is covered by a thin glass slide, which forms a shallow well-like hollow structure with a volume of approximately 75-80 μL . After 80 μL of the reaction solution was filled into the well, a nearly flat liquid surface is expected to form. The formation of a flat liquid surface is beneficial for motion behavior characterization for the following reasons. In a typical observation process, for examples, to form 1% SDS as the surfactant and 5% H_2O_2 as fuel for propulsion. 16 μL of 5% SDS solution, 10 μL of micromotors containing solutions and 38 μL of ultrapure water, and 16 μL of 25% H_2O_2 solutions were mixed together to form the final 80 μL of the micromotors motion behaviors observation liquid. The concentration of the fuel and surfactants could be easily adjusted by using different volumes of the 5% of SDS solutions and 25% of H_2O_2 solutions.

3.3 Results and discussion

Figure 3.1 illustrates the fabrication process of erGO/MnO₂ bilayer microtube micromotors with a customized plating cell (Figure 3.S1) to break the symmetry, the erGO/MnO₂ microtubes were fabricated by

sequential electrodeposition of GO and MnO_2 onto the inner walls of the pores of a gold coated polycarbonate membrane (Figure 3.S2) template. The microtubes were obtained after the membrane template was dissolved and removed. This micromotor structure consists of a graphene outer layer and a MnO_2 inner layer. The MnO_2 inner layer decomposes H_2O_2 into water and oxygen microbubbles. The ejection of microbubbles from one end of the microtubes will thrust the fluid inside the microtubes and behind the micromotors away, thus generating enough counterforce acting on the micromotors for its efficient self-propulsion. The propelling mechanism is similar to the propelling jet engines and rockets in the macroscopic world.

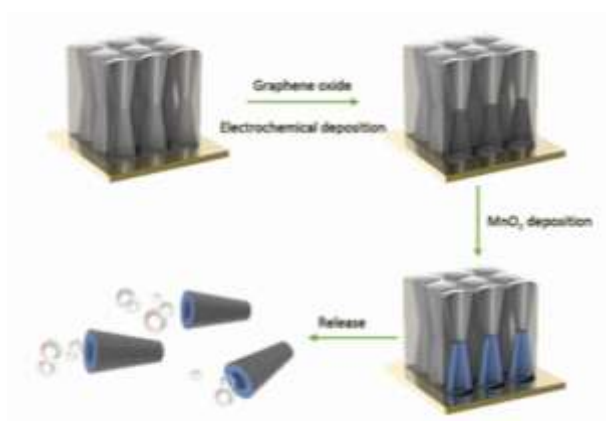


Figure 3.1. Schematic illustration of the fabrication procedure of the erGO/ MnO_2 bilayer microtube micromotors.

Figure 3.S1 is the real product picture of the assembled electrochemical plating cell with electrode stand and the electrodes. The aluminum foil is serving as the conductor to connect with the working electrode and platinum wire as the counter electrode and the Ag/AgCl electrode as the reference electrode.

By the observation of the pores density on the membrane, we could calculate the maximum output of micromotors one membrane could

fabricate. And the result is about 1×10^6 micromotors per membrane by one synthesis.

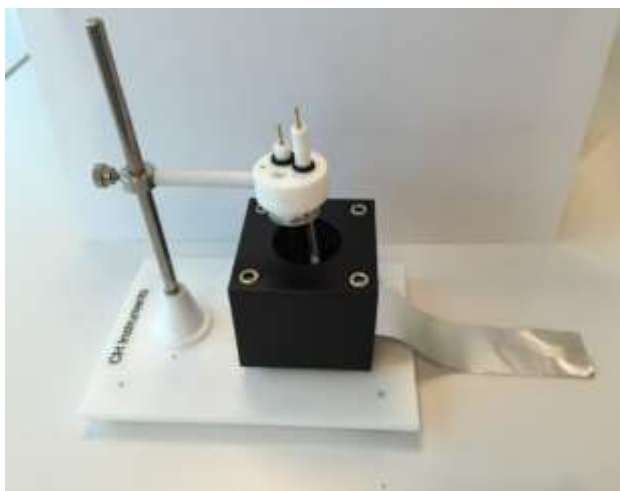


Figure 3.S1. Photograph of the assembled electrochemical plating cell.

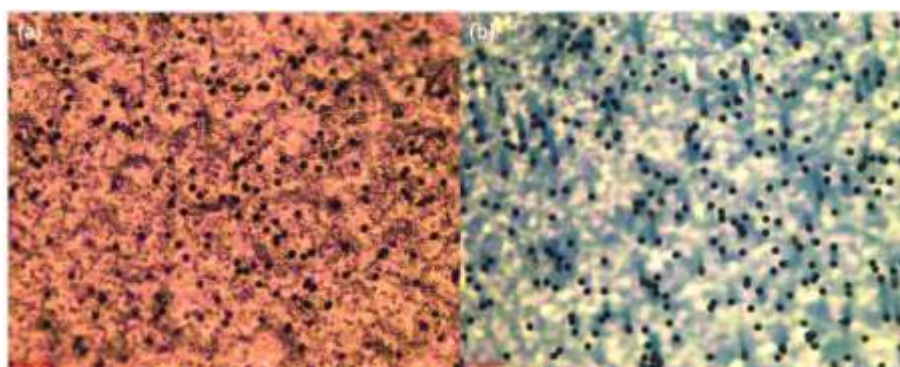


Figure 3.S2. Reflected light optical microscopy images of the polycarbonate membranes. (a) Gold coated side, (b) The uncoated side. Scale bar: 20 μm .

The first GO layer was electrochemically deposited onto the inner walls of the cyclopores of the polycarbonate membrane by the cyclic voltammetry method. Figure 3.2 shows the cyclic voltammograms acquired during the reduction process, $n = 2, 3,$ and 5 corresponding to the relative scan, respectively. GO was electrochemically reduced with a potential cycling at a rate of 50 mV s^{-1} from $+ 0.3$ to $- 1.5 \text{ V}$ for five cycles in a solution containing 0.1 mg mL^{-1} nano-sized GO for the construction

of the graphene outer layer. During the process, large quantities of oxygen functional groups on the surface of GO were removed and the sp^2 -carbon lattices were partially reconstructed.³⁹ The reduction of GO by cyclic voltammetry electrochemical reactions forms the outer erGO layer. This process increases the conductivity and hydrophobicity of the outer graphene layer. The increased conductivity favors the electrochemical reduction and deposition of graphene layer as well as the deposition of the MnO_2 layer. As a semiconductor material, the electrochemical plating fabrication of MnO_2 is not easy if the plating substrate is not a good conductor. The increased conductivity of the erGO outer layer is crucial for the deposition of the MnO_2 . As can be seen from Figure 3.2, the reduction peaks at about -1.0 V corresponding to the reduction of GO to the formation of a thin film of the outer graphene layer on the inner walls of the polycarbonate membrane pores. Most of the oxygen moieties on the surface of GO were removed during the cycling process, resulting in the lowering of the reduction current peaks as the scan number increases. The increased hydrophobic interaction of the graphene layers facilitates the aggregation of the graphene on the inner walls of the polycarbonate membrane pores.⁴⁰ Due to the increased sp^2 -carbons and the removal of the surface hydrophilic oxygen functional groups, the separated graphene layers tend to aggregate, thus forming the outer layer of the micromotors. Then, the formation of the MnO_2 tubular inner layer occurred. Compared with PEDOT, erGO can help the inner MnO_2 layer form a much rougher microporous microstructure due to the large remaining functional groups on the outer erGO layer serving as the nucleation sites, thus enhance the fuel decomposition by the inner MnO_2 layer.³² Chen's group showed the successful formation of the weakly crystalized γ - MnO_2 with different morphologies using an electrolyte containing 0.1 M manganese acetate and 0.1 M sodium sulfate.⁴¹ Due to the hydrolysis process occurred

immediately after the electrochemical deposition process, the produced manganese oxide usually exists as amorphous or weakly crystallized atom lattice. The hydrolysis of manganese hydroxide to form the manganese oxide usually results in the mixed-valence manganese oxides, such as MnO_2 , Mn_3O_4 , and MnO .⁴² Due to the lack of calcination of the electrochemical process to lower the energy state of the MnO_2 , the plated manganese oxide usually presents as amorphous or weakly crystallized structure. This amorphous or weakly crystallized structure is at its high-energy state compared to their crystallized counterpart. The high-energy state of the weakly crystallized or amorphous manganese oxide is sometimes beneficial for the catalysis process. This is also a contributing factor for the good motion behavior of the micromotors. As reported, this similar electrochemical plated MnO_2 for the energy-related applications could be presumed to weakly crystallized or amorphous $\gamma\text{-MnO}_2$.⁴³

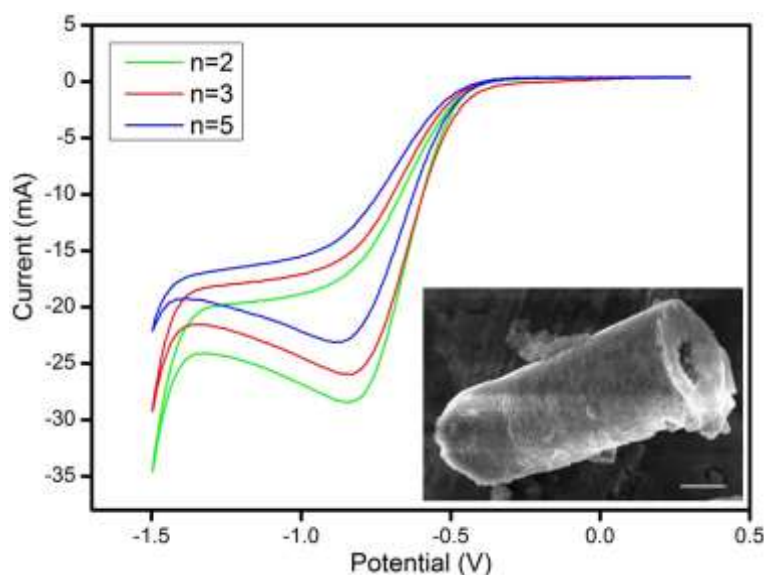


Figure 3.2. Cyclic voltammograms corresponding to the electrochemical reduction of GO, scans $n = 2$ (green line), $n = 3$ (red line) and $n = 5$ (blue line) and SEM image of the side view of an erGO/ MnO_2 bilayer microtube micromotor. Scale bar: 2 μm .

Figure 3.3 shows the scanning electron microscopy (SEM) images of the erGO/MnO₂ bilayer microtube micromotors. Figure 3.3a is a well-formed individual micromotor. This micromotor has an inner diameter of about 2 μm, an outer diameter of about 5 μm and a length of approximately 10 μm. The dimension of the microtube is restricted by the size of the pores on the template. Figure 3.3b demonstrates that the successful formation of large quantities of the microtube micromotors. (Figure. 3.S3) These microtubes have a length in the range from 4 to 12 μm and the average length of the microtubes is about 8 μm. Some of the microtubes are wrecked because the inner MnO₂ tubes are a brittle material and some of the microtubes are prone to be damaged during the washing, centrifugation and separation processes. As shown in Figure 3.3c, the morphology of the inner surface of a wrecked microtube shows a very rough, porous microstructure. This surface morphology is very similar to Chen's results,⁴¹ using the PS electrochemical deposition method. The electrochemical deposited MnO₂ forms a crossed needle-like nanostructure with 5-10 nm in diameter and 50-100 nm in length. Compared with the smooth inner surface, these microtubes with nanoscaled porous inner surface might have a larger surface area. The formation mechanism of MnO₂ could be explained by the following equation: $\text{Mn}^{2+} + 4\text{H}_2\text{O} \rightarrow \text{MnO}_2 + 4\text{H}^+ + 2\text{e}^-$.³⁴ Here, the erGO layer is serving as the anode to oxidize Mn²⁺ ions to its higher valence product MnO₂ at a potential of + 0.75V. The inner surface microstructure is responsible for the efficient motion behaviors of the micromotors due to its large surface area for catalytic H₂O₂ decomposition. The rough surface also favors the generation of the microbubbles. With a nanoscaled porous structure, it is much easier for the decomposition of H₂O₂ to generate oxygen molecules to aggregate and form the microbubbles. These oxygen bubbles formed inside the tubes and ejected from the opening thrust the

liquid behind the micromotors away continuously, thus generating the driving force for propelling. Figure. 3.3d is the energy dispersive X-ray spectrum (EDX) mapping of a micromotor. The carbon element is from the erGO outer layer. The uniform distribution of carbon element on the surface of the micromotors demonstrated the good coverage of the MnO₂ inner tubes by the erGO layer. The formation of erGO/MnO₂ bilayer microtubes can then be evidenced. The oxygen is from the erGO outer layer and the MnO₂ inner layer. The manganese is from the electrochemical plated MnO₂ inner layer only. The EDX results indicate that this micromotor only contains the oxygen, carbon, and manganese elements.

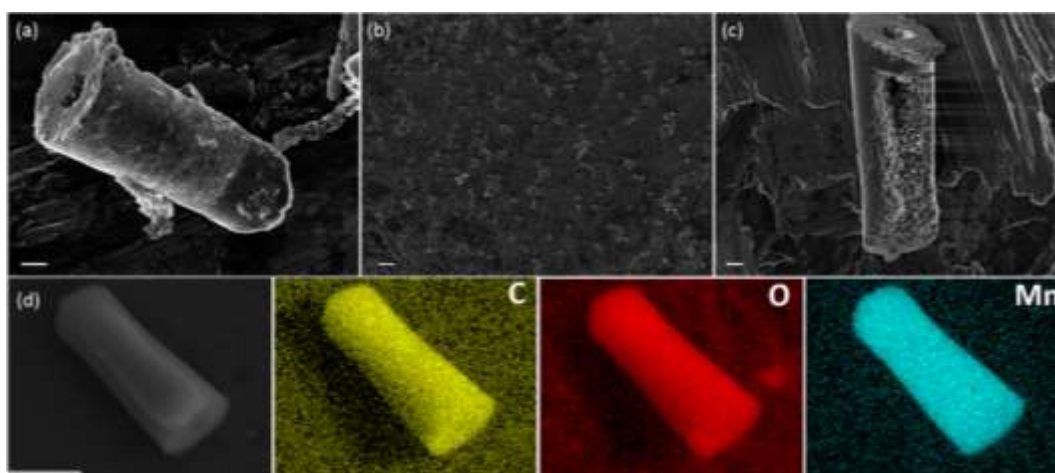


Figure 3.3. SEM images of the erGO/MnO₂ micromotors (a) image of a micromotor, (b) image of large quantities of micromotors, (c) image of a wrecked micromotor. (d) EDX spectrum elemental mapping of a micromotor, illustrating the distribution of carbon (yellow), oxygen (red) and manganese (blue). Scale bars: (a), (c) 2 μm , (b) 20 μm , and (d) 5 μm .

The preparation of this sample is to drop a volume of 2 μL of the micromotors dispersion on the aluminum stub. The micromotors dispersion contains about $10^6/\text{mL}$.

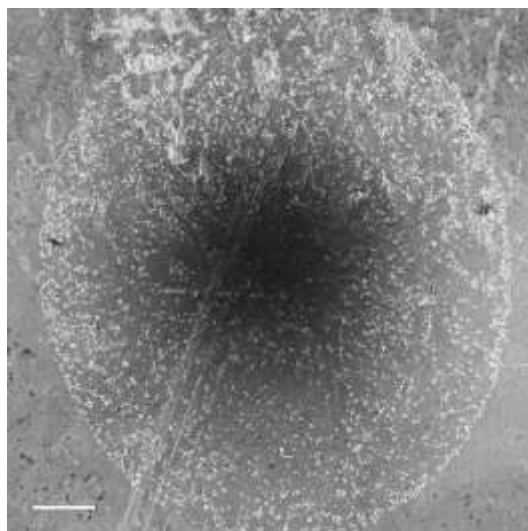


Figure 3.S3. SEM image of a drop of 2 μL of micromotors on the aluminum stub. Scale bar: 200 μm .

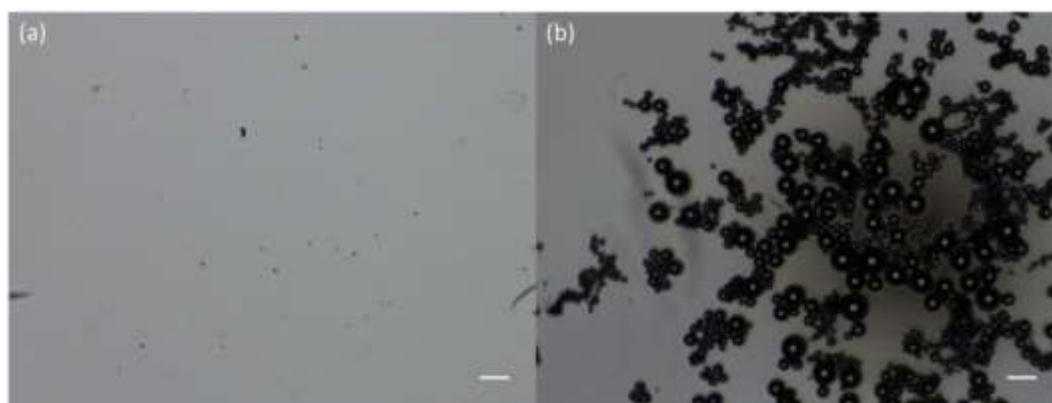


Figure 3.S4. Optical microscopy images of the micromotors (a) before H_2O_2 added, (b) after H_2O_2 fuel added, images were extracted from Video S2. Scale bar: 100 μm .

As shown in Figure 3.4, XPS spectra survey further reveals the presence of carbon (C 1s peak), oxygen (O 1s peak) and manganese (Mn 2p peak) in the erGO/ MnO_2 micromotors. The peaks of high-resolution C 1s spectra (Figure 3.4b) and O 1s spectra (Figure 3.4c) correspond to the binding energy of various functional groups such as C-C/C-H/C=C, C-OH, C=O, and O-C=O, revealing the nature of the covalent bonds of oxygen atoms and carbon atoms (See Table 3.S1). The ratio of all carbon-oxygen

functional groups to all carbon species is about 50%, which denotes the degree of oxidation of the outer layer of erGO/MnO₂ micromotors. The degree of oxidation of erGO/MnO₂ micromotors is slightly larger than the graphene-based microbots fabricated by Vilela et al.⁴⁴. This may be because that the second anodic deposition of the MnO₂ layer at + 0.75 V could partially oxidize the formerly formed erGO layer. Abundant carbonyl and carboxyl groups are present on the surface of erGO/MnO₂ micromotors which is considered very important for the adsorption of pollutants as well as further surface modification of the micromotors for detection and sensing applications. Figure 3.4c shows the peak at 530 eV as the characteristic of the oxygen in metal oxides. The oxidation state of Mn can be examined by the Mn 2p high-resolution XPS spectra (Figure 3.4d). The peaks observed at a binding energy of 642.5 and 652.9 eV were attributed to the Mn 2p XPS lines with the spin-orbit splitting of 11.4 eV between Mn 2p_{3/2} and Mn 2p_{1/2}. The results are in agreement with previously reported values.⁴⁵ The Mn 2p_{3/2} peak was located at 642.5 eV, which indicated that the main oxidation state of Mn in all the manganese oxide is Mn⁴⁺. The XPS spectra of the erGO/MnO₂ micromotors further confirms the oxygen functional groups on the surface of the micromotors and the main component for the catalyst part is MnO₂.

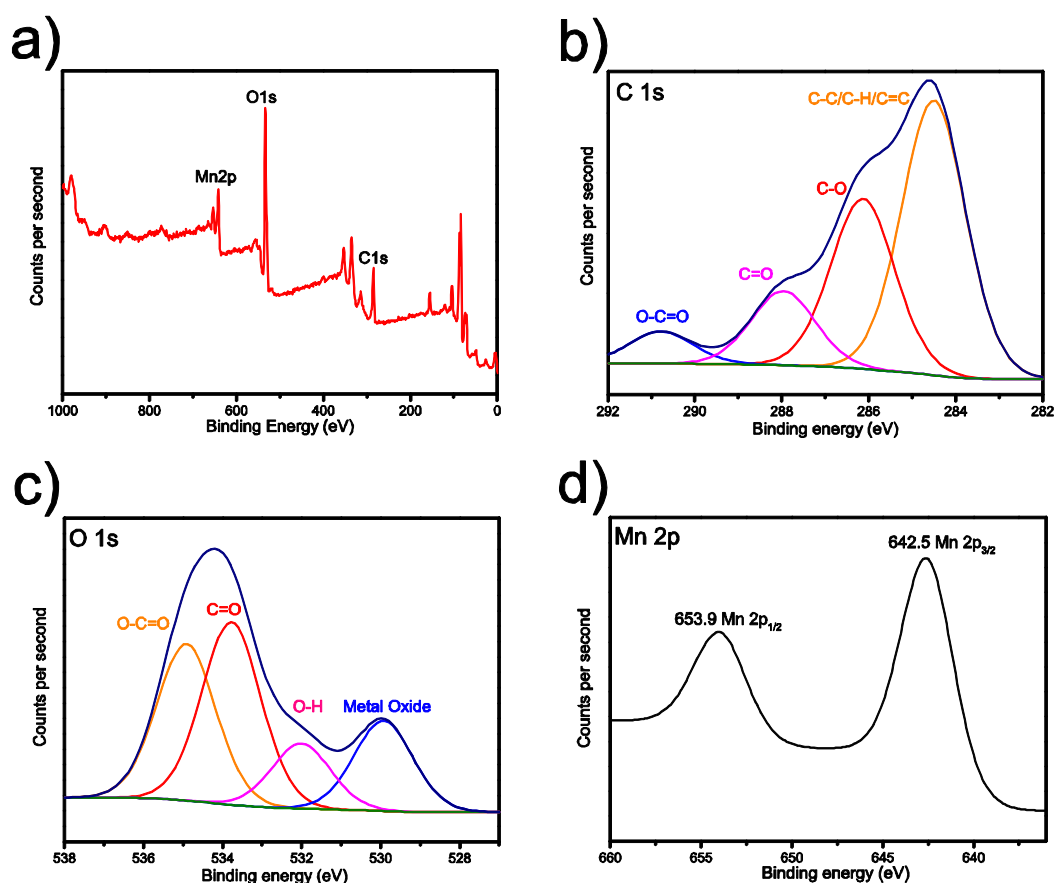


Figure 3.4. XPS spectra survey of erGO/MnO₂ micromotors, (a) wide scan. (b) High-resolution C 1s spectra. (c) High-resolution O 1s spectra. (d) High-resolution Mn 2p spectra.

The surfactants are known to increase the wetting, facilitate the bubble formation, and stabilize the microbubbles, thus enhance the motion behaviors of the bubble propelled MNMs.^{46, 47} Besides the increased bubble formation, increased oxygen production also plays a key role in the propulsion of bubble-propelled MNMs.²⁰ The SDS has been commonly used as a surfactant for the propulsion of micromotors. All the motion behaviors were observed using 1% SDS as a surfactant to lower the surface tension and enhance the wetting of the micromotors for efficient bubble generation. Upon the addition of fuel to the petri dish, the micromotors start to move continuously (see Figure. 3.S4). Figure 3.5 displays time-lapse images, taken from the motion behavior Video S1, for

the motion of the erGO/MnO₂ bilayer microtubes micromotors over a 5s period at 1s intervals in 4% H₂O₂ solution. These images show a trail of oxygen bubbles generated and released behind the motion micromotor. The bubbles show clearly the trajectory of the micromotors. These micromotors show irregular trajectory because the force generated on the MnO₂ inner surface of the micromotors is asymmetrically distributed. Video S2 shows the motion behaviors of micromotors in 15% of H₂O₂ fuel. It shows a much higher speed. The generation of microbubbles can be explained by the following equation: $\text{H}_2\text{O}_2 \rightarrow \text{H}_2\text{O} + \text{O}_2$. Here, MnO₂ is the catalyst for H₂O₂ decomposition. The porous inner surface with a sheet-like microstructure offers plenty of active sites for the catalytic decomposition of H₂O₂. It also provides the perfect place for the generated oxygen molecules to aggregate and form the microbubbles. The outer graphene layer blocks the contact of H₂O₂ with the outer surface of the plated MnO₂ tubes, making the oxygen bubbles generated at the inner surface of the microtubes only. This architecture is the reason for its robust motion behaviors. The SDS in the liquid serves as the surfactant for the easiness of the wetting of the micromotor surface by the solution and facilitates the generation of the microbubbles. The oxygen bubbles generated bounce off the liquid behind the micromotors continuously, resulting in the generation of the net force for propulsion. The micromotor is self-propelled at a speed of nearly 200 $\mu\text{m s}^{-1}$, which corresponds to a relative speed of 25 body-lengths s^{-1} , considering the average length of the micromotors of approximately 8 μm .

Table 3.S1. Various functional groups identified on the surface of erGO/MnO₂ micromotors

Spectra	Group	Position	at. %
C 1s	C-C/C-H/C=C	284.51	49.84
C 1s	C-O	286.14	30.86
C 1s	C=O	287.97	13.48
C 1s	O-C=O	290.79	5.81
O 1s	Metal Oxide	529.94	18.22
O 1s	O-H	532.02	13.18
O 1s	C=O	533.78	36.94
O 1s	O-C=O	534.92	31.66

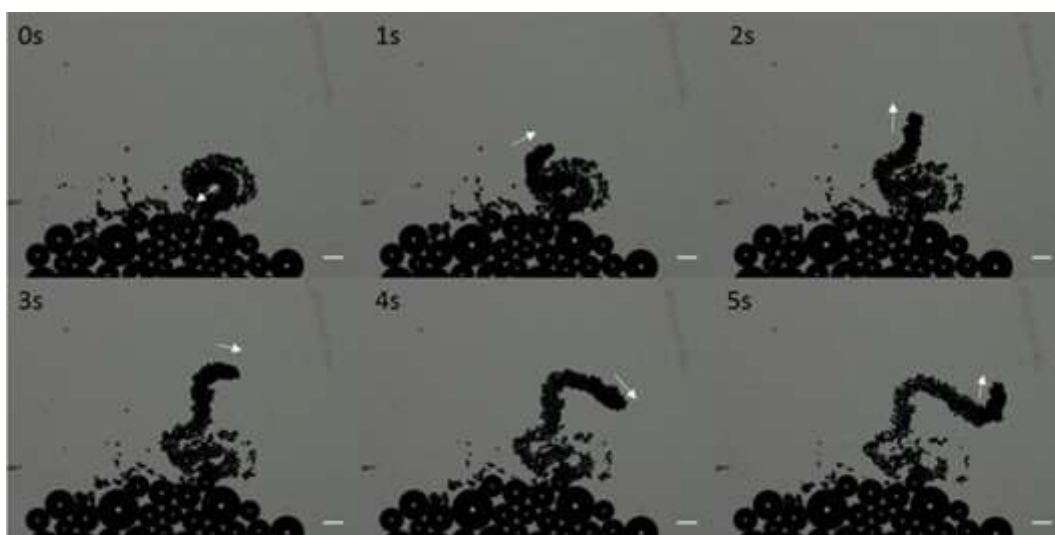


Figure 3.5 Time-lapse images depicting efficient propulsion of an erGO/MnO₂ bilayer micromotors over 5s at time intervals of 1s in 4% H₂O₂ and 1% SDS. Scale bar, 100 μm.

Figure 3.6 shows that the concentration of H₂O₂ fuel strongly influences the velocity of the erGO/MnO₂ micromotors. Below 2% of H₂O₂ fuel solutions, few micromotors show motion behavior, due to the low frequency of microbubbles generation and the weak propelling force generated. At 3% of H₂O₂ concentration, these micromotors start to show efficient motion behavior at an average speed of 77.2 μm s⁻¹, corresponding to a relative speed over 9.6 body-lengths s⁻¹. The speed of the micromotors increases to 210.4 (± 80.4) μm s⁻¹ at 5% H₂O₂, equals to a speed of 29.3 (± 10.0) body-lengths s⁻¹. Fuel depletion would result in the speed decrease when the concentration is below 5% H₂O₂ as time goes by. After the micromotors stopped moving, the motion behaviors could be reinitiated after extra fuel is added, which demonstrates the good lifetime of these micromotors. The speed of the micromotors continues to increase as the concentration of H₂O₂ fuel solution increases. At 15% of the H₂O₂ solution, the average speed of the micromotors reaches its maximum of 466.4 (± 155.3) μm s⁻¹, about 58.3 (± 19.4) body-lengths s⁻¹. The maximum speed of an individual micromotor could exceed 700 μm s⁻¹.

The speed of the graphene/MnO₂ bilayer microtube micromotors greatly increases over the entire range of the H₂O₂ fuel (3% - 15%) resulting from the higher pressure generated by the propelling oxygen microbubbles. Since the fluid cannot flow freely through the bilayer microtubes, the drag force of the micromotors could be estimated roughly using the Stokes' drag force theory.^{3, 48}

$$F_d = \frac{2\pi\mu LU}{\ln(L/a) - 1/2}$$

Where F_d is the fluid resistance, U is the speed of the micromotor (700 $\mu\text{m s}^{-1}$), μ is the fluid dynamic viscosity (1.01 mPa s, equal to $1.01 \times 10^{-3} \text{ N m}^{-2} \text{ s}$), L is the length (8 μm) and a is the radius (2.5 μm) of the micromotor. The calculated maximum drag force of this micromotor, 54 pN, is enough to transport large cargos such as proteins and cells. The performance of this newly synthesized erGO/MnO₂ micromotors is comparable to the conducting polymer/MnO₂ bilayer microtubes micromotor developed by Safdar et al.^{32, 33} in terms of fuel concentration range and speed. While they state that the electrochemical fabricated MnO₂ based micromotors show motion behaviors from above 5% H₂O₂ fuel solutions, we find that the erGO/MnO₂ micromotors show efficient motion from above 3% of H₂O₂. The erGO/MnO₂ micromotors will have more practical applications where a high H₂O₂ fuel concentration is not desired. The comparable performance of these two kinds of micromotors is because both have the same geometry size and electrochemical deposited MnO₂ as the catalyst for H₂O₂ decomposition. From the motion videos, we can see that their motion behaviors are also quite similar, but the graphene-based micromotors could utilize H₂O₂ fuel solution down to 3%. The graphene-based MnO₂ propelled micromotors could be used as a motion platform to perform diverse tasks. For example, the outer graphene surface with

partial oxygen functional groups could be used to functionalize this motion based platform to perform biomedical related applications, such as sensing of chemicals, cargo transportation in the cellular environment, and guided anti-cancer drug delivery.⁴⁹ Beyond biological applications, MnO_2 is also a useful material in environmental remediation. The motion enhanced stirring effect of the catalytic degradation reactions will not only show great promise to accelerate the catalytic degradation of organic pollutants but also the enhanced adsorption capability of aquatic pollutants. The later-on modification of the MnO_2 micromotors and the related environmental based applications are also being conducted in our group.

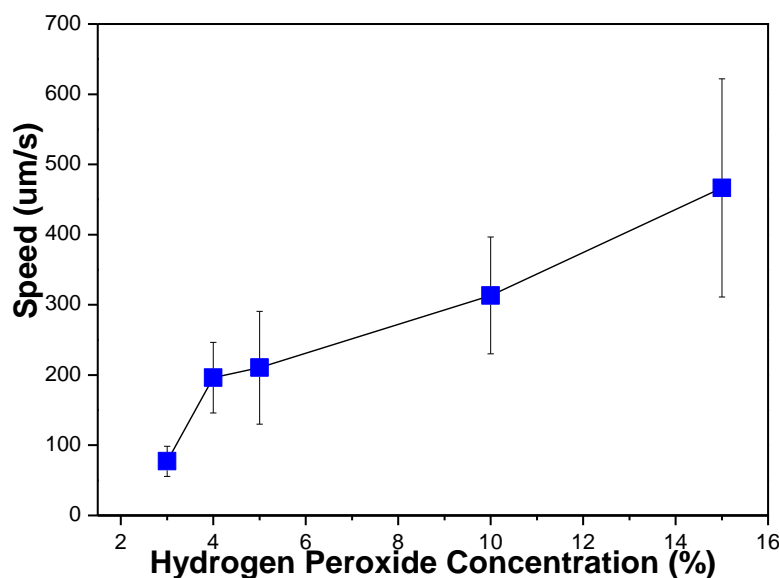


Figure 3.6 The average speed of erGO/MnO_2 micromotors at different fuel concentrations ($n = 50$). Experiments were conducted in the presence of 1% SDS as the surfactant.

3.4 Conclusions

In the present study, we demonstrated that a highly efficient erGO/MnO_2 bilayer microtubes micromotor could be prepared by a simple, template-assisted electrochemical process. The resulting erGO/MnO_2 micromotor has a micro-sized tubular bilayer structure with erGO as the outer layer

and electrochemically deposited MnO₂ as the inner layer. The inner surface of the micromotor has a rough, nanoscale porous microstructure which accounts for the highly efficient catalysis performance over the decomposition of H₂O₂. The erGO/MnO₂ tubular micromotors can move at a high average speed from 77.2 to 466.4 μm s⁻¹ at H₂O₂ fuel concentrations from 3% to 15%. Some of the individual micromotors could show a motion behavior with a velocity larger than 700 μm s⁻¹ in 15% H₂O₂ solutions. The micromotors only contain the low-cost MnO₂ and metal-free graphene materials, holding promises for further environmental based and biomedical applications. The attractive properties of the micromotors, along with their easy synthesis, good motion behaviors, low cost, and robust motion in wide fuel concentration range promise the considerable potentials for biomedical applications as well as environmental remediation.

References

1. Sanchez S, Soler L, Katuri J. Chemically powered micro- and nanomotors. *Angew. Chem. Int. Ed.* 2015; 54(5):1414-1444.
2. Li J, Rozen I, Wang J. Rocket science at the nanoscale. *ACS Nano.* 2016; 10(6):5619-5634.
3. Gao W, Sattayasamitsathit S, Orozco J, Wang J. Highly efficient catalytic microengines: Template electrosynthesis of polyaniline/platinum microtubes. *J. Am. Chem. Soc.* 2011; 133(31):11862-11864.
4. Singh VV, Wang J. Nano/micromotors for security/defense applications. A review. *Nanoscale.* 2015; 7(46):19377-19389.
5. Martin A, Jurado-Sanchez B, Escarpa A, Wang J. Template electrosynthesis of high-performance graphene microengines. *Small.* 2015; 11(29):3568-3574.

6. Lin X, Wu Z, Wu Y, Xuan M, He Q. Self-propelled micro-/nanomotors based on controlled assembled architectures. *Adv. Mater.* 2016; 28(6):1060-1072.
7. Wu Z, Lin X, Wu Y, et al. Near-infrared light-triggered "on/off" motion of polymer multilayer rockets. *ACS Nano.* 2014; 8(6):6097-6105.
8. Singh VV, Martin A, Kaufmann K, de Oliveira SDS, Wang J. Zirconia/graphene oxide hybrid micromotors for selective capture of nerve agents. *Chem. Mater.* 2015; 27(23):8162-8169.
9. Mou FZ, Pan D, Chen CR, et al. Magnetically modulated pot-like MnFe_2O_4 micromotors: Nanoparticle assembly fabrication and their capability for direct oil removal. *Adv. Funct. Mater.* 2015; 25(39):6173-6181.
10. Palacci J, Sacanna S, Vatchinsky A, Chaikin PM, Pine DJ. Photoactivated colloidal dockers for cargo transportation. *J. Am. Chem. Soc.* 2013; 135(43):15978-15981.
11. Wu Z, Wu Y, He W, et al. Self-propelled polymer-based multilayer nanorockets for transportation and drug release. *Angew. Chem. Int. Ed.* 2013; 52(27):7000-7003.
12. Hao J, Yang W, Zhang Z, Tang J. Surfactant-assisted fabrication of 3d prussian blue-reduced graphene oxide hydrogel as a self-propelling motor for water treatment. *Nanoscale.* 2015; 7(23):10498-10503.
13. Soler L, Magdanz V, Fomin VM, Sanchez S, Schmidt OG. Self-propelled micromotors for cleaning polluted water. *ACS Nano.* 2013; 7(11):9611-9620.
14. Dey KK, Bhandari S, Bandyopadhyay D, Basu S, Chattopadhyay A. The pH taxis of an intelligent catalytic microbot. *Small.* 2013; 9(11):1916-1920.
15. Garcia M, Orozco J, Guix M, et al. Micromotor-based lab-on-chip immunoassays. *Nanoscale.* 2013; 5(4):1325-1331.

16. Liu M, Liu L, Gao W, et al. A micromotor based on polymer single crystals and nanoparticles: Toward functional versatility. *Nanoscale*. 2014; 6(15):8601-8605.
17. Dong B, Zhou T, Zhang H, Li CY. Directed self-assembly of nanoparticles for nanomotors. *ACS Nano*. 2013; 7(6):5192-5198.
18. Su Y, Ge Y, Liu L, et al. Motion-based pH sensing based on the cartridge-case-like micromotor. *ACS Appl. Mater. Inter.* 2016; 8(6):4250-4257.
19. Gai MY, Frueh J, Si TY, et al. The collision phenomena of Janus polymer micro-plate motors propelled by oscillating micro-bubbles. *Colloid Surface A*. 2016; 510:113-121.
20. Gai M, Frueh J, Hu N, et al. Self-propelled two dimensional polymer multilayer plate micromotors. *Phys. Chem. Chem. Phys.* 2016; 18(5):3397-3401.
21. Manjare M, Yang B, Zhao YP. Bubble driven quasioscillatory translational motion of catalytic micromotors. *Phys. Rev. Lett.* 2012; 109(12):128305.
22. Yao K, Manjare M, Barrett CA, et al. Nanostructured scrolls from graphene oxide for microjet engines. *J. Phys. Chem. Lett.* 2012; 3(16):2204-2208.
23. Zhao G, Sanchez S, Schmidt OG, Pumera M. Poisoning of bubble propelled catalytic micromotors: The chemical environment matters. *Nanoscale*. 2013; 5(7):2909-2914.
24. Teo WZ, Zboril R, Medrik I, Pumera M. Fe⁰ nanomotors in ton quantities (10²⁰ units) for environmental remediation. *Chem-Eur. J.* 2016; 22(14):4789-4793.
25. Teo WZ, Wang H, Pumera M. Beyond platinum: Silver-catalyst based bubble-propelled tubular micromotors. *Chem. Commun.* 2016; 52(23):4333-4336.

26. Sengupta S, Patra D, Ortiz-Rivera I, et al. Self-powered enzyme micropumps. *Nat. Chem.* 2014; 6(5):415-422.
27. Wani OM, Safdar M, Kinnunen N, Janis J. Dual effect of manganese oxide micromotors: Catalytic degradation and adsorptive bubble separation of organic pollutants. *Chem-Eur. J.* 2016; 22(4):1244-1247.
28. Liu DW, Garcia BB, Zhang QF, et al. Mesoporous hydrous manganese dioxide nanowall arrays with large lithium ion energy storage capacities. *Adv. Funct. Mater.* 2009; 19(7):1015-1023.
29. Zhang H, Cao G, Wang Z, et al. Growth of manganese oxide nanoflowers on vertically-aligned carbon nanotube arrays for high-rate electrochemical capacitive energy storage. *Nano Lett.* 2008; 8(9):2664-2668.
30. Wang H, Zhao G, Pumera M. Beyond platinum: Bubble-propelled micromotors based on Ag and MnO₂ catalysts. *J. Am. Chem. Soc.* 2014; 136(7):2719-2722.
31. Feng XM, Zhang Y, Li Y, et al. Graphene-based highly efficient micromotors. *Chem. Lett.* 2015; 44(3):399-401.
32. Safdar M, Wani OM, Janis J. Manganese oxide-based chemically powered micromotors. *ACS Appl. Mater. Inter.* 2015; 7(46):25580-25585.
33. Safdar M, Minh TD, Kinnunen N, Janis J. Manganese oxide based catalytic micromotors: Effect of polymorphism on motion. *ACS Appl. Mater. Inter.* 2016; 8(47):32624-32629.
34. Wang LL, Chen J, Feng XM, et al. Self-propelled manganese oxide-based catalytic micromotors for drug delivery. *RSC Adv.* 2016; 6(70):65624-65630.
35. Singh AK, Mandal TK, Bandyopadhyay D. Magnetically guided chemical locomotion of self-propelling paperbots. *RSC Adv.* 2015; 5(79):64444-64449.

36. Abramoff MD, Magalhães PJ, Ram SJ. Image processing with imageJ. *Biophotonics international*. 2004; 11(7):36-42.
37. Schneider CA, Rasband WS, Eliceiri KW. Nih image to imageJ: 25 years of image analysis. *Nat. Methods*. 2012; 9(7):671-675.
38. Schindelin J, Arganda-Carreras I, Frise E, et al. Fiji: An open-source platform for biological-image analysis. *Nat. Methods*. 2012; 9(7):676-682.
39. Shao YY, Wang J, Engelhard M, Wang CM, Lin YH. Facile and controllable electrochemical reduction of graphene oxide and its applications. *J. Mater. Chem*. 2010; 20(4):743-748.
40. Martin A, Hernandez-Ferrer J, Vazquez L, Martinez MT, Escarpa A. Controlled chemistry of tailored graphene nanoribbons for electrochemistry: A rational approach to optimizing molecule detection. *RSC Adv*. 2014; 4(1):132-139.
41. Chou SL, Cheng FY, Chen J. Electrodeposition synthesis and electrochemical properties of nanostructured gamma-MnO₂ films. *J. Power Sources*. 2006; 162(1):727-734.
42. Wei W, Cui X, Chen W, Ivey DG. Manganese oxide-based materials as electrochemical supercapacitor electrodes. *Chem. Soc. Rev*. 2011; 40(3):1697-1721.
43. Zhao H, Liu FF, Han GY, et al. Co-electrodeposition of MnO₂/graphene oxide coating on carbon paper from phosphate buffer and the capacitive properties. *J. Solid State Electr*. 2014; 18(2):553-559.
44. Vilela D, Parmar J, Zeng Y, Zhao Y, Sanchez S. Graphene-based microbots for toxic heavy metal removal and recovery from water. *Nano Lett*. 2016; 16(4):2860-2866.
45. Xie XF, Gao L. Characterization of a manganese dioxide/carbon nanotube composite fabricated using an in situ coating method. *Carbon*. 2007; 45(12):2365-2373.

46. Simmchen J, Magdanz V, Sanchez S, et al. Effect of surfactants on the performance of tubular and spherical micromotors - a comparative study. *RSC Adv.* 2014; 4(39):20334-20340.
47. Wang H, Zhao GJ, Pumera M. Crucial role of surfactants in bubble-propelled microengines. *J. Phys. Chem. C.* 2014; 118(10):5268-5274.
48. Li Y, Wu J, Xie Y, Ju H. An efficient polymeric micromotor doped with Pt nanoparticle@carbon nanotubes for complex bio-media. *Chem. Commun.* 2015; 51(29):6325-6328.
49. Wu Z, Gao C, Frueh J, Sun J, He Q. Remote-controllable explosive polymer multilayer tubes for rapid cancer cell killing. *Macromol. Rapid Comm.* 2015; 36(15):1444-1449.

Every reasonable effort has been made to acknowledge the owners of copyright material. I would be pleased to hear from any copyright owner who has been omitted or incorrectly acknowledged.

Chapter 4. High-Speed Graphene/Ag-MnO₂ Micromotors at Low Peroxide Levels by Cathodically Electrochemical Deposition

Abstract

Platinum (Pt) free micro/nanomotors (MNMs) using a low content of fuels are highly desired for many applications. Herein, we demonstrate that cathodic electro-fabrication can produce doped MnO₂ based microtubes and microrods as highly efficient MNMs in hydrogen peroxide (H₂O₂) as low as 0.2%. The speed of graphene/Ag-MnO₂ micromotors could be smartly regulated using a surfactant and the maximum speed of an individual micromotor exceeds 1.3 mm s⁻¹ in 0.5% H₂O₂. The propelling force and output power of the micromotors are 3.4 and 10 times as high as those of the best Pt-based micromotors reported. These Ag-MnO₂ based micromotors are envisioned to be a great promise for practical applications from biomedical to environmental decontamination.

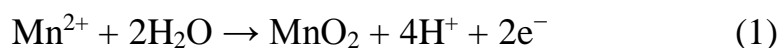
4.1 Introduction

Self-propelled micro/nanomotors (MNMs) have attracted increasing attention because of their wide potential applications from biomedical drug delivery to environmental cleaning.¹⁻¹⁰ MNMs show diverse applications in sensing trace metals,¹¹ selective capture of nerve agents,¹² cargo delivery and release,¹³⁻¹⁶ minimally invasive surgery,¹⁷ diagnostics,¹⁸ environmental monitoring and remediation,¹⁹⁻²² and bioimaging/biosensing.²³⁻²⁵ MNMs based on self-electrophoresis or self-diffusiophoresis mechanism usually exhibit a low speed and weak propelling force.^{26,27} To surpass the limitations, bubble-propelled catalytic MNMs were developed because of their good motion behaviors at a much wider fuel content.²⁸ Up to now, the majority of the MNMs are relying on noble metal platinum (Pt) as the catalyst to decompose H₂O₂ for propelling.^{21, 29-32} The fastest catalytic micromotors are Pt-based tubular microengines,³³ and a Pt-catalyzed rolled-up microjet achieved a high speed of 10 mm s⁻¹ in 5% H₂O₂ at 37 °C.³⁴ Although the Pt-catalyzed MNMs demonstrated the best motion behaviors, the drawbacks of scarcity, high-cost, and susceptibility of deactivation hindered their applications.^{35, 36} A number of other catalysts, such as iridium,³⁷ silver,³⁸ palladium,³⁹ and enzymes^{40, 41} have been tested for the construction of MNMs, but each of them possesses its own limitations and drawbacks and none of them is as good as Pt.⁴²

Recently, MnO₂ based micromotors were developed, but they suffered from a high fuel concentration or low speed due to the inferior catalytic activity.³⁹ Researchers have demonstrated the motion behaviors of MnO₂ based micromotors in biological media⁴³ and salt-rich environment.⁴⁴ The robust nature of MnO₂ is the key to solve the deactivation of Pt-based MNMs. Pumera's group demonstrated that commercial MnO₂ particles

showed motion behaviors of $120 \mu\text{m s}^{-1}$ in 21% H_2O_2 .³⁸ Safdar et al.⁴⁴ developed a MnO_2 hollow particle micromotor with the maximum speed of $1625 \mu\text{m s}^{-1}$ in 10% H_2O_2 . These MnO_2 based MNMs require a much high concentration of fuels. Hence, exploration of new synthesis and modification methods to make MnO_2 suitable for low fuel levels with fast speeds becomes highly desirable.

Electrochemical production of MnO_2 can be realized by anodic oxidation⁴⁵ and cathodic reduction electrodeposition.⁴⁶ For the anodic electrodeposition, electro-oxidation of Mn^{2+} occurs on the anode surface, shown as follows.



For the cathodic electrodeposition process, the electroreduction of high valence Mn (VII) species takes place on the cathode surface.



The anodic electrodeposition and chemical reaction routes have been used exclusively to construct MnO_2 based MNMs. However, for fabrication of a heterogeneous structured metal/ MnO_2 MNMs, the anodic electrodeposition cannot avoid further oxidation and dissolution of the metal. Cathodic electrodeposition of MnO_2 is a reduction process, which can circumvent the drawback successfully. Thus, it is possible to obtain various metal/ MnO_2 hybrid MNMs. Despite the great advantages, to the best of our knowledge, no one has ever reported the synthesis of MnO_2 based MNMs by cathodic electrosynthesis. What is more, no one has ever explored the synthesis of modified MnO_2 based MNMs.

Herein, we attempted the cathodic electroreduction for the synthesis of MnO₂ based MNMs. We demonstrate that silver modified MnO₂ micromotors could also be fabricated by cathodic co-deposition and silver modification is able to significantly enhance the performance of MnO₂ based micromotors. Ag-MnO₂ micromotors will produce benefits for environmental applications as the silver is usually used as a disinfection agent in water treatment. The manganese dioxide is widely applied as the catalyst in advanced oxidation processes for degradation of organic pollutants. In this work, graphene/Ag-MnO₂ micromotors demonstrate much better motion behaviors at 0.2% H₂O₂ with a remarkable high speed of $88 \pm 46 \mu\text{m s}^{-1}$ and a speed up to $1237 \pm 205 \mu\text{m s}^{-1}$ in 10% H₂O₂. By adjusting a surfactant content from 0.1% to 5% in 0.5% H₂O₂, the average speed of graphene/Ag-MnO₂ tubular micromotors could be regulated from 0 to $572 \pm 315 \mu\text{m s}^{-1}$. The surfactant regulation of speed in a wide span as well as the high speeds of the graphene/Ag-MnO₂ at a very low content of fuel suggest that the Ag-MnO₂ based MNMs, along with the simple cathodic electrodeposition, pave a new strategy for fabrication of low-cost and high-performance MNMs and their use at a very low fuel concentration.

4.2. Experimental section

4.2.1 Materials and reagents

Potassium permanganate, silver nitrate, sodium sulfate, ethanol, dichloromethane, sodium dodecyl sulfate (SDS), and sulfuric acid (98%) were purchased from Sigma-Aldrich. H₂O₂ (30%) was purchased from ROWE Scientific Australia. Aluminum oxide paste was purchased from Kemet, NSW, Australia. Porous polycarbonate (PC) membranes with an average pore diameter of 5 μm were purchased from Whatman Inc., NY,

USA. Ultrapure water (Milli-Q) was used in all experiments. Nano-sized graphene oxide (GO) was purchased from graphene supermarket, New York, USA.

4.2.2 Fabrication of MnO₂ based micromotors

Graphene wrapped MnO₂ based micromotors were fabricated using a template-assisted electrochemical deposition protocol. A cyclopore polycarbonate membrane containing 5 μm conical-shaped micropores (Whatman, NY, USA) was employed as the template. An 80 nm of gold film was first deposited on one side of the porous membranes to serve as the working electrode using an Emitech K950X gold evaporator and performed at room temperature under a high vacuum of below 1×10^{-3} mBar at a direct current of 6 A. The deposition rate was about 1 nm s^{-1} . A customized plating cell was used in all electrochemical deposition processes. The membrane was assembled in a self-designed plating cell with an aluminum foil serving as the contact for the working electrode. Electrochemical deposition was carried out using an electrochemical workstation (Zennium Zahner, Germany). A Pt wire and Ag/AgCl with 3M KCl were used as the counter and reference electrodes, respectively. A mixed solution of 0.1 mg mL^{-1} nano-sized graphene oxide in 0.5 M of Na₂SO₄ and 0.1 M H₂SO₄ was prepared as the electrolyte for the electrochemical growth of graphene outer layer. The graphene oxide in the solution was reduced by a cyclic voltammetry (CV) method from 0.3 to -1.5 V for five cycles. After washing with 10 mL of ultrapure water for three times, the inner MnO₂ layer was deposited using a galvanostatic (GS) method at a current of -1 or -1.5 mA for 20 min, respectively, which equals to 1.2 and 1.8 C of charge transferred. For the cathodic reduction deposited MnO₂ inner layer, 1.2 C of charge transfer is the optimal value for the synthesis of graphene wrapped MnO₂ based microtubes. Galvanostatic

deposition at -1.5 mA for 20 min results in the total closure of the microtubes, forming the graphene wrapped microrods architecture. For MnO₂ deposition, the electrolyte solution was 20 mM KMnO₄. For silver modified MnO₂ based micromotors, the solution contains 2 mM of AgNO₃ and 20 mM KMnO₄. Following the electroreduction deposition, the gold layers were removed by hand polishing with alumina slurry. Then the templates were dissolved in dichloromethane for 15 min to release micromotors. Finally, the micromotors were collected by centrifugation at 7000 rpm for 3 min while being repeatedly washed with dichloromethane, ethanol and ultrapure water for three times each. The ultrasonication process was carried out using a Unisonics ultrasonication cleaner (Model FXP12D), and the centrifugation was carried out using an Eppendorf centrifuge 5430. All the micromotors were stored in ultrapure water at room temperature for further use.

4.2.3 Characterization of the micromotors

Scanning electronic microscopy (SEM/EDS) analysis was conducted using a Zeiss 1555 VP-FESEM with a field emission electron gun and the Oxford EDS detector operated by the Aztec software. SEM images were taken at the acceleration voltages from 2 to 5 kV. EDS analysis was taken using the coupled Oxford detector of the microscope and operated by the Aztec software at an acceleration voltage of 15 kV. X-ray photoelectron spectroscopy (XPS) was carried out on a thermos ESCALAB 250 XPS microscope with monochromatic Al-K α X-rays at a photon energy of 1486.7 eV. The measurement was carried out using a Kratos AXIS Ultra DLD system under UHV conditions with a base pressure of less than 1×10^{-9} mBar. The spectra were acquired with the pass energy of 20 eV and fitted using CasaXPS software. All the spectra were calibrated to yield a primary C 1s component at 284.6 eV with the Shirley background, and the

component fitting was applied by Voigt functions with 30% Lorentzian component.

4.2.4 Motion behavior observation

A transparent plastic petri dish (Part No. P35G-1.5-10-C, Mat Tek Corporation, MA, USA) with the holed bottom covered by a thin glass slide was used as the container to prepare different fuel concentrations for observation of motion behavior. A 10 mm diameter bottom hole of the 35 mm diameter plastic petri dish was covered by a thin glass slide, which formed a shallow well-like hollow structure with a volume of approximately 75-80 μL . SDS was used as the surfactant for motion behavior observation in all experiments. Optical microscopy videos and images were obtained using an Olympus IX81 inverted microscope with a Nikon digital sight DS-2Mv camera connected to a computer and operated by the Nikon NIS-Elements software. Motion videos were recorded at 12.5 frames per second using a 4X objective. The time interval between two frames is 0.08 s. For each of the data points in the speed profile figures, at least 50 measurements were taken into account. The error bars stand for the standard deviation. To minimize the effect of fuel depletion, only the videos recorded at the first 5 minutes after fuel added were taken into account for speed calculation. Free Fiji software was used to calculate the speed of micromotors, edit videos and extract pictures. A digital hand-held "Pocket" H_2O_2 refractometer (Model: Atago, PAL-39S) was used to calibrate the concentrations of H_2O_2 solutions.

4.3 Results and discussion

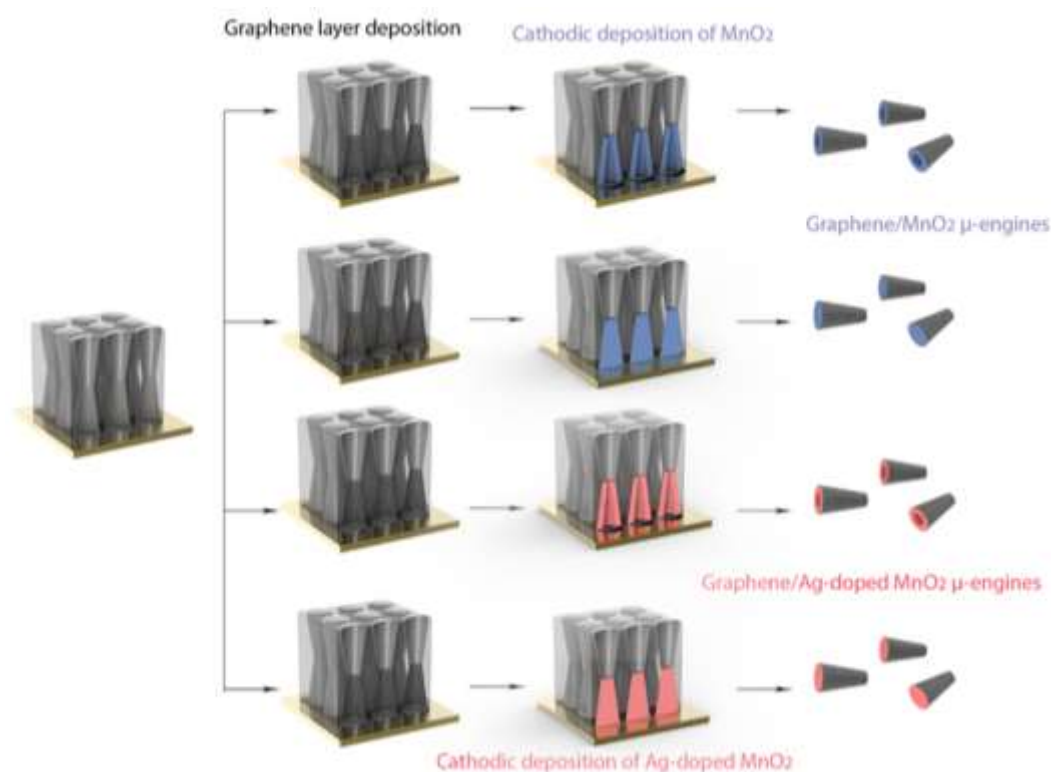


Figure 4.1. Schematic illustration of the fabrication process of the erGO/MnO₂ based micromotors.

The micromotors were constructed by a two-step electroreduction deposition processes as shown in Figure 4.1 Firstly, an outer layer of electrochemically reduced graphene oxide (erGO) was formed by depositing nanosized graphene oxide (GO) onto the pores of the membrane by a cyclic voltammetry method ⁴⁷. The graphene oxide is the substrate for the growth of the second catalytic layers. The graphene layer also serves as the inert layer to shield the outside reactions of catalytic layers, making the catalytically generated oxygen bubbles confined in the microtubes. Due to the large quantities of functional groups remained on the graphene oxide layer, the inner catalyst layer tends to grow on a rough surface with potentially enhanced catalytic performance. The reduced graphene oxide layer could be used as an adsorbent for adsorption of metal ions in the aquatic environment. Secondly, an inner layer of MnO₂ or

silver-modified MnO_2 was produced by the galvanostatic cathodic electroreduction. For the silver-modified MnO_2 micromotors, the electroreduction of MnO_4^- ions and Ag^+ ions occur simultaneously⁴⁸. The inner layer deposition parameters were optimized for the synthesis of rod-shaped and tubular micromotors.

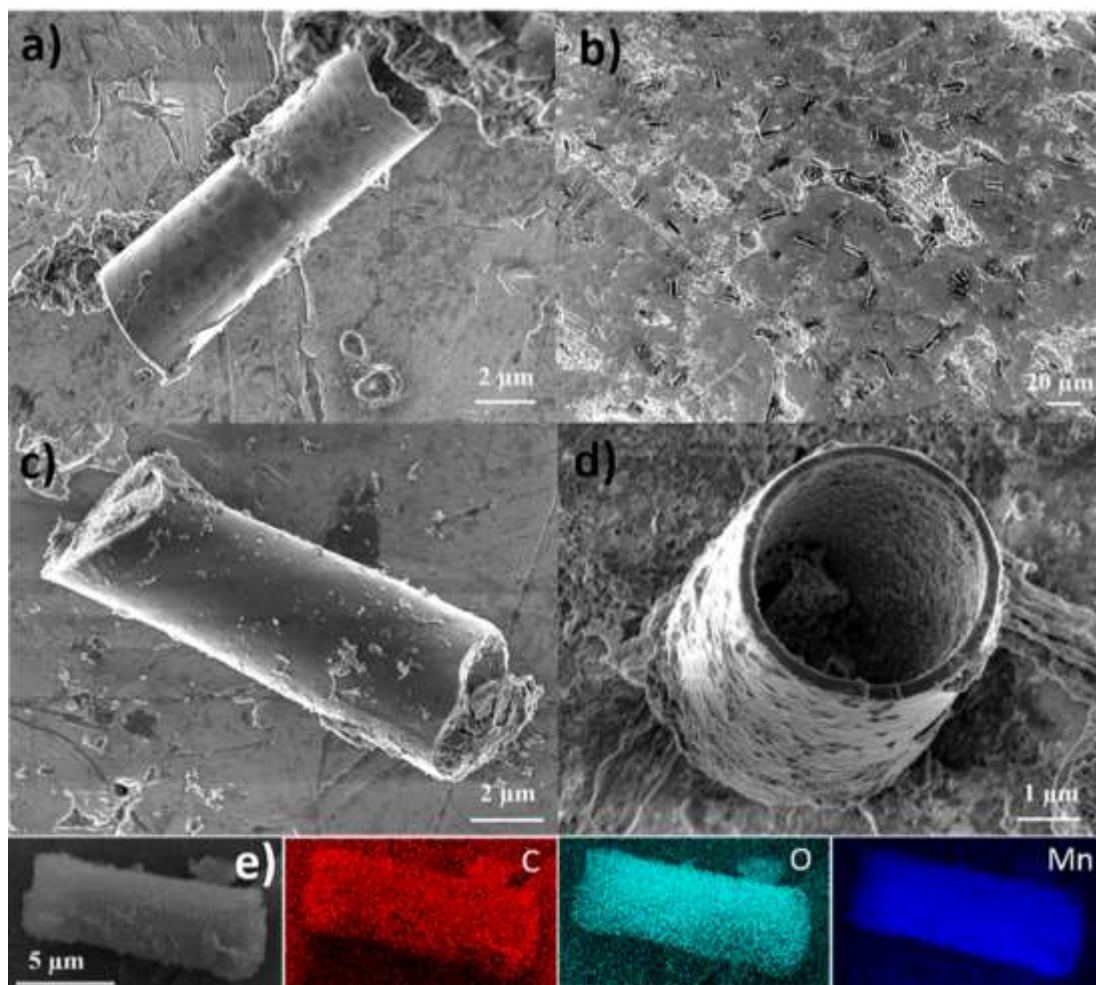


Figure 4.S1. Scanning electron microscope (SEM) and energy dispersive X-ray spectrum (EDX) mapping analysis of the erGO/ MnO_2 micromotors: (a) image of a well-formed microtube, (b) image showing a number of microtubes, (c) a microrod, (d) an upright microtube, (e) EDX analysis of a microtube, illustrating the distributions of carbon (red), oxygen (light blue) and manganese (blue).

Figure 4.S1 demonstrates that erGO/ MnO_2 micromotors in microrods and microtubes are fabricated successfully. The graphene/ MnO_2 microtubes

were electrodeposited at a cathode current of -1 mA for 20 min, meanwhile, the graphene wrapped microrods were synthesized at -1.5 mA for 20 min. The increased cathode current resulted in the transformation of microtubes to microrods. Figure 4.S1a shows a well-formed micromotor with about 5 μm in diameter and about 12 μm in length. Figure 4.S1b shows that large quantities of the erGO/MnO₂ tubular micromotors were obtained. Figure 4.S1c presents the image of a graphene wrapped microrod micromotor. The outer diameter and geometry of the microrods are the same as the microtubes. Figure 4.S1d gives the image of an upright graphene/MnO₂ microtube micromotor. Wang et al.⁴⁷ reported the similar microstructures of graphene/Pt and graphene/Au tubular microengines. Here we demonstrate that the rough porous inner surface could also be constructed by electrochemically plated metal oxide. This microstructure can be attributed to the presence of high density of in-plane and grain-boundary defects of the outer erGO layer, providing a perfect substrate for the nucleation and growth of MnO₂ layer by the cathodic electroreduction. The inner surface of the microstructure offers more reaction sites for the decomposition of fuel. The H₂O₂ solution is decomposed preferably on the inner surface of the microtubes to restrict the formed bubbles inside the microtubes. The continuous recoil of the bubbles from the opening of the microtubes provides the required propelling force for these micromotors to navigate in the fluid environment. Figure 4.S1e shows the elemental mapping of an individual graphene/MnO₂ microtube micromotor. The uniform carbon distribution on the surface further confirms the good coverage of the graphene layer. The oxygen element is from the erGO outer layer and MnO₂ inner layer. The manganese is from the cathodic reduction deposited MnO₂ layer only.

Table 4.S1. Various functional groups identified on the surface of erGO/MnO₂ micromotors.

Spectra	Group	Position (eV)	at. %
C 1s	C-C/C-H/C=C	284.6	65.75
C 1s	C-O	286.18	22.94
C 1s	C=O	287.94	6.09
C 1s	O-C=O	290.30	5.26
O 1s	Metal Oxide	529.98	20.74
O 1s	O-H	531.78	30.74
O 1s	C=O	532.82	34.56
O 1s	O-C=O	533.98	13.96

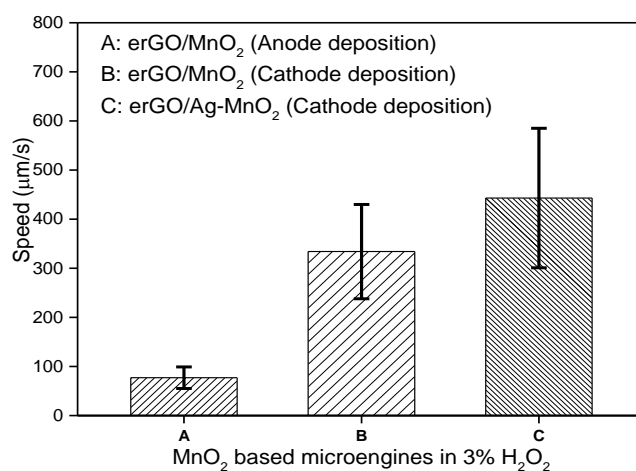


Figure 4.S2. Comparison of the speeds of three erGO/MnO₂ based tubular micromotors in 3% H₂O₂ and 1% SDS as the surfactant.

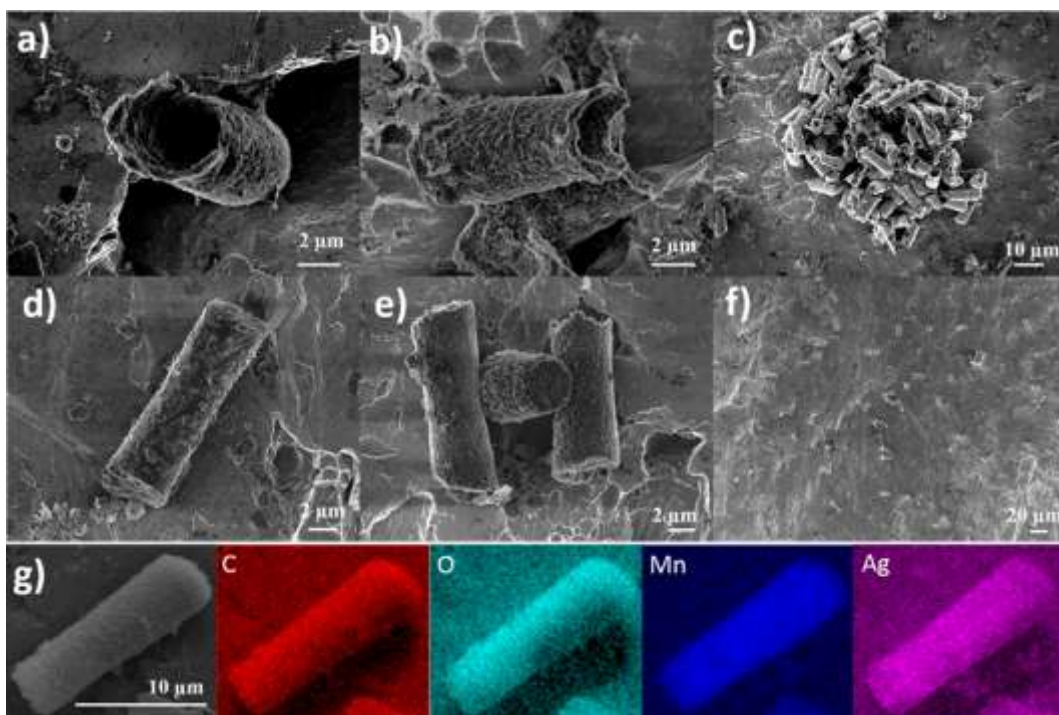


Figure 4.2. SEM and EDX mapping analysis of the erGO/Ag-MnO₂ micromotors: (a) image of a well-formed upright microtube micromotor, (b) image of a lying microtube micromotor, (c) image showing a number of microtubes micromotors, (d) an individual microrod micromotor, (e) an upright and two lying microrod micromotor, (f) a number of microrods micromotors, (g) EDX analysis of an individual microtube micromotor, illustrating the distribution of carbon (red), oxygen (light blue), manganese (blue) and silver (magenta).

Figure 4.2 indicates that erGO/Ag-MnO₂ micromotors in microtube and microrod are fabricated successfully. Figure 4.S1 shows the results of erGO/MnO₂ micromotors. Compared with the smooth tubular microengines, erGO/Ag-MnO₂ microengines exhibit a large surface area of electrochemically active sites for potentially enhanced catalytic activity. The co-deposition of silver and MnO₂ generates a slightly thicker and more porous microstructure and the length of the erGO/Ag-MnO₂ micromotors are slightly shorter than erGO/MnO₂. The uniform distribution of carbon, oxygen, manganese, and silver demonstrates that the silver-modified MnO₂ micromotors are fabricated successfully with a good coverage by graphene layers.

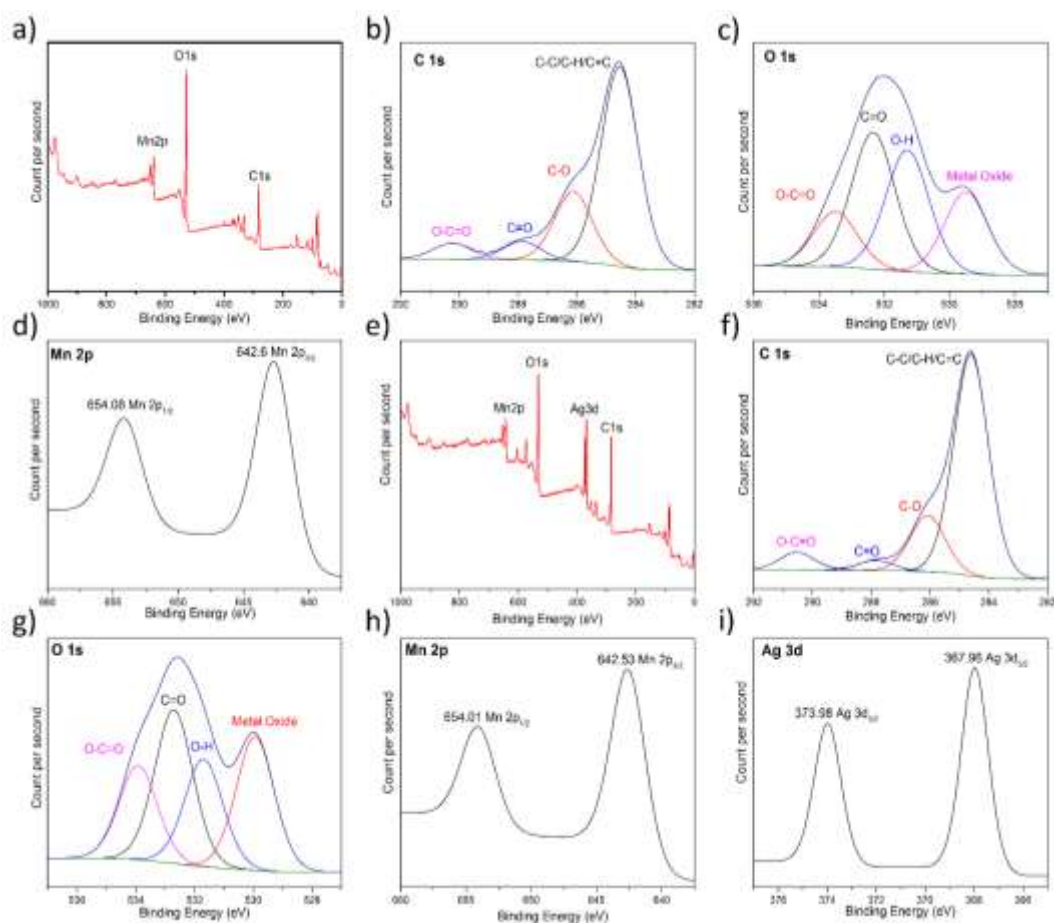


Figure 4.3. XPS surveys of micromotors. (a) Wide scan showing Mn 2p, O 1s and C 1s peaks of the erGO/MnO₂ micromotors. (b) High-resolution C 1s XPS spectra of erGO/MnO₂ micromotors. (c) High-resolution O 1s spectra of erGO/MnO₂ micromotors. (d) High-resolution Mn 2p XPS spectra of erGO/MnO₂ micromotors. (e) Wide scan showing Mn 2p, Ag 3d, O 1s and C 1s peaks of the erGO/Ag-MnO₂ micromotors. (f) High-resolution C 1s XPS spectra of erGO/Ag-MnO₂ micromotors. (g) High-resolution O 1s spectra of erGO/Ag-MnO₂ micromotors. (h) High-resolution Mn 2p XPS spectra of erGO/Ag-MnO₂ micromotors. (i) High-resolution Ag 3d XPS spectra of erGO/Ag-MnO₂ micromotors.

Table 4.S2. Various functional groups identified on the surface of erGO/Ag-MnO₂ micromotors.

Spectra	Group	Position (eV)	at. %
C 1s	C-C/C-H/C=C	284.62	65.75
C 1s	C-O	286.20	22.93
C 1s	C=O	287.96	6.07
C 1s	O-C=O	290.32	5.25
O 1s	Metal Oxide	529.49	34.56
O 1s	O-H	531.29	13.96
O 1s	C=O	532.34	30.74
O 1s	O-C=O	533.50	20.74

As shown in Figure 4.3 and Table 4.S1-S2, XPS surveys further reveal the presence of carbon (C 1s peak), oxygen (O 1s peak), manganese (Mn 2p peak) and silver (Ag 3d peak) in the MnO₂ based micromotors, which are in good agreement with the EDX results. Compared with the unmodified MnO₂ based micromotors, the silver-modified ones show a distinct Ag 3d peak. Both wide scan surveys show that the O 1s peak is higher than the C 1s peak, which is typical characteristics for GO²¹. The peaks of high-resolution C 1s spectra (Figure 4.3b and Figure 4.3f) and O 1s spectra (Figure 4.3c and Figure 4.3g) correspond to the binding energy of various

functional groups such as C-C/C-H/C=C, C-OH, C=O, and O-C=O, revealing the nature of the covalent bonds of oxygen and carbon atoms. The ratios of oxygen functional groups to all the carbon species are 34.29% and 34.25% for erGO/MnO₂ and erGO/Ag-MnO₂ micromotors, respectively, which denote the degree of oxidation of the outer layer of the micromotors. Although various oxygen functional groups are identified on these cathodically electrodeposited MnO₂ based micromotors, the degree of oxidation is much lower than the value of our previous fabricated micromotors by anodic oxidation electrodeposition. Due to the second electroreduction deposition of MnO₂ based inner materials, the erGO outer layer is partially reduced, resulting in the decrease of the oxidation degree. The oxidation state of Mn can be examined by the Mn 2p high-resolution XPS spectra (Figure 4.3d and Figure 4.3h). In both the spectra, the Mn 2p_{3/2} peaks were located at 642.5 and 642.6 eV, which indicates that the main oxidation state of Mn in all the manganese oxides are Mn⁴⁺. In both the cases, the difference of binding energy between Mn 2p_{3/2} and Mn 2p_{1/2} is 11.48 eV. The results are in a good agreement with previously reported values, which further confirms the electrodeposited materials are MnO₂. Figure 4.3i shows the high-resolution XPS spectra of Ag 3d peaks of the erGO/Ag-MnO₂ micromotors. The binding energies of Ag 3d_{5/2} and Ag 3d_{3/2} are 367.96 and 373.98 eV, indicating that the silver is in metallic form (Ag⁰), which is also in a good agreement with previously reported values.⁴⁹ The zero valence of the silver is also due to the electroreduction deposition process. Therefore, the XPS spectra further confirmed the elemental constitution and the valence state of the erGO/MnO₂ and erGO/Ag-MnO₂ micromotors.

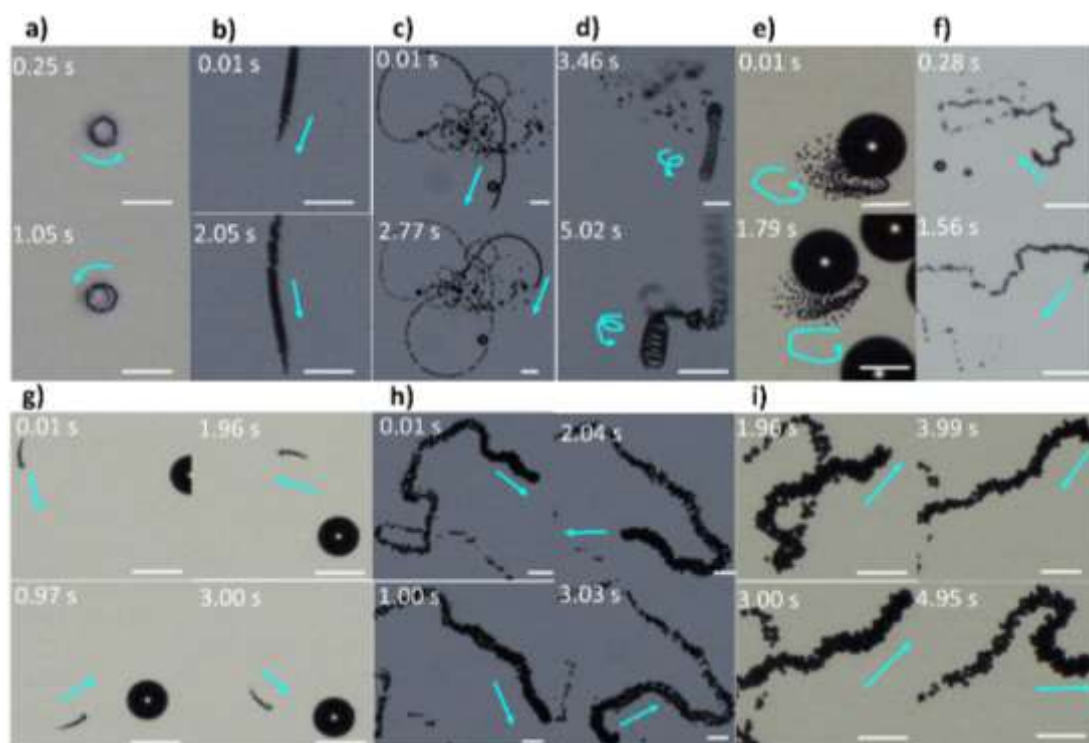


Figure 4.4. Time-lapse images depicting efficient propulsion of the MnO_2 based micromotors in 1% SDS. Blue arrowed lines indicate the directions and trajectories of the motion. (a) The small circular motion of an erGO/Ag- MnO_2 tubular micromotor in 0.2% H_2O_2 . (b) Linear motion of an erGO/Ag- MnO_2 tubular micromotor in 0.3% H_2O_2 . (c) The large circular motion of an erGO/Ag- MnO_2 tubular micromotor in 0.5% H_2O_2 . (d) Helical motion behaviors of an erGO/Ag- MnO_2 tubular micromotor in 1% H_2O_2 . (e) Ultra-fast elliptic orbit motion behaviors of an erGO/Ag- MnO_2 tubular micromotor in 4% H_2O_2 . (f) Irregular motion behaviors of an erGO/Ag- MnO_2 tubular micromotor in 10% H_2O_2 . (g) The circular motion of an erGO/ MnO_2 tubular micromotor in 3% H_2O_2 . (h) The irregular motion of an erGO/Ag- MnO_2 microrod micromotor in 3% H_2O_2 . (i) The irregular motion of an erGO/ MnO_2 microrod micromotor in 4% H_2O_2 . Scale bars: 100 μm .

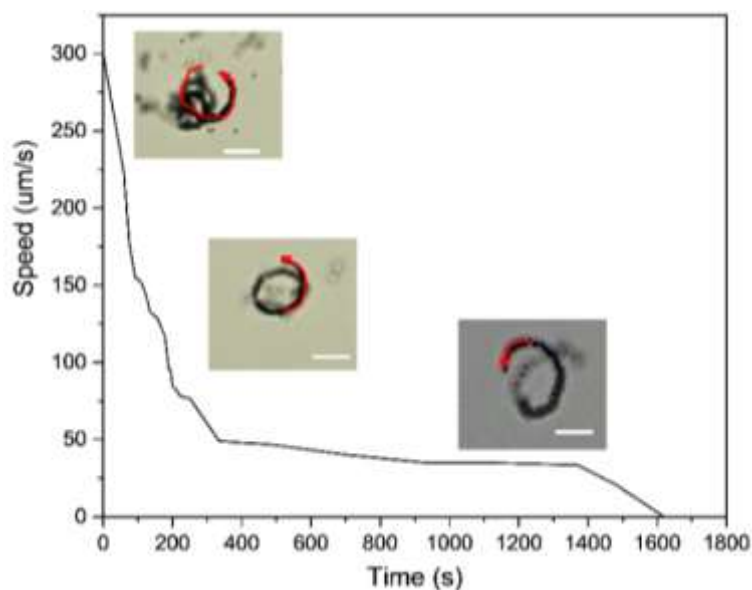


Figure 4.S3. The lifetime of the erGO/Ag-MnO₂ micromotors in 0.3% SDS and 0.5% H₂O₂. The insets show the motion trajectories of the micromotor at different stages in 2 seconds. Scale bars: 100 μ m.

Typical time-lapse images captured from the videos of the moving microtubes and microrods are presented in Figure 4.4. Besides irregular motion trajectory, various motion patterns were recognized. The erGO/Ag-MnO₂ micromotors show fast speeds and complex motion trajectories in H₂O₂ as low as 0.2%. The extraordinary high-performance in a low content of the fuel is attributed to the synergistic effect between Ag and MnO₂ and a large catalytic area offered by the hierarchically porous and rough inner surface of the micromotors for the decomposition of H₂O₂. The tubular microengines show diverse motion patterns at a relatively low fuel concentration range, while the rod-shaped micromotors only exhibit irregular motion trajectories at a higher fuel content. At a very high concentration of fuels, the tubular micromotors show irregular motion trajectories because the violent catalytic reactions and the discontinuous bubble ejection processes will result in the turbulence of the propelling force vectors, thus affecting the motion directions. The microrod micromotors were propelled by the generated microbubbles at the different sides of these microrods. Due to the imbalanced bubble

generation and the unequal propelling force generated at the different sides of the microrods, these rod-shaped micromotors usually show irregular motion behavior.

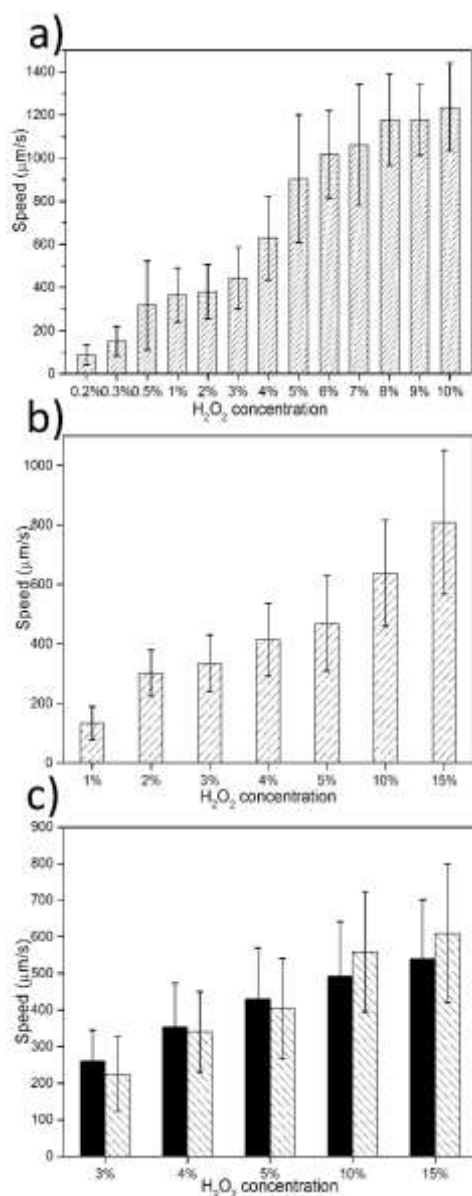


Figure 4.5. Dependence of average speed of graphene wrapped cathodically deposited MnO_2 and co-deposited Ag-MnO_2 micromotors in the presence of 1% SDS surfactant ($n = 50$). The average speed of erGO/Ag-MnO₂ microtube micromotors (a), erGO/MnO₂ microtube micromotors (b), and comparison of the speed profile of erGO/Ag-MnO₂ (black bars) and erGO/MnO₂ (lined bar) microrod micromotors (c).

As demonstrated in Figure 4.5, the speed of the micromotors increases with increased H₂O₂ fuels. The performances of the catalytic MNMs were compared and summarized in Table 4.S3 and Figure 4.S3. The speed of erGO/Ag-MnO₂ tubular microengines is better than Pt-based micromotors in a low level of peroxide. The erGO/Ag-MnO₂ microrockets can propel at speeds of 88 ± 46 , 151 ± 68 , 317 ± 206 , and $365 \pm 124 \mu\text{m s}^{-1}$ in 0.2%, 0.3%, 0.5%, and 1% H₂O₂ fuels, respectively. The ultra-high speed of erGO/Ag-MnO₂ micromotors demonstrate that the hierarchically porous inner layers of erGO/Ag-MnO₂ are more efficient than the rough Pt surface of erGO/Pt microengines (88 vs $81 \mu\text{m s}^{-1}$)⁴⁷ and far more efficient than the smooth Pt layer of PANI/Pt microengines (88 vs $25 \mu\text{m s}^{-1}$) at 0.2% H₂O₂⁵⁰. More favorably, the erGO/Ag-MnO₂ tubular microengines reach a high speed of $317 \pm 206 \mu\text{m s}^{-1}$ in 0.5% H₂O₂, while the speeds of erGO/Pt and PANI/Pt microengines were only 170 ± 40 and $123 \pm 21.4 \mu\text{m s}^{-1}$, respectively.^{47, 50} The average speed of erGO/Ag-MnO₂ tubular micromotors continues to increase from 381 ± 126 to $904 \pm 296 \mu\text{m s}^{-1}$ upon raising H₂O₂ levels from 2 to 5% and further reaches $1237 \pm 205 \mu\text{m s}^{-1}$ at 10% H₂O₂. The average speed of graphene/Pt tubular micromotors rises from 390 ± 80 to $1700 \pm 200 \mu\text{m s}^{-1}$ as the fuel content increases from 1% to 3%, which means that at higher contents of fuel, the Pt-based micromotors are moving much faster than the MnO₂ based micromotors. The reasons for this phenomenon are attributed to the degradation of the MnO₂ based catalysts by the highly oxidizing H₂O₂ fuel at high concentrations, whereas the noble metal Pt catalysts are very inert and stable even at high contents of the oxidizing fuels. Previously, Mei et al. theoretically developed an equation of average speed for the cylindrical-shaped tubular micromotors⁵¹. Later, Li et al. developed a hydrodynamic model for the speed prediction of conically shaped micromotors, which considered the bubble geometric asymmetry and buoyancy force⁵².

Herein, as the high-performance micromotors developed in this work are cylindrical microtubes, we can adopt the body deformation model to analyze the motion of the MnO₂ based microengines. This method has been applied by to analyze graphene/Pt and polymer/Pt based tubular microengines⁴⁷. The analysis provides a good reference for us to elucidate the motion mechanism at different fuel concentrations. According to this model, the speed should be linearly proportional to the concentration of hydrogen peroxide concentrations, while the bubble size and frequency also affect the movement speeds of the tubular microengines. Due to the similar size (Length $L \approx 10 \mu\text{m}$ and inner opening radius $R_j \approx 2.2 \mu\text{m}$) of our developed MnO₂ based tubular micromotors with the Pt-based tubular micromotors from Wang' s group, it is possible to refer to their calculations to analyze the results of our micromotors. Here, R_b is the radius of the bubbles. It seems that at a low peroxide concentration below 1%, the graphene/Ag-MnO₂ micromotors fit well with the curve of $R_b = R_j/5$ and $R_b = R_j/4$. At increases fuel levels, the speed of graphene/Ag-MnO₂ microtubes fits well with the curves between $R_b = R_j/3$ and $R_b = R_j/2$ as the fuel levels rise from 2% to 5%. At further higher fuel levels, the radius of bubbles falls to fit the curve of larger bubbles of $R_b = R_j/2$ and even more. It seems that, as the fuel content rises, the bubble sizes show an increasing tendency, and the bubble frequency shows a decreasing tendency. The merits of the Ag-MnO₂ catalyzed micromotors are the relatively high bubble frequency and small bubble size at low peroxide levels. As illustrated in Figure 4.5b, the speed of erGO/MnO₂ tubular micromotors increases from $134 \pm 55 \mu\text{m s}^{-1}$ in 1% H₂O₂ to $809 \pm 242 \mu\text{m s}^{-1}$ in 15% H₂O₂. The erGO/MnO₂ tubular micromotors are also faster and more efficient than some of the Pt-based⁵³ and MnO₂ based micromotors reported before⁴⁴, implying that the cathodically electrodeposited MnO₂ MNMs are far more efficient than those from

anodic electrodeposition. Similar results were also demonstrated by the graphene/MnO₂ tubular micromotors as the fuel levels rise from 1% to 15% H₂O₂. At 1% fuel level, the speed of pure MnO₂ catalyzed microtubes fits well with the curve between $R_b = R_j/3$ and $R_b = R_j/2$. Later, the bubble size shows an increasing tendency as the fuel level rises, while the expelling frequency shows a decreasing trend. The following reasons account for the good motion performance of the Ag-MnO₂ catalyzed micromotors by theoretical calculations and fitting of the speeds of micromotors with the theoretical curves. The small bubble size and high bubble expelling frequency explained the high mobility at low fuel contents. The synergetic effect of the Ag-MnO₂ catalyst and the high catalytic areas offered by the rough inner surface accounts for the good catalytic performance for generating small microbubbles at low fuel levels. What is more, the cathodic electroreduction fabrication provides additional benefits by avoiding the oxidation and dissolution of the substrate in commonly used anodic electrodeposition, thus paves the way for designing various modified MnO₂ based hybrid MNMs. A comparison of the speeds of the erGO/Ag-MnO₂ and erGO/MnO₂ microrods is presented in Figure 4.5c. It is shown that, at a low fuel concentration range below 5% H₂O₂, the speed of rod-shape erGO/Ag-MnO₂ micromotors are faster than the erGO/MnO₂ micromotors, while at a high fuel concentration range above 10% H₂O₂, the speed of erGO/Ag-MnO₂ microrod micromotors are slower than the unmodified erGO/MnO₂ microrod micromotors, attributing to the poisoning of Ag by concentrated H₂O₂. At a high concentration of H₂O₂ fuel, the silver metal suffers from oxidation. Hence, the speeds of the rod-shaped Ag-MnO₂ catalyzed micromotors are lower than MnO₂ based micromotors. While this is not the case for the tubular micromotors. Although the silver component experiences the oxidation and deactivation by the high concentration of

H₂O₂ fuel, the high-speed flows of the inner tube fluid and bubbles would exfoliate the silver oxides and leave the inner catalytic materials to be the fresh and newly generated Ag-MnO₂ catalysts, thus leading to higher speeds than MnO₂ based microtubes. As we observed that at a high content of H₂O₂, Ag-MnO₂ catalyzed tubular micromotors are moving much faster than MnO₂ catalyzed microtube micromotors.

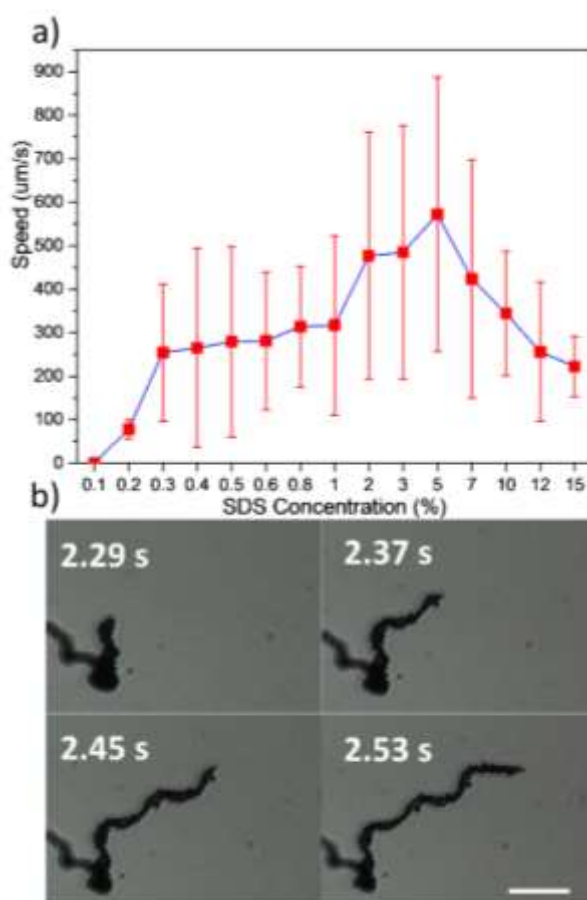


Figure 4.6. Dependence of average speed of graphene/Ag-MnO₂ tubular micromotors with varying SDS content in 0.5% H₂O₂ (n=50) (a); time-lapse images showing an ultrafast graphene/Ag-MnO₂ tubular micromotors in 5% SDS and 0.5% H₂O₂. (b) Scale bar: 100 µm.

Table 4.S3. Comparison of the catalytic MNMs.

Type of the micro-/nanomotor	Ref.	Size [μm]	Fuel concentration range (H_2O_2)	Average speed / $\mu\text{m s}^{-1}$	Max. speed reported / $\mu\text{m s}^{-1}$	Max. relative speed (bl s^{-1})	Efficiency or propelling force (pN)
Rolled up Ti/Cr/Pt microtubes	Sanchez and Schmidt et al. ³⁴	50	0.25-5% (v/v)	140-10000 at 37°C	10000	200	
Multilayered microrockets	Li and Zhang et al. ⁵⁴	20	1-5%	285-1410	1410	70	
Pt-Alloy nanowires	Wang et al. ⁵⁵	2	15%	110	160	75	
Au/Pt-CNT nanowires	Wang et al. ⁵⁶	2	15%	51	91	45.5	
Cu/Pt concentric bimetallic microtubes	Zhao and Pumera et al. ⁵⁷	10	0.2-3%	70-700	n.a.	70	
Cu/Ag segmented bimetallic tubular micromotors	Pumera et al. ³⁸	10-15	0.5-3%	13.1-252.4	n.a.	n.a.	2.52×10^{-9}
Ag and MnO_2 microparticles	Pumera et al. ⁵⁸	Ag \approx 30 MnO ₂ \approx 5	0.1-12% 12-21%	25-100 50-120	n.a.	n.a.	5.81×10^{-8} 1.16×10^{-8}
Au/Graphene/ MnO_2	Feng and Ma et al. ⁴³	6.74	0.15-2.5%	15.79-44.79	111.03	27.69	
PEDOT/ MnO_2 microtubes & microrods And $\text{MnO}_2 @ \text{MnCO}_3$	Saldar and Janis et al. ⁵⁹	12.5 12.5 5	5-15 5-15 1-10	Tubes 200- 510 Rods 200- 410 142-665	n.a. 900	n.a. 180	
Graphene/Pt	Wang et al. ⁴⁷	10	0.1-3	37-1700	n.a.	170	
MnO_2 hallow	Saldar and Janis et al. ⁴⁴	n.a.	5-10	321-996	1625	n.a.	
PANI/Pt microtubes	Gao and Wang et al. ⁵⁰	8	0.2-5	25-1410	3000	375	45 pN
PEDOT/Pt bilayer microtubes PPY/Ag bilayer PPY/Pt-Ni alloy Au/Pt bimetallic microbots	Gao and Wang et al. ⁶⁰	7	10 5-10 15 10 10	10000 at 37°C 2400-3350 500 470 1500	10000 at 37°C 3375 at 20°C	1400 480 70 67	
Paper tubular microjet engines	Singh and Mandal et al. ⁶¹	900	9-16	270-1600	1600	2	
PEDOT/ MnO_2	Wang et al. ⁶²	8	0.4-10	31.57-318.80	n.a.	n.a.	
PEDOT/PtNP@CNT-PPy	Li and Wu et al. ⁵³	12	1-15	62-450	n.a.	n.a.	10 pN
Porous Ti/Cr/Pt microtubes	Mei et al. ³³	10-40	0.2-7	120-1077	>1500	n.a.	
erGO/ MnO_2 microtubes by anodic deposition	Our previous work ⁴⁵	8	3-15	77-466	700	87.5	36 pN
erGO/ MnO_2 microrods	This work	12	3-15	224-609	1149	95.8	43.5 pN
erGO/ MnO_2 microtubes	This work	12	1-15	134-809	1427	118.9	58 pN
erGO/Ag- MnO_2 microrods	This work	12	3-15	261-539	924	77	38.5 pN
erGO/Ag- MnO_2 microtubes	This work	9	0.2-10	88-1237	1888	209.8	90 pN

Taking the microengines as a cylinder microrod, we can adopt the Stokes' drag theory to estimate the drag force or propelling force roughly by the following equation^{50, 53}.

$$F_d = \frac{2\pi\mu LU}{\ln(L/a)-1/2} \quad (1)$$

Where F_d is the fluid resistance, U is the speed of the microengines, μ is the fluid dynamic viscosity, and L and a are the length and radius of the micromotors, respectively. The estimated drag forces for the four types of micromotors are presented in Table 4.S3, which also summarizes the speed profile of different MNMs reported so far. The estimated drag force for the erGO/Ag-MnO₂ micromotors is 90 pN, which is two-fold as high as that of the PANI/Pt tubular microengines and 8 times larger than the polymer micromotors doped with Pt nanoparticle@carbon nanotubes^{50, 53}. The strong drag force exerted by these micromotors is sufficient enough for towing large cargos such as cells. The strong propelling force could be utilized as a powerful tool to penetrate biological tissues such as tumor outer shell for the delivery of anti-cancer drugs. The advantages of the erGO/Ag-MnO₂ tubular micromotors are the higher speed over any Pt catalyzed MNMs at a low H₂O₂ fuel concentration range such as 0.5% H₂O₂ and better environmental tolerance nature, as it already has been proved by other researchers that the efficient motion behaviors of the MnO₂ based micromotors in biological as well as salt-rich aquatic environment^{43, 44}.

The effect of SDS surfactant concentrations on the motion of erGO/Ag-MnO₂ micromotors at 0.5% H₂O₂ is illustrated in Figure 4.6 It is very interesting that at this low content of the fuel, the speed of erGO/Ag-MnO₂ could be regulated from 0 to 572 $\mu\text{m s}^{-1}$ by adjusting the content of the

surfactant. The micromotors are not moving in 0.1% SDS and start to move at a low speed of $78 \pm 22 \mu\text{m s}^{-1}$ in 0.2% SDS. The critical micelle concentration (CMC) of SDS is $\sim 0.24\%$ ⁶³. Below the CMC, the surface tension of the fluid is too high to wet the micromotors for efficient propulsion. Upon reaching the CMC, the speed of micromotors increases to $254 \pm 170 \mu\text{m s}^{-1}$ at 0.3%, and gradually to $317 \pm 206 \mu\text{m s}^{-1}$ as the SDS concentration increases to 1%. Further increasing the surfactant concentration to 5%, the average speed of micromotors reaches its acme of $572 \pm 315 \mu\text{m s}^{-1}$. Under this optimized conditions, the maximum speed of an individual micromotor exceeds 1.3 mm s^{-1} . (Figure 4.6b, time-lapse images) At high concentrations of the surfactant, the fluid viscosity would increase significantly. Due to the effect of fluid viscous resistance, further enhancing the surfactant content decreases the speed of micromotors.

It is noteworthy that the surfactant-assisted wide span speed regulation has never been observed before. This may lead to some fascinating applications, such as active cargo delivery, drilling of biological tissues, motion-based sensing, and detection of an analyte, fast separation of chemicals, and diagnosis of diseases due to its noticeable speed variation and extraordinary high performance at a low content of fuels. Moreover, an erGO/Ag-MnO₂ micromotor shows the continuous motion of nearly 26 min in 0.3% SDS and 0.5% H₂O₂ (Figure 4.S3), demonstrating a good lifetime of the micromotors.

As the propelling force and output power of micromotors are proportional to the velocity and the square of velocity, the average speed of erGO/Ag-MnO₂ micromotors is 3.4-fold of the fastest graphene/Pt micromotors ($572 \text{ vs } 170 \mu\text{m s}^{-1}$ in 0.5% H₂O₂), which means that the propelling force and output power of erGO/Ag-MnO₂ micromotors are 3.4 and 10 times as

high as the values of the Pt-catalyzed micromotor. The speed regulation has long been a pursuit for the MNMs researchers. Geometry design and temperature adjusting have been tested for the tuning of MNMs' motion.^{33, 34, 64} Here, we introduce a new variable for wide span speed regulation at a low content of fuels, which will lead to various practical applications from biomedical to environmental science. Due to the toxicity of H₂O₂ to the biological tissues as well as natural waterbody microorganisms, a high concentration of the fuel is strictly prohibited.

4.4 Conclusions

We demonstrated that Ag-MnO₂ based micromotors with an exceptional high-performance can be produced by a simple and low-cost template assisted cathodic electroreduction deposition. The cathodically electrodeposited MnO₂ based micromotors show better performance than those from anodic deposition. The intrinsic higher catalytic performance and good geometry shape of the tubular MnO₂ based micromotors result in higher speeds at low peroxide contents. The synergistic effect of co-deposited silver and MnO₂ components generated the higher catalytic efficiency than Pt in a low content of H₂O₂. What is more, by regulating the surfactant content to 5% in 0.5% H₂O₂, the average speed of erGO/Ag-MnO₂ tubular micromotors reaches its acme of $572 \pm 315 \mu\text{m s}^{-1}$ and the highest speed of individual micromotor exceeds 1.3 mm s^{-1} . The Ag-MnO₂ based MNMs provide an excellent platform for high-performance motion, which can be used in a wide range of applications in analysis, sensing, diagnostic, monitoring, active cargo delivery, biological entities manipulation, and nano surgeries. The cathodic reduction fabrication also paves the way for designing various hybrid MNMs to meet specific needs and address diverse issues.

References

1. Li JX, Rozen I, Wang J. Rocket science at the nanoscale. *ACS Nano*. 2016; 10(6):5619-5634.
2. Ozin GA, Manners I, Fournier-Bidoz S, Arsenault A. Dream nanomachines. *Adv. Mater.* 2005; 17(24):3011-3018.
3. Lin XK, Wu ZG, Wu YJ, Xuan MJ, He Q. Self-propelled micro-/nanomotors based on controlled assembled architectures. *Adv. Mater.* 2016; 28(6):1060-1072.
4. Duan W, Wang W, Das S, et al. Synthetic nano- and micromachines in analytical chemistry: Sensing, migration, capture, delivery, and separation. *Annu. Rev. Anal. Chem.* 2015; 8(1):311-333.
5. Sanchez S, Soler L, Katuri J. Chemically powered micro- and nanomotors. *Angew. Chem. Int. Ed.* 2015; 54(5):1414-1444.
6. Tu YF, Peng F, Wilson DA. Motion manipulation of micro- and nanomotors. *Adv. Mater.* 2017; 29(39):1701970.
7. Dey KK, Sen A. Chemically propelled molecules and machines. *J. Am. Chem. Soc.* 2017; 139(23):7666-7676.
8. Orozco J, Cheng G, Vilela D, et al. Micromotor-based high-yielding fast oxidative detoxification of chemical threats. *Angew. Chem. Int. Ed.* 2013; 52(50):13276-13279.
9. de Avila BE, Angsantikul P, Li J, et al. Micromotor-enabled active drug delivery for in vivo treatment of stomach infection. *Nat. Commun.* 2017; 8(1):272.
10. Medina-Sanchez M, Schwarz L, Meyer AK, Hebenstreit F, Schmidt OG. Cellular cargo delivery: Toward assisted fertilization by sperm-carrying micromotors. *Nano Lett.* 2016; 16(1):555-561.

11. Kagan D, Calvo-Marzal P, Balasubramanian S, et al. Chemical sensing based on catalytic nanomotors: Motion-based detection of trace silver. *J. Am. Chem. Soc.* 2009; 131(34):12082-12083.
12. Singh VV, Martin A, Kaufmann K, de Oliveira SDS, Wang J. Zirconia/graphene oxide hybrid micromotors for selective capture of nerve agents. *Chem. Mater.* 2015; 27(23):8162-8169.
13. Palacci J, Sacanna S, Vatchinsky A, Chaikin PM, Pine DJ. Photoactivated colloidal dockers for cargo transportation. *J. Am. Chem. Soc.* 2013; 135(43):15978-15981.
14. Patra D, Sengupta S, Duan W, et al. Intelligent, self-powered, drug delivery systems. *Nanoscale.* 2013; 5(4):1273-1283.
15. Peters C, Hoop M, Pane S, Nelson BJ, Hierold C. Degradable magnetic composites for minimally invasive interventions: Device fabrication, targeted drug delivery, and cytotoxicity tests. *Adv. Mater.* 2016; 28(3):533-538.
16. Wu ZG, Wu YJ, He WP, et al. Self-propelled polymer-based multilayer nanorockets for transportation and drug release. *Angew. Chem. Int. Ed.* 2013; 52(27):7000-7003.
17. Nelson BJ, Kaliakatsos IK, Abbott JJ. Microrobots for minimally invasive medicine. *Annu. Rev. Biomed. Eng.* 2010; 12:55-85.
18. Vartholomeos P, Fruchard M, Ferreira A, Mavroidis C. Mri-guided nanorobotic systems for therapeutic and diagnostic applications. *Annu. Rev. Biomed. Eng.* 2011; 13:157-184.
19. Gao W, Wang J. The environmental impact of micro/nanomachines: A review. *ACS Nano.* 2014; 8(4):3170-3180.
20. Soler L, Magdanz V, Fomin VM, Sanchez S, Schmidt OG. Self-propelled micromotors for cleaning polluted water. *ACS Nano.* 2013; 7(11):9611-9620.

21. Vilela D, Parmar J, Zeng YF, Zhao YL, Sanchez S. Graphene-based microbots for toxic heavy metal removal and recovery from water. *Nano Lett.* 2016; 16(4):2860-2866.
22. Orozco J, Garcia-Gradilla V, D'Agostino M, et al. Artificial enzyme-powered microfish for water-quality testing. *ACS Nano.* 2013; 7(1):818-824.
23. Jurado-Sanchez B, Escarpa A. Janus micromotors for electrochemical sensing and biosensing applications: A review. *Electroanalysis.* 2017; 29(1):14-23.
24. Garcia M, Orozco J, Guix M, et al. Micromotor-based lab-on-chip immunoassays. *Nanoscale.* 2013; 5(4):1325-1331.
25. Vilela D, Cossio U, Parmar J, et al. Medical imaging for the tracking of micromotors. *ACS Nano.* 2018; 12(2):1220-1227.
26. Wang W, Duan WT, Ahmed S, Mallouk TE, Sen A. Small power: Autonomous nano- and micromotors propelled by self-generated gradients. *Nano Today.* 2013; 8(5):531-554.
27. Ren L, Zhou D, Mao Z, et al. Rheotaxis of bimetallic micromotors driven by chemical-acoustic hybrid power. *ACS Nano.* 2017; 11(10):10591-10598.
28. Mei YF, Huang GS, Solovev AA, et al. Versatile approach for integrative and functionalized tubes by strain engineering of nanomembranes on polymers. *Adv. Mater.* 2008; 20(21):4085-4090.
29. Li JX, Liu WJ, Wang JY, et al. Nanoconfined atomic layer deposition of TiO₂/Pt nanotubes: Toward ultrasmall highly efficient catalytic nanorockets. *Adv. Funct. Mater.* 2017; 27(24):1700598.
30. Wu Z, Lin X, Wu Y, et al. Near-infrared light-triggered "on/off" motion of polymer multilayer rockets. *ACS Nano.* 2014; 8(6):6097-6105.

31. Wu YJ, Wu ZG, Lin XK, He Q, Li JB. Autonomous movement of controllable assembled Janus capsule motors. *ACS Nano*. 2012; 6(12):10910-10916.
32. Jurado-Sanchez B, Escarpa A, Wang J. Lighting up micromotors with quantum dots for smart chemical sensing. *Chem. Commun*. 2015; 51(74):14088-14091.
33. Li JX, Liu ZQ, Huang GS, et al. Hierarchical nanoporous microtubes for high-speed catalytic microengines. *NPG Asia Mater*. 2014; 6:e94.
34. Sanchez S, Ananth AN, Fomin VM, Viehrig M, Schmidt OG. Superfast motion of catalytic microjet engines at physiological temperature. *J. Am. Chem. Soc*. 2011; 133(38):14860-14863.
35. Wang H, Zhao GJ, Pumera M. Blood proteins strongly reduce the mobility of artificial self-propelled micromotors. *Chem-Eur. J*. 2013; 19(49):16756-16759.
36. Zhao GJ, Sanchez S, Schmidt OG, Pumera M. Poisoning of bubble propelled catalytic micromotors: The chemical environment matters. *Nanoscale*. 2013; 5(7):2909-2914.
37. Gao W, Pei A, Dong RF, Wang J. Catalytic iridium-based Janus micromotors powered by ultralow levels of chemical fuels. *J. Am. Chem. Soc*. 2014; 136(6):2276-2279.
38. Teo WZ, Wang H, Pumera M. Beyond platinum: Silver-catalyst based bubble-propelled tubular micromotors. *Chem. Commun*. 2016; 52(23):4333-4336.
39. Maria-Hormigos R, Jurado-Sanchez B, Vazquez L, Escarpa A. Carbon allotrope nanomaterials based catalytic micromotors. *Chem. Mater*. 2016; 28(24):8962-8970.
40. Dey KK, Zhao X, Tansi BM, et al. Micromotors powered by enzyme catalysis. *Nano Lett*. 2015; 15(12):8311-8315.

41. Ma X, Hortelao AC, Miguel-Lopez A, Sanchez S. Bubble-free propulsion of ultrasmall tubular nanojets powered by biocatalytic reactions. *J. Am. Chem. Soc.* 2016; 138(42):13782-13785.
42. Li JX, Yu X, Xu ML, et al. Metal-organic frameworks as micromotors with tunable engines and brakes. *J. Am. Chem. Soc.* 2017; 139(2):611-614.
43. Feng XM, Zhang Y, Li Y, et al. Graphene-based highly efficient micromotors. *Chem. Lett.* 2015; 44(3):399-401.
44. Safdar M, Minh TD, Kinnunen N, Janis J. Manganese oxide based catalytic micromotors: Effect of polymorphism on motion. *ACS Appl. Mater. Inter.* 2016; 8(47):32624-32629.
45. Ye H, Sun H, Wang S. Electrochemical synthesis of graphene/MnO₂ in an architecture of bilayer microtubes as micromotors. *Chem. Eng. J.* 2017; 324:251-258.
46. Ye H, Ma G, Kang J, Sun H, Wang S. Pt-Free microengines at extremely low peroxide levels. *Chem. Commun.* 2018; 54:4653-4656.
47. Martin A, Jurado-Sanchez B, Escarpa A, Wang J. Template electrosynthesis of high-performance graphene microengines. *Small.* 2015; 11(29):3568-3574.
48. Wang YH, Zhitomirsky I. Cathodic electrodeposition of Ag-doped manganese dioxide films for electrodes of electrochemical supercapacitors. *Mater. Lett.* 2011; 65(12):1759-1761.
49. Tjeng LH, Meinders MB, van Elp J, et al. Electronic structure of Ag₂O. *Phys. Rev. B Condens. Matter.* 1990; 41(5):3190-3199.
50. Gao W, Sattayasamitsathit S, Orozco J, Wang J. Highly efficient catalytic microengines: Template electrosynthesis of polyaniline/platinum microtubes. *J. Am. Chem. Soc.* 2011; 133(31):11862-11864.

51. Li J, Huang G, Ye M, et al. Dynamics of catalytic tubular microjet engines: Dependence on geometry and chemical environment. *Nanoscale*. 2011; 3(12):5083-5089.
52. Li L, Wang J, Li T, Song W, Zhang G. Hydrodynamics and propulsion mechanism of self-propelled catalytic micromotors: Model and experiment. *Soft Matter*. 2014; 10(38):7511-7518.
53. Li YN, Wu J, Xie YZ, Ju HX. An efficient polymeric micromotor doped with Pt nanoparticle@carbon nanotubes for complex bio-media. *Chem. Commun*. 2015; 51(29):6325-6328.
54. Li TL, Li LQ, Song WP, et al. Self-propelled multilayered microrockets for pollutants purification. *ECS J. Solid State Sci. Technol*. 2015; 4(10):S3016-S3019.
55. Demirok UK, Laocharoensuk R, Manesh KM, Wang J. Ultrafast catalytic alloy nanomotors. *Angew. Chem. Int. Ed*. 2008; 47(48):9349-9351.
56. Laocharoensuk R, Burdick J, Wang J. Carbon-nanotube-induced acceleration of catalytic nanomotors. *ACS Nano*. 2008; 2(5):1069-1075.
57. Zhao GJ, Pumera M. Concentric bimetallic microjets by electrodeposition. *RSC Adv*. 2013; 3(12):3963-3966.
58. Wang H, Zhao GJ, Pumera M. Beyond platinum: Bubble-propelled micromotors based on Ag and MnO₂ catalysts. *J. Am. Chem. Soc*. 2014; 136(7):2719-2722.
59. Safdar M, Wani OM, Janis J. Manganese oxide-based chemically powered micromotors. *ACS Appl. Mater. Inter*. 2015; 7(46):25580-25585.
60. Gao W, Sattayasamitsathit S, Uygun A, et al. Polymer-based tubular microbots: Role of composition and preparation. *Nanoscale*. 2012; 4(7):2447-2453.

61. Singh AK, Mandal TK, Bandyopadhyay D. Magnetically guided chemical locomotion of self-propelling paperbots. RSC Adv. 2015; 5(79):64444-64449.
62. Wang LL, Chen J, Feng XM, et al. Self-propelled manganese oxide-based catalytic micromotors for drug delivery. RSC Adv. 2016; 6(70):65624-65630.
63. Wang H, Zhao GJ, Pumera M. Crucial role of surfactants in bubble-propelled microengines. J. Phys. Chem. C. 2014; 118(10):5268-5274.
64. Tu YF, Peng F, Sui XF, et al. Self-propelled supramolecular nanomotors with temperature-responsive speed regulation. Nat. Chem. 2017; 9(5):480-486.

Every reasonable effort has been made to acknowledge the owners of copyright material. I would be pleased to hear from any copyright owner who has been omitted or incorrectly acknowledged.

Chapter 5. High-Performance Pt-Free Microengines at Extremely Low Peroxide Levels

Abstract

Herein, we demonstrate that iron oxide modified MnO_2 (FeO_x-MnO_2) catalyzed micromotors can be fabricated by electrochemical co-reduction and that they exhibit exceptional high-performance at an extremely low hydrogen peroxide (H_2O_2) fuel concentration. We observed that the graphene/ FeO_x-MnO_2 microtubes could show motion behaviors at as low as 0.03% H_2O_2 , which is nearly one order of magnitude lower than Pt-based micromotors (normally at around 0.2% H_2O_2). Moreover, the micromotors exhibit higher speeds than any other reported catalytic micro/nanomotors (MNM) at low peroxide levels. The FeO_x-MnO_2 systems present as better catalytic MNMs, due to their excellent catalytic activity, easy fabrication, robust structure, and movement, as well as low-cost, biocompatible and abundance nature, showing a great potential for future applications.

5.1 Introduction

Micro/nanomotors (MNMs) have attracted extensive attention because of their wide potential applications in diverse areas.¹⁻⁹ Due to the good catalytic activity for hydrogen peroxide (H_2O_2) decomposition, precious rare metal platinum (Pt) has always been the most widely used catalytic material to construct the MNMs in different geometry shapes, such as micro/nano tubular engines,¹⁰⁻¹² Janus particles,^{13, 14} and bi-segment nanorods.¹⁵ However, the scarcity, high cost, and deactivation of Pt render its further application. Hence, researchers are searching for new catalysts and propelling mechanisms for MNMs.¹⁶ For examples, based on hydrogen bubbles generated by reactive metals with water or acids for propulsion, the reactive MNMs have been generated but they exhibit very short lifetime and the harsh reaction conditions limit them in real applications.¹⁷ Enzyme-based MNMs were also developed in a new propulsion strategy, because of the good catalytic performance over a wide range of biocatalytic reactions in mild environmental conditions.¹⁸ Nevertheless, the enzyme-based MNMs also suffer from quick deactivation in various media and harsh environment. The sophisticated synthetic procedures and low power output also hindered their future use.

MnO_2 based MNMs was developed to be an alternative to Pt, due to their low-cost, good propulsion, and robust nature.^{16, 19} The polycrystallinity and various synthesis and modification methods provide good opportunities for researchers to design MnO_2 catalyzed MNMs.²⁰ By geometry design and crystallinity tuning, some MnO_2 -based MNMs have been developed and tested.²¹ Although fruitful achievements have been made, the performance of MnO_2 based MNMs still cannot compete with the Pt-based MNMs due to inferior catalytic activity.²²

Herein we introduce a new catalyst for catalytic MNMs by doping MnO₂ with mixed valence iron oxide (denoted as FeO_x-MnO₂) by cathodic electrochemical co-deposition. We fabricated graphene/FeO_x-MnO₂ bilayer tubular and rod-shaped micromotors and evaluated their mobility performance. It is astounding to find that, the newly designed micromotors move much faster than any reported MNMs at a low peroxide fuel concentration below 1% H₂O₂. What is more, these MnO₂ based MNMs exceed the fuel concentration range limit of the Pt-based MNMs by nearly an order of magnitude, reaching an extremely low value of 0.03% H₂O₂ with an acceptable speed of $89 \pm 59 \mu\text{m s}^{-1}$. Due to the easiness of fabrication, high catalytic performance, low-cost, eco-friendly and biocompatible properties of the newly developed FeO_x-MnO₂ catalyst, we anticipate that a range of new MNMs based on this groundbreaking new strategy could be developed, and navigated at the very favorably low content of fuels to address diverse issues not limiting to the biomedical and environmental areas.

5.2 Experimental section

5.2.1 Materials and reagents

Potassium permanganate, iron (III) nitrate, sodium sulfate, ethanol, dichloromethane, sodium dodecyl sulfate (SDS), and sulfuric acid (98%) were purchased from Sigma-Aldrich. Hydrogen peroxide (30%) was purchased from ROWE Scientific Australia. Aluminum oxide paste was purchased from Kemet, NSW, Australia. Porous polycarbonate (PC) membranes with an average pore diameter of 5 μm were purchased from Whatman Inc., NY, USA. Ultrapure water (Milli-Q) was used in all experiments. Nano-sized graphene oxide (GO) was purchased from graphene supermarket, New York, USA.

5.2.2 Fabrication of MnO₂ based micromotors

Graphene/FeO_x-MnO₂ based micromotors were fabricated using a template-assisted electrochemical deposition protocol. A cyclopore polycarbonate membrane containing 5 μm conical-shaped micropores (Whatman, NY, USA) was employed as the template. An 80 nm of gold film was first deposited on one side of the porous membranes to serve as the working electrode using an Emitech K950X gold evaporator and performed at room temperature under a high vacuum of below 1×10^{-3} mBar at a direct current of 6 A. The deposition rate was about 1 nm s^{-1} . A customized plating cell was used in all electrochemical deposition processes.

The membrane was assembled in a self-designed plating cell with an aluminum foil serving as the contact for the working electrode. Electrochemical deposition was carried out using an electrochemical workstation (Zennium Zahner, Germany). A Pt wire and Ag/AgCl with 3M KCl were used as the counter and reference electrodes, respectively. A mixed solution of 0.1 mg mL^{-1} nano-sized graphene oxide in 0.5 M of Na₂SO₄ and 0.1 M H₂SO₄ was prepared as the electrolyte for the electrochemical growth of graphene outer layer. The graphene oxide in the solution was reduced by a cyclic voltammetry (CV) method from 0.3 to -1.5 V for five cycles.

After washing with 10 mL of ultrapure water for three times, the inner FeO_x-MnO₂ catalyst was deposited using a galvanostatic (GS) method at a cathodic current of -3 mA for 10 min or 30 min, respectively, which equals to 1.8 C or 5.4 C of charge transferred. Galvanostatic deposition at -3 mA for 10 min results in the formation of tubularly shaped micromotors. Galvanostatic deposition at -3 mA for 30 min results in the total closure

of the microtubes, forming the graphene wrapped microrods architecture. The electrolyte contains 20 mM of $\text{Fe}(\text{NO}_3)_3$ and 20 mM KMnO_4 .

Following the electroreduction deposition, the gold layer was removed by hand polishing with alumina slurry. Then the templates were dissolved in dichloromethane for 15 min to release the micromotors. Finally, the micromotors were collected by centrifugation at 7000 rpm for 3 min while being repeatedly washed with dichloromethane, ethanol and ultrapure water for three times each. The ultrasonication process was carried out using a Unisonics ultrasonication cleaner (Model FXP12D), and the centrifugation was carried out using an Eppendorf centrifuge 5430. All the micromotors were stored in ultrapure water at room temperature for further use.

5.2.3 Characterization of the micromotors

Scanning electronic microscopy (SEM/EDS) analysis was conducted using a Zeiss 1555 VP-FESEM with a field emission electron gun and the Oxford EDS detector operated by the Aztec software. SEM images were taken at the acceleration voltages from 2 to 5 kV. EDS analysis was taken using the coupled Oxford detector of the microscope and operated by the Aztec software at an acceleration voltage of 15 kV. X-ray photoelectron spectroscopy (XPS) was carried out on a thermos ESCALAB 250 XPS microscope with monochromatic $\text{Al-K}\alpha$ X-rays at a photo energy of 1486.7 eV. The measurement was carried out using a Kratos AXIS Ultra DLD system under UHV conditions with a base pressure of less than 1×10^{-9} mBar. The spectra were acquired with the pass energy of 20 eV and fitted using CasaXPS software. All the spectra were calibrated to yield a primary C 1s component at 284.6 eV with the Shirley background, and the

component fitting was applied by Voigt functions with 30% Lorentzian component.

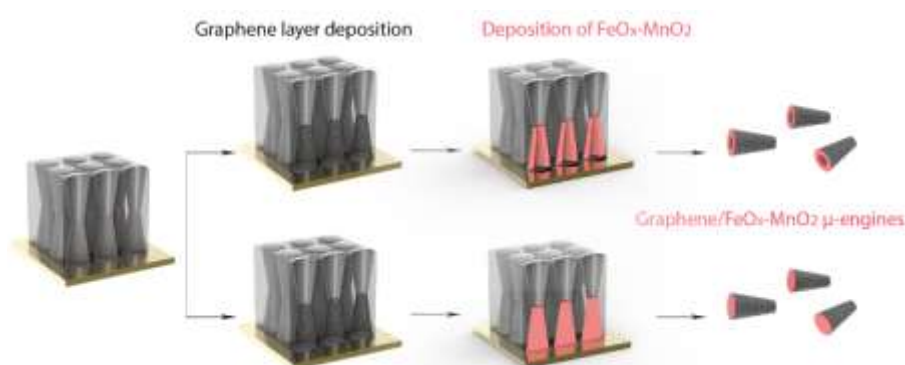
5.2.4 Motion behavior observation

A transparent plastic petri dish (Part No. P35G-1.5-10-C, Mat Tek Corporation, MA, USA) with the holed bottom covered by a thin glass slide was used as the container for the observation of motion behaviors. A 10 mm diameter bottom hole of the 35 mm diameter plastic petri dish was covered by a thin glass slide, which formed a shallow well-like hollow structure with a volume of approximately 75-80 μL . SDS was used as the surfactant for motion behavior observation. Optical microscopy videos were obtained using an Olympus IX81 inverted microscope with a Nikon digital sight DS-2Mv camera connected to a computer and operated by the Nikon NIS-Elements software. Motion behavior videos were recorded at about 12.5 frames per second using a 4X objective. The time interval between two frames is 0.08 s. Free Fiji software was used to calculate the speed of micromotors, edit videos and extract pictures. A digital hand-held "Pocket" H_2O_2 refractometer (Model: Atago, PAL-39S) was used to calibrate the concentrations of H_2O_2 solutions.

5.3 Results and discussion

Scheme 5.1 illustrates the fabrication process of the graphene/ $\text{FeO}_x\text{-MnO}_2$ micromotors. These bilayer micromotors were constructed by a two-step electrochemical deposition process. Firstly, an outer layer of electrochemically reduced graphene oxide (erGO) was formed by the deposition of graphene oxide into the pores of the membrane by a cyclic voltammetry (CV) method.²³ Secondly, an inner layer of $\text{FeO}_x\text{-MnO}_2$ catalyst was produced by the cathodically electrochemical co-deposition. The electrochemical reduction of MnO_4^- ions and Fe^{3+} ions occur

simultaneously. The synthetic parameters can be tailored to obtain rod-shaped and tubular micromotors.



Scheme 5.1. Schematic illustration of the fabrication of erGO/FeO_x-MnO₂ micromotors.

Figure 5.1 indicates that erGO/FeO_x-MnO₂ micromotors in microtube and microrod are fabricated successfully. Compared with the smooth tubular microengines, the inner surface of erGO/FeO_x-MnO₂ microengines exhibits a larger surface area of electrochemically active sites for improving the catalytic activity.²⁴ The co-deposition of iron oxide and MnO₂ generates a much thinner wall. As shown in Figure 5.1A and 5.1B, the wall thickness of the tubular micromotors is far less than 1 μm, which demonstrates its good mechanical properties. Without good mechanical strength and toughness, these tiny micro structures are very easy to be torn apart or crushed into pieces. This implies that the doping of iron oxide improves the mechanical strength of the micromotors, allowing the formation of the thin wall structured tubular micromotors with good structural integrity. The uniform distribution of carbon, oxygen, manganese, and iron demonstrates that the inner layer of iron oxide doped MnO₂ was fabricated successfully with good coverage by the outer graphene layer.

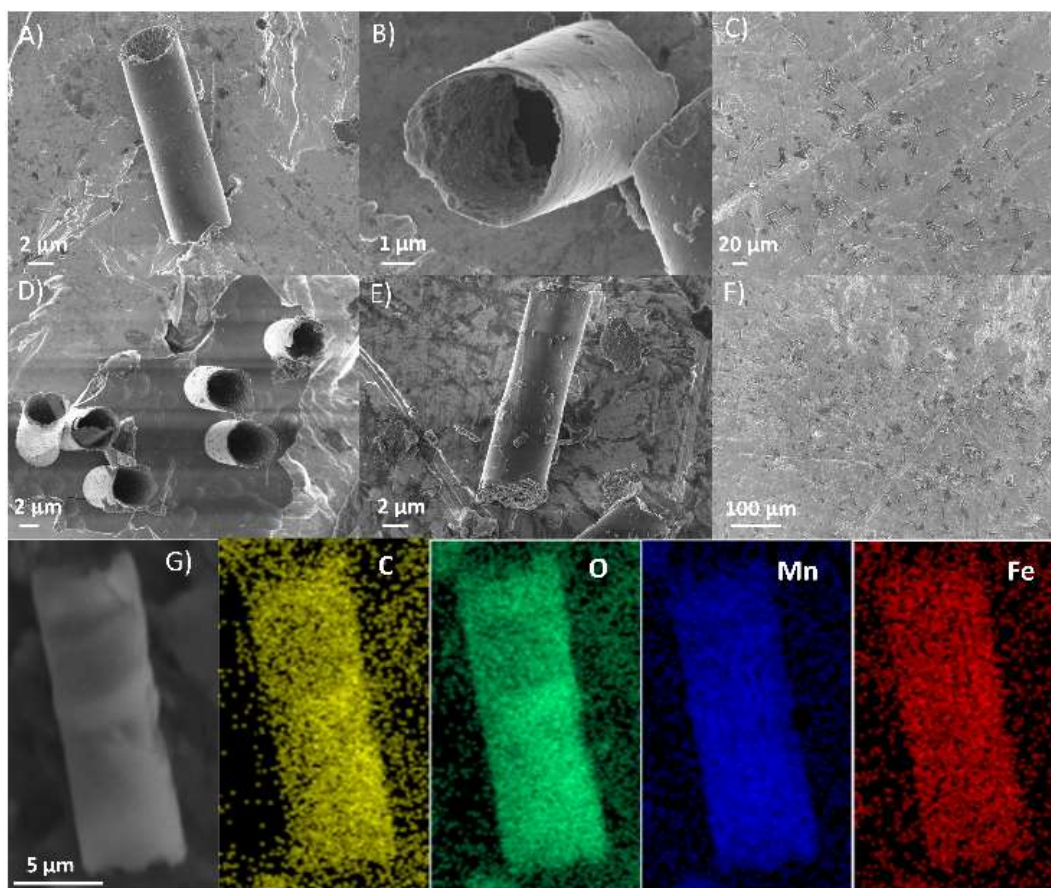


Figure 5.1. SEM and EDX mapping analysis of the erGO/FeO_x-MnO₂ micromotors: (A) a lying microtube, (B) an upright microtube, (C) many a microtubes, (D) an array of microtubes, (E) a microrods, (F) many a microrods, (G) EDX mapping analysis of a microtube.

As illustrated in Figure 5.2, XPS survey further reveals the presence of carbon (C 1s peak), oxygen (O 1s peak), manganese (Mn 2p peaks) and iron (Fe 2p peaks). The results are in good agreement with the SEM and EDX. The peaks of high-resolution C 1s (Figure 5.2B) and O 1s spectra (Figure 5.S1) correspond to the binding energy of various functional groups, such as C-C/C-H/C=C, C-OH, C=O, and O-C=O, revealing the nature of the covalent bonds of oxygen and carbon atoms.²⁵ The quantities of the various functional groups are summarized in Table 5.1. The ratio of sp² carbons is at 68.33%, which indicates the degree of oxidation of the outer layer of the micromotor.

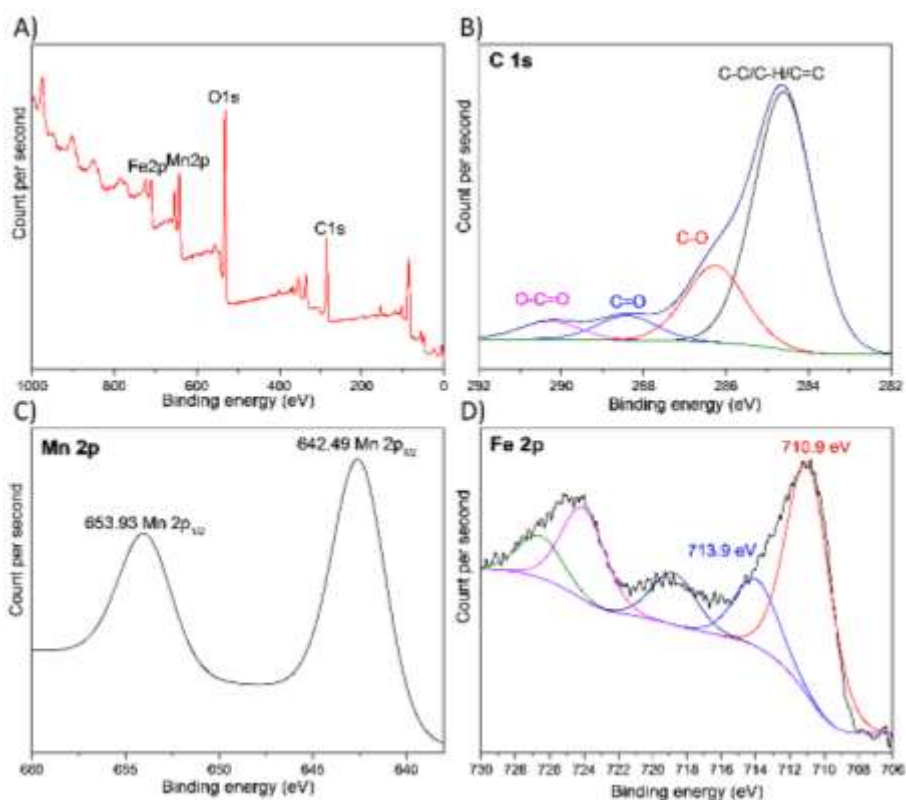


Figure 5.2. XPS survey of the erGO/FeO_x-MnO₂ micromotors. (A) Wide scan showing Mn 2p, O 1s, C 1s, and Fe 2p peaks. (B) High-resolution C 1s XPS spectra. (C) High-resolution Mn 2p XPS spectra. (D) High-resolution Fe 2p XPS spectra.

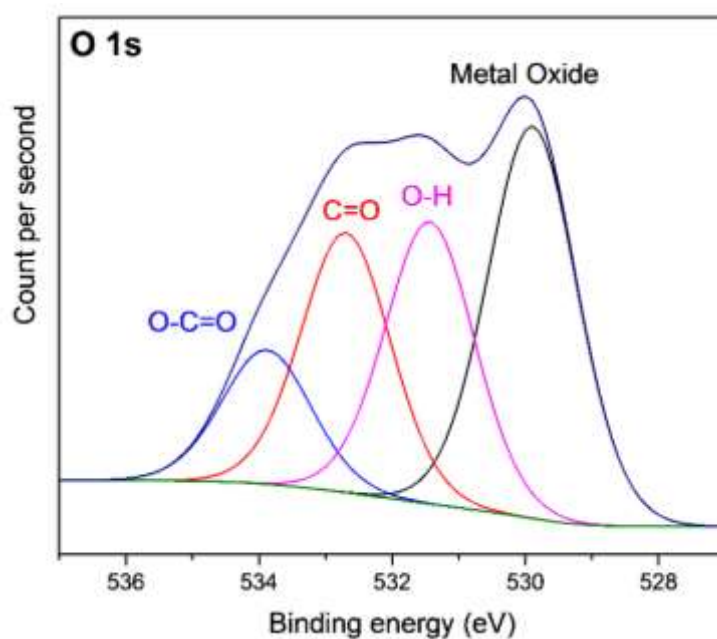


Figure 5.S1. XPS results of the O1s spectra of the erGO/FeO_x-MnO₂ micromotors.

Table 5.1. Various functional groups identified on the surface of erGO/FeO_x-MnO₂ micromotors.

Spectra	Group	Position (eV)	at. %
C 1s	C-C/C-H/C=C	284.6	68.33
C 1s	C-O	286.26	20.41
C 1s	C=O	288.40	6.47
C 1s	O-C=O	290.28	4.79
O 1s	Metal Oxide	529.89	36.71
O 1s	O-H	531.44	26.41
O 1s	C=O	532.70	24.32
O 1s	O-C=O	533.88	12.57

Due to a higher cathode current for reduction of the iron oxide doped MnO₂ catalyst, the oxidation degree is much lower than our previously designed MnO₂ based micromotors, which means that more graphene carbon lattice is recovered by the cathode galvanostatic electroreduction.²⁶ The high-resolution Mn 2p XPS spectra reveal the oxidation state of Mn (Fig. 5.2C). The peaks observed at the binding energies of 642.49 and 653.93 eV were attributed to the Mn 2p with the spin-orbit splitting of 11.44 eV. The Mn 2p_{3/2} peak located at 642.49 eV indicates the main oxidation state of Mn⁴⁺.²⁶

Figure 5.2D shows the high-resolution XPS spectra of Fe 2p for the iron oxide doped MnO₂ micromotors. The peaks at binding energies of 710.9 and 724.2 eV correspond to Fe 2p_{3/2} and Fe 2p_{1/2}, respectively.²⁷ It can be noted that the Fe atomic distribution is a mixture of Fe²⁺ (710.9 eV), and Fe³⁺ (713.9 eV) with 77.5% of the iron species as Fe²⁺.²⁸ Due to the electrochemical reduction process, Fe²⁺ ions are generated, but no zero valence iron (Fe⁰ peak usually exists at around 707.1 eV) was generated. Instead, a small proportion of Fe³⁺ was also doped into the MnO₂ matrix, as shown by the peak around 713.9 eV. Hence, the inner layer catalyst can be denoted as mixed-valence iron doped MnO₂.

As demonstrated in Figure 5.3A, the speed of all the micromotors exhibits an increasing tendency over the entire H₂O₂ fuel range with 1% SDS as the surfactant. The tubular micromotors demonstrate exceptionally high performance at extremely low peroxide levels. The speed of erGO/FeO_x-MnO₂ tubular micromotors is 4 times faster than that of the erGO/Pt micromotors (187 ± 80 vs $37 \pm 10 \mu\text{m s}^{-1}$) in 0.1% H₂O₂, which is the minimum fuel requirement for the best reported Pt catalyzed micromotors.²³ What is more, the erGO/FeO_x-MnO₂ micromotors can easily utilize even a lower fuel concentration of 0.03% H₂O₂ with a speed of $89 \pm 59 \mu\text{m s}^{-1}$, which is more than two-fold the speed of the erGO/Pt micromotors at a much higher fuel concentration of 0.1% H₂O₂. Moreover, the minimal fuel content is two order of magnitude lower than the 3% value of the graphene/MnO₂ micromotors.²⁶ At a slightly higher fuel concentration of 3%, the erGO/FeO_x-MnO₂ micromotors can easily exceed 1 mm s^{-1} , which is also remarkably high compared with polymer/Pt micromotors, PANI/Pt, PPy/Pt, and PEDOT/Pt, which cannot exceed 1 mm s^{-1} in 3% H₂O₂.²⁴ The erGO/FeO_x-MnO₂ micromotors also exceed the

speed of all the Pt-based rolled-up multi-layer tubular micromotors and Janus motors at a relatively higher fuel content.^{10, 29}

As shown in Figure 5.3B, the tubular micromotors show circular motion behaviors at 0.03% H₂O₂. Ultrafast helical and irregular motion behaviors were also observed (Figure 5.3C and 5.3D). As far as we know, Pt-based micromotors require at least 0.1% H₂O₂ for propulsion, and MnO₂ based micromotors demand an even higher fuel concentration, while we demonstrate here that the Pt-free mixed-valence iron oxide doped MnO₂ catalyzed micromotors could extend the fuel concentration to a very low threshold value of 0.03% with an acceptable velocity. The groundbreaking new catalyst along with the simple and low-cost fabrication method provides a new strategy to fabricate MNMs and will greatly boost motion in the tiny world.

As the surfactants are quite indispensable for the motion of bubble propelled tubular MNMs, the effect of the SDS surfactant on motion of FeO_x-MnO₂ micromotors could provide insight for us to manipulate the motion behaviors.^{30, 31} Hence we investigated the mobility of the micromotors in 1%, 0.5%, and 0.05% H₂O₂ with different SDS concentrations, as shown in Figure 5.4A, 5.4B, and 5.4C, respectively. At an extremely low content of surfactant, the micromotors could not move, while at a very high content of the surfactant, the high viscosity of fluid would have an adverse effect on the motion to decrease the speed of micromotors. Hence, the minimal and optimal SDS surfactant contents for the micromotors at certain H₂O₂ fuel contents are important.

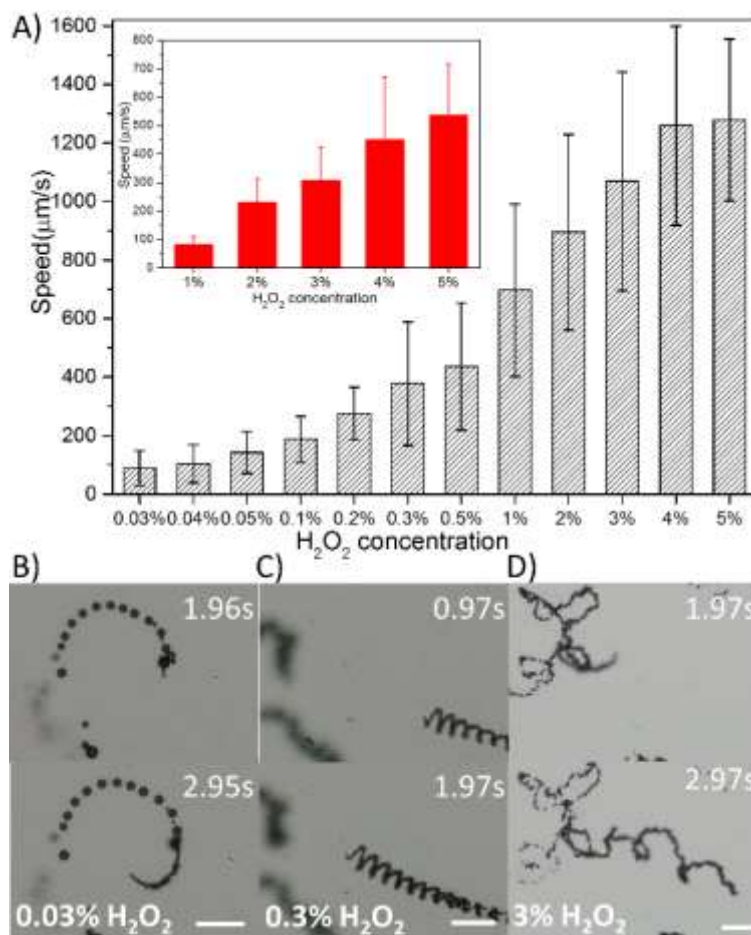


Figure 5.3. Speed profile of erGO/FeO_x-MnO₂ micromotors in 1% SDS (n = 50). Average speed of tubular micromotors (inset: rod-shape micromotor) (A); Time-lapse images of tubular micromotors in 0.03% (B), 0.3% (C), and 3% (D) H₂O₂. (Scale bars: 100 μm).

As shown in Figure 5.4, the blue bar corresponds to the minimal SDS concentration, while the red bar corresponds to the optimal surfactant content. It is interesting that as the fuel concentration drops from 1% to 0.05%, the minimal SDS concentration increases from 0.05% at 1% H₂O₂ to 0.3% at 0.5% H₂O₂ and finally reaches 0.6% at 0.05% H₂O₂. Meanwhile, the optimal SDS concentrations are 7%, 5%, and 3%, respectively. Under the optimized conditions, the speed of erGO/FeO_x-MnO₂ tubular micromotors are $1102 \pm 262 \mu\text{m s}^{-1}$, $453 \pm 97 \mu\text{m s}^{-1}$, and $222 \pm 91 \mu\text{m s}^{-1}$ in 1%, 0.5%, and 0.05% H₂O₂, respectively.

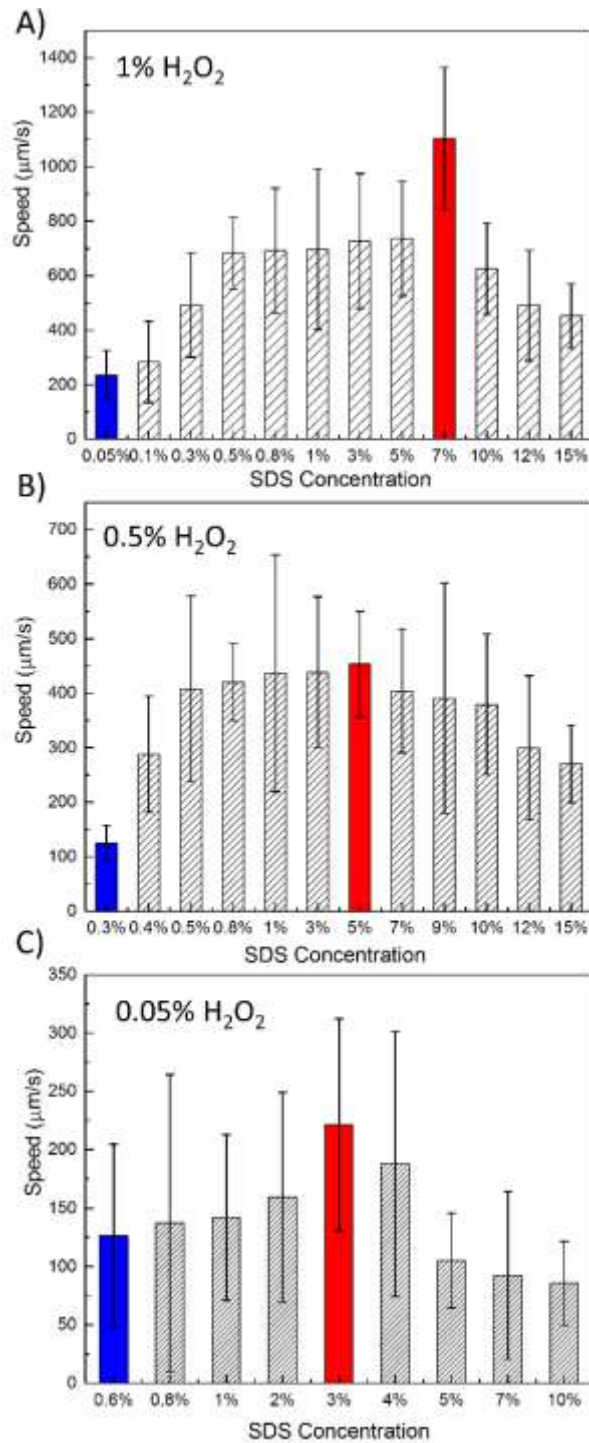


Figure 5.4. Dependence of average speed of erGO/FeO_x-MnO₂ micromotors with varying SDS contents in 1% H₂O₂ (A); 0.5% H₂O₂ (B); and 0.05% H₂O₂ (C) (n=50).

The higher performance is usually obtained at moderate surfactant concentrations. This phenomenon can be used in sensing, detection, and motion-based analysis applications. To the best of our knowledge, the

unveiled high-speed mobility property at this low content of fuels far exceeds other reported MNMs under the same fuel conditions (Table 5.2). As the toxicity of high concentration of H_2O_2 fuels are the major obstacles for biomedical application, the iron-doped manganese oxide MNMs will show a good prospect in biomedical and environmental applications due to lower toxicity of the MNMs. The advantage of the new types of MNMs provides a new route to minimize the use of toxic fuel and surfactants thus paves the way for biomedical applications, such as drug delivery. This new strategy could also minimize the environmental impact as lower contents of fuel and surfactants are needed for efficient motion.

For such fascinating mobility performance of this new-type microengines, several effects take place. First and most importantly, the mixed valence iron doped MnO_2 catalyst exhibits a much high catalytic activity for H_2O_2 decomposition to produce oxygen, which gives faster generation and ejection of microbubbles. The rough inner catalytic layer also contributes to the improved catalytic performance. Secondly, the improved mechanical strength of the $\text{FeO}_x\text{-MnO}_2$ catalyst allows for the formation of a thin-wall tubular structure, thus significantly reducing the weight of the micromotors. Thirdly, the big difference of the density between the iron oxide doped MnO_2 (usually the density is $\approx 5 \text{ g/cm}^3$) and Pt (the density is $\approx 20 \text{ g/cm}^3$) makes MnO_2 based MNMs much lighter than Pt-based tubular microengines. Fourthly, the ultra-thin wall of the graphene/ $\text{FeO}_x\text{-MnO}_2$ tubular microengines would facilitate the fluid flow in the microtubes and minimize the effect of fluid resistance. Therefore, the structure design of the thin wall and the improved catalytic performance of the tubular microengines resulted in the exceptional high mobility at extremely low peroxide levels.

Upon fuel added, microbubbles were generated and the micromotors start to move. The lifetime of these micromotors could exceed 25 min but only the first few minutes were taken into account for the speed calculation as the depletion of fuel will have a significant effect on the speed of micromotors. At a very high content of fuels, such as 10% of H₂O₂, the fuel solution reacts very fast with the catalytic micromotors, thus the observed lifetime of micromotors is shortened due to the consumption of the catalytic materials. At a very low content of the fuel, such as 0.03% H₂O₂, although the reaction consumption of catalytic materials is not a problem, the fuel depletion will significantly affect the lifetime of these micromotors, these micromotors will stop moving very soon. Upon refuel the petri dish, these micromotors will initiate motion. What we have observed is that at moderate fuel levels and surfactant content, it is very easy for these micromotors to navigate for more than 25 min.

Taking the microengines as a cylinder microrod, we can adopt the Stokes' drag theory to estimate the drag force or propelling force roughly by the following equation.^{11, 32}

$$F_d = \frac{2\pi\mu LU}{\ln(L/a)-1/2} \quad (\text{Eq. 5.1})$$

Where F_d is the fluid resistance, U is the speed of the microengines, μ is the fluid dynamic viscosity, and L and a are the length and radius of the micromotors, respectively. The estimated drag forces for the four types of micromotors are presented in Table 5.2, which also summarizes the speed profile of different MNMs reported so far. The estimated drag force for the graphene/FeO_x-MnO₂ micromotors is 6.3 pN in 0.03% H₂O₂ and 91.1 pN in 5% H₂O₂.

Table 5.2. Comparison of the performance of catalytic MNMs.

Type of the micro-/nanomotor	Ref.	Size [μm]	H ₂ O ₂ fuel content [%]	Average speed [$\mu\text{m s}^{-1}$]	Max. speed reported [$\mu\text{m s}^{-1}$]	Max. relative speed (bl s ⁻¹)	Efficiency or propelling force (pN)
Rolled up Ti/Cr/Pt microtubes	Sanchez and Schmidt et al. ¹²	50	0.25-5	140-10000 at 37°C	10000	200	
Multilayered microrockets	Li and Zhang et al. ³³	20	1-5	285-1410	1410	70	
Pt-Alloy nanowires	Wang et al. ¹⁵	2	15	110	160	75	
Au/Pt-CNT nanowires	Wang et al. ³⁴	2	15	51	91	45.5	
Cu/Pt concentric bimetallic microtubes	Zhao and Pumera et al. ³⁵	10	0.2-3	70-700	n.a.	70	
Cu/Ag segmented bimetallic tubular micromotors	Pumera et al. ³⁶	10-15	0.5-3	13.1-252.4	n.a.	n.a.	2.52×10 ⁻⁹
Ag and MnO ₂ microparticles	Pumera et al. ¹⁶	Ag≈30 MnO ₂ ≈5	0.1-12 12-21	25-100 50-120	n.a.	n.a.	5.81×10 ⁻⁸ 1.16×10 ⁻⁸
Au/Graphene/MnO ₂	Feng and Ma et al. ³⁷	6.74	0.15-2.5	15.79-44.79	111.03	27.69	
PEDOT/MnO ₂ microtubes & microrods And MnO ₂ @MnCO ₃	Saldar and Janis et al. ¹⁹	12.5 12.5 5	5-15 5-15 1-10	Tubes 200-510 Rods 200-410 142-665	n.a. 900	n.a. 180	
Graphene/Pt	Wang et al. ²³	10	0.1-3	37-1700	n.a.	170	
MnO ₂ hallow	Saldar and Janis et al. ²¹	n.a.	5-10	321-996	1625	n.a.	
PANI/Pt microtubes	Gao and Wang et al. ¹¹	8	0.2-5	25-1410	3000	375	45 pN
PEDOT/Pt bilayer microtubes PPy/Ag bilayer PPy/Pt-Ni alloy Au/Pt bimetallic microbots	Gao and Wang et al. ²⁴	7	10 5-10 15 10 10	10000 at 37°C 2400-3350 500 470 1500	10000 at 37°C 3375 at 20°C	1400 480 70 67	
Paper tubular microjet engines	Singh and Mandal et al. ³⁸	900	9-16	270-1600	1600	2	
PEDOT/MnO ₂	Wang et al. ³⁹	8	0.4-10	31.57-318.80	n.a.	n.a.	
PEDOT/PtNP@CNT-PPy	Li and Wu et al. ³²	12	1-15	62-450	n.a.	n.a.	10 pN
Porous Ti/Cr/Pt microtubes	Mei et al. ⁴⁰	10-40	0.2-7	120-1077	>1500	n.a.	
erGO/MnO ₂ microtubes by anodic deposition	Our previous work ²⁶	8	3-15	77-466	700	87.5	36 pN
erGO/FeO _x -MnO ₂ microtubes	This work	12	0.03-5	89-1279	1779	148.25	6-91 pN

5.4 Conclusions

In conclusion, we demonstrate the first example of tubular microengines that propel efficiently by the thrust of oxygen bubbles in an extremely low H₂O₂ level (0.03%), which is nearly an order of magnitude lower than the previously reported values at around 0.2%. At below 1% of H₂O₂ fuel, the graphene/FeO_x-MnO₂ micromotors can move at a far exceeded speed of any reported MNMs. Such high-performance, low-cost micromotors could greatly expand the research and applications of micro/nano scale motion tools and devices, and could thus lead to new biomedical and environmental applications for drug delivery or biological entity manipulation and environmental cleaning. In addition, the doping fabrication strategy provides a new approach to the designing of new types of MNMs.

References

1. Tu YF, Peng F, Wilson DA. Motion manipulation of micro- and nanomotors. *Adv. Mater.* 2017; 29(39):1701970.
2. Peng F, Tu Y, Wilson DA. Micro/nanomotors towards in vivo application: Cell, tissue and biofluid. *Chem. Soc. Rev.* 2017; 46(17):5289-5310.
3. Dey KK, Sen A. Chemically propelled molecules and machines. *J. Am. Chem. Soc.* 2017; 139(23):7666-7676.
4. Li JX, Rozen I, Wang J. Rocket science at the nanoscale. *ACS Nano.* 2016; 10(6):5619-5634.
5. Wang H, Pumera M. Fabrication of micro/nanoscale motors. *Chem. Rev.* 2015; 115(16):8704-8735.
6. Sanchez S, Soler L, Katuri J. Chemically powered micro- and nanomotors. *Angew. Chem. Int. Ed.* 2015; 54(5):1414-1444.

7. Duan W, Wang W, Das S, et al. Synthetic nano- and micromachines in analytical chemistry: Sensing, migration, capture, delivery, and separation. *Annu. Rev. Anal. Chem.* 2015; 8(1):311-333.
8. Guix M, Mayorga-Martinez CC, Merkoci A. Nano/micromotors in (bio)chemical science applications. *Chem. Rev.* 2014; 114(12):6285-6322.
9. Gao W, Wang J. The environmental impact of micro/nanomachines: A review. *ACS Nano.* 2014; 8(4):3170-3180.
10. Yao K, Manjare M, Barrett CA, et al. Nanostructured scrolls from graphene oxide for microjet engines. *J. Phys. Chem. Lett.* 2012; 3(16):2204-2208.
11. Gao W, Sattayasamitsathit S, Orozco J, Wang J. Highly efficient catalytic microengines: Template electrosynthesis of polyaniline/platinum microtubes. *J. Am. Chem. Soc.* 2011; 133(31):11862-11864.
12. Sanchez S, Ananth AN, Fomin VM, Viehrig M, Schmidt OG. Superfast motion of catalytic microjet engines at physiological temperature. *J. Am. Chem. Soc.* 2011; 133(38):14860-14863.
13. Orozco J, Mercante LA, Pol R, Merkoci A. Graphene-based Janus micromotors for the dynamic removal of pollutants. *J. Mater. Chem. A.* 2016; 4(9):3371-3378.
14. Ma X, Hahn K, Sanchez S. Catalytic mesoporous Janus nanomotors for active cargo delivery. *J. Am. Chem. Soc.* 2015; 137(15):4976-4979.
15. Demirok UK, Laocharoensuk R, Manesh KM, Wang J. Ultrafast catalytic alloy nanomotors. *Angew. Chem. Int. Ed.* 2008; 47(48):9349-9351.
16. Wang H, Zhao GJ, Pumera M. Beyond platinum: Bubble-propelled micromotors based on Ag and MnO₂ catalysts. *J. Am. Chem. Soc.* 2014; 136(7):2719-2722.

17. Li J, Singh VV, Sattayasamitsathit S, et al. Water-driven micromotors for rapid photocatalytic degradation of biological and chemical warfare agents. *ACS Nano*. 2014; 8(11):11118-11125.
18. Ma X, Hortelao AC, Miguel-Lopez A, Sanchez S. Bubble-free propulsion of ultrasmall tubular nanojets powered by biocatalytic reactions. *J. Am. Chem. Soc.* 2016; 138(42):13782-13785.
19. Safdar M, Wani OM, Janis J. Manganese oxide-based chemically powered micromotors. *ACS Appl. Mater. Inter.* 2015; 7(46):25580-25585.
20. Wani OM, Safdar M, Kinnunen N, Janis J. Dual effect of manganese oxide micromotors: Catalytic degradation and adsorptive bubble separation of organic pollutants. *Chem-Eur. J.* 2016; 22(4):1244-1247.
21. Safdar M, Minh TD, Kinnunen N, Janis J. Manganese oxide based catalytic micromotors: Effect of polymorphism on motion. *ACS Appl. Mater. Inter.* 2016; 8(47):32624-32629.
22. He X, Bahk YK, Wang J. Organic dye removal by MnO₂ and Ag micromotors under various ambient conditions: The comparison between two abatement mechanisms. *Chemosphere*. 2017; 184:601-608.
23. Martin A, Jurado-Sanchez B, Escarpa A, Wang J. Template electrosynthesis of high-performance graphene microengines. *Small*. 2015; 11(29):3568-3574.
24. Gao W, Sattayasamitsathit S, Uygun A, et al. Polymer-based tubular microbots: Role of composition and preparation. *Nanoscale*. 2012; 4(7):2447-2453.
25. Vilela D, Parmar J, Zeng Y, Zhao Y, Sanchez S. Graphene-based microbots for toxic heavy metal removal and recovery from water. *Nano Lett.* 2016; 16(4):2860-2866.

26. Ye H, Sun H, Wang S. Electrochemical synthesis of graphene/MnO₂ in an architecture of bilayer microtubes as micromotors. *Chem. Eng. J.* 2017; 324:251-258.
27. Parmar J, Vilela D, Pellicer E, et al. Reusable and long-lasting active microcleaners for heterogeneous water remediation. *Adv. Funct. Mater.* 2016; 26(23):4152-4161.
28. Jia Z, Duan XG, Qin P, et al. Disordered atomic packing structure of metallic glass: Toward ultrafast hydroxyl radicals production rate and strong electron transfer ability in catalytic performance. *Adv. Funct. Mater.* 2017; 27(38):1702258-n/a.
29. Ma X, Katuri J, Zeng Y, Zhao Y, Sanchez S. Surface conductive graphene-wrapped micromotors exhibiting enhanced motion. *Small.* 2015; 11(38):5023-5027.
30. Simmchen J, Magdanz V, Sanchez S, et al. Effect of surfactants on the performance of tubular and spherical micromotors - a comparative study. *RSC Adv.* 2014; 4(39):20334-20340.
31. Wang H, Zhao GJ, Pumera M. Crucial role of surfactants in bubble-propelled microengines. *J. Phys. Chem. C.* 2014; 118(10):5268-5274.
32. Li YN, Wu J, Xie YZ, Ju HX. An efficient polymeric micromotor doped with Pt nanoparticle@carbon nanotubes for complex bio-media. *Chem. Commun.* 2015; 51(29):6325-6328.
33. Li TL, Li LQ, Song WP, et al. Self-propelled multilayered microrockets for pollutants purification. *ECS J. Solid State Sci. Technol.* 2015; 4(10):S3016-S3019.
34. Laocharoensuk R, Burdick J, Wang J. Carbon-nanotube-induced acceleration of catalytic nanomotors. *ACS Nano.* 2008; 2(5):1069-1075.
35. Zhao GJ, Pumera M. Concentric bimetallic microjets by electrodeposition. *RSC Adv.* 2013; 3(12):3963-3966.

36. Teo WZ, Wang H, Pumera M. Beyond platinum: Silver-catalyst based bubble-propelled tubular micromotors. *Chem. Commun.* 2016; 52(23):4333-4336.
37. Feng XM, Zhang Y, Li Y, et al. Graphene-based highly efficient micromotors. *Chem. Lett.* 2015; 44(3):399-401.
38. Singh AK, Mandal TK, Bandyopadhyay D. Magnetically guided chemical locomotion of self-propelling paperbots. *RSC Adv.* 2015; 5(79):64444-64449.
39. Wang LL, Chen J, Feng XM, et al. Self-propelled manganese oxide-based catalytic micromotors for drug delivery. *RSC Adv.* 2016; 6(70):65624-65630.
40. Li JX, Liu ZQ, Huang GS, et al. Hierarchical nanoporous microtubes for high-speed catalytic microengines. *NPG Asia Mater.* 2014; 6:e94.

Every reasonable effort has been made to acknowledge the owners of copyright material. I would be pleased to hear from any copyright owner who has been omitted or incorrectly acknowledged.

Chapter 6. Robust MnO₂ Based Microengines for Surfactant Independent Propulsion

Abstract

Micro/nanomotors (MNMs) have attracted tremendous research interest due to their wide potential applications in biomedicine and environmental fields. MnO₂ based catalysts are alternatives to platinum chemically powered MNMs due to their low cost, low toxicity, good performance, and abundance. Various MnO₂ based micromotors have been demonstrated in H₂O₂-surfactant driven systems, but there is no systematic investigation on the effect of different surfactants, which is a basic requirement for moving of MNMs. Herein, we choose four types of surfactants and two types of commercial detergents to investigate the influence of the surfactants on the motion behaviors of a typical graphene/MnO₂ tubular micromotors. The results suggested that the graphene/MnO₂ tubular micromotors are active nanomaterials, showing robust performance at different conditions, better than Pt-MNMs. This investigation improves our understanding of the microscaled motion of MNMs and provides a guide for the further application of the emerging MnO₂ based MNMs for environmental remediation.

6.1 Introduction

As a versatile tool for motion-based nanoscale operation and practice, self-propelled micro/nanomotors (MNM)s are expected to address diverse issues in biomedicine and environmental fields.¹⁻¹⁰ Tremendous proof-of-concept applications were demonstrated based on the catalytic decomposition of hydrogen peroxide (H_2O_2) for propulsion, such as cleaning wastewater,⁸ targeted cargo delivery,¹⁰ tumor cell manipulation,⁵ and chemical sensing.¹¹ Previously, the majority of the catalytic MNMs are relying on the precious rare metal platinum (Pt) as a catalyst to decompose H_2O_2 for propulsion.¹²⁻¹⁵ Pt-based catalysts with various geometry forms, such as Janus particles,¹⁶ tubular microengines,¹⁷ bi-segment microrods,¹⁸ and Pt nanoparticles¹⁹ were incorporated as the engine part for MNMs. However, Pt-based MNMs suffer from the high-cost, scarcity, and possibility of deactivation in various media, impeding their further applications.^{20, 21} MnO_2 based MNMs could circumvent the drawbacks of Pt due to the good catalytic performance, low-cost, and abundance, as well as various fabrication and modification methods.²²⁻²⁴ MnO_2 based micromotors are emerging as the next generation MNMs for many applications, such as drug delivery²⁵ and environmental cleaning.²⁶ ²⁷ Despite great efforts made to study the alternative fuel for H_2O_2 , little attention has been paid to the role of a surfactant in the micro/nano scale motion. Two reports have already studied the effect of surfactants on the motion behaviors of Pt-based micromotors exclusively,^{28, 29} but no investigation has been reported on MnO_2 based micromotors. Up to now, the choice of surfactants for the MNMs are quite random.^{17, 30, 31} To fully exploit MnO_2 as catalytic MNMs, it is imperative to study the role of different surfactant solutions in the motion behaviors.

Surfactants are usually amphiphilic bipolar organic compounds, which have a hydrophobic group as the tail and a hydrophilic group as the head. Previously, Pumera's group studied the effect of surfactants on the motion behaviors of Pt-based tubular microengines.³² They found that the Pt-based microengines are much more active in the presence of an anionic surfactant sodium dodecyl sulfate (SDS) than the non-ionic surfactant Tween 20. However, the microengines lost their mobility in the presence of a cationic surfactant cetyltrimethylammonium bromide (CTAB). They suggested that the charging property affects the surfactant adsorption process. The anionic surfactant would easily adsorb onto the positively charged Pt surface of microjets due to electrostatic attraction, while the cationic surfactant CTAB has to overcome repulsion to be adsorbed onto the inner catalytic surface.³² Schmidt et al.²⁸ investigated the effect of surfactants on the performance of Pt-based tubular and Janus particle micromotors. The Janus particles propel at a much higher speed at a low content of surfactants, while the tubular micromotors require a much higher surfactant content to acquire the maximum speeds. The reasons for these phenomena are not totally clear, as most of the explanations are based on empirical or description reasoning. In addition, the results obtained at different research groups using different MNMs systems cannot always show consistency. Hence, a systematic investigation is needed to generate a more comprehensive insight on the role of surfactants to promote the motion at a micro scale.

Herein, we choose four types of pure surfactants and two types of commercial dishwashing liquids as the surfactants to study the influence of a surfactant on the motion of MnO₂ based tubular micromotors. The surfactants are SDS as the anionic surfactant, CTAB as the cationic surfactant, N-Dodecyl-N, N-dimethyl-3-ammonio-1-propanesulfonate

(DDPS) as a zwitterionic surfactant, and Triton-X-100 as the non-ionic surfactant. (Table 6.1) Two commercially available detergents were also chosen as the mixture of surfactants. (Table 6.2-6.3). It seems that the propulsion of MnO₂ based micromotors is quite independent of the surfactants, which is different from Pt-based MNMs. The speed profiles of the MnO₂ based micromotors in each surfactant show a similar style. After passing the minimal surfactant requirement, these micromotors speed up to its maximum value or plateau as the surfactant concentration reaches its optimal region. Then the speed of the micromotors shows a decreasing tendency as the higher surfactant levels would increase the fluid resistance. The first ever demonstrated surfactant independent propulsion phenomena paves a better way for environmental remediation strategy as well as novel biomedical applications.

6.2 Experimental section

6.2.1 Materials and reagents

Potassium permanganate, sodium sulfate, ethanol, dichloromethane, SDS, Triton-X-100, DDPS, CTAB, and sulfuric acid (98%) were purchased from Sigma-Aldrich. H₂O₂ (30%) was purchased from ROWE Scientific Australia. Aluminum oxide paste was purchased from Kemet, NSW, Australia. Two commercial dishwashing liquids were collected from the lab, Palmolive ultra-original (denoted as Palmolive) dish wash liquid and Earth Choice dish wash Liquid – Lemon Fresh and Aloe Fresh (denoted as Earth Choice). Porous polycarbonate (PC) membranes with an average pore diameter of 5 μm were purchased from Whatman Inc., NY, USA. Ultrapure water (Milli-Q) was used in all experiments. Nano-sized graphene oxide (GO) was purchased from graphene supermarket, New York, USA.

6.2.2 Fabrication of MnO₂ based micromotors

Graphene wrapped MnO₂ based micromotors were fabricated using a template-assisted electrochemical deposition protocol. A cyclopores polycarbonate membrane containing 5 μm conical-shaped micropores (Whatman, NY, USA) was employed as the template. An 80 nm of gold film was first deposited on one side of the porous membranes to serve as the working electrode using an Emitech K950X gold evaporator and performed at room temperature under a high vacuum of below 1×10^{-3} mBar at a direct current of 6 A. The deposition rate was about 1 nm s^{-1} . A customized plating cell was used in all electrochemical deposition processes. The membrane was assembled in a self-designed plating cell with an aluminum foil serving as the contact for the working electrode. Electrochemical deposition was carried out using an electrochemical workstation (Zennium Zahner, Germany). A Pt wire and Ag/AgCl with 3M KCl were used as the counter and reference electrodes, respectively. A mixed solution of 0.1 mg mL^{-1} nano-sized graphene oxide in 0.5 M of Na₂SO₄ and 0.1 M H₂SO₄ was prepared as the electrolyte for the electrochemical growth of graphene outer layer. The graphene oxide in the solution was reduced by a cyclic voltammetry (CV) method from 0.3 to -1.5 V for five cycles. After washing with 10 mL of ultrapure water for three times, the inner MnO₂ layer was deposited using a galvanotactic (GS) method at a current of -1 mA for 20 min, which equals to 1.2 C of charge transferred. For the cathodic reduction deposited MnO₂ inner layer, 1.2 C of charge transfer is the optimal value for the synthesis of graphene wrapped MnO₂ based microtubes. For MnO₂ deposition, the electrolyte solution was 20 mM KMnO₄. Following the electroreduction deposition, the gold layers were removed by hand polishing with alumina slurry. Then the templates were dissolved in dichloromethane for 15 min to release

micromotors. Finally, the micromotors were collected by centrifugation at 7000 rpm for 3 min while being repeatedly washed with dichloromethane, ethanol and ultrapure water for three times each. The ultrasonication process was carried out using a Unisonics ultrasonication cleaner (Model FXP12D), and the centrifugation was carried out using an Eppendorf centrifuge 5430. All the micromotors were stored in ultrapure water at room temperature for further use.

6.2.3 Motion behaviors observation

A transparent plastic petri dish (Part No. P35G-1.5-10-C, Mat Tek Corporation, MA, USA) with a holed bottom covered by a thin glass slide was used as the container to prepare different fuel concentrations for observation of motion behavior. A 10-mm diameter bottom hole of the 35 mm diameter plastic petri dish was covered by a thin glass slide, which formed a shallow well-like hollow structure with a volume of approximately 75-80 μL . Optical microscopy videos and images were obtained using an Olympus IX81 inverted microscope with a Nikon digital sight DS-2Mv camera connected to a computer and operated by the Nikon NIS-Elements software. Motion videos were recorded at 12.5 frames per second using a 4X objective. The time interval between two frames is 0.08 s. For each of the data points in the speed profile figures, at least 50 measurements were taken into count. The error bars stand for the standard deviation. To minimize the effect of fuel depletion, only the videos recorded at the first 5 minutes after fuel added were taken into account for speed calculation. Unless otherwise stated, all the percentage about the fuel and surfactant are weight by volume (w/v %). Free Fiji software was used to calculate the speed of micromotors, edit videos and extract pictures. A digital hand-held "Pocket" H_2O_2 refractometer (Model: Atago, PAL-39S) was used to calibrate the concentrations of H_2O_2 solutions.

6.3 Results and discussions

We investigated the influence of pure surfactants on the motion behaviors of a typical MnO₂ based tubular micromotor. The speed variations of graphene/MnO₂ bilayer tubular micromotors show similar trends under the surfactant conditions with slight differences in the top speed and initial speed occurring at different minimal and optimal surfactant levels. When dissolved in water, the surfactants would adsorb at the interface between the air and water phases, and thus, significantly lower the surface tension or interfacial free energy of the fluid. The surfactant would also be adsorbed on the catalytic surface of the microengines and decrease the interfacial free energy, thus facilitating the ejection of microbubbles. Below the minimal surfactant concentration, the tubular microengines would not move. It is apparent that the surfactants play a crucial role in the motion of MNMs. Surfactants can be classified according to the charging properties of their hydrophilic heads. That is, the hydrophilic group of cationic surfactants carries a net positive charge, while the anionic surfactant contains a negatively charged hydrophilic head. The zwitterionic surfactants contain a negatively charged and a positively charged end in the hydrophilic head, while the non-ionic surfactants do not have a charged group in their hydrophilic head. The properties of the surfactants are summarized in Table 6.1. The most important parameters of the surfactants are the critical micelle concentration (CMC), where micelles began to form and the surface tension of the fluid tended to be constant as the surfactant concentration reached the CMC. As the most widely used anionic surfactant for MNMs, SDS has a CMC of 0.24%, which is the highest among the four surfactants used.

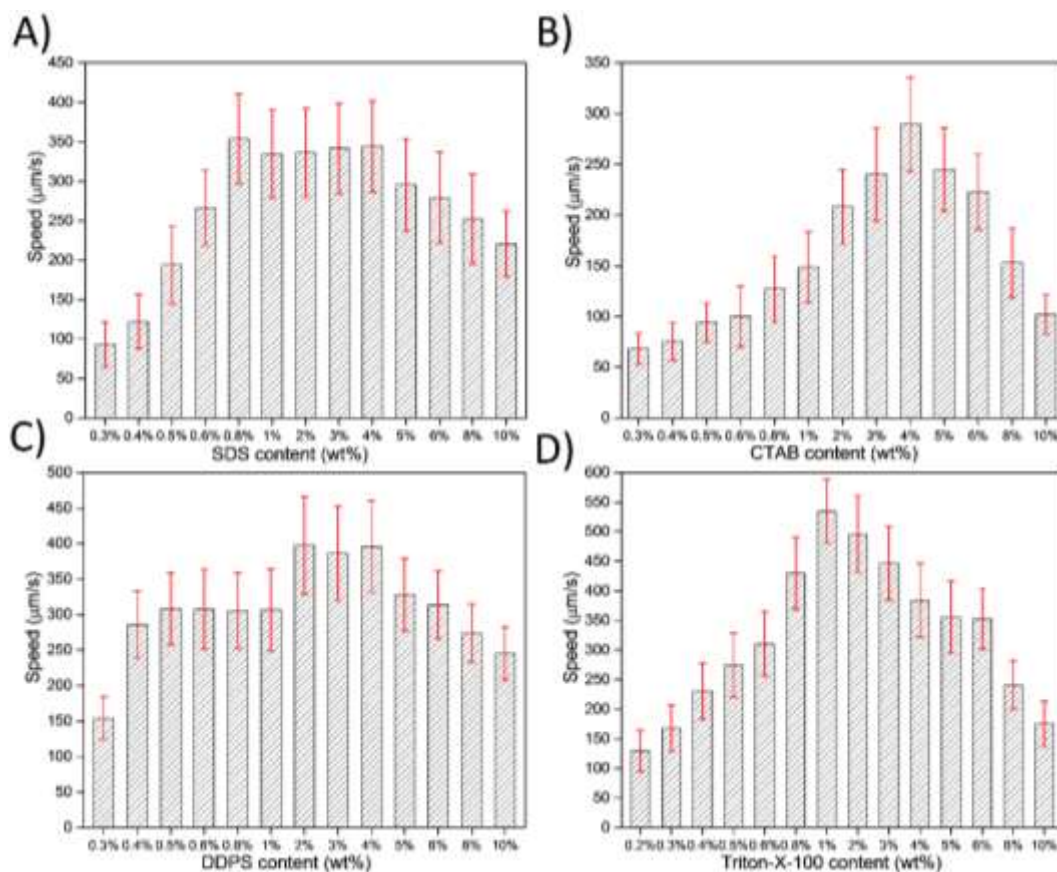


Figure 6.1. Dependence of the motion speeds of graphene/MnO₂ tubular microengines upon the concentration of surfactants in the solutions. (A) SDS; (B) CTAB; (C) DDPS; (D) Triton-X-100. (n=50). Condition in all experiments: at room temperature of 23 °C and 3% H₂O₂ as a fuel.

As shown in Figure 6.1A, below the concentration of 0.3%, the microengines could not move. The speed of graphene/MnO₂ tubular micromotors increases rapidly from 93 ± 29 to $354 \pm 57 \mu\text{m s}^{-1}$ as the SDS content increases from 0.3% to 0.8%. The speed of micromotors reached a plateau of $350 \mu\text{m s}^{-1}$ as the surfactant content further increased to 4%. Due to the increased fluid resistance, further increasing of the SDS content slows down the microengine moving. Figure 6.1B shows that the speed of micromotors increases from $68 \pm 15 \mu\text{m s}^{-1}$ at 0.3% CTAB to $290 \pm 46 \mu\text{m s}^{-1}$ at the CTAB content of 4%. Further increasing the CTAB content to 10% results in a decreased speed to $102 \pm 19 \mu\text{m s}^{-1}$. Figure 6.1C shows the speed profile of micromotors in an amphoteric surfactant DDPS.

Under the minimal surfactant content of 0.3%, the speed of micromotors slightly exceeded $150 \mu\text{m s}^{-1}$ and then it reached a plateau of about $300 \mu\text{m s}^{-1}$ at the surfactant concentrations of 0.4% to 1%. A further increase in the surfactant concentration from 2% to 4%, the speed elevated to the second plateau of approximately $400 \mu\text{m s}^{-1}$. After that, the speed of micromotors gradually decreased to less than $250 \mu\text{m s}^{-1}$ at 10% DDPS. Figure 6.1D demonstrates the speed variations of micromotors in a non-ionic surfactant Triton-X-100. The speed increases from 130 ± 35 to $534 \pm 54 \mu\text{m s}^{-1}$ as the surfactant content increases from the minimal value of 0.2% to the optimal value of 1%. Upon further increasing the concentration to 10%, the speed of micromotors drops to $175 \pm 39 \mu\text{m s}^{-1}$.

Generally, at 3% H_2O_2 as a fuel, a minimal surfactant content of 0.2-0.3% is needed to initiate micromotors moving, although the CMCs of the 4 surfactants have a big difference. The non-ionic surfactant Triton-X-100 has a much lower CMC than the anionic surfactant SDS (0.01% vs 0.23%), the minimal surfactant content for micromotor moving is only slightly lower than the SDS (0.2% vs 0.3%). This means that the surface tension of fluid does not have a very influential effect on the motion of the micromotors. The surface tension affects the wetting of the micromotors with the fluid. At a very high content of surfactant, the bubbles are more stable than those formed at a low content of surfactant. The ejections of stable bubbles from the opening of the microtubes generate the propelling force.

By comparing the speed of MNMs at different surfactant conditions, we can compare the performance of the surfactant to MNMs. It seems that the non-ionic surfactant Triton-X-100 is the best surfactant for the graphene/ MnO_2 micromotors and a much lower surfactant content is

needed for efficient propulsion and higher speeds could be generated at around 1% surfactant content. As the molecular weight of Triton-X-100 is apparently larger than the other three surfactants used, the larger molecule may have a good effect on stabilizing the microbubbles. As the interface between the water and air is at least one layer of surfactant, the larger the surfactant molecules, the harder the diffusion of the oxygen molecules to the fluid. The stabilized bubbles are more efficient to expel the water from the opening of the tube, thus enhancing the motion behaviors especially at a low content of the surfactant. The zwitterionic surfactant DDPS is the second efficient surfactant for the MNMs motion. At the same surfactant content, the DDPS could generate a higher speed than SDS. It seems that the most widely used surfactant SDS is not the best efficient surfactant. Other surfactants can make better motion behaviors of MNMs than SDS. The cationic surfactant CTAB is the worst surfactant for MNMs motion. Previous observation shows the Pt-based microjets were not moving in CTAB at all, attributed to the repulsion between CTAB and the microjets.²⁹ Schmidt et al. also found that the cationic surfactant is inefficient for tubular microengines and Janus particles micromotors²⁸ and they suggested that the ammonium moiety of CTAB has a high affinity to Pt to deactivate the Pt. Our results are in good agreement with previous reports. Hence, we can conclude that the cationic surfactant is the most inefficient surfactant for the MNMs. The study provides a good reference for the future applications of MnO₂ and Pt-based MNMs.

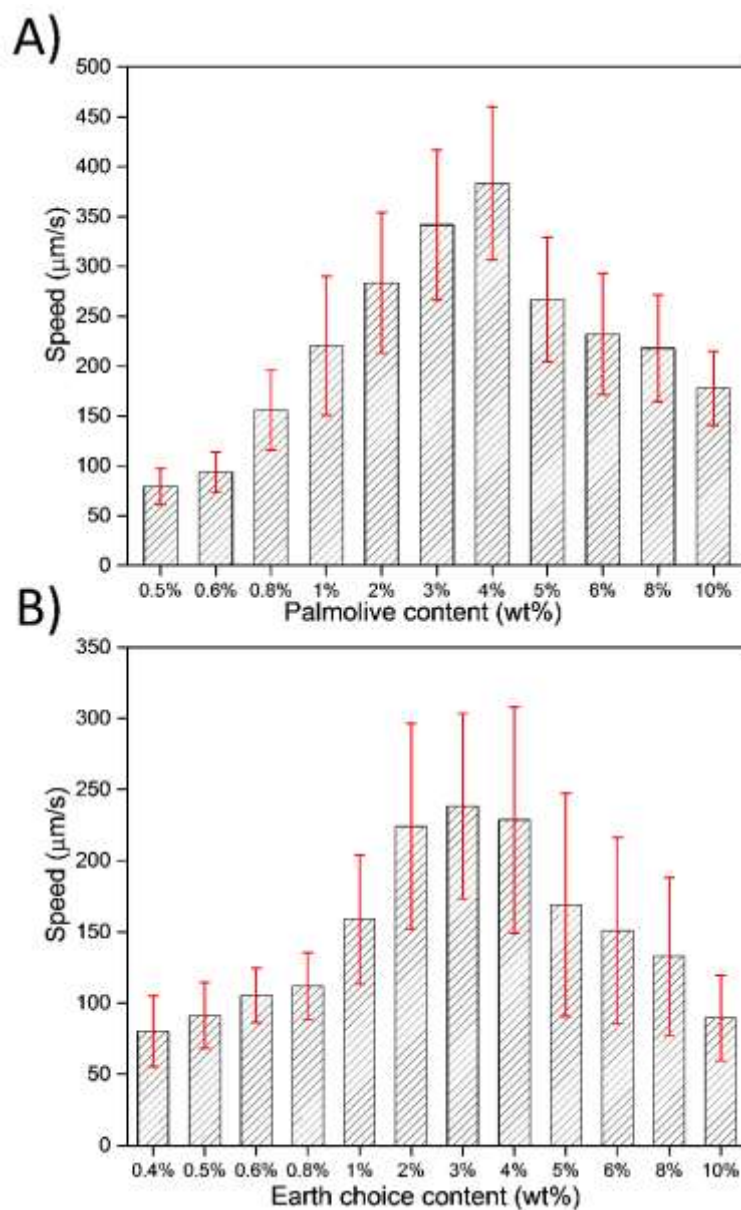


Figure 6.2. Motion speed profiles of graphene/MnO₂ tubular microengines at the concentration of surfactants in the solutions. (A) Palmolive; (B) Earth Choice. (n=50). Condition in all experiments: at room temperature of 23 °C and 3% H₂O₂ as fuel.

Table 6.1. The properties of four different surfactants used.

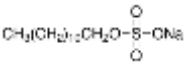
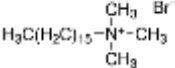
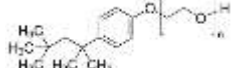
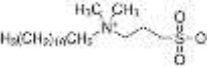
Surfactant	SDS	CTAB	Triton-X-100	DDPS
Category	anionic	cationic	non-ionic	zwitterionic
Formula Weight	288.38	364.45	647	335.55
Formula	$\text{NaC}_{12}\text{H}_{25}\text{SO}_4$	$\text{C}_{19}\text{H}_{42}\text{BrN}$	$\text{C}_{14}\text{H}_{22}\text{O}(\text{C}_2\text{H}_4\text{O})_n$ (n = 9-10)	$\text{C}_{17}\text{H}_{37}\text{NO}_3\text{S}$
Formula graph				
Aggregation number	62	170	100-155	55
Average micellar mole weight	18000	62000	80000	18500
CMC	7-10 mM	~1mM	0.2-0.9 mM	2-4 mM(20-25°C)
	~0.24 wt. %	0.04 wt. %	0.01 wt. %	0.12%
Solubility (mol)	0.1M	H2O: 0.1 M at 40°C,	soluble	H2O: 1 M at 20 °C,
Solubility (Weight)	>15g	0.1g/mL at 25°C	0.1g/mL	Good
HLB	40	10	13.5	Not clear

Table 6.2. Information of the commercial Palmolive® Ultra Original dishwashing liquids.

Ingredient (INCI Name)	Purpose
Water	Consistency
C12-14 Alcohol EO 2:1 Sodium Sulphate	Cleaning and foaming agent
Lauramidopropyldimethylamine Oxide	Cleaning and foaming agent
Sodium Chloride	Controls viscosity
Sodium Xylene Sulphonate	Solubiliser
Myristamidopropylamine Oxide	Cleaning and foaming agent
Poloxamer 124	Controls viscosity
Citric Acid	pH adjuster
Fragrance	Pleasant scent
Isothiazolinones	Preservatives
Dyes	Color
Tetrasodium EDTA	Chelating agent

Previously, a commercial soap FIT was tested in the Pt-based systems.¹⁵ Since all the single-component surfactants could be used to facilitate the movement of bubble-propelled MnO₂ based tubular micromotors, we then test commercial dishwashing liquid for the motion of MnO₂ based micromotors. We chose two commercial dish soaps as mixed surfactant solutions, and the results are summarized in Figure 6.2. The information about the commercial dish wash liquid is summarized in Tables 6.2 and 6.3. Both the dish soaps are a mixture of anionic and non-ionic surfactants.

The commercial dish soaps also contain a minor amount of stabilizer, salt, fragrance, and dyes as additives.

Table 6.3. Information of the commercial Earth Choice[®] Dishwash Liquid – Lemon Fresh and Aloe Fresh.

Chemical Name	CAS Number	Proportion (%)
Water	7732-18-5	> 60
Sodium Dodecylbenzene Sulfonate	25155-30-0	10 - 30
Sodium Laureth Sulfate	68603-42-9	< 10
Cocamide DEA	61790-63-4	< 10
Sodium Citrate	6132-04-3	< 10
Aloe Vera Extract	85507-69-3	< 10
Fragrance		< 10
Benzisothiazolinone	2634-33-5	< 10
CI 42090	3844-45-9	< 10

Figure 6.2A shows the motion of graphene/MnO₂ tubular microjets in the commercial Palmolive soap. In the Palmolive soap, at least 0.5% of its content is needed to initiate the propulsion of the micromotors at a speed of around 80 $\mu\text{m s}^{-1}$. As the detergent content increases to 4%, the speed of micromotors rises to $383 \pm 77 \mu\text{m s}^{-1}$. A further rise of the detergent levels results in a decreased speed of micromotors due to the increased fluid resistance. The effect of Earth Choice soap on the speed of micromotors shows a similar trend as the Palmolive detergent. Initiation

of motion of the micromotors required 0.4% of Earth Choice to reach a speed of $80 \pm 25 \mu\text{m s}^{-1}$, and rising of the detergent content to 3%, the micromotors could generate the highest speed of $238 \pm 65 \mu\text{m s}^{-1}$. Then the speed of micromotors drops to $90 \pm 30 \mu\text{m s}^{-1}$ as the soap content reaches 10%. The above results demonstrate that the MnO_2 based micromotors are very robust to the real environmental water matrix. As the organics, salt, fragrances, and pigment are widely present in a natural water body, the effective motion of the MnO_2 based MNMs make them promise as self-propelled cleaners, for environmental remediation.

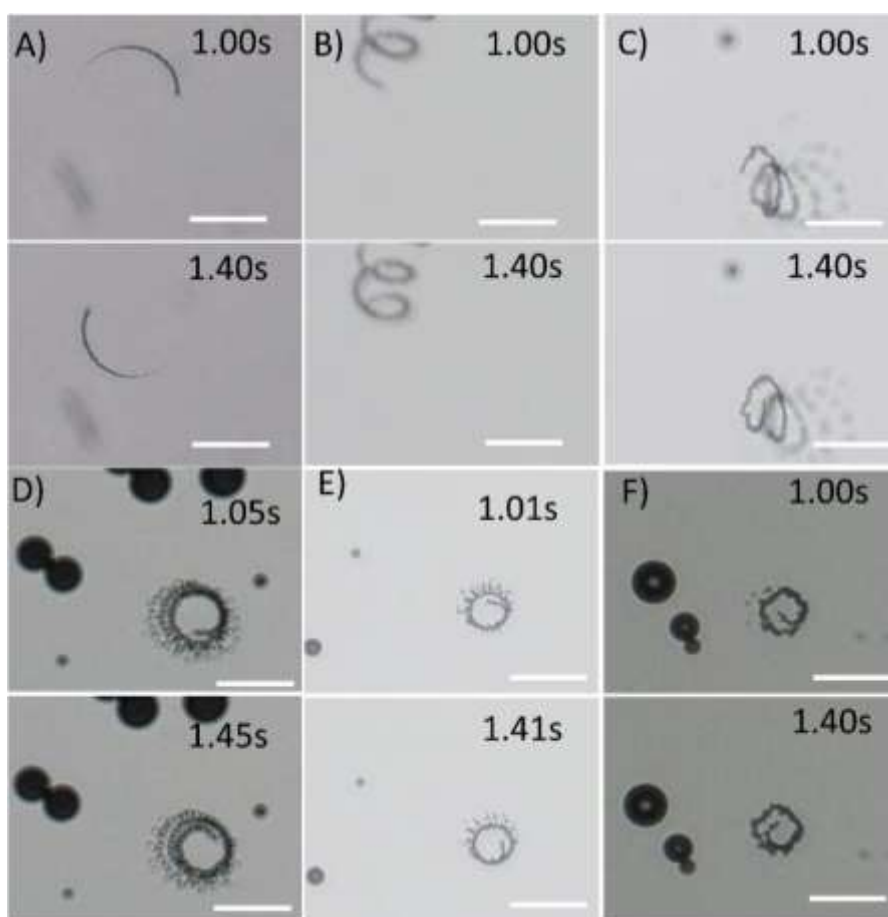


Figure 6.3. Typical time-lapse images extracted from the motion behaviors videos depicting the motion of graphene/ MnO_2 tubular micromotors in different surfactant conditions in a time interval of 0.4 s with 3% H_2O_2 as a fuel. (A) 0.8% SDS; (B) 2% CTAB; (C) 1% DDPS; (D) 0.2% Triton-X-100; (E) 1% Palmolive; (F) 8% Earth Choice. Scale bars: 100 μm .

Figure 6.3 demonstrates the typical time-lapse images of the motion behaviors of graphene/MnO₂ micromotors in different surfactant solutions. As can be seen from the representative pictures, all the micromotors demonstrate similar circular motion patterns regardless of the surfactant used. The circular motion behaviors are the most typical motion patterns of the tubular micromotors. At a high fuel concentration, some of the micromotors could demonstrate irregular motion patterns. The motion pattern of micromotors is relied on the geometry shape of the micromotors and bubble propelling. However, in this investigation, the micromotors are active in all kinds of surfactants, which means the motion behaviors of MnO₂ based micromotors are surfactant independent propulsion. This behavior is very different from a previous report, but the Pt-based micromotors' motion behaviors are quite dependent on the surfactant used.²⁹

6.4 Conclusions

Self-propelling MnO₂ based micromotors using catalytic H₂O₂ decomposition are surfactant independent MNMs, significantly to differentiate from the previously developed Pt-based systems. The CMC of a surfactant does not have a much effect on the motion of MnO₂ based microjets, and the MnO₂ tubular micromotors can move at high speeds at 0.2-0.3% content of four different surfactants. Moreover, they can also show moving behavior in commercial dish soaps with the similar profile of speed, demonstrating the robustness in various conditions. Hence, MnO₂ based micromotors will be a good alternative to Pt MNMs for a wide application in wastewater treatment.

Table 6.4. Types of the surfactants and fuel used for catalytic MNMs.

Type of the MNMs	Ref.	Size (μm)	Surfactant	H ₂ O ₂ fuel (%)	Motion speed (μm/s)
Ti/Cr/Pt microtubes	Schmidt et al. ¹⁵	50	0.5% commercial soap FIT:	0.25-5	140-10000 at 37°C
Multilayered microrockets	Zhang et al. ³³	20	Sodium cholate 0.33%	1-5	285-1410
Cu/Pt bimetallic microtubes	Pumera et al. ³⁴	10	1% SDS	0.2-3	70-700
Cu/Pt concentric bimetallic microtubes	Pumera et al. ²⁹	10	0.01-10% SDS 0.01-10% Tween 20 0.01-10% CTAB	3	50-365 65 0
Ti/Cr/Fe/Pt microjets	Schmidt et al. ²⁸	50	without surfactant 0.0001%-10% SDS 0.0001%-10% BACl 0.0001%-10% Triton-X 0.1%-10% FIT dish soap	10-20 5 5 5 5	Around 250 0-200 0-100 50-200 60-260
Pt/SiO ₂ Janus particles	Schmidt et al. ²⁸	4.78	without surfactant 0.0001%-1% SDS 0.0001%-1% BACl 0.0001%-10% Triton-X 0.1%-1% FIT dish soap	1-20 5 5 5 5	2-13 3.5-0 0 8-1 6.5-7-0
Cu/Ag microtubes	Pumera et al. ³⁵	10-15	1% SDS	0.5-3	13.1-252.4
Ag and MnO ₂ microparticles	Pumera et al. ²³	Ag≈30 MnO ₂ ≈5	0.5% SDS	0.1-12 12-21	25-100 50-120
Au/Graphene/MnO ₂	Ma et al. ³¹	6.74	0.33% Triton-X-100	0.15-2.5	15.79-44.79
PEDOT/MnO ₂ micro tubes & rods & MnO ₂ @MnCO ₃	Janis et al. ³⁶	12.5 12.5 5	0.5% Triton-X-100 for microtubes and microrods 0.5% SDS for micro particles	5-15 5-15 1-10	Tubes 200-510 Rods 200-410 142-665
Graphene/Pt microtubes	Wang et al. ³⁷	10	1.5% sodium cholate	0.1-3	37-1700
MnO ₂ hallow	Janis et al. ³⁸	n.a	0.5% SDS or Triton-X-100	5-10	321-996
PANI/Pt microtubes	Wang et al. ¹⁴	8	1.6% sodium cholate	0.2-5	25-1410
PEDOT/Pt microtubes PPY/Ag bilayer PPY/Pt-Ni alloy Au/Pt bimetallic microbots	Wang et al. ³⁹	7	5% sodium cholate 3% sodium cholate 5% Sodium cholate 2% Sodium cholate	10 15 10 5	10000 at 37°C 3500 at 23 °C 500 470 1500
GOx/Ni/Pt GOx/Ni/Pt/MnO ₂ HS/Au/GOx/Ni/Pt/MnO ₂	Janis et al. ⁴⁰	13	0.1% SDS	0.5-4	100-150 to 800-900
Janus Ag/ZIF-Zn-Fe	Guo et al. ⁴¹	80	0.2% SDS	1-20	316-1650
Fe/Pt Janus	Chang et al. ⁴²	1-5	0.01% Triton-X-100	0.5-5	50-207.89
PEDOT/MnO ₂	Wang et al. ⁴³	8	0.33% Triton-X-100	0.4-10	31.57-318.80
PEDOT/PtNP@CNT-PPy	Wu et al. ³⁰	12	1.6% sodium Cholate	1-15	62-450
C/Pt				1	176-409
C/Pt-NP	Escarpa et al. ⁴⁴		1.5% Sodium cholate	1	261-502

C/Ag		12		5	73-104
C/Pd				5	98-139
C/MnO ₂				5	39-65
erGO/MnO ₂ microtubes	Our work ²²	8	1% SDS	3-15	77-466
erGO/MnO ₂ microrods	Our work ⁴⁵	12	1% SDS	3-15	224-609
erGO/MnO ₂ microtubes	Our work ⁴⁵	12	1% SDS	1-15	134-809
erGO/Ag-MnO ₂ microrods	Our work ⁴⁵	12	1% SDS	3-15	261-539
erGO/Ag-MnO ₂ microtubes	Our work ⁴⁵	9	1% SDS	0.2-10	88-1237
erGO/FeO _x -MnO ₂ microtubes	Our work ²⁴	12	1% SDS	0.03-5	89-1279

References

1. de Avila BE, Angsantikul P, Li J, et al. Micromotor-enabled active drug delivery for in vivo treatment of stomach infection. *Nat. Commun.* 2017; 8(1):272.
2. Vilela D, Parmar J, Zeng YF, Zhao YL, Sanchez S. Graphene-based microbots for toxic heavy metal removal and recovery from water. *Nano Lett.* 2016; 16(4):2860-2866.
3. Orozco J, Mercante LA, Pol R, Merkoci A. Graphene-based Janus micromotors for the dynamic removal of pollutants. *J. Mater. Chem. A.* 2016; 4(9):3371-3378.
4. Uygun DA, Jurado-Sanchez B, Uygun M, Wang J. Self-propelled chelation platforms for efficient removal of toxic metals. *Environ Sci-Nano.* 2016; 3(3):559-566.
5. Balasubramanian S, Kagan D, Jack Hu C-M, et al. Micromachine-enabled capture and isolation of cancer cells in complex media. *Angew. Chem. Int. Ed.* 2011; 50(18):4161-4164.
6. Orozco J, Cheng G, Vilela D, et al. Micromotor-based high-yielding fast oxidative detoxification of chemical threats. *Angew. Chem. Int. Ed.* 2013; 52(50):13276-13279.

7. Parmar J, Vilela D, Pellicer E, et al. Reusable and long-lasting active microcleaners for heterogeneous water remediation. *Adv. Funct. Mater.* 2016; 26(23):4152-4161.
8. Soler L, Magdanz V, Fomin VM, Sanchez S, Schmidt OG. Self-propelled micromotors for cleaning polluted water. *ACS Nano.* 2013; 7(11):9611-9620.
9. Li J, Singh VV, Sattayasamitsathit S, et al. Water-driven micromotors for rapid photocatalytic degradation of biological and chemical warfare agents. *ACS Nano.* 2014; 8(11):11118-11125.
10. Larysa B, Denys M, Robert S, et al. Catalytic Janus motors on microfluidic chip: Deterministic motion for targeted cargo delivery. *ACS Nano.* 2012; 6(4):3383-3389.
11. Jurado-Sanchez B, Escarpa A, Wang J. Lighting up micromotors with quantum dots for smart chemical sensing. *Chem. Commun.* 2015; 51(74):14088-14091.
12. Solovev AA, Mei Y, Bermúdez Ureña E, Huang G, Schmidt OG. Catalytic microtubular jet engines self-propelled by accumulated gas bubbles. *Small.* 2009; 5(14):1688-1692.
13. Gibbs JG, Fragnito NA, Zhao Y. Asymmetric Pt/Au coated catalytic micromotors fabricated by dynamic shadowing growth. *Appl. Phys. Lett.* 2010; 97(25).
14. Gao W, Sattayasamitsathit S, Orozco J, Wang J. Highly efficient catalytic microengines: Template electrosynthesis of polyaniline/platinum microtubes. *J. Am. Chem. Soc.* 2011; 133(31):11862-11864.
15. Sanchez S, Ananth AN, Fomin VM, Viehrig M, Schmidt OG. Superfast motion of catalytic microjet engines at physiological temperature. *J. Am. Chem. Soc.* 2011; 133(38):14860-14863.
16. Gibbs JG, Zhao YP. Autonomously motile catalytic nanomotors by bubble propulsion. *Appl. Phys. Lett.* 2009; 94(16):163104.

17. Mei YF, Huang GS, Solovev AA, et al. Versatile approach for integrative and functionalized tubes by strain engineering of nanomembranes on polymers. *Adv. Mater.* 2008; 20(21):4085-4090.
18. Paxton WF, Baker PT, Kline TR, et al. Catalytically induced electrokinetics for motors and micropumps. *J. Am. Chem. Soc.* 2006; 128(46):14881-14888.
19. Tu YF, Peng F, Sui XF, et al. Self-propelled supramolecular nanomotors with temperature-responsive speed regulation. *Nat. Chem.* 2017; 9(5):480-486.
20. Zhao GJ, Sanchez S, Schmidt OG, Pumera M. Poisoning of bubble propelled catalytic micromotors: The chemical environment matters. *Nanoscale.* 2013; 5(7):2909-2914.
21. Wang H, Zhao G, Pumera M. Blood electrolytes exhibit a strong influence on the mobility of artificial catalytic microengines. *Phys. Chem. Chem. Phys.* 2013; 15(40):17277-17280.
22. Ye H, Sun H, Wang S. Electrochemical synthesis of graphene/MnO₂ in an architecture of bilayer microtubes as micromotors. *Chem. Eng. J.* 2017; 324:251-258.
23. Wang H, Zhao GJ, Pumera M. Beyond platinum: Bubble-propelled micromotors based on Ag and MnO₂ catalysts. *J. Am. Chem. Soc.* 2014; 136(7):2719-2722.
24. Ye H, Ma G, Kang J, Sun H, Wang S. Pt-Free microengines at extremely low peroxide levels. *Chem. Commun.* 2018; 54:4653-4656.
25. Wang L, Chen J, Feng X, et al. Self-propelled manganese oxide-based catalytic micromotors for drug delivery. *RSC Adv.* 2016; 6(70):65624-65630.
26. He X, Bahk YK, Wang J. Organic dye removal by MnO₂ and Ag micromotors under various ambient conditions: The comparison between two abatement mechanisms. *Chemosphere.* 2017; 184:601-608.

27. Wani OM, Safdar M, Kinnunen N, Janis J. Dual effect of manganese oxide micromotors: Catalytic degradation and adsorptive bubble separation of organic pollutants. *Chem-Eur. J.* 2016; 22(4):1244-1247.
28. Simmchen J, Magdanz V, Sanchez S, et al. Effect of surfactants on the performance of tubular and spherical micromotors - a comparative study. *RSC Adv.* 2014; 4(39):20334-20340.
29. Wang H, Zhao GJ, Pumera M. Crucial role of surfactants in bubble-propelled microengines. *J. Phys. Chem. C.* 2014; 118(10):5268-5274.
30. Li YN, Wu J, Xie YZ, Ju HX. An efficient polymeric micromotor doped with Pt nanoparticle@carbon nanotubes for complex bio-media. *Chem. Commun.* 2015; 51(29):6325-6328.
31. Feng XM, Zhang Y, Li Y, et al. Graphene-based highly efficient micromotors. *Chem. Lett.* 2015; 44(3):399-401.
32. Solovev AA, Sanchez S, Pumera M, Mei YF, Schmidt OG. Magnetic control of tubular catalytic microbots for the transport, assembly, and delivery of micro-objects. *Adv. Funct. Mater.* 2010; 20(15):2430-2435.
33. Li TL, Li LQ, Song WP, et al. Self-propelled multilayered microrockets for pollutants purification. *ECS J. Solid State Sci. Technol.* 2015; 4(10):S3016-S3019.
34. Zhao GJ, Pumera M. Concentric bimetallic microjets by electrodeposition. *RSC Adv.* 2013; 3(12):3963-3966.
35. Teo WZ, Wang H, Pumera M. Beyond platinum: Silver-catalyst based bubble-propelled tubular micromotors. *Chem. Commun.* 2016; 52(23):4333-4336.
36. Safdar M, Wani OM, Janis J. Manganese oxide-based chemically powered micromotors. *ACS Appl. Mater. Inter.* 2015; 7(46):25580-25585.

37. Martin A, Jurado-Sanchez B, Escarpa A, Wang J. Template electrosynthesis of high-performance graphene microengines. *Small*. 2015; 11(29):3568-3574.
38. Safdar M, Minh TD, Kinnunen N, Janis J. Manganese oxide based catalytic micromotors: Effect of polymorphism on motion. *ACS Appl. Mater. Inter.* 2016; 8(47):32624-32629.
39. Gao W, Sattayasamitsathit S, Uygun A, et al. Polymer-based tubular microbots: Role of composition and preparation. *Nanoscale*. 2012; 4(7):2447-2453.
40. Minh TD, Safdar M, Janis J. Protection of platinum-based micromotors from thiol toxicity by using manganese oxide. *Chem-Eur. J.* 2017; 23(34):8134-8136.
41. Wang R, Guo W, Li X, et al. Highly efficient MOF-based self-propelled micromotors for water purification. *RSC Adv.* 2017; 7(67):42462-42467.
42. Lee C-S, Gong J, Oh D-S, Jeon J-R, Chang Y-S. Zero-valent iron/platinum Janus micromotors with spatially separated functionalities for efficient water decontamination. *ACS Appl. Nano Mater.* 2018.
43. Wang LL, Chen J, Feng XM, et al. Self-propelled manganese oxide-based catalytic micromotors for drug delivery. *RSC Adv.* 2016; 6(70):65624-65630.
44. Maria-Hormigos R, Jurado-Sanchez B, Vazquez L, Escarpa A. Carbon allotrope nanomaterials based catalytic micromotors. *Chem. Mater.* 2016; 28(24):8962-8970.
45. Ye H, Kang J, Ma G, Sun H, Wang S. High-speed graphene@Ag-MnO₂ micromotors at low peroxide levels. *J. Colloid Interface Sci.* 2018; 528:271-280.

Every reasonable effort has been made to acknowledge the owners of copyright material. I would be pleased to hear from any copyright owner who has been omitted or incorrectly acknowledged

Chapter 7. How Surfactants Affect the Mobility of Silver-Containing Microengines

Abstract

Micro/nanomotors (MNMs) that can convert chemical energy into movement and force have attracted great interest due to their wide potential applications for fundamental chemistry and biological science-related fields. Silver-based materials are replacing platinum (Pt) as the next generation self-propelled MNMs due to their low-cost, good motion performance, robust, and more abundance advantages, and potentially wide area applications for disinfection and water treatment. Various proof-of-concept applications have been demonstrated by the silver-containing MNMs, but there is no systematic investigation on how different types of surfactants will affect the mobility. Herein, four types of surfactant and two types of commercial detergent soap were chosen to investigate the influence of the surfactants upon motion behaviors of a typical silver containing micromotor. The results improve our understanding of microscale motion and provide a reference for the future applications of the emerging silver containing MNMs.

7.1 Introduction

The use of micro/nano scale tools and machines to perform tasks and address issues has attracted tremendous attention in the last decade.¹⁻⁹ The development of molecular machines has led to the award of the Nobel prize in chemistry in 2016.¹⁰ Self-propelled catalytic micro/nanomotors (MNMs) are the most fundamental component to construct micro/nano scale machines and factories, which would fundamentally change the nanoscience and nanotechnology. Tremendous proof of concept applications was demonstrated based on the decomposition of H_2O_2 as a fuel and the precious metal platinum (Pt) as a catalyst for bubble recoil propulsion, such as water treatment,¹¹ targeted cargo delivery,¹² cell manipulation,¹³ and chemical sensing.¹⁴ Up to now, a large portion of the catalytic MNMs are based on the precious noble metal Pt as a catalyst for hydrogen peroxide (H_2O_2) decomposition.¹⁵⁻¹⁸ Pt-containing MNMs with various geometry shapes, such as Janus particles,¹¹ microtubes engines,¹⁹ bi-segment microrods,²⁰ and Pt nanoparticles²¹ were designed and incorporated as the engine part for MNMs, due to its superb catalytic activities for H_2O_2 decomposition. However, Pt-based MNMs suffer from the drawbacks of high-cost, scarcity and possible deactivation in various media impeded their further applications.^{22, 23} Hence, there is great interests in searching for a new catalyst for MNMs.²⁴⁻²⁶

Silver-based materials are emerging as new catalytic materials as well as the functional parts for MNMs.^{27, 28} Silver containing MNMs have demonstrated various applications, such as killing pathogenic bacterial^{9, 29} and aquatic pollutants degradation.³⁰ Silver-containing MNMs can be fabricated via electrochemical plating and physical vapor depositions.^{9, 29, 31-34} The use of raw silver particles without modification has also been demonstrated as MNMs.^{30, 31} The published results have demonstrated the

versatility of silver for MNMs objectives. Besides the metallic zero valence silver metal, the silver-containing compounds and alloys have also been incorporated for the construction of MNMs.^{27, 35, 36} The use of silver containing materials to replace the precious Pt catalyst for MNMs provides the following advantages of good motion performance, low materials cost, versatile fabrication, and modification techniques, and multiple functionalities. Since the first demonstration of silver particles as MNMs by Pumera's group, various silver containing MNMs have been designed and tested.³¹ Up to now, the most powerful MNMs are the bubble propelled tubular microjet engines, which moves by expelling the gas bubbles and the fluid inside the microtubes away. Recently, we designed the graphene/Ag-MnO₂ tubular micromotors with good motion performance at relative low H₂O₂ contents. Due to the synergistic effect of the silver and MnO₂ catalyst, good geometry shape, and rough inner surface microstructure, the motion performance of the Ag-MnO₂ catalyzed micromotors are comparable to the Pt-based microengines at low peroxide fuel levels, demonstrating the great potential as an alternative for Pt in designing MNMs. As the fuel and surfactants are quite indispensable for the mobility of catalytic bubble propelled MNMs, and most of the research focuses on the search of alternative fuels, such as hydrozine³⁷ and glucose,³⁸ for improving MNMs' performance, very few studies investigated the role of surfactants in promoting microscale motion. Currently, only two reports have already studied the effect of surfactants on the motion behaviors of Pt-based micromotors exclusively,^{39, 40} but no one has investigated how different surfactants affect the movement of silver containing micromotors systematically. By now, the choice of surfactants to facilitate the movement of MNMs are quite random.^{19, 41, 42} To fully exploit the potential of silver containing catalytic MNMs, it is of

great significance to study how different types of surfactant and its concentrations affect the movement of MNMs.

Surfactants are amphiphilic organic compounds, which has a hydrophobic group and a hydrophilic group. Surfactants can be classified according to the charging properties of their hydrophilic groups. The hydrophilic group of cationic surfactants carries a net positive charge, while the anionic surfactant contains a negatively charged hydrophilic head. Zwitterionic surfactants contain a negatively charged and a positively charged end in the hydrophilic group, while the non-ionic surfactants have no charged groups. Previously, Pumera's group studied how different surfactants affect the mobility of Pt-catalyzed tubular microengines.⁴³ They found that different types of surfactant greatly affect the motion behaviors. The sodium dodecyl sulfate (SDS) is much better than Tween 20, while the cetyltrimethylammonium bromide (CTAB) would deactivate the microengines.⁴³ Simmchen et al.³⁹ studied the effect of surfactants on the motion performance of Pt-catalyzed tubular and Janus particle micromotors. The Janus micromotors move at a much higher speed at a relative lower content of surfactant, while the tubular microengines demand a much higher surfactant concentration to achieve the maximum speed. The reasons for these phenomena are not totally clear, as most of the explanations are based on empirical or descriptive reasoning. What's more, the results obtained at different research groups using different types of MNMs systems cannot always show consistent results. Hence, a systematic investigation is needed to generate a more comprehensive insight on the role of surfactants to facilitate the mobility at the micro/nano scale.

Herein, we choose two types of commercial detergents and four types of pure surfactant to study the influence of surfactants upon the motion of silver containing MNMs. The choice of each type of surfactants are as follows: SDS as the anionic surfactant, CTAB as the cationic surfactant, N-Dodecyl-N, N-dimethyl-3-ammonio-1-propanesulfonate (DDPS) as the zwitterionic surfactant, and Triton-X-100 as the non-ionic surfactant. (Table 6.1) Two types of commercially available detergents were chosen as a mixture of surfactants. (Table 6.2-6.3). We hope to generate a guide for the further application of silver containing MNMs and improve the understanding of the motion behaviors at a micro/nano scale. The results show that efficient motion can be achieved under every surfactant condition. The data acquired here paves the way for further environmental remediation strategy as well as novel biomedical applications of the emerging silver containing MNMs.

7.2 Experimental section

7.2.1 Materials and reagents

Potassium permanganate, silver nitrate, sodium sulfate, ethanol, dichloromethane, SDS, Triton-X-100, N-Dodecyl-N,N-dimethyl-3-ammonio-1-propanesulfonate (DDPS), CTAB, and sulfate acid (98%) were purchased from Sigma-Aldrich. H₂O₂ (30%) was purchased from ROWE Scientific Australia. Aluminum oxide paste was purchased from Kemet, NSW, Australia. Two types of commercial dishwashing liquid were collected from the chemistry lab, the Palmolive and the Earth Choice brand washing-up liquid. Porous polycarbonate (PC) membranes with an average pore diameter of 5 μm were purchased from Whatman Inc., NY, USA. Ultrapure water (Milli-Q) was used in all experiments. Nano-sized

graphene oxide (GO) was purchased from graphene supermarket, New York, USA.

7.2.2 Fabrication of graphene/Ag-MnO₂ micromotors

Graphene/Ag-MnO₂ tubular micromotors were fabricated by a template-assisted electrochemical deposition protocol, as with our previous publication.²⁵ A cyclopore polycarbonate membrane containing 5 μm diameter conical-shaped micropores (Whatman, NY, USA) was employed as the template. An 80 nm of gold film was first deposited on one side of the porous membranes to serve as the working electrode using an Emitech K950X gold evaporator and performed at room temperature under a high vacuum of below 1×10^{-3} mBar at a direct current of 6 A. The deposition rate was about 1 nm s⁻¹. A customized plating cell was used in all electrochemical deposition processes. The membrane was assembled in a self-designed plating cell with an aluminum foil serving as the contact for the working electrode. Electrochemical deposition was carried out using an electrochemical workstation (Zennium Zahner, Germany). A Pt wire and Ag/AgCl with 3M KCl were used as the counter and reference electrodes, respectively. A mixed solution of 0.1 mg mL⁻¹ nano-sized GO in 0.5 M of Na₂SO₄ and 0.1 M H₂SO₄ was prepared as the electrolyte for the electrochemical growth of graphene outer layer. The GO in the solution was reduced by a cyclic voltammetry (CV) method from 0.3 to -1.5 V for five cycles. After washing with 10 mL of ultrapure water for three times, the inner Ag-MnO₂ layer was deposited using a galvanostatic (GS) method at a current of -1 mA for 20 min, which equals to 1.2 C of charge transferred. For the cathodic reduction deposited of the Ag-MnO₂ inner layer, 1.2 C of charge transfer is the optimal value for the synthesis of graphene/Ag-MnO₂ tubular microtubes. For Ag-MnO₂ deposition, the electrolyte solution was 2 mM of AgNO₃ and 20 mM KMnO₄. Following

the electroreduction deposition, the gold layers were removed by hand polishing with alumina slurry. Then the templates were dissolved in dichloromethane for 15 min to release the micromotors. Finally, the micromotors were collected by centrifugation at 7000 rpm for 3 min while being repeatedly washed with dichloromethane, ethanol and ultrapure water for three times each. The ultrasonication process was carried out using a Unisonics ultrasonication cleaner (Model FXP12D), and the centrifugation was carried out using an Eppendorf centrifuge 5430. All the micromotors were stored in ultrapure water at room temperature for further use.

7.2.3 Motion behavior observation

A transparent plastic petri dish (Part No. P35G-1.5-10-C, Mat Tek Corporation, MA, USA) with the holed bottom covered by a thin glass slide was used as the container to prepare different fuel concentrations for observation of motion behavior. A 10 mm diameter bottom hole of the 35 mm diameter plastic petri dish was covered by a thin glass slide, which formed a shallow well-like hollow structure with a volume of approximately 75-80 μL . Optical microscopy videos and images were obtained using an Olympus IX81 inverted microscope with a Nikon digital sight DS-2Mv camera connected to a computer and operated by the Nikon NIS-Elements software. Motion videos were recorded at 12.5 frames per second using a 4X objective. The time interval between two frames is 0.08 s. For each of the data points in the speed profile figures, at least 50 measurements were taken into account. The error bars stand for the standard deviation. To minimize the effect of fuel depletion, only the videos recorded at the first 5 minutes after fuel added were taken into account for speed calculation. Unless otherwise stated, all the percentage about the fuel and surfactant are weight by volume (w/v %). Free Fiji

software was used to calculate the speed of micromotors, edit videos and extract pictures. A digital hand-held "Pocket" H_2O_2 refractometer (Model: Atago, PAL-39S) was used to calibrate the concentrations of H_2O_2 solutions.

7.3 Results and discussion

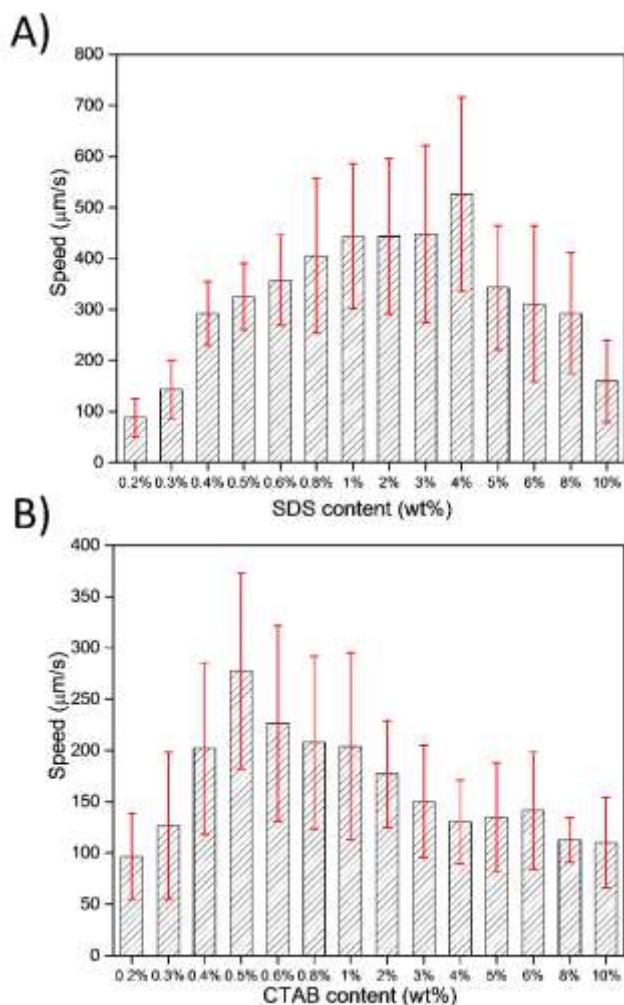


Figure 7.1. Dependence of the motion speed of graphene/Ag-MnO₂ microjets. (n=50) (A) Influence of SDS concentration upon the speed of micromotors. (B) Influence of CTAB concentration upon the speed of micromotors. Conditions in all experiments: room temperature of 23°C and 3% H_2O_2 as a fuel.

As the surfactants have a hydrophobic group and a hydrophilic group, they are very likely to be adsorbed at the interface between the air, water, and

solid phases. The amphiphilic surfactants would adsorb at the interface between the air and water phases, and thus, significantly lower the surface tension or interfacial free energy of the fluid. The surfactant would also adsorb on the catalytic surface of the microengines and decrease the interfacial free energy to a marked degree, thus facilitating the ejection of the microbubbles. The most important parameter of surfactants is the critical micelle concentration (CMC), where micelles began to form and the surface tension of the fluid tends to be constant. When dissolved in the liquid phase at a very tiny amount below the CMC, the micelle cannot form and the surfactant tends to be in the free-floating state. When the surfactant content rises to CMC, micelles of different geometry tend to form due to the requirement of lowering the free energy.

Previously, Mei and co-workers developed the theoretical model for the dynamics of catalytic cylindrical tubular microengines.⁴⁴ According to this model, the speed of micromotors should be linearly proportional to the concentration of fuels. As the fuel concentrations affect the generation of gas volume and the bubbling frequency, thus, the most influential factor in micro/nano scale motion is the fuel levels. The geometry of the microtubes also affects the movement speed of micromotors. Wang and his co-workers analyzed the motion behaviors of the graphene/Pt and a polymer/Pt tubular microengines using this body deformation model theoretically.⁴⁵ They found that the catalyst property, such as the surface roughness, improves the mobility by generating higher frequency bubbles with smaller diameters to facilitate the motion at a low content of fuels. Similar results were also obtained by the analysis of the graphene/Ag-MnO₂ tubular micromotors at constant surfactant content with varying fuel levels by our previous report.²⁵ But how the surfactant conditions affect the motion behaviors remains unknown. Previous reports about the

surfactant used in the MNMs purposes are summarized in Table 6.4. The Ag-MnO₂ catalyst is comparable with Pt for promoting motion at a low content of fuels, thus it is of great importance to study how different types of surfactant and its concentration affect the mobility of the emerging silver containing MNMs.

The bubble formation and ejection can be affected to a large extent by the surfactant, as the surfactants are a key component for the generation and stabilization of bubbles. Below the lowest surfactant requirement, the tubular microengines would not move, as the bubbles are hard to form and the frequency of bubbling is too low to propel the microengines. At the minimal surfactant requirement, the force generated by the propelling bubbles could overcome the resistance and the microengines start to move. The results about the influence of anionic surfactants SDS and the cationic surfactants CTAB on the mobility of the graphene/Ag-MnO₂ tubular micromotor are summarized in Figure 7.1. The speeds of graphene/Ag-MnO₂ bilayer tubular micromotors show similar increasing and decreasing trends under the anionic and cationic surfactant conditions with variations in speeds at different surfactant levels. As the most widely used anionic surfactant for bubble propelled MNMs, SDS has a CMC of 0.24%, which is the highest among the four types of surfactant used. The CTAB has a much lower CMC of 0.04%, while the minimal surfactant requirement for the two types of surfactant is the same at 0.2% with very close motion performance of slightly less than 100 $\mu\text{m s}^{-1}$. As the surfactant levels continue to increase, the graphene/Ag-MnO₂ tubular micromotors show a faster speed under the anionic surfactant SDS. The results are in good agreement with a previous report regarding the performance of Pt-based micromotors.⁴⁰ While the Pt-based tubular microengines were deactivated by the cationic surfactant CTAB, the

silver-containing micromotors demonstrated efficient motion performance in a wide range of the cationic surfactant CTAB. The graphene/Ag-MnO₂ tubular micromotors speed up to its acme of $526 \pm 190 \mu\text{m s}^{-1}$ as the SDS content increases to 4%, while under the cationic surfactant CTAB, the maximum speed of $278 \pm 96 \mu\text{m s}^{-1}$ was achieved at a relative low CTAB content of 0.5%. Upon on passing the optimal surfactant levels, the graphene/Ag-MnO₂ microengines show decreasing speeds due to the increased fluid resistance at higher surfactant levels.

The property of zwitterionic surfactant is very similar to the non-ionic surfactant. As a whole, the hydrophilic group contains no charge. The performances of these two types of surfactant for facilitating motion at a micro/nano scale are also quite similar. The speed profiles of the graphene/Ag-MnO₂ bilayer microtubes in zwitterionic surfactant DDPS and the non-ionic surfactant Triton-X-100 solutions are presented in Figure 7.2, both are very effective in promoting the movement. Only 0.1% of the surfactants is needed for the MNMs to propel at speeds of around $100 \mu\text{m s}^{-1}$, which shows a better result than the ionic surfactants SDS and CTAB. It seems that the charging property of the surfactant has an adverse effect on the motion behaviors. Under the surfactant DDPS, the speed of micromotors accelerates very fast to $332 \pm 102 \mu\text{m s}^{-1}$ as the surfactant levels increase to 1%. Then the speed of micromotors decreases as the surfactant levels increase to 10%. While the speed of micromotors shows a gradual increase to the top speed of $457 \pm 176 \mu\text{m s}^{-1}$ as the surfactant Triton-X-100 rises to 4%. Further increase Triton-X-100 contents results in the reduced speeds, due to the increased fluid resistance at a higher level of surfactants. At 10% of Triton-X-100, the average speed of micromotors decreases to less than $200 \mu\text{m s}^{-1}$. While the non-ionic surfactant requires

a lower content to activate motion, the ionic surfactant SDS demonstrates faster speeds at 4% than Triton-X-100.

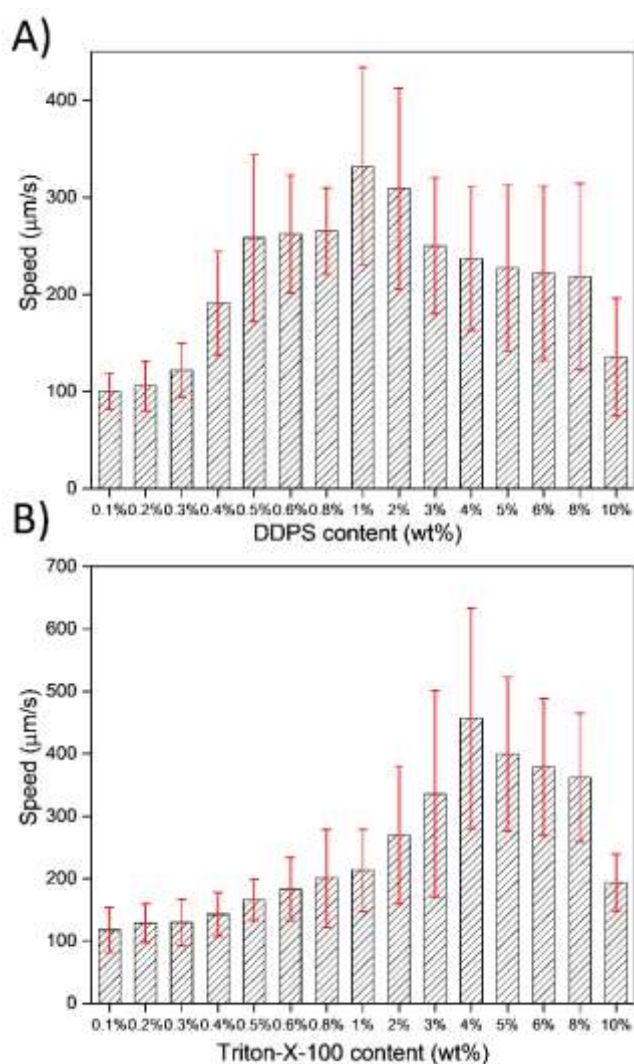


Figure 7.2. Dependence of the motion speed of graphene/Ag-MnO₂ microjets. (n=50) (A) Influence of DDPS concentration upon the speed of micromotors. (B) Influence of Triton-X-100 concentration upon the speed of micromotors. Condition in all experiments: at room temperature of 23°C and 3% H₂O₂ as fuel.

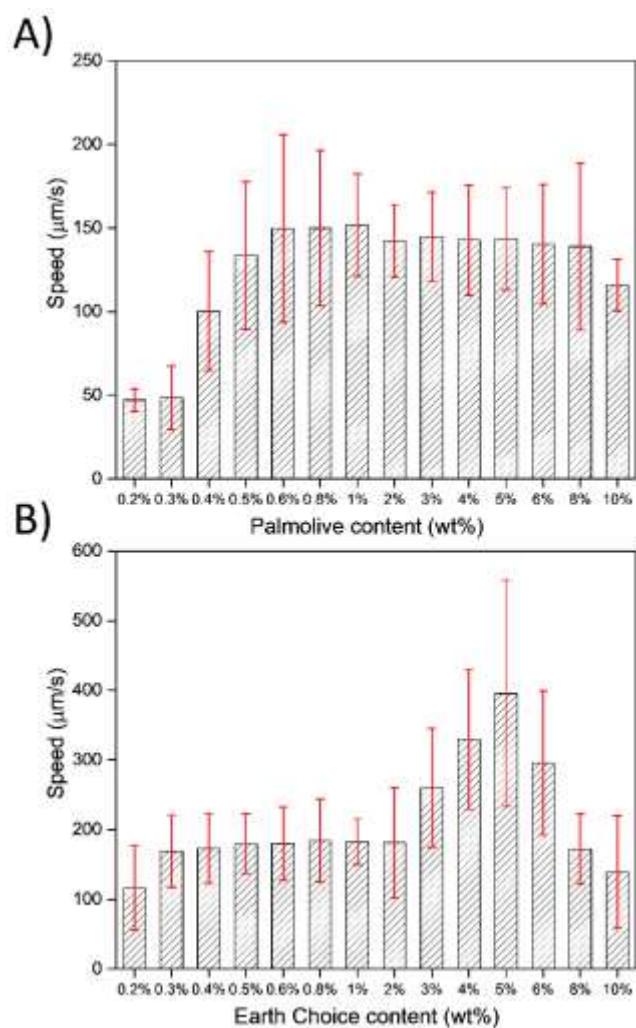


Figure 7.3. Dependence of the motion speed of graphene/Ag-MnO₂ microjets upon the content of detergents. (n=50) (A) Palmolive ultra original (denoted as Palmolive) dish wash liquid; (B) Earth Choice dish wash Liquid – Lemon Fresh and Aloe Fresh (denoted as Earth Choice). Condition in all experiments: at room temperature of 23°C and 3% H₂O₂ as fuel.

Previously, commercial soap liquid has been used as a surfactant in Pt catalyzed tubular micromotors.^{18, 46} As the silver-containing micromotors show efficient motion performance in all the pure surfactant solutions, two types of commercially available dish-washing liquid in mixed surfactants and additives solutions are also employed to investigate their influence on motion behaviors and the robustness of the silver-containing micromotors, and the results are summarized in Figure 7.3. The commercial detergents are composed of a mixture of anionic and non-ionic surfactant. The

detergents also contain minor amounts of stabilizers, salts, fragrances, and dyes as additives. The Palmolive is a commonly used detergent made mainly by the industrial feedstock, while the Earth Choice is a more environmentally friendly biodegradable detergent made mainly by the natural organics. Both types of commercial soap show good results as the mixed surfactants to initiate the motion of graphene/Ag-MnO₂ tubular micromotors. At least 0.2% of Palmolive soap is needed to initiate the propulsion at a speed less than 50 $\mu\text{m s}^{-1}$, while at the same content of Earth Choice, the speed of micromotors are $116 \pm 60 \mu\text{m s}^{-1}$, which means that the Earth Choice detergent is far better than the Palmolive detergent for MNMs motions. The speed of micromotors increased to a plateau of around 180 $\mu\text{m s}^{-1}$ as the Earth Choice content increased from 0.3% to 2%, while under the same content of Palmolive detergent, the speed of micromotors increased to around 150 $\mu\text{m s}^{-1}$ at 0.5% and maintained this speed as the surfactant further rose to 2%. Above 2% of the surfactant, the micromotors in Earth Choice detergent increase the motion dramatically to around 400 $\mu\text{m s}^{-1}$ at 5%, while the micromotors in Palmolive show a slight decrease as the surfactant level continued to rise. Above 5% of the detergent as a surfactant, the micromotors in Earth Choice surfactant dropped dramatically to $139 \pm 81 \mu\text{m s}^{-1}$ as the surfactant level increased to 10%, while under the Palmolive detergent as a surfactant, the micromotors' speed decreased to $116 \pm 15 \mu\text{m s}^{-1}$ in 10%. The use of Earth Choice detergent demonstrates higher speeds than Palmolive under the whole range of surfactant concentration, which demonstrated its great potential as the low cost environmentally friendly surfactant for the applications of the emerging silver containing micromotors. The above results also demonstrate that the silver-containing MNMs are very robust to the real environmental water matrix. The organics, salt, fragrances, and pigment widely exist in the natural water body. Previously, we

demonstrated the propulsion of MnO_2 based micromotors is quite independent of the surfactant used. Here, we also demonstrated that the silver-containing micromotors can also be propelled by all the surfactant conditions. These behaviors are very different from a previous report, the Pt-based micromotors' motion behaviors are quite dependent on the surfactant used.⁴⁰

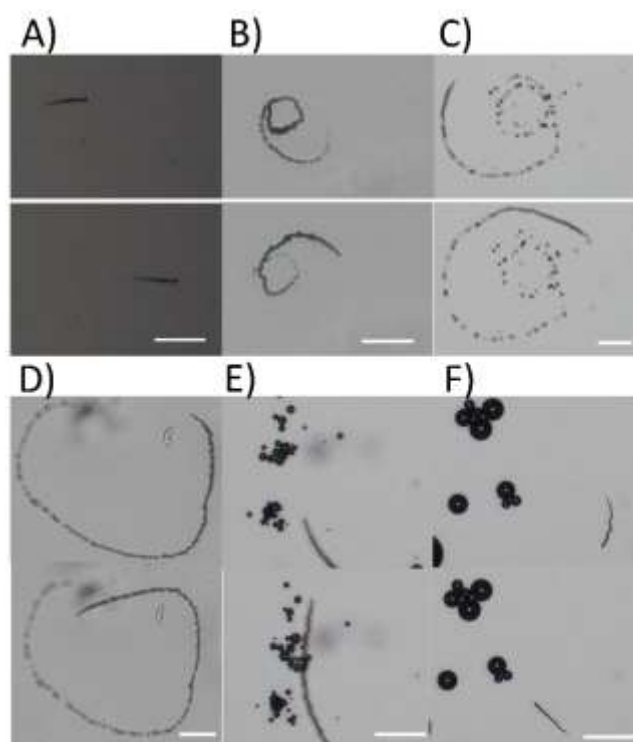


Figure 7.4. Time-lapse images extracted from the motion behaviors videos depicting the motion behaviors of graphene/Ag- MnO_2 tubular micromotors in different surfactant conditions in 1 s time interval with 3% H_2O_2 as fuel. (A) 4% SDS; (B) 0.8% CTAB; (C) 0.5% DDPS; (D) 2% Triton-X-100; (E) 8% Palmolive; (F) 8% Earth Choice. Scale bars: $100\mu\text{m}$.

Typical time-lapse images for the motion behaviors are presented in Figure 7.4. The graphene/Ag- MnO_2 micromotors show efficient motion behaviors and diverse motion patterns in all the surfactant conditions. There are many factors affecting the motion speed and directionality of micromotors. The fuel and surfactants affect the motion speeds by affecting the generation and ejection of the bubbles, while the motion

directions are affected by the fluid resistance and the geometry of the microtubes.⁴⁷ As the microtubes are not perfectly tubular in geometry and contain some asymmetry at the openings. That asymmetry can be accidentally produced by the electrochemical deposition process and the later-on cleaning and separation. If the edge of the tubes is not symmetrically distributed, the ejecting bubbles leave the microtubes in an angle, resulting in a torque force on the microtubes, which leads to various trajectories. Various motion patterns were recognized, such as circular, spiral, curved, flower-like, and snake-like motion. If the microtubes have more degree in symmetry, the expelling of bubbles will result in a direct force vector applied on the axial direction of the microtubes, which leads to linear motion.

7.4 Conclusions

The results demonstrate that the motion of graphene/Ag-MnO₂ micromotors are quite independent on the surfactants used, which is the biggest difference between the emerging silver containing micromotors and the previously developed Pt catalyzed micromotors. The CMC doesn't have a much effect on the motion of the silver-containing microjets, only 0.1-0.2% single component surfactants are needed for the initiation of silver containing micromotor in 3% H₂O₂ as a fuel. The commercial dish soap could be a good choice as a surfactant for silver containing micromotors with slightly higher surfactant concentration and lower speeds. The silver-containing micromotors are very robust in nature, resulting in efficient motion patterns. As different MNMs have different catalytic performances under different surfactant and fuel conditions, hence, the data revealed here could provide a good reference for the future application of the silver-containing micromotors.

References

1. Pacheco M, Jurado-Sanchez B, Escarpa A. Sensitive monitoring of enterobacterial contamination of food using self-propelled Janus microsensors. *Anal. Chem.* 2018; 90(4):2912-2917.
2. Li ZL, Wang W, Li M, et al. Facile fabrication of bubble-propelled micromotors carrying nanocatalysts for water remediation. *Ind. Eng. Chem. Res.* 2018; 57(13):4562-4570.
3. Xu T, Gao W, Xu LP, Zhang X, Wang S. Fuel-free synthetic micro-/nanomachines. *Adv. Mater.* 2017; 29(9):1603250.
4. Xu L, Mou F, Gong H, Luo M, Guan J. Light-driven micro/nanomotors: From fundamentals to applications. *Chem. Soc. Rev.* 2017; 46(22):6905-6926.
5. Molinero-Fernandez A, Moreno-Guzman M, Lopez MA, Escarpa A. Biosensing strategy for simultaneous and accurate quantitative analysis of mycotoxins in food samples using unmodified graphene micromotors. *Anal. Chem.* 2017; 89(20):10850-10857.
6. Li J, Angsantikul P, Liu W, et al. Micromotors spontaneously neutralize gastric acid for pH-responsive payload release. *Angew. Chem. Int. Ed.* 2017; 56(8):2156-2161.
7. Pan D, Mou FZ, Li XF, et al. Multifunctional magnetic oleic acid-coated MnFe_2O_4 /polystyrene Janus particles for water treatment. *J. Mater. Chem. A.* 2016; 4(30):11768-11774.
8. Mushtaq F, Asani A, Hoop M, et al. Highly efficient coaxial TiO_2 -PtPd tubular nanomachines for photocatalytic water purification with multiple locomotion strategies. *Adv. Funct. Mater.* 2016; 26(38):6995-7002.

9. Hoop M, Shen Y, Chen XZ, et al. Magnetically driven silver-coated nanocoils for efficient bacterial contact killing. *Adv. Funct. Mater.* 2016; 26(7):1063-1069.
10. Cheng C, Stoddart JF. Wholly synthetic molecular machines. *Chemphyschem.* 2016; 17(12):1780-1793.
11. Lee C-S, Gong J, Oh D-S, Jeon J-R, Chang Y-S. Zerovalent-iron/platinum Janus micromotors with spatially separated functionalities for efficient water decontamination. *ACS Appl. Nano Mater.* 2018; 1(2):768-776.
12. Tu Y, Peng F, Andre AA, et al. Biodegradable hybrid stomatocyte nanomotors for drug delivery. *ACS Nano.* 2017; 11(2):1957-1963.
13. Kuralay F, Sattayasamitsathit S, Gao W, et al. Self-propelled carbohydrate-sensitive microtransporters with built-in boronic acid recognition for isolating sugars and cells. *J. Am. Chem. Soc.* 2012; 134(37):15217-15220.
14. Jurado-Sanchez B, Escarpa A, Wang J. Lighting up micromotors with quantum dots for smart chemical sensing. *Chem. Commun.* 2015; 51(74):14088-14091.
15. Solovev AA, Mei Y, Bermúdez Ureña E, Huang G, Schmidt OG. Catalytic microtubular jet engines self-propelled by accumulated gas bubbles. *Small.* 2009; 5(14):1688-1692.
16. Gibbs JG, Fragnito NA, Zhao Y. Asymmetric Pt/Au coated catalytic micromotors fabricated by dynamic shadowing growth. *Appl. Phys. Lett.* 2010; 97(25).
17. Gao W, Sattayasamitsathit S, Orozco J, Wang J. Highly efficient catalytic microengines: Template electrosynthesis of polyaniline/platinum microtubes. *J. Am. Chem. Soc.* 2011; 133(31):11862-11864.

18. Sanchez S, Ananth AN, Fomin VM, Viehrig M, Schmidt OG. Superfast motion of catalytic microjet engines at physiological temperature. *J. Am. Chem. Soc.* 2011; 133(38):14860-14863.
19. Mei YF, Huang GS, Solovev AA, et al. Versatile approach for integrative and functionalized tubes by strain engineering of nanomembranes on polymers. *Adv. Mater.* 2008; 20(21):4085-4090.
20. Paxton WF, Baker PT, Kline TR, et al. Catalytically induced electrokinetics for motors and micropumps. *J. Am. Chem. Soc.* 2006; 128(46):14881-14888.
21. Tu YF, Peng F, Sui XF, et al. Self-propelled supramolecular nanomotors with temperature-responsive speed regulation. *Nat. Chem.* 2017; 9(5):480-486.
22. Zhao GJ, Sanchez S, Schmidt OG, Pumera M. Poisoning of bubble propelled catalytic micromotors: The chemical environment matters. *Nanoscale.* 2013; 5(7):2909-2914.
23. Wang H, Zhao G, Pumera M. Blood electrolytes exhibit a strong influence on the mobility of artificial catalytic microengines. *Phys. Chem. Chem. Phys.* 2013; 15(40):17277-17280.
24. Ye H, Sun H, Wang S. Electrochemical synthesis of graphene/MnO₂ in an architecture of bilayer microtubes as micromotors. *Chem. Eng. J.* 2017; 324:251-258.
25. Ye H, Kang J, Ma G, Sun H, Wang S. High-speed graphene@Ag-MnO₂ micromotors at low peroxide levels. *J. Colloid Interface Sci.* 2018; 528:271-280.
26. Ye H, Ma G, Kang J, Sun H, Wang S. Pt-Free microengines at extremely low peroxide levels. *Chem. Commun.* 2018; 54:4653-4656.
27. Zhou C, Zhang HP, Tang JY, Wang W. Photochemically powered AgCl Janus micromotors as a model system to understand ionic self-diffusiophoresis. *Langmuir.* 2018; 34(10):3289-3295.

28. Wang RQ, Guo WL, Li XH, et al. Highly efficient MOF-based self-propelled micromotors for water purification. *RSC Adv.* 2017; 7(67):42462-42467.
29. Vilela D, Stanton MM, Parmar J, Sanchez S. Microbots decorated with silver nanoparticles kill bacteria in aqueous media. *ACS Appl. Mater. Inter.* 2017.
30. He X, Bahk YK, Wang J. Organic dye removal by MnO₂ and Ag micromotors under various ambient conditions: The comparison between two abatement mechanisms. *Chemosphere.* 2017; 184:601-608.
31. Wang H, Zhao GJ, Pumera M. Beyond platinum: Bubble-propelled micromotors based on Ag and MnO₂ catalysts. *J. Am. Chem. Soc.* 2014; 136(7):2719-2722.
32. Singh VV, Jurado-Sanchez B, Sattayasamitsathit S, et al. Multifunctional silver-exchanged zeolite micromotors for catalytic detoxification of chemical and biological threats. *Adv. Funct. Mater.* 2015; 25(14):2147-2155.
33. Maria-Hormigos R, Jurado-Sanchez B, Vazquez L, Escarpa A. Carbon allotrope nanomaterials based catalytic micromotors. *Chem. Mater.* 2016; 28(24):8962-8970.
34. Teo WZ, Wang H, Pumera M. Beyond platinum: Silver-catalyst based bubble-propelled tubular micromotors. *Chem. Commun.* 2016; 52(23):4333-4336.
35. Demirok UK, Laocharoensuk R, Manesh KM, Wang J. Ultrafast catalytic alloy nanomotors. *Angew. Chem. Int. Ed.* 2008; 47(48):9349-9351.
36. Simmchen J, Baeza A, Miguel-Lopez A, et al. Dynamics of novel photoactive AgCl microstars and their environmental applications. *ChemNanoMat.* 2017; 3(1):65-71.

37. Gao W, Pei A, Dong RF, Wang J. Catalytic iridium-based Janus micromotors powered by ultralow levels of chemical fuels. *J. Am. Chem. Soc.* 2014; 136(6):2276-2279.
38. Matsuda Y, Yoshii M, Suematsu NJ, Izumi S, Nakata S. Self-propelled motor driven by a glucose engine. *Chem. Lett.* 2014; 43(4):453-455.
39. Simmchen J, Magdanz V, Sanchez S, et al. Effect of surfactants on the performance of tubular and spherical micromotors - a comparative study. *RSC Adv.* 2014; 4(39):20334-20340.
40. Wang H, Zhao GJ, Pumera M. Crucial role of surfactants in bubble-propelled microengines. *J. Phys. Chem. C.* 2014; 118(10):5268-5274.
41. Li YN, Wu J, Xie YZ, Ju HX. An efficient polymeric micromotor doped with Pt nanoparticle@carbon nanotubes for complex bio-media. *Chem. Commun.* 2015; 51(29):6325-6328.
42. Feng XM, Zhang Y, Li Y, et al. Graphene-based highly efficient micromotors. *Chem. Lett.* 2015; 44(3):399-401.
43. Solovev AA, Sanchez S, Pumera M, Mei YF, Schmidt OG. Magnetic control of tubular catalytic microbots for the transport, assembly, and delivery of micro-objects. *Adv. Funct. Mater.* 2010; 20(15):2430-2435.
44. Li J, Huang G, Ye M, et al. Dynamics of catalytic tubular microjet engines: Dependence on geometry and chemical environment. *Nanoscale.* 2011; 3(12):5083-5089.
45. Martin A, Jurado-Sanchez B, Escarpa A, Wang J. Template electrosynthesis of high-performance graphene microengines. *Small.* 2015; 11(29):3568-3574.
46. Solovev AA, Mei Y, Bermudez Urena E, Huang G, Schmidt OG. Catalytic microtubular jet engines self-propelled by accumulated gas bubbles. *Small.* 2009; 5(14):1688-1692.

47. Parmar J, Vilela D, Sanchez S. Tubular microjets: Fabrication, factors affecting the motion and mechanism of propulsion. Eur. Phys. J-Spec. Top. 2016; 225(11-12):2255-2267.

Every reasonable effort has been made to acknowledge the owners of copyright material. I would be pleased to hear from any copyright owner who has been omitted or incorrectly acknowledged.

Chapter 8. Conclusions and Perspectives

8.1 Conclusions

The main objective of this research is to develop low-cost and high-performance MNMs with the capability of addressing environmental issues. MnO₂ based micromotors are developed as a low-cost alternative to the precious metal Pt-based microengines by electrochemical fabrication. Due to the intrinsic lower catalytic activity than the noble metal Pt for the most widely used H₂O₂ fuel, the performance of MnO₂ based catalysts cannot compete with the Pt-MNMs. Hence, various fabrication and modification methods have been used to construct the precious metals free MnO₂ based micromotors. We demonstrate that graphene/MnO₂ bilayer microtubes could be fabricated by a low-cost multi-step electrochemical deposition. By changing the electrodeposition electrolytes and parameters, various MnO₂ based micromotors could be fabricated with regulated mobilities performance.

We also demonstrate that the MnO₂ based micromotors could be activated in different types of surfactant conditions. This phenomenon is quite different from the previously developed Pt-based microengines, whose mobility is quite dependent on the surfactant. Both pure MnO₂ based microengines and silver containing micromotors demonstrate efficient mobility performance at all typical surfactant conditions, demonstrating the robustness of these MnO₂ based micromotors.

8.1.1 Graphene/MnO₂ micromotors by anodic electrosynthesis

The fabrication of graphene/MnO₂ bilayer tubular micromotors was achieved by anodic electrochemical fabrication. The anodic deposited MnO₂ based micromotors require at least 3% of H₂O₂ as the fuel for

propulsion. The average speeds are much slower than Pt catalyzed micromotors under the same fuel conditions. Although the performance of MnO₂ based micromotors is not very good, the template-assisted electrochemical deposition is a good method for the fabrication of tubular micromotors.

8.1.2 MnO₂ based micromotors by cathodic electrofabrication

Since the MnO₂ based micromotors by anodic electrochemical oxidation synthesis require at least 3% H₂O₂ as a fuel for propulsion, we explored the fabrication of MnO₂ based micromotors via cathodic electrochemical reduction deposition. We found that the MnO₂ based micromotors by the cathodic fabrication require only 1% of H₂O₂ as a fuel for propulsion. Another advantage of the cathodic fabrication over anodic fabrication is the reduction process, which makes it possible to fabricate the metal modified MnO₂ based micromotors by electrochemical co-reduction deposition. The graphene/Ag-MnO₂ bilayer tubular micromotors need only 0.2% of H₂O₂ for propulsion, demonstrating the versatility and capability of this method for synthesis of micromotors.

8.1.3 High-performance graphene/FeO_x-MnO₂ micromotors

Based on the developed cathodic deposition method, we further designed metal oxide modified MnO₂ based microengines. The graphene/FeO_x-MnO₂ tubular micromotors require an even lower fuel content of 0.03% H₂O₂ to activate the motion, which is nearly one order of magnitude lower than Pt-based micromotors. Due to the good motion performance, low-cost, and easy functionality of the iron oxide modified MnO₂ based microengines, graphene/FeO_x-MnO₂ demonstrates as a very competitive alternative to Pt MNMs. The metal oxide based micromotors could be a

good choice as the catalyst for advanced oxidation process to degrade organic pollutant in the aquatic environment.

8.1.4 The role of surfactants in MnO₂ based micromotors system

Different types of surfactants affect the mobility as well as the function of MNMs for specific applications. We demonstrated that the MnO₂ based micromotors have another advantage over Pt-based micromotors in various surfactants. However, Pt-based microengines' performance is quite dependent on the surfactant used. These surfactant independent propulsion behaviors pave the way for the wide applications of the MnO₂ based and the silver-containing MNMs.

8.2 Perspectives and suggestions for future work

The development of micro/nano scale motion-based tools and devices would fundamentally change the nanoscience and nanotechnology today, as these self-propelled mobile devices and tools could be used for the regulation of chemical reactions and biological processes at a very precisely micro/nano scale. The development of MNMs could provide an opportunity for the chemists, materials scientist, and biologists to regulate the related chemical or biological process.

8.2.1 Environmental applications of the developed micromotors

As the outer layer of our developed MNMs is the electrochemically reduced graphene oxide, which contains many oxygen functional groups. Thus, it could be used as a micro scale adsorbent for adsorption of heavy metal ions in the aquatic environment. The inner layer catalytic materials are MnO₂ based materials, which are good candidates for various advanced oxidation processes. The iron oxide modified MnO₂ based

catalyst could be a good choice for the catalytic degradation of organic pollutants, such as dyes and phenolic compounds.

8.2.2 Development of new types of metal oxide based MNMs

The MnO₂ based materials fabricated by the cathodic electrochemical depositions are far more capable than those by the previously developed anodic fabrications. Due to the reduction deposition process, the substrate dissolution and oxidations are avoided. This method is very cheap and could be extended to fabricate various kinds of modified MnO₂ based MNMs. We demonstrated that the iron oxide could be a good choice to modify MnO₂ based materials with mobility performance even higher than that of Pt-based microengines at a very favorable low content of fuels. As the current fabrication methods are time-consuming, laborious, and always relying on the high vacuum equipment, it is very appealing to design the asymmetrically structured MNMs using cheap and reliable materials at the same time without the use of physical vapor deposition equipment. The electrochemical fabrication is much cheaper and faster than the sequential physical vapor deposition, but the use of porous membranes restricted the quantity of material synthesized. Hence, exploring new synthetic materials and avoiding the use of membrane template by electrochemical methods could be a good choice for future research focus.

8.2.3 MNMs based analytical applications

The use of MNMs for environmental monitoring and remediation has been demonstrated. MNMs could also be applied as novel analytical tools for food safety, security, defense, and biochemistry areas, due to the noticeable speed variation and the electrochemical signals, as the MNMs react with the analytes and regulate the speed of the chemical process.

Thus, these intelligent tools could be used at various applications from assays to food safety insurance.

Currently, the most widely explored areas of MNMs applications are the biomedical science and environmental fields. MNMs cannot be restricted to these areas, new fields are being explored by researchers from different backgrounds. As the development of MNMs is still at its early stage, there are numerous problems to be solved and improvement and progress could be made from every aspect relating to the synthesis and application. The innovation in synthesis and application of MNMs could generate a plethora of knowledge and technology for mankind to address diverse issues not limiting to the environmental and biomedical areas.

Appendix

The copyright licenses for some references in Chapter 2 (literature review) are attached below:

1. Ref. 9 (Figure 2.1A)
2. Ref. 43 (Figure 2.1B)
3. Ref. 44 (Figure 2.1C)
4. Ref. 45 (Figure 2.1D)
5. Ref. 46 (Figure 2.1E)
6. Ref. 32 (Figure 2.1F)
7. Ref. 63 (Figure 2.2A)
8. Ref. 48 (Figure 2.2B)
9. Ref. 64 (Figure 2.2C)
10. Ref. 47 (Figure 2.2D)
11. Ref. 95 (Figure 2.3A)
12. Ref. 96 (Figure 2.3B)
13. Ref. 97 (Figure 2.3C)

Adapted under the term of ACS Author Choice publication permission. Direct link <https://pubs.acs.org/doi/abs/10.1021/nm405075d>. Further permissions related to the material excerpted should be directed to the ACS.

14. Ref. 98 (Figure 2.3D)
15. Ref. 61 (Figure 2.3E)
16. Ref. 99 (Figure 2.3F)

Adapted under the term of ACS Author Choice publication permission. Direct link <https://pubs.acs.org/doi/abs/10.1021/acs.nanolett.6b00768>. Further permissions related to the material excerpted should be directed to the ACS.

17. Ref. 100 (Figure 2.3G)

[Home](#)[Account Info](#)[Help](#)

Title: Characterizing the Swimming Properties of Artificial Bacterial Flagella

Author: Li Zhang, Jake J. Abbott, Lixin Dong, et al

Publication: Nano Letters

Publisher: American Chemical Society

Date: Oct 1, 2009

Logged in as:

Heng Ye

Account #:

3001174420

[LOGOUT](#)

Copyright © 2009,
American Chemical
Society

PERMISSION/LICENSE IS GRANTED FOR YOUR ORDER AT NO CHARGE

This type of permission/license, instead of the standard Terms & Conditions, is sent to you because no fee is being charged for your order. Please note the following:

- Permission is granted for your request in both print and electronic formats, and translations.
- If figures and/or tables were requested, they may be adapted or used in part.
- Please print this page for your records and send a copy of it to your publisher/graduate school.
- Appropriate credit for the requested material should be given as follows: "Reprinted (adapted) with permission from (COMPLETE REFERENCE CITATION). Copyright (YEAR) American Chemical Society." Insert appropriate information in place of the capitalized words.
- One-time permission is granted only for the use specified in your request. No additional uses are granted (such as derivative works or other editions). For any other uses, please submit a new request.

If credit is given to another source for the material you requested, permission must be obtained from that source.

[BACK](#)[CLOSE WINDOW](#)



RightsLink®

Home

Account
Info

Help



Title:

Catalytic Nanomotors:
Autonomous Movement of
Striped Nanorods

Author:

Walter F. Paxton, Kevin C.
Kistler, Christine C. Olmeda,
et al

Publication:

Journal of the American
Chemical Society

Publisher:

American Chemical Society

Date:

Oct 1, 2004

Copyright © 2004,
American Chemical
Society

Logged in as:

Heng Ye

Account #:

3001174420

LOGOUT

PERMISSION/LICENSE IS GRANTED FOR YOUR ORDER AT NO CHARGE

This type of permission/license, instead of the standard Terms & Conditions, is sent to you because no fee is being charged for your order. Please note the following:

- Permission is granted for your request in both print and electronic formats, and translations.
- If figures and/or tables were requested, they may be adapted or used in part.
- Please print this page for your records and send a copy of it to your publisher/graduate school.
- Appropriate credit for the requested material should be given as follows:
"Reprinted (adapted) with permission from (COMPLETE REFERENCE CITATION). Copyright (YEAR) American Chemical Society." Insert appropriate information in place of the capitalized words.
- One-time permission is granted only for the use specified in your request. No additional uses are granted (such as derivative works or other editions). For any other uses, please submit a new request.

If credit is given to another source for the material you requested, permission must be obtained from that source.

BACK

CLOSE WINDOW



Title: Catalytically Induced
Electrokinetics for Motors and
Micropumps

Author: Walter F. Paxton, Paul T. Baker,
Timothy R. Kline, et al

Publication: Journal of the American
Chemical Society

Publisher: American Chemical Society

Date: Nov 1, 2006

Copyright © 2006, American Chemical Society

Logged in as:
Heng Ye
Account #:
3001174420

LOGOUT

PERMISSION/LICENSE IS GRANTED FOR YOUR ORDER AT NO CHARGE

This type of permission/license, instead of the standard Terms & Conditions, is sent to you because no fee is being charged for your order. Please note the following:

- Permission is granted for your request in both print and electronic formats, and translations.
- If figures and/or tables were requested, they may be adapted or used in part.
- Please print this page for your records and send a copy of it to your publisher/graduate school.
- Appropriate credit for the requested material should be given as follows: "Reprinted (adapted) with permission from (COMPLETE REFERENCE CITATION). Copyright (YEAR) American Chemical Society." Insert appropriate information in place of the capitalized words.
- One-time permission is granted only for the use specified in your request. No additional uses are granted (such as derivative works or other editions). For any other uses, please submit a new request.

If credit is given to another source for the material you requested, permission must be obtained from that source.

BACK

CLOSE WINDOW

Copyright © 2018 [Copyright Clearance Center, Inc.](#) All Rights Reserved. [Privacy statement.](#) [Terms and Conditions.](#)
Comments? We would like to hear from you. E-mail us at customer@copyright.com





Title: Chemical Sensing Based on Catalytic Nanomotors: Motion-Based Detection of Trace Silver

Author: Daniel Kagan, Percy Calvo-Marzal, Shankar Balasubramanian, et al

Publication: Journal of the American Chemical Society

Publisher: American Chemical Society

Date: Sep 1, 2009

Copyright © 2009, American Chemical Society

Logged in as:
Heng Ye
Account #:
3001174420

LOGOUT

PERMISSION/LICENSE IS GRANTED FOR YOUR ORDER AT NO CHARGE

This type of permission/license, instead of the standard Terms & Conditions, is sent to you because no fee is being charged for your order. Please note the following:

- Permission is granted for your request in both print and electronic formats, and translations.
- If figures and/or tables were requested, they may be adapted or used in part.
- Please print this page for your records and send a copy of it to your publisher/graduate school.
- Appropriate credit for the requested material should be given as follows: "Reprinted (adapted) with permission from (COMPLETE REFERENCE CITATION). Copyright (YEAR) American Chemical Society." Insert appropriate information in place of the capitalized words.
- One-time permission is granted only for the use specified in your request. No additional uses are granted (such as derivative works or other editions). For any other uses, please submit a new request.

If credit is given to another source for the material you requested, permission must be obtained from that source.

BACK

CLOSE WINDOW

Copyright © 2018 [Copyright Clearance Center, Inc.](#) All Rights Reserved. [Privacy statement](#). [Terms and Conditions](#).
Comments? We would like to hear from you. E-mail us at customer care@copyright.com



RightsLink®

Home

Account Info

Help



Title: Highly Efficient Catalytic Microengines: Template

Logged in as:
Heng Ye

Electrosynthesis of
Polyaniline/Platinum Microtubes

Author: Wei Gao, Sirilak
Sattayasamitsathit, Jahir
Orozco, et al

Publication: Journal of the American
Chemical Society

Publisher: American Chemical Society

Date: Aug 1, 2011

Copyright © 2011, American Chemical Society

Account #:
3001174420

LOGOUT

PERMISSION/LICENSE IS GRANTED FOR YOUR ORDER AT NO CHARGE

This type of permission/license, instead of the standard Terms & Conditions, is sent to you because no fee is being charged for your order. Please note the following:

- Permission is granted for your request in both print and electronic formats, and translations.
- If figures and/or tables were requested, they may be adapted or used in part.
- Please print this page for your records and send a copy of it to your publisher/graduate school.
- Appropriate credit for the requested material should be given as follows: "Reprinted (adapted) with permission from (COMPLETE REFERENCE CITATION). Copyright (YEAR) American Chemical Society." Insert appropriate information in place of the capitalized words.
- One-time permission is granted only for the use specified in your request. No additional uses are granted (such as derivative works or other editions). For any other uses, please submit a new request.

If credit is given to another source for the material you requested, permission must be obtained from that source.

BACK

CLOSE WINDOW

Copyright © 2018 [Copyright Clearance Center, Inc.](#) All Rights Reserved. [Privacy statement.](#) [Terms and Conditions.](#)
Comments? We would like to hear from you. E-mail us at customercare@copyright.com



RightsLink®

Home

Account
Info

Help



Title: Superhydrophobic Alkanethiol-
Coated Microsubmarines for
Effective Removal of Oil

Logged in as:
Heng Ye
Account #:
3001174420

Author: Maria Guix, Jahir Orozco, Miguel García, et al

LOGOUT

Publication: ACS Nano

Publisher: American Chemical Society

Date: May 1, 2012

Copyright © 2012, American Chemical Society

PERMISSION/LICENSE IS GRANTED FOR YOUR ORDER AT NO CHARGE

This type of permission/license, instead of the standard Terms & Conditions, is sent to you because no fee is being charged for your order. Please note the following:

- Permission is granted for your request in both print and electronic formats, and translations.
- If figures and/or tables were requested, they may be adapted or used in part.
- Please print this page for your records and send a copy of it to your publisher/graduate school.
- Appropriate credit for the requested material should be given as follows: "Reprinted (adapted) with permission from (COMPLETE REFERENCE CITATION). Copyright (YEAR) American Chemical Society." Insert appropriate information in place of the capitalized words.
- One-time permission is granted only for the use specified in your request. No additional uses are granted (such as derivative works or other editions). For any other uses, please submit a new request.

If credit is given to another source for the material you requested, permission must be obtained from that source.

BACK

CLOSE WINDOW

Copyright © 2018 [Copyright Clearance Center, Inc.](#) All Rights Reserved. [Privacy statement](#). [Terms and Conditions](#).
Comments? We would like to hear from you. E-mail us at customer care@copyright.com



RightsLink®

Home

Create Account

Help



ACS Publications
Most Trusted. Most Cited. Most Read.

Title:

Water-Driven Micromotors for Rapid Photocatalytic Degradation of Biological and Chemical Warfare Agents

LOGIN

Author: Jinxing Li, Virendra V. Singh,
Sirilak Sattayasamitsathit, et al
Publication: ACS Nano
Publisher: American Chemical Society
Date: Nov 1, 2014

Copyright © 2014, American Chemical Society

If you're a [copyright.com user](#), you can login to RightsLink using your [copyright.com](#) credentials.

Already a [RightsLink user](#) or want to [learn more?](#)

PERMISSION/LICENSE IS GRANTED FOR YOUR ORDER AT NO CHARGE

This type of permission/license, instead of the standard Terms & Conditions, is sent to you because no fee is being charged for your order. Please note the following:

- Permission is granted for your request in both print and electronic formats, and translations.
- If figures and/or tables were requested, they may be adapted or used in part.
- Please print this page for your records and send a copy of it to your publisher/graduate school.
- Appropriate credit for the requested material should be given as follows: "Reprinted (adapted) with permission from (COMPLETE REFERENCE CITATION). Copyright (YEAR) American Chemical Society." Insert appropriate information in place of the capitalized words.
- One-time permission is granted only for the use specified in your request. No additional uses are granted (such as derivative works or other editions). For any other uses, please submit a new request.

If credit is given to another source for the material you requested, permission must be obtained from that source.

BACK

CLOSE WINDOW

Copyright © 2018 [Copyright Clearance Center, Inc.](#) All Rights Reserved. [Privacy statement](#). [Terms and Conditions](#).
Comments? We would like to hear from you. E-mail us at customer care@copyright.com



RightsLink®

Home

Create Account

Help



ACS Publications
Most Trusted. Most Cited. Most Read.

Title: "Shoot and Sense" Janus
Micromotors-Based Strategy for
the Simultaneous Degradation
and Detection of Persistent
Organic Pollutants in Food and
Biological Samples

Author: D. Rojas, B. Jurado-Sánchez, A.
Escarpa

Publication: Analytical Chemistry

[LOGIN](#)

If you're a [copyright.com user](#), you can login to RightsLink using your [copyright.com](#) credentials.

Already a [RightsLink user](#) or want to [learn more?](#)

Publisher: American Chemical Society

Date: Apr 1, 2016

Copyright © 2016, American Chemical Society

PERMISSION/LICENSE IS GRANTED FOR YOUR ORDER AT NO CHARGE

This type of permission/license, instead of the standard Terms & Conditions, is sent to you because no fee is being charged for your order. Please note the following:

- Permission is granted for your request in both print and electronic formats, and translations.
- If figures and/or tables were requested, they may be adapted or used in part.
- Please print this page for your records and send a copy of it to your publisher/graduate school.
- Appropriate credit for the requested material should be given as follows: "Reprinted (adapted) with permission from (COMPLETE REFERENCE CITATION). Copyright (YEAR) American Chemical Society." Insert appropriate information in place of the capitalized words.
- One-time permission is granted only for the use specified in your request. No additional uses are granted (such as derivative works or other editions). For any other uses, please submit a new request.

If credit is given to another source for the material you requested, permission must be obtained from that source.

BACK

CLOSE WINDOW

Copyright © 2018 [Copyright Clearance Center, Inc.](#) All Rights Reserved. [Privacy statement.](#) [Terms and Conditions.](#)
Comments? We would like to hear from you. E-mail us at customercare@copyright.com

AIP PUBLISHING LICENSE TERMS AND CONDITIONS

Sep 28, 2018

This Agreement between Heng Ye ("You") and AIP Publishing ("AIP Publishing") consists of your license details and the terms and conditions provided by AIP Publishing and Copyright Clearance Center.

License Number 4437060635715

License date Sep 27, 2018

Licensed Content Publisher	AIP Publishing
Licensed Content Publication	Applied Physics Letters
Licensed Content Title	Autonomously motile catalytic nanomotors by bubble propulsion
Licensed Content Author	J. G. Gibbs, Y.-P. Zhao
Licensed Content Date	Apr 20, 2009
Licensed Content Volume	94
Licensed Content Issue	16
Type of Use	Thesis/Dissertation
Requestor type	Student
Format	Print and electronic
Portion	Figure/Table
Number of figures/tables	1
Title of your thesis / dissertation	Self-Propelled Micro/Nanomotors (MNMs) and Their Applications
Expected completion date	Oct 2018
Estimated size (number of pages)	200
Requestor Location	Heng Ye 141 basinghall St East Victoria Park Perth, other 6101 Australia Attn:
Billing Type	Invoice
Billing Address	Heng Ye 141 basinghall St East Victoria Park Perth, Australia 6101 Attn: Heng Ye
Total	0.00 AUD

Terms and Conditions

AIP Publishing -- Terms and Conditions: Permissions Uses

AIP Publishing hereby grants to you the non-exclusive right and license to use and/or distribute the Material according to the use specified in your order, on a one-time basis, for the specified term, with a maximum distribution equal to the number that you have ordered. Any links or other content accompanying the Material are not the subject of this license.

1. You agree to include the following copyright and permission notice with the reproduction of the Material: "Reprinted from [FULL CITATION], with the permission of AIP Publishing." For an article, the credit line and permission notice must be printed on the first page of the article or book chapter. For photographs, covers, or tables, the notice may appear with the Material, in a footnote, or in the reference list.
2. If you have licensed reuse of a figure, photograph, cover, or table, it is your responsibility to ensure that the material is original to AIP Publishing and does not contain the copyright of another entity, and that the copyright notice of the figure, photograph, cover, or table does not indicate that it was reprinted by AIP Publishing, with permission, from another source. Under no circumstances does AIP Publishing

purport or intend to grant permission to reuse material to which it does not hold appropriate rights.

You may not alter or modify the Material in any manner. You may translate the Material into another language only if you have licensed translation rights. You may not use the Material for promotional purposes.

3. The foregoing license shall not take effect unless and until AIP Publishing or its agent, Copyright Clearance Center, receives the Payment in accordance with Copyright Clearance Center Billing and Payment Terms and Conditions, which are incorporated herein by reference.
4. AIP Publishing or Copyright Clearance Center may, within two business days of granting this license, revoke the license for any reason whatsoever, with a full refund payable to you. Should you violate the terms of this license at any time, AIP Publishing, or Copyright Clearance Center may revoke the license with no refund to you. Notice of such revocation will be made using the contact information provided by you. Failure to receive such notice will not nullify the revocation.
5. AIP Publishing makes no representations or warranties with respect to the Material. You agree to indemnify and hold harmless AIP Publishing, and their officers, directors, employees or agents from and against any and all claims arising out of your use of the Material other than as specifically authorized herein.
6. The permission granted herein is personal to you and is not transferable or assignable without the prior written permission of AIP Publishing. This license may not be amended except in a writing signed by the party to be charged.
7. If purchase orders, acknowledgments or check endorsements are issued on any forms containing terms and conditions which are inconsistent with these provisions, such inconsistent terms and conditions shall be of no force and effect. This document, including the CCC Billing and Payment Terms and Conditions, shall be the entire agreement between the parties relating to the subject matter hereof.

This Agreement shall be governed by and construed in accordance with the laws of the State of New York. Both parties hereby submit to the jurisdiction of the courts of New York County for purposes of resolving any disputes that may arise hereunder.

V1.2

Questions? customercare@copyright.com or +1-855-239-3415 (toll free in the US) or +1-978-646-2777.

JOHN WILEY AND SONS LICENSE TERMS AND CONDITIONS

Sep 29, 2018

This Agreement between Heng Ye ("You") and John Wiley and Sons ("John Wiley and Sons") consists of your license details and the terms and conditions provided by John Wiley and Sons and Copyright Clearance Center.

License Number	4437520156583
License date	Sep 28, 2018

Licensed Content Publisher	John Wiley and Sons
Licensed Content Publication	Angewandte Chemie International Edition
Licensed Content Title	A Polymerization-Powered Motor
Licensed Content Author	Ryan A. Pavlick, Samudra Sengupta, Timothy McFadden, et al
Licensed Content Date	Aug 30, 2011
Licensed Content Volume	50
Licensed Content Issue	40
Licensed Content Pages	4
Type of use	Dissertation/Thesis
Requestor type	University/Academic
Format	Print and electronic
Portion	Figure/table
Number of figures/tables	1
Original Wiley figure/table number(s)	Figure 5
Will you be translating?	No
Title of your thesis / dissertation	Self-Propelled Micro/Nanomotors (MNMs) and Their Applications
Expected completion date	Oct 2018
Expected size (number of pages)	200
Requestor Location	Heng Ye 141 basinghall St East Victoria Park Perth, other 6101 Australia Attn:
Publisher Tax ID	EU826007151
Total	0.00 AUD
Terms and Conditions	

TERMS AND CONDITIONS

This copyrighted material is owned by or exclusively licensed to John Wiley & Sons, Inc. or one of its group companies (each a "Wiley Company") or handled on behalf of a society with which a Wiley Company has exclusive publishing rights in relation to a particular work (collectively "WILEY"). By clicking "accept" in connection with completing this licensing transaction, you agree that the following terms and conditions apply to this transaction (along with the billing and payment terms and conditions established by the Copyright Clearance Center Inc., ("CCC's Billing and Payment terms and conditions"), at the time that you opened your RightsLink account (these are available at any time at <http://myaccount.copyright.com>).

Terms and Conditions

- The materials you have requested permission to reproduce or reuse (the "Wiley Materials") are protected by copyright.
- You are hereby granted a personal, non-exclusive, non-sub licensable (on a stand-alone basis), non-transferable, worldwide, limited license to reproduce the Wiley Materials for the purpose specified in the licensing process. This license, **and any CONTENT (PDF or image file) purchased as part of your order,** is for a one-time use only and limited to any maximum distribution number specified in the license. The first instance of republication or reuse granted by this license must be completed within two years of the date of the grant of this license (although copies prepared before the end date may be distributed thereafter). The Wiley Materials shall not be used in any other manner or for any other purpose, beyond what is granted in the license. Permission is granted subject to an appropriate acknowledgement given to the author, title of the material/book/journal and the publisher. You shall also duplicate the copyright notice that appears in the Wiley publication in your use of the Wiley Material. Permission is also granted on the understanding that nowhere in the text is a previously published source acknowledged for all or part of this Wiley Material. Any third party content is expressly excluded from this permission.
- With respect to the Wiley Materials, all rights are reserved. Except as expressly granted by the terms of the license, no part of the Wiley Materials may be copied, modified, adapted (except for minor reformatting required by the new Publication), translated, reproduced, transferred or distributed, in any form or by any means, and no derivative works may be made based on the Wiley Materials without the prior permission of the respective copyright owner. **For STM Signatory Publishers clearing permission under the terms of the [STM Permissions Guidelines](#) only, the terms of the license are extended to include subsequent editions and for editions in other languages, provided such editions are for the work as a whole in situ and does not involve the separate exploitation of the permitted figures or extracts,** You may not alter, remove or suppress in any manner any copyright, trademark or other notices displayed by the Wiley Materials. You may not license, rent, sell, loan, lease, pledge, offer as security,

transfer or assign the Wiley Materials on a stand-alone basis, or any of the rights granted to you hereunder to any other person.

- The Wiley Materials and all of the intellectual property rights therein shall at all times remain the exclusive property of John Wiley & Sons Inc, the Wiley Companies, or their respective licensors, and your interest therein is only that of having possession of and the right to reproduce the Wiley Materials pursuant to Section 2 herein during the continuance of this Agreement. You agree that you own no right, title or interest in or to the Wiley Materials or any of the intellectual property rights therein. You shall have no rights hereunder other than the license as provided for above in Section 2. No right, license or interest to any trademark, trade name, service mark or other branding ("Marks") of WILEY or its licensors is granted hereunder, and you agree that you shall not assert any such right, license or interest with respect thereto
- NEITHER WILEY NOR ITS LICENSORS MAKES ANY WARRANTY OR REPRESENTATION OF ANY KIND TO YOU OR ANY THIRD PARTY, EXPRESS, IMPLIED OR STATUTORY, WITH RESPECT TO THE MATERIALS OR THE ACCURACY OF ANY INFORMATION CONTAINED IN THE MATERIALS, INCLUDING, WITHOUT LIMITATION, ANY IMPLIED WARRANTY OF MERCHANTABILITY, ACCURACY, SATISFACTORY QUALITY, FITNESS FOR A PARTICULAR PURPOSE, USABILITY, INTEGRATION OR NON-INFRINGEMENT AND ALL SUCH WARRANTIES ARE HEREBY EXCLUDED BY WILEY AND ITS LICENSORS AND WAIVED BY YOU.
- WILEY shall have the right to terminate this Agreement immediately upon breach of this Agreement by you.
- You shall indemnify, defend and hold harmless WILEY, its Licensors and their respective directors, officers, agents and employees, from and against any actual or threatened claims, demands, causes of action or proceedings arising from any breach of this Agreement by you.
- IN NO EVENT SHALL WILEY OR ITS LICENSORS BE LIABLE TO YOU OR ANY OTHER PARTY OR ANY OTHER PERSON OR ENTITY FOR ANY SPECIAL, CONSEQUENTIAL, INCIDENTAL, INDIRECT, EXEMPLARY OR PUNITIVE DAMAGES, HOWEVER CAUSED, ARISING OUT OF OR IN CONNECTION WITH THE DOWNLOADING, PROVISIONING, VIEWING OR USE OF THE MATERIALS REGARDLESS OF THE FORM OF ACTION, WHETHER FOR BREACH OF CONTRACT, BREACH OF WARRANTY, TORT, NEGLIGENCE, INFRINGEMENT OR OTHERWISE (INCLUDING, WITHOUT LIMITATION, DAMAGES BASED ON LOSS OF PROFITS,

DATA, FILES, USE, BUSINESS OPPORTUNITY OR CLAIMS OF THIRD PARTIES), AND WHETHER OR NOT THE PARTY HAS BEEN ADVISED OF THE POSSIBILITY OF SUCH DAMAGES. THIS LIMITATION SHALL APPLY NOTWITHSTANDING ANY FAILURE OF ESSENTIAL PURPOSE OF ANY LIMITED REMEDY PROVIDED HEREIN.

- Should any provision of this Agreement be held by a court of competent jurisdiction to be illegal, invalid, or unenforceable, that provision shall be deemed amended to achieve as nearly as possible the same economic effect as the original provision, and the legality, validity and enforceability of the remaining provisions of this Agreement shall not be affected or impaired thereby.
- The failure of either party to enforce any term or condition of this Agreement shall not constitute a waiver of either party's right to enforce each and every term and condition of this Agreement. No breach under this agreement shall be deemed waived or excused by either party unless such waiver or consent is in writing signed by the party granting such waiver or consent. The waiver by or consent of a party to a breach of any provision of this Agreement shall not operate or be construed as a waiver of or consent to any other or subsequent breach by such other party.
- This Agreement may not be assigned (including by operation of law or otherwise) by you without WILEY's prior written consent.
- Any fee required for this permission shall be non-refundable after thirty (30) days from receipt by the CCC.
- These terms and conditions together with CCC's Billing and Payment terms and conditions (which are incorporated herein) form the entire agreement between you and WILEY concerning this licensing transaction and (in the absence of fraud) supersedes all prior agreements and representations of the parties, oral or written. This Agreement may not be amended except in writing signed by both parties. This Agreement shall be binding upon and inure to the benefit of the parties' successors, legal representatives, and authorized assigns.
- In the event of any conflict between your obligations established by these terms and conditions and those established by CCC's Billing and Payment terms and conditions, these terms and conditions shall prevail.

- WILEY expressly reserves all rights not specifically granted in the combination of (i) the license details provided by you and accepted in the course of this licensing transaction, (ii) these terms and conditions and (iii) CCC's Billing and Payment terms and conditions.
- This Agreement will be void if the Type of Use, Format, Circulation, or Requestor Type was misrepresented during the licensing process.
- This Agreement shall be governed by and construed in accordance with the laws of the State of New York, USA, without regards to such state's conflict of law rules. Any legal action, suit or proceeding arising out of or relating to these Terms and Conditions or the breach thereof shall be instituted in a court of competent jurisdiction in New York County in the State of New York in the United States of America and each party hereby consents and submits to the personal jurisdiction of such court, waives any objection to venue in such court and consents to service of process by registered or certified mail, return receipt requested, at the last known address of such party.

WILEY OPEN ACCESS TERMS AND CONDITIONS

Wiley Publishes Open Access Articles in fully Open Access Journals and in Subscription journals offering Online Open. Although most of the fully Open Access journals publish open access articles under the terms of the Creative Commons Attribution (CC BY) License only, the subscription journals and a few of the Open Access Journals offer a choice of Creative Commons Licenses. The license type is clearly identified on the article.

The Creative Commons Attribution License

The [Creative Commons Attribution License \(CC-BY\)](#) allows users to copy, distribute and transmit an article, adapt the article and make commercial use of the article. The CC-BY license permits commercial and non-

Creative Commons Attribution Non-Commercial License

The [Creative Commons Attribution Non-Commercial \(CC-BY-NC\) License](#) permits use, distribution and reproduction in any medium, provided the original work is properly cited and is not used for commercial purposes. (see below)

Creative Commons Attribution-Non-Commercial-NoDerivs License

The [Creative Commons Attribution Non-Commercial-NoDerivs License](#) (CC-BY-NC-ND) permits use, distribution and reproduction in any medium,

provided the original work is properly cited, is not used for commercial purposes and no modifications or adaptations are made. (see below)

Use by commercial "for-profit" organizations

Use of Wiley Open Access articles for commercial, promotional, or marketing purposes requires further explicit permission from Wiley and will be subject to a fee.

Further details can be found on Wiley Online

Library <http://olabout.wiley.com/WileyCDA/Section/id-410895.html>

Other Terms and Conditions:

v1.10 Last updated September 2015

Questions? customercare@copyright.com or +1-855-239-3415 (toll free in the US) or +1-978-646-2777.



**JOHN WILEY AND SONS LICENSE
TERMS AND CONDITIONS**

Sep 29, 2018



This Agreement between Heng Ye ("You") and John Wiley and Sons ("John Wiley and Sons") consists of your license details and the terms and conditions provided by John Wiley and Sons and Copyright Clearance Center.

License Number

4437511128892

License date	Sep 28, 2018
Licensed Content Publisher	John Wiley and Sons
Licensed Content Publication	Chemistry - A European Journal
Licensed Content Title	External-Energy-Independent Polymer Capsule Motors and Their Cooperative Behaviors
Licensed Content Author	Guanjia Zhao, Tzu Hui Seah, Martin Pumera
Licensed Content Date	Sep 23, 2011
Licensed Content Volume	17
Licensed Content Issue	43
Licensed Content Pages	7
Type of use	Dissertation/Thesis
Requestor type	University/Academic
Format	Print and electronic
Portion	Figure/table
Number of figures/tables	1
Original Wiley figure/table number(s)	Scheme 1
Will you be translating?	No
Title of your thesis / dissertation	Self-Propelled Micro/Nanomotors (MNMs) and Their Applications
Expected completion date	Oct 2018
Expected size (number of pages)	200
Requestor Location	Heng Ye 141 basinghall St East Victoria Park Perth, other 6101 Australia Attn:
Publisher Tax ID	EU826007151
Total	0.00 AUD
Terms and Conditions	

TERMS AND CONDITIONS

This copyrighted material is owned by or exclusively licensed to John Wiley & Sons, Inc. or one of its group companies (each a "Wiley Company") or handled on behalf of a society with which a Wiley Company has exclusive publishing rights in relation to a particular work (collectively "WILEY"). By clicking "accept" in connection with completing this licensing transaction, you agree that the following terms and conditions apply to this transaction (along with the billing and payment terms and conditions established by the Copyright Clearance Center Inc., ("CCC's Billing and Payment terms and conditions"), at the

time that you opened your RightsLink account (these are available at any time at <http://myaccount.copyright.com>).

Terms and Conditions

- The materials you have requested permission to reproduce or reuse (the "Wiley Materials") are protected by copyright.
- You are hereby granted a personal, non-exclusive, non-sub licensable (on a stand-alone basis), non-transferable, worldwide, limited license to reproduce the Wiley Materials for the purpose specified in the licensing process. This license, **and any CONTENT (PDF or image file) purchased as part of your order,** is for a one-time use only and limited to any maximum distribution number specified in the license. The first instance of republication or reuse granted by this license must be completed within two years of the date of the grant of this license (although copies prepared before the end date may be distributed thereafter). The Wiley Materials shall not be used in any other manner or for any other purpose, beyond what is granted in the license. Permission is granted subject to an appropriate acknowledgement given to the author, title of the material/book/journal and the publisher. You shall also duplicate the copyright notice that appears in the Wiley publication in your use of the Wiley Material. Permission is also granted on the understanding that nowhere in the text is a previously published source acknowledged for all or part of this Wiley Material. Any third party content is expressly excluded from this permission.
- With respect to the Wiley Materials, all rights are reserved. Except as expressly granted by the terms of the license, no part of the Wiley Materials may be copied, modified, adapted (except for minor reformatting required by the new Publication), translated, reproduced, transferred or distributed, in any form or by any means, and no derivative works may be made based on the Wiley Materials without the prior permission of the respective copyright owner. **For STM Signatory Publishers clearing permission under the terms of the [STM Permissions Guidelines](#) only, the terms of the license are extended to include subsequent editions and for editions in other languages, provided such editions are for the work as a whole in situ and does not involve the separate exploitation of the permitted figures or extracts,** You may not alter, remove or suppress in any manner any copyright, trademark or other notices displayed by the Wiley Materials. You may not

license, rent, sell, loan, lease, pledge, offer as security, transfer or assign the Wiley Materials on a stand-alone basis, or any of the rights granted to you hereunder to any other person.

- The Wiley Materials and all of the intellectual property rights therein shall at all times remain the exclusive property of John Wiley & Sons Inc, the Wiley Companies, or their respective licensors, and your interest therein is only that of having possession of and the right to reproduce the Wiley Materials pursuant to Section 2 herein during the continuance of this Agreement. You agree that you own no right, title or interest in or to the Wiley Materials or any of the intellectual property rights therein. You shall have no rights hereunder other than the license as provided for above in Section 2. No right, license or interest to any trademark, trade name, service mark or other branding ("Marks") of WILEY or its licensors is granted hereunder, and you agree that you shall not assert any such right, license or interest with respect thereto
- NEITHER WILEY NOR ITS LICENSORS MAKES ANY WARRANTY OR REPRESENTATION OF ANY KIND TO YOU OR ANY THIRD PARTY, EXPRESS, IMPLIED OR STATUTORY, WITH RESPECT TO THE MATERIALS OR THE ACCURACY OF ANY INFORMATION CONTAINED IN THE MATERIALS, INCLUDING, WITHOUT LIMITATION, ANY IMPLIED WARRANTY OF MERCHANTABILITY, ACCURACY, SATISFACTORY QUALITY, FITNESS FOR A PARTICULAR PURPOSE, USABILITY, INTEGRATION OR NON-INFRINGEMENT AND ALL SUCH WARRANTIES ARE HEREBY EXCLUDED BY WILEY AND ITS LICENSORS AND WAIVED BY YOU.
- WILEY shall have the right to terminate this Agreement immediately upon breach of this Agreement by you.
- You shall indemnify, defend and hold harmless WILEY, its Licensors and their respective directors, officers, agents and employees, from and against any actual or threatened claims, demands, causes of action or proceedings arising from any breach of this Agreement by you.
- IN NO EVENT SHALL WILEY OR ITS LICENSORS BE LIABLE TO YOU OR ANY OTHER PARTY OR ANY OTHER PERSON OR ENTITY FOR ANY SPECIAL, CONSEQUENTIAL, INCIDENTAL, INDIRECT, EXEMPLARY OR PUNITIVE DAMAGES, HOWEVER CAUSED, ARISING OUT OF OR IN CONNECTION WITH THE DOWNLOADING, PROVISIONING, VIEWING OR USE OF THE MATERIALS REGARDLESS OF THE FORM OF ACTION, WHETHER FOR BREACH OF CONTRACT, BREACH OF WARRANTY, TORT, NEGLIGENCE, INFRINGEMENT OR OTHERWISE

(INCLUDING, WITHOUT LIMITATION, DAMAGES BASED ON LOSS OF PROFITS, DATA, FILES, USE, BUSINESS OPPORTUNITY OR CLAIMS OF THIRD PARTIES), AND WHETHER OR NOT THE PARTY HAS BEEN ADVISED OF THE POSSIBILITY OF SUCH DAMAGES. THIS LIMITATION SHALL APPLY NOTWITHSTANDING ANY FAILURE OF ESSENTIAL PURPOSE OF ANY LIMITED REMEDY PROVIDED HEREIN.

- Should any provision of this Agreement be held by a court of competent jurisdiction to be illegal, invalid, or unenforceable, that provision shall be deemed amended to achieve as nearly as possible the same economic effect as the original provision, and the legality, validity and enforceability of the remaining provisions of this Agreement shall not be affected or impaired thereby.
- The failure of either party to enforce any term or condition of this Agreement shall not constitute a waiver of either party's right to enforce each and every term and condition of this Agreement. No breach under this agreement shall be deemed waived or excused by either party unless such waiver or consent is in writing signed by the party granting such waiver or consent. The waiver by or consent of a party to a breach of any provision of this Agreement shall not operate or be construed as a waiver of or consent to any other or subsequent breach by such other party.
- This Agreement may not be assigned (including by operation of law or otherwise) by you without WILEY's prior written consent.
- Any fee required for this permission shall be non-refundable after thirty (30) days from receipt by the CCC.
- These terms and conditions together with CCC's Billing and Payment terms and conditions (which are incorporated herein) form the entire agreement between you and WILEY concerning this licensing transaction and (in the absence of fraud) supersedes all prior agreements and representations of the parties, oral or written. This Agreement may not be amended except in writing signed by both parties. This Agreement shall be binding upon and inure to the benefit of the parties' successors, legal representatives, and authorized assigns.
- In the event of any conflict between your obligations established by these terms and conditions and those established by CCC's Billing and Payment terms and conditions, these terms and conditions shall prevail.

- WILEY expressly reserves all rights not specifically granted in the combination of (i) the license details provided by you and accepted in the course of this licensing transaction, (ii) these terms and conditions and (iii) CCC's Billing and Payment terms and conditions.
- This Agreement will be void if the Type of Use, Format, Circulation, or Requestor Type was misrepresented during the licensing process.
- This Agreement shall be governed by and construed in accordance with the laws of the State of New York, USA, without regards to such state's conflict of law rules. Any legal action, suit or proceeding arising out of or relating to these Terms and Conditions or the breach thereof shall be instituted in a court of competent jurisdiction in New York County in the State of New York in the United States of America and each party hereby consents and submits to the personal jurisdiction of such court, waives any objection to venue in such court and consents to service of process by registered or certified mail, return receipt requested, at the last known address of such party.

WILEY OPEN ACCESS TERMS AND CONDITIONS

Wiley Publishes Open Access Articles in fully Open Access Journals and in Subscription journals offering Online Open. Although most of the fully Open Access journals publish open access articles under the terms of the Creative Commons Attribution (CC BY) License only, the subscription journals and a few of the Open Access Journals offer a choice of Creative Commons Licenses. The license type is clearly identified on the article.

The Creative Commons Attribution License

The [Creative Commons Attribution License \(CC-BY\)](#) allows users to copy, distribute and transmit an article, adapt the article and make commercial use of the article. The CC-BY license permits commercial and non-

Creative Commons Attribution Non-Commercial License

The [Creative Commons Attribution Non-Commercial \(CC-BY-NC\) License](#) permits use, distribution and reproduction in any medium, provided the original work is properly cited and is not used for commercial purposes. (see below)

Creative Commons Attribution-Non-Commercial-NoDerivs License

The [Creative Commons Attribution Non-Commercial-NoDerivs License](#) (CC-BY-NC-ND) permits use, distribution and reproduction in any medium,

provided the original work is properly cited, is not used for commercial purposes and no modifications or adaptations are made. (see below)

Use by commercial "for-profit" organizations

Use of Wiley Open Access articles for commercial, promotional, or marketing purposes requires further explicit permission from Wiley and will be subject to a fee.

Further details can be found on Wiley Online

Library <http://olabout.wiley.com/WileyCDA/Section/id-410895.html>

Other Terms and Conditions:

v1.10 Last updated September 2015

Questions? customercare@copyright.com or +1-855-239-3415 (toll free in the US) or +1-978-646-2777.

**JOHN WILEY AND SONS LICENSE
TERMS AND CONDITIONS**

Sep 29, 2018

This Agreement between Heng Ye ("You") and John Wiley and Sons ("John Wiley and Sons") consists of your license details and the terms and conditions provided by John Wiley and Sons and Copyright Clearance Center.

License Number	4437501257039
License date	Sep 28, 2018
Licensed Content Publisher	John Wiley and Sons
Licensed Content Publication	Advanced Functional Materials
Licensed Content Title	Magnetic Control of Tubular Catalytic Microbots for the Transport, Assembly, and Delivery of Micro-objects
Licensed Content Author	Alexander A. Solovev, Samuel Sanchez, Martin Pumera, et al
Licensed Content Date	Jul 29, 2010
Licensed Content Volume	20
Licensed Content Issue	15
Licensed Content Pages	6
Type of use	Dissertation/Thesis
Requestor type	University/Academic
Format	Print and electronic
Portion	Figure/table
Number of figures/tables	1
Original Wiley figure/table number(s)	Figure 1
Will you be translating?	No
Title of your thesis / dissertation	Self-Propelled Micro/Nanomotors (MNMs) and Their Applications
Expected completion date	Oct 2018
Expected size (number of pages)	200
Requestor Location	Heng Ye 141 basinghall St East Victoria Park Perth, other 6101 Australia Attn:
Publisher Tax ID	EU826007151
Total	0.00 AUD
Terms and Conditions	

TERMS AND CONDITIONS

This copyrighted material is owned by or exclusively licensed to John Wiley & Sons, Inc. or one of its group companies (each a "Wiley Company") or handled on behalf of a society with which a Wiley Company has exclusive publishing rights in relation to a particular work (collectively "WILEY"). By clicking "accept" in connection with completing this licensing transaction, you agree that the following terms and conditions apply to this transaction (along with the billing and payment terms and conditions established by the Copyright Clearance Center Inc., ("CCC's Billing and Payment terms and conditions"), at the

time that you opened your RightsLink account (these are available at any time at <http://myaccount.copyright.com>).

Terms and Conditions

- The materials you have requested permission to reproduce or reuse (the "Wiley Materials") are protected by copyright.
- You are hereby granted a personal, non-exclusive, non-sub licensable (on a stand-alone basis), non-transferable, worldwide, limited license to reproduce the Wiley Materials for the purpose specified in the licensing process. This license, **and any CONTENT (PDF or image file) purchased as part of your order,** is for a one-time use only and limited to any maximum distribution number specified in the license. The first instance of republication or reuse granted by this license must be completed within two years of the date of the grant of this license (although copies prepared before the end date may be distributed thereafter). The Wiley Materials shall not be used in any other manner or for any other purpose, beyond what is granted in the license. Permission is granted subject to an appropriate acknowledgement given to the author, title of the material/book/journal and the publisher. You shall also duplicate the copyright notice that appears in the Wiley publication in your use of the Wiley Material. Permission is also granted on the understanding that nowhere in the text is a previously published source acknowledged for all or part of this Wiley Material. Any third party content is expressly excluded from this permission.
- With respect to the Wiley Materials, all rights are reserved. Except as expressly granted by the terms of the license, no part of the Wiley Materials may be copied, modified, adapted (except for minor reformatting required by the new Publication), translated, reproduced, transferred or distributed, in any form or by any means, and no derivative works may be made based on the Wiley Materials without the prior permission of the respective copyright owner. **For STM Signatory Publishers clearing permission under the terms of the [STM Permissions Guidelines](#) only, the terms of the license are extended to include subsequent editions and for editions in other languages, provided such editions are for the work as a whole in situ and does not involve the separate exploitation of the permitted figures or extracts,** You may not alter, remove or suppress in any manner any copyright, trademark or other notices displayed by the Wiley Materials. You may not

license, rent, sell, loan, lease, pledge, offer as security, transfer or assign the Wiley Materials on a stand-alone basis, or any of the rights granted to you hereunder to any other person.

- The Wiley Materials and all of the intellectual property rights therein shall at all times remain the exclusive property of John Wiley & Sons Inc, the Wiley Companies, or their respective licensors, and your interest therein is only that of having possession of and the right to reproduce the Wiley Materials pursuant to Section 2 herein during the continuance of this Agreement. You agree that you own no right, title or interest in or to the Wiley Materials or any of the intellectual property rights therein. You shall have no rights hereunder other than the license as provided for above in Section 2. No right, license or interest to any trademark, trade name, service mark or other branding ("Marks") of WILEY or its licensors is granted hereunder, and you agree that you shall not assert any such right, license or interest with respect thereto
- NEITHER WILEY NOR ITS LICENSORS MAKES ANY WARRANTY OR REPRESENTATION OF ANY KIND TO YOU OR ANY THIRD PARTY, EXPRESS, IMPLIED OR STATUTORY, WITH RESPECT TO THE MATERIALS OR THE ACCURACY OF ANY INFORMATION CONTAINED IN THE MATERIALS, INCLUDING, WITHOUT LIMITATION, ANY IMPLIED WARRANTY OF MERCHANTABILITY, ACCURACY, SATISFACTORY QUALITY, FITNESS FOR A PARTICULAR PURPOSE, USABILITY, INTEGRATION OR NON-INFRINGEMENT AND ALL SUCH WARRANTIES ARE HEREBY EXCLUDED BY WILEY AND ITS LICENSORS AND WAIVED BY YOU.
- WILEY shall have the right to terminate this Agreement immediately upon breach of this Agreement by you.
- You shall indemnify, defend and hold harmless WILEY, its Licensors and their respective directors, officers, agents and employees, from and against any actual or threatened claims, demands, causes of action or proceedings arising from any breach of this Agreement by you.
- IN NO EVENT SHALL WILEY OR ITS LICENSORS BE LIABLE TO YOU OR ANY OTHER PARTY OR ANY OTHER PERSON OR ENTITY FOR ANY SPECIAL, CONSEQUENTIAL, INCIDENTAL, INDIRECT, EXEMPLARY OR PUNITIVE DAMAGES, HOWEVER CAUSED, ARISING OUT OF OR IN CONNECTION WITH THE DOWNLOADING, PROVISIONING, VIEWING OR USE OF THE MATERIALS REGARDLESS OF THE FORM OF ACTION, WHETHER FOR BREACH OF CONTRACT, BREACH OF WARRANTY, TORT, NEGLIGENCE, INFRINGEMENT OR OTHERWISE

(INCLUDING, WITHOUT LIMITATION, DAMAGES BASED ON LOSS OF PROFITS, DATA, FILES, USE, BUSINESS OPPORTUNITY OR CLAIMS OF THIRD PARTIES), AND WHETHER OR NOT THE PARTY HAS BEEN ADVISED OF THE POSSIBILITY OF SUCH DAMAGES. THIS LIMITATION SHALL APPLY NOTWITHSTANDING ANY FAILURE OF ESSENTIAL PURPOSE OF ANY LIMITED REMEDY PROVIDED HEREIN.

- Should any provision of this Agreement be held by a court of competent jurisdiction to be illegal, invalid, or unenforceable, that provision shall be deemed amended to achieve as nearly as possible the same economic effect as the original provision, and the legality, validity and enforceability of the remaining provisions of this Agreement shall not be affected or impaired thereby.
- The failure of either party to enforce any term or condition of this Agreement shall not constitute a waiver of either party's right to enforce each and every term and condition of this Agreement. No breach under this agreement shall be deemed waived or excused by either party unless such waiver or consent is in writing signed by the party granting such waiver or consent. The waiver by or consent of a party to a breach of any provision of this Agreement shall not operate or be construed as a waiver of or consent to any other or subsequent breach by such other party.
- This Agreement may not be assigned (including by operation of law or otherwise) by you without WILEY's prior written consent.
- Any fee required for this permission shall be non-refundable after thirty (30) days from receipt by the CCC.
- These terms and conditions together with CCC's Billing and Payment terms and conditions (which are incorporated herein) form the entire agreement between you and WILEY concerning this licensing transaction and (in the absence of fraud) supersedes all prior agreements and representations of the parties, oral or written. This Agreement may not be amended except in writing signed by both parties. This Agreement shall be binding upon and inure to the benefit of the parties' successors, legal representatives, and authorized assigns.
- In the event of any conflict between your obligations established by these terms and conditions and those established by CCC's Billing and Payment terms and conditions, these terms and conditions shall prevail.

- WILEY expressly reserves all rights not specifically granted in the combination of (i) the license details provided by you and accepted in the course of this licensing transaction, (ii) these terms and conditions and (iii) CCC's Billing and Payment terms and conditions.
- This Agreement will be void if the Type of Use, Format, Circulation, or Requestor Type was misrepresented during the licensing process.
- This Agreement shall be governed by and construed in accordance with the laws of the State of New York, USA, without regards to such state's conflict of law rules. Any legal action, suit or proceeding arising out of or relating to these Terms and Conditions or the breach thereof shall be instituted in a court of competent jurisdiction in New York County in the State of New York in the United States of America and each party hereby consents and submits to the personal jurisdiction of such court, waives any objection to venue in such court and consents to service of process by registered or certified mail, return receipt requested, at the last known address of such party.

WILEY OPEN ACCESS TERMS AND CONDITIONS

Wiley Publishes Open Access Articles in fully Open Access Journals and in Subscription journals offering Online Open. Although most of the fully Open Access journals publish open access articles under the terms of the Creative Commons Attribution (CC BY) License only, the subscription journals and a few of the Open Access Journals offer a choice of Creative Commons Licenses. The license type is clearly identified on the article.

The Creative Commons Attribution License

The [Creative Commons Attribution License \(CC-BY\)](#) allows users to copy, distribute and transmit an article, adapt the article and make commercial use of the article. The CC-BY license permits commercial and non-

Creative Commons Attribution Non-Commercial License

The [Creative Commons Attribution Non-Commercial \(CC-BY-NC\) License](#) permits use, distribution and reproduction in any medium, provided the original work is properly cited and is not used for commercial purposes. (see below)

Creative Commons Attribution-Non-Commercial-NoDerivs License

The [Creative Commons Attribution Non-Commercial-NoDerivs License](#) (CC-BY-NC-ND) permits use, distribution and reproduction in any medium,

provided the original work is properly cited, is not used for commercial purposes and no modifications or adaptations are made. (see below)

Use by commercial "for-profit" organizations

Use of Wiley Open Access articles for commercial, promotional, or marketing purposes requires further explicit permission from Wiley and will be subject to a fee.

Further details can be found on Wiley Online

Library <http://olabout.wiley.com/WileyCDA/Section/id-410895.html>

Other Terms and Conditions:

v1.10 Last updated September 2015

Questions? customercare@copyright.com or +1-855-239-3415 (toll free in the US) or +1-978-646-2777.

**JOHN WILEY AND SONS LICENSE
TERMS AND CONDITIONS**

Sep 29, 2018

This Agreement between Heng Ye ("You") and John Wiley and Sons ("John Wiley and Sons") consists of your license details and the terms and conditions provided by John Wiley and Sons and Copyright Clearance Center.

License Number
4436850486629

License date
Sep 26, 2018

Licensed Content Publisher
John Wiley and Sons
Licensed Content Publication
Small
Licensed Content Title
Catalytic Microtubular Jet Engines Self-Propelled by Accumulated Gas Bubbles
Licensed Content Author
Alexander A. Solovev, Yongfeng Mei, Esteban Bermúdez Ureña, et al
Licensed Content Date
Apr 16, 2009
Licensed Content Volume
5
Licensed Content Issue
14
Licensed Content Pages
5
Type of use
Dissertation/Thesis
Requestor type
University/Academic
Format
Print and electronic
Portion
Figure/table
Number of figures/tables
2
Original Wiley figure/table number(s)
Figure 1 and Figure 2
Will you be translating?
No
Title of your thesis / dissertation
Self-Propelled Micro/Nanomotors (MNM)s and Their Applications
Expected completion date
Oct 2018
Expected size (number of pages)
200
Requestor Location
Heng Ye
141 basinghall St
East Victoria Park

Perth, other 6101
Australia
Attn:
Publisher Tax ID
EU826007151
Total
0.00 AUD
Terms and Conditions

TERMS AND CONDITIONS

This copyrighted material is owned by or exclusively licensed to John Wiley & Sons, Inc. or one of its group companies (each a "Wiley Company") or handled on behalf of a society with which a Wiley Company has exclusive publishing rights in relation to a particular work (collectively "WILEY"). By clicking "accept" in connection with completing this licensing transaction, you agree that the following terms and conditions apply to this transaction (along with the billing and payment terms and conditions established by the Copyright Clearance Center Inc., ("CCC's Billing and Payment terms and conditions"), at the time that you opened your RightsLink account (these are available at any time at <http://myaccount.copyright.com>).

Terms and Conditions

- The materials you have requested permission to reproduce or reuse (the "Wiley Materials") are protected by copyright.
- You are hereby granted a personal, non-exclusive, non-sub licensable (on a stand-alone basis), non-transferable, worldwide, limited license to reproduce the Wiley Materials for the purpose specified in the licensing process. This license, **and any CONTENT (PDF or image file) purchased as part of your order**, is for a one-time use only and limited to any maximum distribution number specified in the license. The first instance of republication or reuse granted by this license must be completed within two years of the date of the grant of this license (although copies prepared before the end date may be distributed thereafter). The Wiley Materials shall not be used in any other manner or for any other purpose, beyond what is granted in the license. Permission is granted subject to an appropriate acknowledgement given to the author, title of the material/book/journal and the publisher. You shall also duplicate the copyright notice that appears in the Wiley publication in your use of the Wiley Material. Permission is also granted on the understanding that nowhere in the text is a previously published source acknowledged for all or part of this Wiley Material. Any third party content is expressly excluded from this permission.
- With respect to the Wiley Materials, all rights are reserved. Except as expressly granted by the terms of the license, no part of the Wiley Materials may be copied, modified, adapted (except for minor reformatting required by the new Publication), translated, reproduced, transferred or distributed, in any form or by any means, and no derivative works may be made based on the Wiley Materials without the prior permission of the respective copyright owner. **For STM Signatory Publishers clearing permission under the terms of the [STM Permissions Guidelines](#) only, the terms of the license are extended to include subsequent editions and for editions in other languages, provided such editions are for the work as a whole in situ and does not involve the separate exploitation of the permitted figures or extracts,** You may not alter, remove or suppress in any manner any copyright, trademark or other notices displayed by the Wiley Materials. You may not license, rent, sell, loan, lease, pledge, offer as security, transfer or assign the Wiley Materials on a stand-alone basis, or any of the rights granted to you hereunder to any other person.
- The Wiley Materials and all of the intellectual property rights therein shall at all times remain the exclusive property of John Wiley & Sons Inc, the Wiley Companies, or their respective licensors, and your interest therein is only that of having possession of and the right to reproduce the Wiley Materials pursuant to Section 2 herein during the continuance of this Agreement. You agree that you own no right, title or interest in or to the Wiley Materials or any of the intellectual property rights therein. You shall have no rights hereunder other than the license as provided for above in Section 2. No right, license or interest to any trademark, trade name, service mark or other branding ("Marks") of WILEY or its licensors is granted hereunder, and you agree that you shall not assert any such right, license or interest with respect thereto
- NEITHER WILEY NOR ITS LICENSORS MAKES ANY WARRANTY OR REPRESENTATION OF ANY KIND TO YOU OR ANY THIRD PARTY, EXPRESS, IMPLIED OR STATUTORY, WITH RESPECT TO THE MATERIALS OR THE ACCURACY OF ANY INFORMATION CONTAINED IN THE MATERIALS, INCLUDING, WITHOUT LIMITATION, ANY IMPLIED

WARRANTY OF MERCHANTABILITY, ACCURACY, SATISFACTORY QUALITY, FITNESS FOR A PARTICULAR PURPOSE, USABILITY, INTEGRATION OR NON-INFRINGEMENT AND ALL SUCH WARRANTIES ARE HEREBY EXCLUDED BY WILEY AND ITS LICENSORS AND WAIVED BY YOU.

- WILEY shall have the right to terminate this Agreement immediately upon breach of this Agreement by you.
- You shall indemnify, defend and hold harmless WILEY, its Licensors and their respective directors, officers, agents and employees, from and against any actual or threatened claims, demands, causes of action or proceedings arising from any breach of this Agreement by you.
- IN NO EVENT SHALL WILEY OR ITS LICENSORS BE LIABLE TO YOU OR ANY OTHER PARTY OR ANY OTHER PERSON OR ENTITY FOR ANY SPECIAL, CONSEQUENTIAL, INCIDENTAL, INDIRECT, EXEMPLARY OR PUNITIVE DAMAGES, HOWEVER CAUSED, ARISING OUT OF OR IN CONNECTION WITH THE DOWNLOADING, PROVISIONING, VIEWING OR USE OF THE MATERIALS REGARDLESS OF THE FORM OF ACTION, WHETHER FOR BREACH OF CONTRACT, BREACH OF WARRANTY, TORT, NEGLIGENCE, INFRINGEMENT OR OTHERWISE (INCLUDING, WITHOUT LIMITATION, DAMAGES BASED ON LOSS OF PROFITS, DATA, FILES, USE, BUSINESS OPPORTUNITY OR CLAIMS OF THIRD PARTIES), AND WHETHER OR NOT THE PARTY HAS BEEN ADVISED OF THE POSSIBILITY OF SUCH DAMAGES. THIS LIMITATION SHALL APPLY NOTWITHSTANDING ANY FAILURE OF ESSENTIAL PURPOSE OF ANY LIMITED REMEDY PROVIDED HEREIN.
- Should any provision of this Agreement be held by a court of competent jurisdiction to be illegal, invalid, or unenforceable, that provision shall be deemed amended to achieve as nearly as possible the same economic effect as the original provision, and the legality, validity and enforceability of the remaining provisions of this Agreement shall not be affected or impaired thereby.
- The failure of either party to enforce any term or condition of this Agreement shall not constitute a waiver of either party's right to enforce each and every term and condition of this Agreement. No breach under this agreement shall be deemed waived or excused by either party unless such waiver or consent is in writing signed by the party granting such waiver or consent. The waiver by or consent of a party to a breach of any provision of this Agreement shall not operate or be construed as a waiver of or consent to any other or subsequent breach by such other party.
- This Agreement may not be assigned (including by operation of law or otherwise) by you without WILEY's prior written consent.
- Any fee required for this permission shall be non-refundable after thirty (30) days from receipt by the CCC.
- These terms and conditions together with CCC's Billing and Payment terms and conditions (which are incorporated herein) form the entire agreement between you

and WILEY concerning this licensing transaction and (in the absence of fraud) supersedes all prior agreements and representations of the parties, oral or written. This Agreement may not be amended except in writing signed by both parties. This Agreement shall be binding upon and inure to the benefit of the parties' successors, legal representatives, and authorized assigns.

- In the event of any conflict between your obligations established by these terms and conditions and those established by CCC's Billing and Payment terms and conditions, these terms and conditions shall prevail.
- WILEY expressly reserves all rights not specifically granted in the combination of (i) the license details provided by you and accepted in the course of this licensing transaction, (ii) these terms and conditions and (iii) CCC's Billing and Payment terms and conditions.
- This Agreement will be void if the Type of Use, Format, Circulation, or Requestor Type was misrepresented during the licensing process.
- This Agreement shall be governed by and construed in accordance with the laws of the State of New York, USA, without regards to such state's conflict of law rules. Any legal action, suit or proceeding arising out of or relating to these Terms and Conditions or the breach thereof shall be instituted in a court of competent jurisdiction in New York County in the State of New York in the United States of America and each party hereby consents and submits to the personal jurisdiction of such court, waives any objection to venue in such court and consents to service of process by registered or certified mail, return receipt requested, at the last known address of such party.

WILEY OPEN ACCESS TERMS AND CONDITIONS

Wiley Publishes Open Access Articles in fully Open Access Journals and in Subscription journals offering Online Open. Although most of the fully Open Access journals publish open access articles under the terms of the Creative Commons Attribution (CC BY) License only, the subscription journals and a few of the Open Access Journals offer a choice of Creative Commons Licenses. The license type is clearly identified on the article.

The Creative Commons Attribution License

The [Creative Commons Attribution License \(CC-BY\)](#) allows users to copy, distribute and transmit an article, adapt the article and make commercial use of the article. The CC-BY license permits commercial and non-

Creative Commons Attribution Non-Commercial License

The [Creative Commons Attribution Non-Commercial \(CC-BY-NC\) License](#) permits use, distribution and reproduction in any medium, provided the original work is properly cited and is not used for commercial purposes.(see below)

Creative Commons Attribution-Non-Commercial-NoDerivs License

The [Creative Commons Attribution Non-Commercial-NoDerivs License](#) (CC-BY-NC-ND) permits use, distribution and reproduction in any medium, provided the original work is properly cited, is not used for commercial purposes and no modifications or adaptations are made. (see below)

Use by commercial "for-profit" organizations

Use of Wiley Open Access articles for commercial, promotional, or marketing purposes requires further explicit permission from Wiley and will be subject to a fee.

Further details can be found on Wiley Online
Library <http://olabout.wiley.com/WileyCDA/Section/id-410895.html>

Other Terms and Conditions:

v1.10 Last updated September 2015

Questions? customercare@copyright.com or +1-855-239-3415 (toll free in the US) or +1-978-646-2777.

**JOHN WILEY AND SONS LICENSE
TERMS AND CONDITIONS**

Sep 29, 2018

This Agreement between Heng Ye ("You") and John Wiley and Sons ("John Wiley and Sons") consists of your license details and the terms and conditions provided by John Wiley and Sons and Copyright Clearance Center.

License Number

4438561351026

License date	Sep 29, 2018
Licensed Content Publisher	John Wiley and Sons
Licensed Content Publication	Angewandte Chemie International Edition
Licensed Content Title	Autonomous Movement and Self-Assembly
Licensed Content Author	Rustem F. Ismagilov, Alexander Schwartz, Ned Bowden, et al
Licensed Content Date	Feb 14, 2002
Licensed Content Volume	41
Licensed Content Issue	4
Licensed Content Pages	3
Type of use	Dissertation/Thesis
Requestor type	University/Academic
Format	Print and electronic
Portion	Figure/table
Number of figures/tables	1
Original Wiley figure/table number(s)	Figure 1
Will you be translating?	No
Title of your thesis / dissertation	Self-Propelled Micro/Nanomotors (MNMs) and Their Applications
Expected completion date	Oct 2018
Expected size (number of pages)	200
Requestor Location	Heng Ye 141 basinghall St East Victoria Park Perth, other 6101 Australia Attn:
Publisher Tax ID	EU826007151
Total	0.00 AUD

Terms and Conditions

TERMS AND CONDITIONS

This copyrighted material is owned by or exclusively licensed to John Wiley & Sons, Inc. or one of its group companies (each a "Wiley Company") or handled on behalf of a society with which a Wiley Company has exclusive publishing rights in relation to a particular work (collectively "WILEY"). By clicking "accept" in connection with completing this licensing transaction, you agree that the following terms and conditions apply to this transaction (along with the billing and payment terms and conditions established by the Copyright Clearance Center Inc., ("CCC's Billing and Payment terms and conditions"), at the time that you opened your RightsLink account (these are available at any time at <http://myaccount.copyright.com>).

Terms and Conditions

- The materials you have requested permission to reproduce or reuse (the "Wiley Materials") are protected by copyright.
- You are hereby granted a personal, non-exclusive, non-sub licensable (on a stand-alone basis), non-transferable, worldwide, limited license to reproduce the Wiley Materials for the purpose specified in the licensing process. This license, **and any CONTENT (PDF or image file) purchased as part of your order**, is for a one-time use only and limited to any maximum distribution number specified in the license. The first instance of republication or reuse granted by this license must be completed within two years of the date of the grant of this license (although copies prepared before the end date may be distributed thereafter). The Wiley Materials shall not be used in any other manner or for any other purpose, beyond what is granted in the license. Permission is granted subject to an appropriate acknowledgement given to the author, title of the material/book/journal and the publisher. You shall also duplicate the copyright notice that appears in the Wiley publication in your use of the Wiley Material. Permission is also granted on the understanding that nowhere in the text is a previously published source acknowledged for all or part of this Wiley Material. Any third party content is expressly excluded from this permission.
- With respect to the Wiley Materials, all rights are reserved. Except as expressly granted by the terms of the license, no part of the Wiley Materials may be copied, modified, adapted (except for minor reformatting required by the new Publication), translated, reproduced, transferred or distributed, in any form or by any means, and no derivative works may be made based on the Wiley Materials without the prior permission of the respective copyright owner. **For STM Signatory Publishers clearing permission under the terms of the [STM Permissions Guidelines](#) only, the terms of the license are extended to include subsequent editions and for editions in other languages, provided such editions are for the work as a whole in situ and does not involve the separate exploitation of the permitted figures or extracts**, You may not alter, remove or suppress in any manner any copyright, trademark or other notices displayed by the Wiley Materials. You may not license, rent, sell, loan, lease, pledge, offer as security, transfer or assign the Wiley Materials on a stand-alone basis, or any of the rights granted to you hereunder to any other person.
- The Wiley Materials and all of the intellectual property rights therein shall at all times remain the exclusive property of John Wiley & Sons Inc, the Wiley Companies, or their respective licensors, and your interest therein is only that of having possession of and the right to reproduce the Wiley Materials pursuant to Section 2 herein during the continuance of this Agreement. You agree that you own no right, title or interest in or to the Wiley Materials or any of the intellectual property rights therein. You shall have no rights hereunder other than the license as provided for above in Section 2. No right, license or interest to any trademark, trade name, service mark or other branding ("Marks") of WILEY or its licensors is granted hereunder, and you agree that you shall not assert any such right, license or interest with respect thereto

- NEITHER WILEY NOR ITS LICENSORS MAKES ANY WARRANTY OR REPRESENTATION OF ANY KIND TO YOU OR ANY THIRD PARTY, EXPRESS, IMPLIED OR STATUTORY, WITH RESPECT TO THE MATERIALS OR THE ACCURACY OF ANY INFORMATION CONTAINED IN THE MATERIALS, INCLUDING, WITHOUT LIMITATION, ANY IMPLIED WARRANTY OF MERCHANTABILITY, ACCURACY, SATISFACTORY QUALITY, FITNESS FOR A PARTICULAR PURPOSE, USABILITY, INTEGRATION OR NON-INFRINGEMENT AND ALL SUCH WARRANTIES ARE HEREBY EXCLUDED BY WILEY AND ITS LICENSORS AND WAIVED BY YOU.
- WILEY shall have the right to terminate this Agreement immediately upon breach of this Agreement by you.
- You shall indemnify, defend and hold harmless WILEY, its Licensors and their respective directors, officers, agents and employees, from and against any actual or threatened claims, demands, causes of action or proceedings arising from any breach of this Agreement by you.
- IN NO EVENT SHALL WILEY OR ITS LICENSORS BE LIABLE TO YOU OR ANY OTHER PARTY OR ANY OTHER PERSON OR ENTITY FOR ANY SPECIAL, CONSEQUENTIAL, INCIDENTAL, INDIRECT, EXEMPLARY OR PUNITIVE DAMAGES, HOWEVER CAUSED, ARISING OUT OF OR IN CONNECTION WITH THE DOWNLOADING, PROVISIONING, VIEWING OR USE OF THE MATERIALS REGARDLESS OF THE FORM OF ACTION, WHETHER FOR BREACH OF CONTRACT, BREACH OF WARRANTY, TORT, NEGLIGENCE, INFRINGEMENT OR OTHERWISE (INCLUDING, WITHOUT LIMITATION, DAMAGES BASED ON LOSS OF PROFITS, DATA, FILES, USE, BUSINESS OPPORTUNITY OR CLAIMS OF THIRD PARTIES), AND WHETHER OR NOT THE PARTY HAS BEEN ADVISED OF THE POSSIBILITY OF SUCH DAMAGES. THIS LIMITATION SHALL APPLY NOTWITHSTANDING ANY FAILURE OF ESSENTIAL PURPOSE OF ANY LIMITED REMEDY PROVIDED HEREIN.
- Should any provision of this Agreement be held by a court of competent jurisdiction to be illegal, invalid, or unenforceable, that provision shall be deemed amended to achieve as nearly as possible the same economic effect as the original provision, and the legality, validity and enforceability of the remaining provisions of this Agreement shall not be affected or impaired thereby.
- The failure of either party to enforce any term or condition of this Agreement shall not constitute a waiver of either party's right to enforce each and every term and condition of this Agreement. No breach under this agreement shall be deemed waived or excused by either party unless such waiver or consent is in writing signed by the party granting such waiver or consent. The waiver by or consent of a party to a breach of any provision of this Agreement shall not operate or be construed as a waiver of or consent to any other or subsequent breach by such other party.
- This Agreement may not be assigned (including by operation of law or otherwise) by you without WILEY's prior written consent.

- Any fee required for this permission shall be non-refundable after thirty (30) days from receipt by the CCC.
- These terms and conditions together with CCC's Billing and Payment terms and conditions (which are incorporated herein) form the entire agreement between you and WILEY concerning this licensing transaction and (in the absence of fraud) supersedes all prior agreements and representations of the parties, oral or written. This Agreement may not be amended except in writing signed by both parties. This Agreement shall be binding upon and inure to the benefit of the parties' successors, legal representatives, and authorized assigns.
- In the event of any conflict between your obligations established by these terms and conditions and those established by CCC's Billing and Payment terms and conditions, these terms and conditions shall prevail.
- WILEY expressly reserves all rights not specifically granted in the combination of (i) the license details provided by you and accepted in the course of this licensing transaction, (ii) these terms and conditions and (iii) CCC's Billing and Payment terms and conditions.
- This Agreement will be void if the Type of Use, Format, Circulation, or Requestor Type was misrepresented during the licensing process.
- This Agreement shall be governed by and construed in accordance with the laws of the State of New York, USA, without regards to such state's conflict of law rules. Any legal action, suit or proceeding arising out of or relating to these Terms and Conditions or the breach thereof shall be instituted in a court of competent jurisdiction in New York County in the State of New York in the United States of America and each party hereby consents and submits to the personal jurisdiction of such court, waives any objection to venue in such court and consents to service of process by registered or certified mail, return receipt requested, at the last known address of such party.

WILEY OPEN ACCESS TERMS AND CONDITIONS

Wiley Publishes Open Access Articles in fully Open Access Journals and in Subscription journals offering Online Open. Although most of the fully Open Access journals publish open access articles under the terms of the Creative Commons Attribution (CC BY) License only, the subscription journals and a few of the Open Access Journals offer a choice of Creative Commons Licenses. The license type is clearly identified on the article.

The Creative Commons Attribution License

The [Creative Commons Attribution License \(CC-BY\)](#) allows users to copy, distribute and transmit an article, adapt the article and make commercial use of the article. The CC-BY license permits commercial and non-

Creative Commons Attribution Non-Commercial License

The [Creative Commons Attribution Non-Commercial \(CC-BY-NC\) License](#) permits use, distribution and reproduction in any medium, provided the original work is properly cited and is not used for commercial purposes.(see below)

Creative Commons Attribution-Non-Commercial-NoDerivs License

The [Creative Commons Attribution Non-Commercial-NoDerivs License](#) (CC-BY-NC-ND) permits use, distribution and reproduction in any medium, provided the original work is

properly cited, is not used for commercial purposes and no modifications or adaptations are made. (see below)

Use by commercial "for-profit" organizations

Use of Wiley Open Access articles for commercial, promotional, or marketing purposes requires further explicit permission from Wiley and will be subject to a fee.

Further details can be found on Wiley Online Library

<http://olabout.wiley.com/WileyCDA/Section/id-410895.html>

Other Terms and Conditions:

v1.10 Last updated September 2015

Questions? customercare@copyright.com or +1-855-239-3415 (toll free in the US) or +1-978-646-2777.

**JOHN WILEY AND SONS LICENSE
TERMS AND CONDITIONS**

Sep 30, 2018

This Agreement between Heng Ye ("You") and John Wiley and Sons ("John Wiley and Sons") consists of your license details and the terms and conditions provided by John Wiley and Sons and Copyright Clearance Center.

License Number	4438571268231
License date	Sep 30, 2018
Licensed Content Publisher	John Wiley and Sons
Licensed Content Publication	Angewandte Chemie International Edition

Licensed Content Title	Micromotor-Based High-Yielding Fast Oxidative Detoxification of Chemical Threats
Licensed Content Author	Jahir Orozco, Guanzhi Cheng, Diana Vilela, et al
Licensed Content Date	Oct 24, 2013
Licensed Content Volume	52
Licensed Content Issue	50
Licensed Content Pages	4
Type of use	Dissertation/Thesis
Requestor type	University/Academic
Format	Print and electronic
Portion	Figure/table
Number of figures/tables	1
Original Wiley figure/table number(s)	Figure 1
Will you be translating?	No
Title of your thesis / dissertation	Self-Propelled Micro/Nanomotors (MNMs) and Their Applications
Expected completion date	Oct 2018
Expected size (number of pages)	200
Requestor Location	Heng Ye 141 basinghall St East Victoria Park Perth, other 6101 Australia Attn:
Publisher Tax ID	EU826007151
Total	0.00 AUD
Terms and Conditions	

TERMS AND CONDITIONS

This copyrighted material is owned by or exclusively licensed to John Wiley & Sons, Inc. or one of its group companies (each a "Wiley Company") or handled on behalf of a society with which a Wiley Company has exclusive publishing rights in relation to a particular work (collectively "WILEY"). By clicking "accept" in connection with completing this licensing transaction, you agree that the following terms and conditions apply to this transaction (along with the billing and payment terms and conditions established by the Copyright Clearance Center Inc., ("CCC's Billing and Payment terms and conditions"), at the time that you opened your RightsLink account (these are available at any time at <http://myaccount.copyright.com>).

Terms and Conditions

- The materials you have requested permission to reproduce or reuse (the "Wiley Materials") are protected by copyright.

- You are hereby granted a personal, non-exclusive, non-sub licensable (on a stand-alone basis), non-transferable, worldwide, limited license to reproduce the Wiley Materials for the purpose specified in the licensing process. This license, **and any CONTENT (PDF or image file) purchased as part of your order,** is for a one-time use only and limited to any maximum distribution number specified in the license. The first instance of republication or reuse granted by this license must be completed within two years of the date of the grant of this license (although copies prepared before the end date may be distributed thereafter). The Wiley Materials shall not be used in any other manner or for any other purpose, beyond what is granted in the license. Permission is granted subject to an appropriate acknowledgement given to the author, title of the material/book/journal and the publisher. You shall also duplicate the copyright notice that appears in the Wiley publication in your use of the Wiley Material. Permission is also granted on the understanding that nowhere in the text is a previously published source acknowledged for all or part of this Wiley Material. Any third party content is expressly excluded from this permission.
- With respect to the Wiley Materials, all rights are reserved. Except as expressly granted by the terms of the license, no part of the Wiley Materials may be copied, modified, adapted (except for minor reformatting required by the new Publication), translated, reproduced, transferred or distributed, in any form or by any means, and no derivative works may be made based on the Wiley Materials without the prior permission of the respective copyright owner. **For STM Signatory Publishers clearing permission under the terms of the [STM Permissions Guidelines](#) only, the terms of the license are extended to include subsequent editions and for editions in other languages, provided such editions are for the work as a whole in situ and does not involve the separate exploitation of the permitted figures or extracts,** You may not alter, remove or suppress in any manner any copyright, trademark or other notices displayed by the Wiley Materials. You may not license, rent, sell, loan, lease, pledge, offer as security, transfer or assign the Wiley Materials on a stand-alone basis, or any of the rights granted to you hereunder to any other person.
- The Wiley Materials and all of the intellectual property rights therein shall at all times remain the exclusive property of John Wiley & Sons Inc, the Wiley Companies, or their respective licensors, and your interest therein is only that of having possession of and the right to reproduce the Wiley Materials pursuant to Section 2 herein during the continuance of this Agreement. You agree that you own no right, title or interest in or to the Wiley Materials or any of the intellectual property rights therein. You shall have no rights hereunder other than the license as provided for above in Section 2. No right, license or interest to any trademark, trade name, service mark or other branding ("Marks") of WILEY or its licensors is granted hereunder, and you agree that you shall not assert any such right, license or interest with respect thereto
- NEITHER WILEY NOR ITS LICENSORS MAKES ANY WARRANTY OR REPRESENTATION OF ANY KIND TO YOU OR ANY THIRD PARTY, EXPRESS, IMPLIED OR STATUTORY, WITH RESPECT TO THE MATERIALS OR THE ACCURACY OF ANY INFORMATION CONTAINED IN THE MATERIALS, INCLUDING, WITHOUT LIMITATION, ANY IMPLIED

WARRANTY OF MERCHANTABILITY, ACCURACY, SATISFACTORY QUALITY, FITNESS FOR A PARTICULAR PURPOSE, USABILITY, INTEGRATION OR NON-INFRINGEMENT AND ALL SUCH WARRANTIES ARE HEREBY EXCLUDED BY WILEY AND ITS LICENSORS AND WAIVED BY YOU.

- WILEY shall have the right to terminate this Agreement immediately upon breach of this Agreement by you.
- You shall indemnify, defend and hold harmless WILEY, its Licensors and their respective directors, officers, agents and employees, from and against any actual or threatened claims, demands, causes of action or proceedings arising from any breach of this Agreement by you.
- IN NO EVENT SHALL WILEY OR ITS LICENSORS BE LIABLE TO YOU OR ANY OTHER PARTY OR ANY OTHER PERSON OR ENTITY FOR ANY SPECIAL, CONSEQUENTIAL, INCIDENTAL, INDIRECT, EXEMPLARY OR PUNITIVE DAMAGES, HOWEVER CAUSED, ARISING OUT OF OR IN CONNECTION WITH THE DOWNLOADING, PROVISIONING, VIEWING OR USE OF THE MATERIALS REGARDLESS OF THE FORM OF ACTION, WHETHER FOR BREACH OF CONTRACT, BREACH OF WARRANTY, TORT, NEGLIGENCE, INFRINGEMENT OR OTHERWISE (INCLUDING, WITHOUT LIMITATION, DAMAGES BASED ON LOSS OF PROFITS, DATA, FILES, USE, BUSINESS OPPORTUNITY OR CLAIMS OF THIRD PARTIES), AND WHETHER OR NOT THE PARTY HAS BEEN ADVISED OF THE POSSIBILITY OF SUCH DAMAGES. THIS LIMITATION SHALL APPLY NOTWITHSTANDING ANY FAILURE OF ESSENTIAL PURPOSE OF ANY LIMITED REMEDY PROVIDED HEREIN.
- Should any provision of this Agreement be held by a court of competent jurisdiction to be illegal, invalid, or unenforceable, that provision shall be deemed amended to achieve as nearly as possible the same economic effect as the original provision, and the legality, validity and enforceability of the remaining provisions of this Agreement shall not be affected or impaired thereby.
- The failure of either party to enforce any term or condition of this Agreement shall not constitute a waiver of either party's right to enforce each and every term and condition of this Agreement. No breach under this agreement shall be deemed waived or excused by either party unless such waiver or consent is in writing signed by the party granting such waiver or consent. The waiver by or consent of a party to a breach of any provision of this Agreement shall not operate or be construed as a waiver of or consent to any other or subsequent breach by such other party.
- This Agreement may not be assigned (including by operation of law or otherwise) by you without WILEY's prior written consent.
- Any fee required for this permission shall be non-refundable after thirty (30) days from receipt by the CCC.
- These terms and conditions together with CCC's Billing and Payment terms and conditions (which are incorporated herein) form the entire agreement between you

and WILEY concerning this licensing transaction and (in the absence of fraud) supersedes all prior agreements and representations of the parties, oral or written. This Agreement may not be amended except in writing signed by both parties. This Agreement shall be binding upon and inure to the benefit of the parties' successors, legal representatives, and authorized assigns.

- In the event of any conflict between your obligations established by these terms and conditions and those established by CCC's Billing and Payment terms and conditions, these terms and conditions shall prevail.
- WILEY expressly reserves all rights not specifically granted in the combination of (i) the license details provided by you and accepted in the course of this licensing transaction, (ii) these terms and conditions and (iii) CCC's Billing and Payment terms and conditions.
- This Agreement will be void if the Type of Use, Format, Circulation, or Requestor Type was misrepresented during the licensing process.
- This Agreement shall be governed by and construed in accordance with the laws of the State of New York, USA, without regards to such state's conflict of law rules. Any legal action, suit or proceeding arising out of or relating to these Terms and Conditions or the breach thereof shall be instituted in a court of competent jurisdiction in New York County in the State of New York in the United States of America and each party hereby consents and submits to the personal jurisdiction of such court, waives any objection to venue in such court and consents to service of process by registered or certified mail, return receipt requested, at the last known address of such party.

WILEY OPEN ACCESS TERMS AND CONDITIONS

Wiley Publishes Open Access Articles in fully Open Access Journals and in Subscription journals offering Online Open. Although most of the fully Open Access journals publish open access articles under the terms of the Creative Commons Attribution (CC BY) License only, the subscription journals and a few of the Open Access Journals offer a choice of Creative Commons Licenses. The license type is clearly identified on the article.

The Creative Commons Attribution License

The [Creative Commons Attribution License \(CC-BY\)](#) allows users to copy, distribute and transmit an article, adapt the article and make commercial use of the article. The CC-BY license permits commercial and non-

Creative Commons Attribution Non-Commercial License

The [Creative Commons Attribution Non-Commercial \(CC-BY-NC\) License](#) permits use, distribution and reproduction in any medium, provided the original work is properly cited and is not used for commercial purposes.(see below)

Creative Commons Attribution-Non-Commercial-NoDerivs License

The [Creative Commons Attribution Non-Commercial-NoDerivs License](#) (CC-BY-NC-ND) permits use, distribution and reproduction in any medium, provided the original work is properly cited, is not used for commercial purposes and no modifications or adaptations are made. (see below)

Use by commercial "for-profit" organizations

Use of Wiley Open Access articles for commercial, promotional, or marketing purposes requires further explicit permission from Wiley and will be subject to a fee.

Further details can be found on Wiley Online Library

<http://olabout.wiley.com/WileyCDA/Section/id-410895.html>

Other Terms and Conditions:

v1.10 Last updated September 2015

Questions? customercare@copyright.com or +1-855-239-3415 (toll free in the US) or +1-978-646-2777.

Dear Dr. Ye:

Thank you for contacting ACS Publications Support.

Your permission request is granted and there is no fee for this reuse. In your planned reuse, you must cite the ACS article as the source, add this direct link <<https://pubs.acs.org/doi/abs/10.1021/nn405075d>>, and include a notice to readers that further permissions related to the material excerpted should be directed to the ACS.

Please let me know if I can be of further assistance.

Sincerely,

Maria Flona-Amor Odevilas

ACS Customer Services & Information

<https://help.acs.org/>

Dear heng.ye@postgrad.curtin.edu.au,

Incident Information:

Incident #: 2259285

Date Created: 2018-09-30T13:12:38

Priority: 3

Customer: heng.ye@postgrad.curtin.edu.au

Title: Request for the reuse of a figure in ACS Nano Journal

Description: Dear Support team from ACS,

Hello! I am a student from Curtin University, Australia. I would like to reuse a figure of the ACS Author Choice paper in the ACS Nano journal. The title of the paper is: "Self-Propelled Micromotors for Cleaning Polluted Water"

The link is: <https://pubs.acs.org/doi/abs/10.1021/nn405075d>

The portion of the article I want to use is Figure 1.

I would like to use this part in my PhD thesis. The title is "Self-Propelled Micro/Nanomotors (MNMs) and Their Applications"

Kind regards!

Heng Ye

Dear Dr. Ye:

Thank you for contacting ACS Publications Support.

Your permission request is granted and there is no fee for this reuse. In your planned reuse, you must cite the ACS article as the source, add this direct link <<https://pubs.acs.org/doi/abs/10.1021/acs.nanolett.6b00768>>, and include a notice to readers that further permissions related to the material excerpted should be directed to the ACS.

Please let me know if I can be of further assistance.

Sincerely,

Maria Flona-Amor Odevilas

ACS Customer Services & Information

<https://help.acs.org/>

Dear heng.ye@postgrad.curtin.edu.au,

Incident Information:

Incident #: 2259292

Date Created: 2018-09-30T13:27:38

Priority: 3

Customer: heng.ye@postgrad.curtin.edu.au

Title: Request for the reuse of a figure in Nano Letters Journal

Description: Dear Support team from ACS,

Hello! I am a student from Curtin University, Australia. I would like to reuse a figure of the ACS Author Choice paper in the Nano Letters journal. The title of the paper is: “Graphene-Based Microbots for Toxic Heavy Metal Removal and Recovery from Water”

The link is: <https://pubs.acs.org/doi/abs/10.1021/acs.nanolett.6b00768>

The portion of the article I want to use is Figure 1.

I would like to use this part in my PhD thesis. The title is “Self-Propelled Micro/Nanomotors (MNM)s and Their Applications”

Kind regards!

Heng Ye